Structure Based Drug Design and *in vitro* Biological Screening for Various Enzymes of *Mycobacterium tuberculosis*

THESIS

Submitted in partial fulfilment
of the requirements for the degree of
DOCTOR OF PHILOSOPHY

by

SHALINI SAXENA
ID No 2011PHXF025H

Under the Supervision of
D. SRIRAM

BIRLA INSTITUTE OF TECHNOLOGY AND SCIENCE, PILANI

2015

BIRLA INSTITUTE OF TECHNOLOGY AND SCIENCE, PILANI

CERTIFICATE

This is to certify that the thesis entitled "**Structure Based Drug Design and *in vitro* Biological Screening for Various Enzymes of *Mycobacterium tuberculosis***" submitted by **SHALINI SAXENA** ID. No **2011PHXF025H** for award of Ph.D. of the Institute embodies original work done by her under my supervision.

Signature in full of the Supervisor:

Name in capital Block letters : **D. SRIRAM**

Designation : **Professor**

Date:

ACKNOWLEDGEMENT

Imagination is the beginning of creation, you imagine what you desire, you will what you imagine and at last you create what you will.

George Bernard Shaw

Words are tools of expression, but they fail miserably when it comes to thanks giving. I might not able to do adequate justice in this task of acknowledging my indebtedness to all those who have directly as well as indirectly made it possible to complete my thesis. I am going to try anyway, and if your name is not listed, rest assured that my gratitude is not less than for those listed below.

*It's a fact that every mission needs a spirit of hard work and dedication but it needs to be put on the right path to meet its destination and in my case this credit goes to my esteem supervisor respected **Prof. D.Sriram**, for his constant encouragement, continuous support, valuable suggestion and timely advice, without whom my thesis would not have been a success. This has thus been a memorable phase and he shall always remain my greatest inspiration. I am short of words to thank him for his affectionate behavior and patience throughout the duration of the thesis work.*

*I deeply acknowledge and heartfelt thanks to **Prof. P. Yogeeswari**, Professor, Department of Pharmacy, BITS, Pilani-Hyderabad campus, for her valuable suggestions, guidance and precious time which she offered me throughout my research.*

*With immense pleasure and profound sense of gratitude, I take this golden opportunity to express my heartfelt and sincere indebtness to my DAC member **Dr. Balaram Ghosh** Department of Pharmacy, BITS, Pilani-Hyderabad campus, for the precious suggestions and guidance during my research work.*

*I am grateful to **Prof. Bijendra Nath Jain**, Vice-Chancellor (BITS) and Director **Prof. V.S.Rao** (Hyderabad campus), for allowing me to carry out my doctoral research work in the institute.*

ABSTRACT

In the present study we explore the pharmaceutically underexploited domains of *M. tuberculosis* DNA Gyrase B (GyrB) and L-Alanine dehydrogenase (L-AlaDH) as potential platform for developing novel agents that target *M. tuberculosis* which is an air born infection that has infected one third of the world population.

Utilizing the computational tools of structure based and ligand based drug design methods; 5-phenyl-2-C-thiophene-2-thiophene-2,3-diamido was identified as potential DNA Gyrase B lead and 5-(4-benzyloxy)benzylidene-2-imino-3-(5-nitrothiazol-2-yl)thiazolidin-4-one and 2-(5-nitrothiophene-2-carboxamido)-4,5-dihydro-N6-(4-methoxyphenyl)thieno[2,3-c]pyridine-3,6(7H) dicarboxamide were identified as *M. tuberculosis* L-AlaDH leads.

The leads obtained from both the targets were further customized using a combination of molecular docking and chemical synthesis to develop various analogues that displayed considerable *in vitro* enzyme efficacy and bactericidality activity against *M. tuberculosis* $H_{37}Rv$ strain.

By using structure based approach, compound **S23** emerged as the most potent GyrB lead with *M. smegmatis* GyrB IC_{50} of 1.35 ± 0.58 μM; supercoiling inhibitory IC_{50} value of 0.86 ± 0.25 μM; *M. tuberculosis* MIC of 4.84 μM. The binding affinity of the potent ligand towards the GyrB domain was re-ascertained by differential scanning fluorimetry experiment wherein a shift in the melting temperature T_M was monitored. The tested compounds brought a positive shift in T_M in the range of 2-3.1°C compared to the native protein, a repercussion of strong inhibitor binding.

Similarly, for the identification of *M. tuberculosis* L-AlaDH inhibitors, an e-pharmcophore based high throughput virtual screening protocol was used. Since no inhibitors were reported till date for *M. tuberculosis* L-AlaDH, thus we have report the first set of novel diverse inhibitors using crystal structure of *M. tuberculosis* L-AlaDH protein complex with N_6-methyl adenosine and substrate NAD^+. Two molecules identified as leads were modified synthetically to obtain thirty novel analogues belonging to 2-iminothiazolidine-4-ones and 4,5,6,7-tetrahydrothieno[2,3-c]pyridine-3-carboxamides. Among the screened compounds

four (**4n, 4o, 12** and **14**) emerged as potent inhibitors displaying IC_{50} values ranging from 0.58 ± 0.02 to 1.74 ± 0.03 µM against *M. tuberculosis* L-AlaDH and was non-cytotoxic at 50 µM. Some of these synthesized compounds also exhibited good activity against nutrient starved dormant *M. tuberculosis*. The most potent inhibitors were found to stabilize the protein which was confirmed biophysically through differential scanning fluorimetry.

With new anti-TB agents desperately needed, we believe that the present class of inhibitors reported in this work would be interesting as potential leads to be worked for rational drug design against *M. tuberculosis* from pharmaceutical point of view.

TABLE OF CONTENTS

Contents	*Page No.*

Contents	Page No.

Contents	Page No.

Contents	Page No.

Contents	Page No.

Contents	*Page No.*

LIST OF TABLES

LIST OF FIGURES

ABBREVIATIONS

2D	:	Two-Dimensional
3D	:	Three-Dimensional
A	:	Acceptor
AlaDH	:	Alanine dehydrogenase
ATP	:	Adenosine triphosphate
AZ	:	AstraZeneca
BITS-Pilani	:	Birla Institute of Technology and Science, Pilani
BDQ	:	Bedaquiline
bp	:	Basepair
BTZ043	:	Benzothiazinones
^{13}C NMR	:	Carbon Nuclear Magnetic Resonance
CG	:	Conjugate gradient
CTD	:	C-terminal Domain
CM	:	Capuramycin
DOTS	:	Directly observed treatment, short course
DNA	:	Deoxyribonucleic acid
DMSO	:	Dimethyl sulfoxide
DTT	:	Dithiothreitol
DSF	:	Differential scanning fluorimetry
D	:	Donor
EDTA	:	Ethylenediaminetetraacetic acid
ELISA	:	Enzyme-linked immunosorbent assay
EF	:	Enrichment factor
e-pharmacophore	:	Energy based pharmacophore
EMB	:	Ethambutol
ETH	:	Ethionamide
FBS	:	Fetal bovine serum

GyrA	:	DNA Gyrase A subunit
GyrB	:	DNA Gyrase B subunit
GSK	:	GalaxoSmithKline
GH	:	Goodness of hits
GOLD	:	Genetic Optimization for Ligand Docking
HIV	:	Human Immunodeficiency Virus
HTS	:	High-Throughput Screening
hERG	:	Human Ether-à-go-go-Related Gene
^{1}H NMR	:	Proton Nuclear Magnetic Resonance
HPLC	:	High-Performance Liquid Chromatography
HTVS	:	High throuput virtual screening
HY	:	Hydrophobic
HBD	:	Hydrogen bond donor
HBA	:	Hydrogen bond acceptor
HY-Ar	:	Hydrophobic Aromatic
HEPES	:	(4-(2-hydroxyethyl)-1-piperazineethanesulfonic acid)
IPTG	:	Isopropyl β-D-1-thiogalactopyranoside
INH	:	Isoniazid
K_i	:	Dissociation constant
K_d	:	Dissociation constant
KCl	:	Potassium chloride
KOH	:	Potassium hydroxide
LB	:	Luria-Bertani
L	:	Liter
LHS	:	Left hand side
MDR-TB	:	Multi-drug resistant *Mycobacterium tuberculosis*
ml	:	Mililiter
μg	:	Microgram
mg	:	Milligram
MIC	:	Minimum inhibitory concentration

μM	:	Micromolar
MPN	:	Most probable number
MTT	:	(4,5-dimethylthiazol-2-yl)-2,5-diphenyltetrazolium bromide
mmol	:	Millimole
M.p	:	Melting point
$MgCl_2$	:	Magnesium chloride
NBTIs	:	Non-fluoroquinoline topoisomerase inhibitors
NTD	:	N-terminal Domain
nM	:	Nanomolar
NAD	:	Nicotinamide adenine dinucleotide
NADH	:	Nicotinamide adenine dinucleotide (reduced form)
ns	:	Nanosecond
NI	:	Negative ionizable
NaCl	:	Sodium chloride
OADC	:	Oleic acid, Albumin, Dextrose, and Catalase
PAS	:	*Para*-aminosalicylic acid
PTH	:	Prothionamide
PDB	:	Protein Data Bank
PCR	:	Polymerase Chain Reaction
PI	:	Positive ionizable
PBS	:	Phosphate buffered saline
RIF	:	Rifampin
RHS	:	Right hand side
RMSD	:	Root mean square deviation
ROC	:	Receiver operating characteristic
rpm	:	Rotation per minute
rt	:	Room temperature
R	:	Ring aromatic
RPMI	:	Roswell Park Memorial Institute medium
SD	:	Steepest descent

SP	:	Standard precision
SAR	:	Structure activity relationship
TB	:	Tuberculosis
TDR-TB	:	Totally-drug resistant *Mycobacterium tuberculosis*
TL-1	:	Translocase-1
T_M	:	Melting temperature
TAE	:	Tris-acetate-EDTA
WHO	:	World Health Organization
XDR-TB	:	Extensively-drug resistant *Mycobacterium tuberculosis*
XP	:	Extra precision
zERG	:	Zebrafish ether-a-go-go-related gene

Chapter **1**

Introduction

Tuberculosis (TB) is a chronic disease caused by bacteria called *Mycobacterium tuberculosis* which is an obligate aerobic bacilli that divides at a very slow rate and is transmitted as a highly infectious aerosol. The bacteria, usually attacks the lungs but can also damage other parts of the body such as brain, intestines, kidneys and spine. Patients with active pulmonary TB are the main source of infection and majority of people infected with TB suffer from asymptomatic latent TB infection. TB remains to be a leading cause of morbidity and mortality in many Asian countries like Afghanistan, Bangladesh, Bhutan, India and also in other developing countries. With the discovery of chemotherapy in the 1940s and adoption of the standardized short course in the 1980s, it was supposed that TB would decline globally. Although a declining trend was observed, in most developed countries, this was not evident in many developing countries. In developing countries, about 7% of all deaths are due to TB, which is the most common cause of death from a single source of infection among adults.

1.1. Epidemiology

It is the first infectious disease declared by the World Health Organization (WHO) as a global health emergency. It is the second greatest killer due to a single infectious agent worldwide and the WHO estimates in 2012 that 1.3 million people died from the disease, with 8.6 million falling ill [WHO Report., 2013]. The Centers for Disease Control and Prevention (CDC) report, that in 2010, there were 11,182 cases of TB in the United States. The current global picture of TB showed that in 2012, most of the cases were found in South-East Asia (29%), Africa (27%) and Western Pacific (19%) regions with more than 255 cases per 100,000 people. India and China alone accounted for 26% and 12% of total cases, respectively [WHO Report., 2013] and fewer than 10 per 100,000 populations in parts of the America and several countries in Western Europe, Japan, Australia and New Zealand. Globally in 2012, an estimated 450,000 people developed multi-drug-resistant-TB (MDR-TB) and there were an estimated 170,000 deaths from MDR-TB. In 84 countries, extensively

drug-resistant TB (XDR-TB) has been reported [WHO Report., 2013]. More people in the developing world contract TB because of poor immune system, largely due to high rates of HIV infection and the corresponding development of AIDS.

Data from drug resistance surveys, suggests that 3.6% of newly diagnosed TB cases and 20% of those previously treated for TB had MDR-TB, caused by organisms resistant to isoniazid and rifampin. In developing countries, where the TB burden is high, this situation highlights the relative shortcomings of the current treatment strategies for TB and the limited effectiveness of public health systems.

1.2. The causative agent of TB

TB is one of the oldest recorded human afflictions and is still one of the biggest killers among infectious diseases, despite the use of a worldwide, live attenuated vaccine and several antibiotics [I. Smith., 2003]. *M. tuberculosis*, along with *M. bovis, M. africanum and M. microti* are all causative agents of TB and are the members of the tuberculosis species complex. Each member of the TB complex is pathogenic, but *M. tuberculosis* is pathogenic for humans while *M. bovis* is usually pathogenic for animals. *M. tuberculosis* is the etiologic agent of tuberculosis in humans and it is facultative intracellular organism discovered by Robert Koch in 1882 [Koch R., 1882]. Humans are the only reservoir for the bacterium and it is spread from person to person by the germs being sent through air by carriers coughing, sneezing or spitting. In the classic case of TB, *M. tuberculosis* complexes are always found in the well-aerated upper lobes of the lungs [Singh G., *et al.*, 2010]. *M. tuberculosis* is gram-positive and non-spore forming bacteria. The TB bacterium is a facultative intracellular parasite; usually of macrophages which have a slow generation time of 15-20 hours as compared to other bacteria. The hard cell wall of the bacterium prevents passage of nutrients into and excreted from the cell, leading to its slow growth rate. The cell wall of the pathogen looks like a Gram-positive cell wall. The cell envelope contains a polypeptide layer, a peptidoglycan layer, complex free lipids and it is unique among all prokaryotes. It is a major determinant of virulence for the bacterium [Cole S.T., *et al.*, 1998]. Over 60% of the mycobacterial cell wall is composed of lipid. The lipid fraction of *M. tuberculosis* cell wall consists of three major components, i.e. mycolic acids, cord factor and wax-D [Rivers E.C., *et al.*, 2008; Barrera L., 2007; Godreuil S., *et al.*, 2007]. Infection with *M. tuberculosis* is believed to be contacted, following the inhalation of droplets (aerosols) containing a small number of bacilli [Kaufmann S.H., 2001]. Once in the lung, bacilli are internalized through

phagocytosis by the resident macrophages of the lung, called the alveolar macrophages. The bacteria replicate within the macrophage and induce cytokines that initiate the inflammatory response in the lungs. Macrophages and lymphocytes migrate to the site of infection and form granulomas (**Figure 1.1**). The unique structure of the cell wall of *M. tuberculosis* allows it to lie dormant for many years as a latent infection, particularly as it can grow readily inside macrophages, hiding it from the host's immune system but not eliminating the pathogen [Russell., 2007]. This contributes to the chronic nature of the disease, imposes lengthy treatment regimens and represents a difficult problem for researchers.
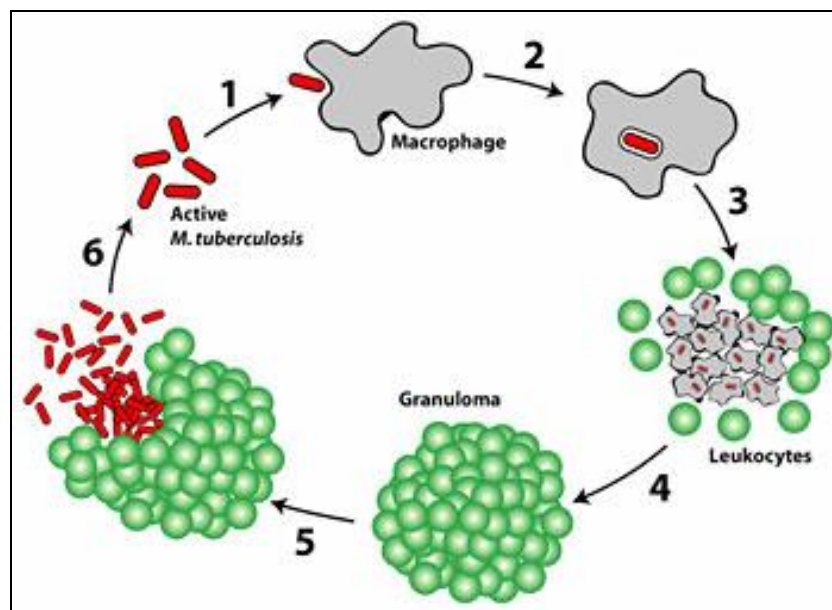
Figure 1.1: Pathogenesis of *M. tuberculosis* [Larsen, M. H., *et al*.; 2006]

1.3. History of the current TB drug therapy

In 1944, the major historical landmarks of TB therapy evolved with the discovery of effective medications like streptomycin and *para*-aminosalicylic acid (PAS), while in the 1970's the revelation of "triple therapy" [streptomycin, PAS and isoniazid (INH)] emerged which assured cure. In the same year INH and rifampin (RIF) could reduce the duration of treatment from 18 months to 9 months and the observation in the 1980's pyrazinamide was added to these drugs which promised a cure in 6 months. Most of the drugs which composed the arsenal of the first-line TB treatment were discovered during the 1950's and the 60's [Villemagne D., *et al*., 2012]. In 1943, the first effective anti-tuberculosis agent streptomycin brought much excitement and hope to the world. Later the aminoglycoside class of antibiotics was discovered which consists of many different agents. This aminoglycoside interferes with

protein biosynthesis through an interaction with the small 30S subunit of the ribosome [Schatz A., *et al*., 1944; Jones D., *et al*., 1944] followed by the discovery of PAS in 1946. In the same year mycolic acid biosynthesis inhibitor INH [Bernstein J., *et al*., 1952] and pyrazinamide (PAZ) [Malone L., *et al*., 1952] emerged as one of the most active anti-TB drugs. In 1956, further investigation of the anti-TB activity of polyamines and diamines prompted the production of a series of diamine analogues that gave rise to ethambutol (EMB) [Thomas J.P., *et al*., 1961]. Later, development of the same lead gave rise to ethionamide (ETH) and prothionamide (PTH). In 1961 the discovery of a new anti-tuberculosis agent [Thomas *et al*., 1961] N, N'diisopropylethylenediamine was found to protect mice from lethal infection with *M. tuberculosis* strain H37Rv. Finally, in 1971 RIF the last member of the present first line TB drugs appeared as a drug of choice for TB treatment [Binda G., *et al*., 1971] and was found to be effective against replicating and non-replicating mycobacteria. In spite of the significant efficiency showed by these drugs, soon it was observed that TB bacteria quickly developed resistance to these drugs. To overcome this problem, combination therapy was introduced by grouping some current TB drugs according to their effectiveness, experience of use and drug class. The WHO-recommended DOTS (directly observed treatment, short course) anti-TB therapy involving a 6-month chemotherapy regimen using a combination of 4 drugs (RIF, INH, ETH, and PAZ) for 2 months, followed by RIF and INH for 4 months with cure rates of approximately 90% in human immunodeficiency virus (HIV) negative patients. This is the globally accepted standard treatment of drug-susceptible, active tuberculosis. It is essential to take several TB drugs together because if only one TB drug is taken on its own, then the patient will very quickly become resistant to that drug. The drugs that are taken for the treatment of TB have the aim to kill all TB bacteria present in a person's body. However, TB bacteria die very slowly and so the drugs have to be taken for quite a few months. Even when a patient starts to feel better they can still have bacteria alive in their body and hence the person needs to keep taking the treatment until all the bacteria are dead. All the TB drugs must be taken for the entire period of treatment. If only one or two TB drugs are taken then all the bacteria may not be killed and they can become resistant to the drugs which then don't work. If the person becomes sick again, then different TB drugs may be needed. Treatment with these so called first-line drugs is carried out initially over two months, leading to the destruction of bacteria in all growth stages, after which treatment continues with RIF and INH alone for four months. The residual dormant bacilli are eliminated by RIF and any remaining RIF-resistant mutants are killed by INH [Bayer R., *et al*., 1995; Raviglione M.C., *et al*., 2007; Bhowruth V., *et al*., 2007].

1.4. Problems with current TB treatment

In spite of newer modalities for diagnosis and treatment of TB, unfortunately, millions of people are still suffering and dying from this disease. There are several major problems associated with the currently available TB treatment. The most problematic issue with the current first-line TB regimen is the duration and complexity of treatment which resulted in the nonadherence to treatment. This leads to suboptimal response (failure and relapse), the emergence of resistance and continuous spread of the disease. Another problem with current TB treatment is the increasing incidence of MDR-TB and XDR-TB. Inadequate adherence to treatment occurs despite extensive global efforts by the WHO, ministries of health and others to implement the highly labor-intensive TB treatment program known as DOTS, which includes direct observation of treatment by public health workers. Resistant TB occurs in the presence of partially suppressive drug concentrations that enable replication of bacteria with the formation of mutants and overgrowth of wild-type strains by mutants. Due to the long treatment time required, the treatment of TB differs from that of other infectious diseases to treat the patient arising from the slow-growing nature of *M. tuberculosis* bacteria along with its ability to enter a non-replicating persistent (NRP) state where in a certain subpopulations of bacteria survive within the granulomas lesions surrounded by foamy macrophages, with lacking clinical symptoms. This phenomenon, called phenotypic resistance or tolerance, is also commonly referred to as 'persistence', and the bacilli that remain in the host for relatively long periods despite appropriate drug treatment are referred to as 'persistors'. Investigators have demonstrated that INH alone at the standard dose kills over 90% of the infecting mycobacteria in the first two days of treatment [Ginsberg A.M., *et al*., 2007]. Most bactericidal drugs are only effective against the actively growing bacilli. Thus extended treatment is required to inhibit the re-growth of the bacteria. Genetic and molecular analysis of drug resistance in *M. tuberculosis* suggests that resistance is usually acquired by the bacilli either by alteration of the drug target through mutation or by titration of the drug through overproduction of the target [Solanki R.N., 2012]. Under such conditions, the sensitive strains are killed and the drug-resistant mutants flourish. TB treatment in HIV-positive patients is further complicated by drug-drug interactions between some of the antiretroviral agents (ARVs) and key anti-tubercular drugs, especially RIF. In order to intensify our fight against this deadly disease, we need to further strengthen our surveillance programs to accurately estimate the burden of all kinds of TB (childhood, HIV/TB, MDR-TB).

1.4.1. MDR-TB

MDR-TB is caused by bacteria that are resistant to the most effective anti-TB drugs - INH and RIF. MDR-TB results from either primary infection with resistant bacteria or may develop in the course of a patient's treatment. Drug resistance in *M. tuberculosis* occurs due to genetic factor, resistance factors related to previous anti tuberculosis treatment and other factors [Jain A., *et al*., 2008]. While TB is curable, MDR-TB may be fatal and the cure rates are very low. Management of MDR-TB is most difficult, complicated, challenging, costlier and needs experienced and highly skilled persons [Rai and Panda 2004]. TB is easy to diagnose but diagnosis of MDR-TB depends on reliable and expensive culture and sensitivity test that are not available in most parts of the world. The second line drugs used in cases of MDR-TB are often less effective, more likely to cause side effects and are expensive [Sharma and Mohan 2004]. To cure MDR-TB, healthcare providers must turn to a combination of second-line drugs. MDR-TB demands treatment with second line drugs that have limited sterilizing capacity and are more toxic [Sharma and Mohan 2004; Ormerod 2005]. MDR-TB treatment is rather complicated as it requires second line drugs some of which are only injectables, less efficacious, more toxic and more expensive than the first line agents. Treatment lasts for 18-24 months but only around 50%–60% of MDR-TB patients will be cured compared to 95%-97% cure rate for patients with drug-susceptible strains treated with first line agents [Ma Z., *et al*., 2010].

1.4.2. XDR-TB

The global emergence of XDR-TB heralds the advent of widespread, virtually untreatable TB [Dalton T., *et al*., 2012; Shah N.S., *et al*., 2007]. XDR-TB is defined as resistance to at least INH, RIF, fluoroquinolone and one of three injectables drugs (amikacin, kanamycin or capreomycin). Because XDR-TB is resistant to first- and second-line drugs, treatment options are seriously limited and because of the lack of potent anti-TB drugs, it is challenging to treat patients suffering from XDR-TB. However, the approach to designing a treatment regimen is the same as with MDR-TB. First, begin with any first-line drugs that demonstrate *in vitro* activity, followed by second and third line drugs. Surgery should be a strong consideration in patients with XDR-TB.

1.4.3. Totally drug resistant TB (TDR-TB)

In 2009, the new term TDR-TB is evolved for TB strains that showed *in vitro* resistance to all first and second line drugs tested. However, data on the TDR-TB may not provide an adequate indication of its prevalence. Giovanni Migliori, director of the WHO Collaborating Centre for Tuberculosis and Lung Diseases in Tradate, Italy, suggests that TDR-TB is a deadlier iteration of the highly resistant forms of TB that have been increasingly reported over the past decade. "Totally resistant TB is not new at all," he says. National Reference TB laboratory (NRL) of Iran was the first laboratories which could identify TDR-TB bacilli. Based on availability of TDR-culture isolates, investigation was started at cellular and molecular level. The primary results using transmission and atomic force microscopes, confirmed morphological variation in TDR-TB isolates. TDR-TB has resulted from further mutations within the bacterial genome to give resistance, beyond those seen in XDR and MDR-TB.

1.5. The current TB drugs in pipeline

There are currently at least twelve compounds in various stages of clinical development for TB. Four of these are existing drugs that are either being redeveloped or repurposed for the treatment of TB and there are six new chemical compounds that are being specifically developed as TB drugs. This is not however considered to be a very extensive drugs "pipeline" for such a major disease as TB. Twenty one new TB drugs are in clinical investigation, nine in preclinical development, eight in phase 2 (early bactericidal activity and sputum culture conversion), and four in phase 3 (safety and efficacy) trials (**Figure 1.2**).

A selection of promising new compounds is on the scope for the first time in 40 years as substantial progress has been made in development of new drugs during the past decade. Some have the potential to become the keystone of future TB treatment. Some of the drugs have been discussed in this section.

The first drug which is presently in their pre-clinical stage development is **CPZEN-45**. It is a nucleoside antibiotic developed by Institute of Microbial Chemistry (BIKAKEN), Tokyo, Japan and is active against both replicating and non-replicating bacteria. It is the most promising derivative of the caprazamycins [Yoshimasa I., *et al*., 2013].
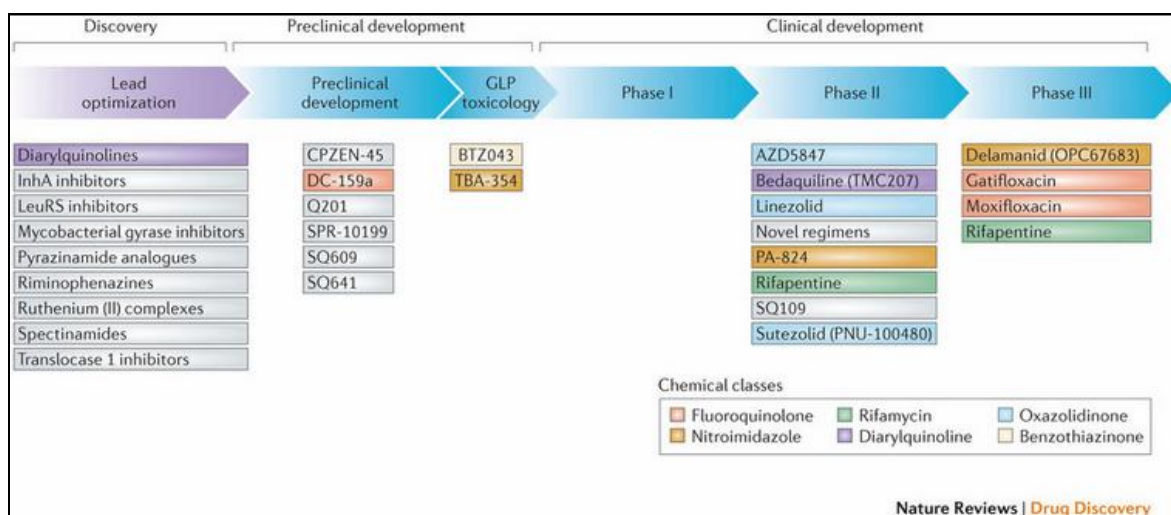
Figure 1.2: Current global pipeline of new TB drugs [Zumla A., *et al*., 2013].

The **Benzothiazinones** (**BTZ043**) is another drug which is also currently in preclinical stage. It is the most potent inhibitors of *M. tuberculosis* yet described and display low nanomolar bactericidal activity against mycobacteria growing *in vitro* and in *ex vivo* models [Stanley S.A., *et al.*, 2012]. It kills MTB bacteria by blocking arabinan synthesis. The benzothiazinone lead compound, BTZ043, kills MTB bacteria by inhibiting the essential flavo-enzyme DprE1, decaprenylphosphoryl-beta-D-ribose 2-epimerase [Makarov V., 2014].

Another drug of same class is **PBTZ169**, which has improved potency, safety and efficacy in zebra fish and mouse models of TB as compared to BTZ043. When combined with other TB drugs, PBTZ169 showed additive activity against *M. tuberculosis in vitro* except with bedaquiline (BDQ) where synergy was observed. A new regimen comprising PBTZ169, BDQ and pyrazinamide was found to be more efficacious than the standard three drug treatment in a murine model of this chronic disease. PBTZ169 is thus an attractive drug candidate to treat TB in humans [Makarov V., 2014].

The **DC-159a** is a new fluoroquinolone drug with more potent *in vitro* activity than available fluoroquinolones against both drug-susceptible and fluoroquinolone-resistant *M. tuberculosis*. DC-159a is the most active compound against quinolone-resistant multidrug-resistant *M. tuberculosis* (MIC=0.5 µg/ml) as well as drug-susceptible isolates (MIC=0.06 µg/ml). DC-159a also demonstrated the highest activities against clinically important non-tuberculous mycobacteria [Disratthakit A., *et al.*, 2010].

SQ609 and **SQ641**were identified by Sequella and they have promising activity against drug-susceptible and drug-resistant TB. SQ641 is an analogue of capuramycin (CM), a naturally occurring nucleoside-based compound produced by *Streptomyces griseus*. It was derived from a library of over 7,000 CM analogues created by Daiichi-Sankyo (Japan) and was identified as the most potent of the translocase-1 (TL1) inhibitors, with good activity against mycobacteria. These classes of compounds are mainly targeting cell wall of the bacteria. It is an ideal drug target because inhibition of TL1 leads to cell death and the enzyme is unique to bacteria, reducing the likelihood of toxicity [Boris V.N., *et al.*, 2009].

The other drug from the riminophenazine class **Clofazimine** (**TBI-166**) is also in its pre-clinical stage and is effective in treating the mycobacterial infection Hansen's disease (also known as leprosy) while clofazimine and other compounds of this class demonstrate impressive bactericidal and sterilizing efficacy against TB *in vitro* and in mouse models of the disease.

Q203 is another potent inhibitor of *M. tuberculosis* in both outside and inside of the host cell. It inhibited the growth of both MDR and XDR-TB, in addition, Q203 displays pharmacokinetic and safety profiles compatible with once-daily dosing. Together, this data indicate that Q203 is a promising new clinical candidate for the treatment of TB [Pethe K., *et al.*, 2013].

As a part of new combination therapy when other alternatives have failed, **Bedaquiline**, a novel adenosine triphosphate synthase inhibitor has recently been granted license by the U.S. Food and Drug Administration under its accelerated approval procedure for treatment of MDR-TB patients [Cohen J., 2013]. It is unique and specific anti-mycobacterial activity derives from inhibition of the proton pump of mycobacterial ATP synthase. ATP synthase is a critical enzyme in the ATP synthesis of *M. tuberculosis*. Binding of Bedaquiline to the oligomeric and proteolipic subunit-c of mycobacterial ATP synthase leads to inhibition of ATP synthesis, which subsequently results in bacterial death.

The nitroimidazoles are an existing class of drugs known to have antimicrobial activity. Two nitroimidazoles, **PA-824** and **OPC-67683** (now also known as Delamanid), are currently in Phase II clinical trials for the treatment of TB and the outcome of these may determine the future directions of drug development for anti-tubercular nitroimidazoles. **Delamanid** is a member of the nitroimidazo-oxazole family, and although early studies showed it to be a

potentially effective drug for both drug resistant and drug susceptible TB, it is currently being initially developed by the Otsuka pharmaceutical company as a treatment for MDR-TB. **PA-824** potentially used for the treatment of both drug sensitive and drug resistant TB and it has also shown activity against both latent and active TB. Another drug in the same class is **TBA-354**, a new member of the nitroimidazole class, was discovered by the Global Alliance for TB Drug Development (TB Alliance), in partnership with two academic institutions, the University of Auckland and the University of Illinois at Chicago. This compound was discovered with the aim to maximize the potential of this emerging class of anti-tubercular compounds for the treatment of both drug-sensitive and drug-resistant TB. It is a drug in the same class as **PA-824** but it has been more potent in preclinical studies and also said to be longer lasting and has greater activity against resistant strains of the disease. **TBA-354** has now been selected by the TB Alliance for further development and it is hoped that trials in humans will soon start.

AZD5847 is a potential new TB drug being developed by AstraZeneca (AZ). It acts by the inhibition of translation by binding at the "A" site of peptidyl transferase center. In December 2012, it was announced that the first patient had been enrolled in a Phase 2a trial of the drug in South Africa, to assess the effectiveness of the drug for patients with TB, including patients with HIV and TB co-infection [Balasubramanian V., *et al.*, 2013].

The other drug of this class is **Sutezolid** (PNU 100480) which was discovered by Pfizer. Ethylenediamine class of drug **SQ109** is being developed by Sequella and it is a new TB drug candidate with a novel mechanism of action that was safe and well tolerated in Phase I and early Phase II clinical trials [Sacksteder K.A., *et al.*, 2013]. It acts by Inhibition of MmpL3 transporter of trehalose mycolate across cell membrane for incorporation into cell wall. It is an oxazolidinone that was identified contemporaneously with linezolid, which is FDA approved for severe infections caused by Gram-positive bacteria that are resistant to other antibiotics. **RIF** is a key component of first line drug treatment for TB and **Rifapentine** is attractive as a possible TB drug for shortening the treatment. Further, the clinical trials are under way to assess these drugs.

Several members of the fluoroquinoles class of drugs are already in use as second line TB drugs for the treatment of MDR-TB. **Moxifloxacin** and **Gatifloxacin** are now being developed specially for the treatment of drug sensitive TB. Each of these potential TB drugs is currently undergoing evaluation in a phase 3 trial, to see how effective it is when

substituted for either ethambutol or isoniazid, to shorten the treatment of drug sensitive TB from the standard six months to four months [Laurenzi M., *et al*., 2007]. **Gatifloxacin** trial is being conducted by the Oflotub, Consortium and **Moxifloxacin** is being developed by Bayer and the TB Alliance. What is ideally needed is not just one new TB drug but several which can be used together. In July 2012 it was announced that a phase 2A study had been carried out investigating a number of drug combinations including PA-824 over a 14 day period to assess their suitability for further development. The combination of PA-824, moxifloxacin and pyrazinamide had the greatest early bactericidal activity. One advantage of this drug combination is that it does not involve either INH or RIF and it is therefore suitable for use with those patients who were resistant to these drugs. These three drug combination now needs to be further investigated over a longer period of time, taking into account that PA-824 and moxifloxacin have at least some potential to cause cardiac side effect.

Nitroimidazole compounds, such as the classic metronidazole, were first investigated as TB drugs because of their known activity against anaerobic microorganisms, and anaerobiosis is thought to lead to LTBI [Migliori G.B., *et al*., 2012]. Metronidazole kills *M. tuberculosis in vitro* under hypoxic but not aerobic conditions and displays widely contrasting effects in different animal models.

In search for novel drug targets, more research must go into understanding the biology of persistence, the factors involved in tissue liquefaction and cavity formation, and the host immune mechanisms that control latent infection. The outcome of such research will not only provide improved understanding of the disease, but also new relevant biology-based targets for drug intervention. This is a battle that might not be easily won, but given persistent effort and sustained support, it is quite likely that the current endeavors will bear fruit and lead to more effective treatment.

Chapter 2

Literature Review

In the search of new TB drugs that can overcome the increasing spread of MDR and XDR-TB and emergence of drug resistance along with the problem of mycobacterial persistence, highlights the need to develop novel TB drugs that are active against drug resistant bacteria and also more importantly, kill persistent bacteria and shorten the length of treatment. It can be approached from the identification and validation of novel targets. One such attractive strategy is to inhibit **DNA Gyrase (Gyr)**, an ATP-dependent type IIA topoisomerase enzyme. The other target is **L-alanine dehydrogenase** (**L-AlaDH**) from *M. tuberculosis*. The major problem associated with TB is that the TB bacteria survive in the human host for decades evading the immune system in a latent or persistent state. In such conditions, the Rv2780 gene that codes for L-AlaDH enzyme catalyzes the reversible oxidative deamination of L-alanine to pyruvate and also it is over-expressed under hypoxic and nutrient starvation conditions. At present, as there is no suitable drug available to treat dormant tuberculosis; it is essential to identify drug candidates that could potentially treat dormant TB. These two targets are the focus of the present study.

2.1. DNA Gyrase as an anti-tubercular drug target

Bacterial DNA gyrase, a type II DNA topoisomerase found in all bacteria, is a proven target for antibacterial chemotherapy [Ferrero *et al*., 1994]. Topoisomerases maintain the topology of DNA, and is essential for the survival of the organisms. The important processes of replication, transcription and recombination involve the change in DNA topology aided by the topoisomerases and these enzymes catalyse the changes in the tertiary structure of DNA both *in vitro* and *in vivo*.

This is the only enzyme which is able to introduce negative supercoils into the DNA at the expense of ATP hydrolysis and regulates the super helical state of the bacterial chromosomes [Chopra S., *et al*., 2011]. This results in a condensed form of the chromosome for proper partitioning during cell division. Negative supercoiling of bacterial DNA by DNA gyrase

influences all metabolic processes involving DNA and is essential for replication. Gyrase supercoils DNA by a mechanism called sign inversion, whereby a positive supercoil is directly inverted to a negative one by passing a DNA segment through a transient double-strand break. Reversal of this scheme relaxes DNA and this mechanism also accounts for the ability of gyrase to catenate and uncatenate DNA rings (**Figure 2.1**). Upon binding to DNA (the "Gyrase-DNA" state), there is a competition between DNA wrapping and dissociation, where increasing DNA tension increases the probability of dissociation.
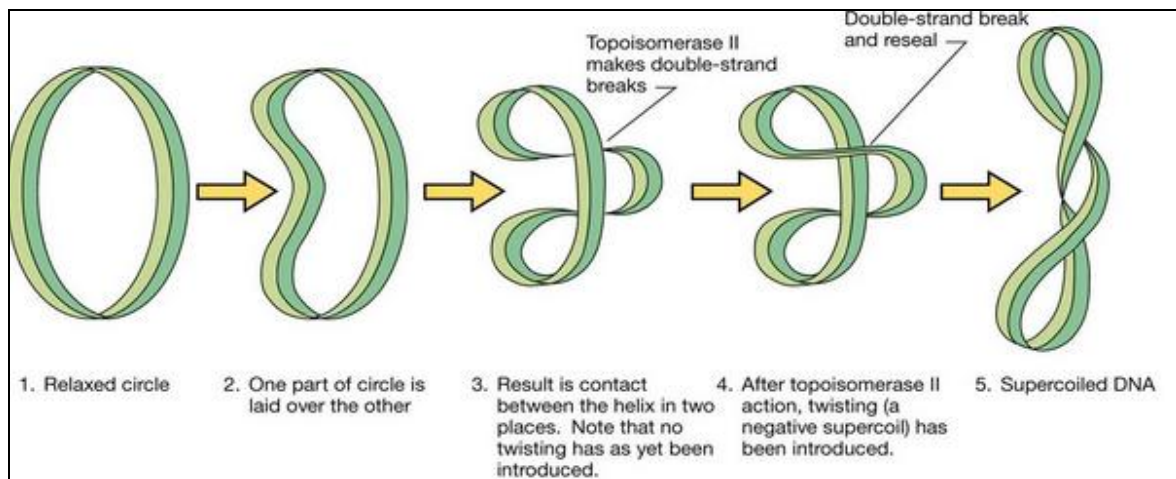
Figure 2.1: Introduction of supercoiling into a circular DNA by activity of topoisomerase II, which makes double-strand breaks [Glick B.R., *et al*., 1998]

Each round of supercoiling is driven by a conformational change induced by adenosine triphosphate (ATP) binding [Kreuzer K.N., *et al*., 1980]. *M. tuberculosis* DNA gyrase is a validated target for antitubercular drug discovery; its inhibition results in highly mycobactericidal activity. Inhibitors of this enzyme are also active against non-replicating, persistent mycobacteria, which might be important for shortening the duration of TB therapy. A novel inhibitor of *M. tuberculosis* DNA gyrase would also be effective against MDR-TB, and will likely be effective against fluoroquinolones resistant *M. tuberculosis.* Gyrase is the first enzyme required for initiation of DNA replication. Instead of targeting the bacterial cell at the level of transcription and translation, targeting Gyrase may stop the infections from spreading at the preliminary stages of replication so that an infected cell may not give rise to another infected one.

2.1.1. Structure of DNA Gyrase

In a 1978, it was found that gyrase contains two subunits; one smaller subunit that is directly responsible for interacting with ATP and a larger subunit. As we discusses that gyrase belongs to a class of enzymes known as topoisomerases that are involved in the control of topological transitions of DNA. Members of the type II subfamily of topoisomerases as represented by DNA gyrase have a three domain structure: the GyrB domain, the GyrA domain, and a C-terminal tail. Both the subunit contains domains significant to the introduction of negative supercoils into the DNA helix.

The structure of the N-terminal ATPase domain of gyrase (Wigley, Davies, Dodson, Maxwell, and Dodson, Nature 1991) and yeast topo II (Classen and Berger, Proceedings of the National Academy of Science, 2003, PDB ID=1PVG) have been solved in complex with AMPPNP (an ATP analogue) showing that two ATPase domains dimerize to form a closed conformation. For gyrase, the structure has a substantial hole in the middle, presumably to capture the T-segment. Linking the ATPase domain to the Toprim fold is a helical element known as the transducer domain. This domain is thought to communicate the nucleotide state of the ATPase domain to the rest of the protein. The first gyrase DNA binding core was solved by Morais Cabral *et al*., (Nature 1997, PDB ID = 1AB4). The structure solved by Berger revealed important insights into the function of the enzyme.

GyrA is a dimer subunit that is responsible for interacting directly with only the DNA strand and not ATP. In 2007, Raghu Ram and his team of scientists studied the structure of GyrA and found that there was extensive fold conservation exhibited between the GyrA subunit of *E. coli* and of *Plasmodium falciparum* (PfGyrase). They found that the Tyrosine 122 residue was exactly the same throughout all species that contain DNA gyrase. They concluded that this residue is critical to the function of the enzyme, because it directly interacts with the broken 5'-end of each DNA strand. Another segment that saw complete conservation was the quinolone resistant region between residues 67-106. Another region that is important to the function of gyrase is the CAP region (residues 71-140) in GyrA, which is a region that strongly resembles the DNA binding region in *E.coli* catabolite activator protein. This region must be conserved because it plays an integral part in binding to the DNA T-segment, allowing the gyrase to introduce negative supercoils in the DNA helix [Champoux J., 2001].
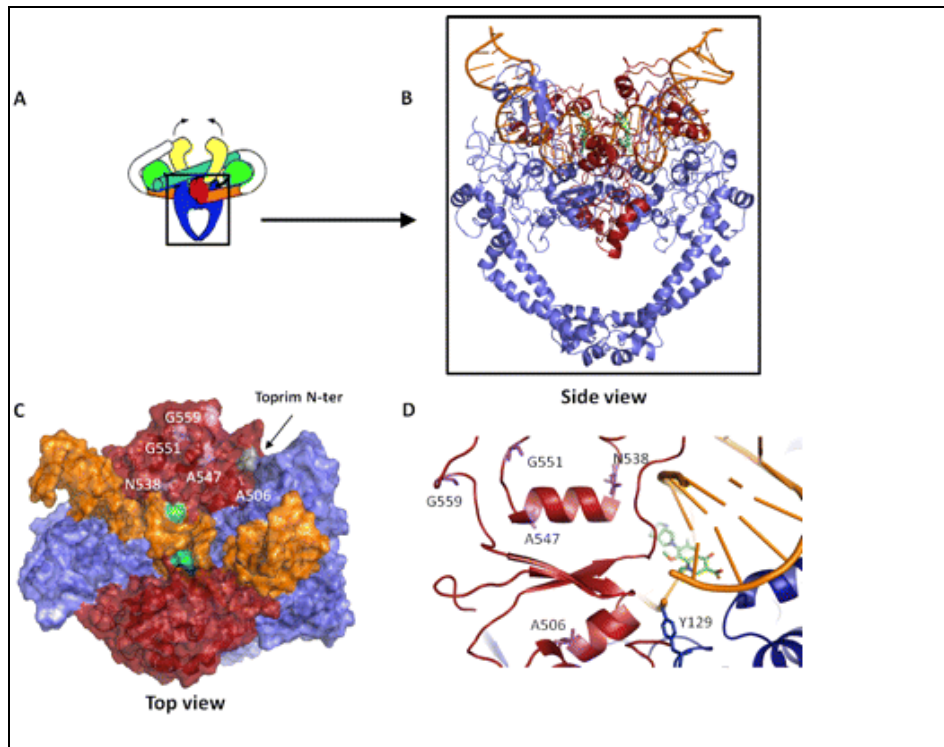
Figure 2.2: (A) Schematic representation of the *M. tuberculosis* DNA gyrase in complex with DNA. Protein domains are colored as follows: for GyrB, the ATPase domain is in yellow and the Toprim domain is in red; the GyrA breakage-reunion domain is in blue, and the C-terminal domain domain is in green. DNA within the catalytic core is in orange. (B) Side view of the catalytic core in ribbon representation in complex with DNA in orange and moxifloxacin in green (C) Top view of the catalytic core represented in molecular surface. The pink surface indicates the substituted amino acids, and the surface in gray and the black arrow indicate the beginning of the Toprim N-terminal GyrB structure. (D) Cartoon representation of a close-up view of the catalytic core in complex with DNA and moxifloxacin. The catalytic Tyr129 and the substituted amino acids are in stick representation [Pantel A., *et al.*, 2011]

In 2007, a team of scientists examined the DNA gyrase of *E. coli* and was able to report the structural model of the GyrB subunit at ~12-15 Å resolution. They found that the dimer GyrB subunit, or the subunit responsible for interacting with ATP, is composed of three subdomains, the ATPase, Toprim, and Tail [Costenaro L., *et. al.*, 2007]. These three domains take the shape of a tadpole, with the ATPase forming the head, the Tail subdomain forming the tadpole's tail, and the Toprim connecting the head and tail. Scientists use the term "tadpole" in order to better visualize the structure of the GyrB subunit.

DNA Gyrase binds ~128 bp of DNA, which includes the G segment [Orphanides G., *et al*., 1994] and directs T-segment capture using the C-terminal DNA wrapping domains of GyrA. DNA gyrase is unique amongst this class, because it can introduce supercoils as well as remove them. To wind or unwind DNA it must break both strands of DNA, capture another segment of the same DNA molecule and pass this through the double strand break before resealing. However, it can only introduce supercoils with a given chirality *i.e.* negative supercoils. It is thought to achieve this by wrapping DNA around itself in a right-handed sense, which determines the direction of strand capture and passage. It needs the free energy release of ATP hydrolysis to drive this energetically unfavourable process [Thomson N., 2001].

2.1.2. The mechanism of action of DNA Gyrase

DNA gyrase is a tetrameric enzyme (A_2B_2) with two A subunits and two B subunits, which are encoded by GyrA and GyrB genes respectively. Similar to gyrase, topoisomerase IV is an A_2B_2 enzyme encoded by parC and parE genes. These ParC and ParE of topoisomerase IV are highly homologous to GyrA and GyrB of topoisomerase II.

The A and B subunits of DNA gyrase perform distinct functions, while the N-terminal of GyrA subunit is responsible for the DNA breakage and reunion of the C-terminal domain part (GyrA-CTD) which is the wrapped around the DNA [Critchlow S.E., *et al*., 1996]. As a whole the tetramer functions to impart negative supercoils into the DNA. Binding of ATP molecule to gyrase drives the supercoiling reaction in which ATP hydrolysis the enzyme to reset for the second round of catalysis. Within the holoenzyme, two A and two B subunits form dimmer gates that control the passage of DNA through the enzyme. The enzyme binds to DNA and a segment of about 140 bp is wrapped around the C-terminal tail domain of the GyrA protein into a positive supercoil. The bound DNA (the G-segment) is then cleaved in each strand at sites separated by 4 bp leaving the active site tyrosines (Tyr22) from the two A subunits covalently attached to the 5'-phosphate groups on the cleaved ends. Another segment of DNA (the T-segment) is transported through this double-stranded break and through the enzyme itself. Upon resealing of the cleaved DNA, the linking number is reduced by two, which results in the introduction of negative supercoils, altering the topology of the DNA molecule. The DNA strand-passage reaction is coupled to the hydrolysis of ATP, but how exactly the energy from the ATP hydrolysis is used in the strand passage process is not clear.
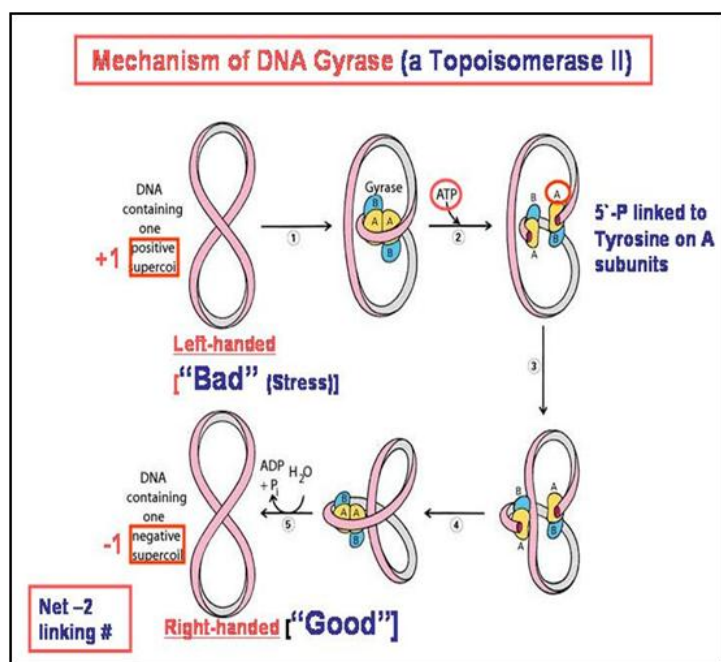
Figure 2.3: Mechanism of DNA Gyrase [Critchlow S.E., *et al*., 1996].

2.1.3. Quinolones and fluoroquinolones as DNA Gyrase A inhibitors

The type II topoisomerase DNA Gyrase has been of tremendous interest ever since, it was discovered as the biological target of quinolones (as GyrA inhibitor) and of coumarin (as GyrB inhibitor) antibiotics. This enzyme is a lethal antibacterial drug for numerous reasons. Some of them are: (1) They are the necessary components of all bacteria. (2) Bacterial DNA replication and cell division depends on these proteins to be viable. (3) A bactericidal (versus bacteriostatic) incident can occur if their function is inhibited. (4) It shows bacterial specificity due to distinct structural differences from that of mammalian enzyme counterparts. (5) These enzymes of multiple site for target and (6) Both GyrA and GyrB are structurally similar which allows the ligands to inhibit both. [Mdluli K., *et al*., 2007].

Among the various classes of inhibitors reported for DNA Gyrase till date, the quinolone classes of antibiotics are the most promising leads, displaying broad spectrum antibacterial potency. Fluoroquinolones, the only DNA Gyrase inhibitors used in clinical practice, inhibit the activity of bacterial DNA Gyrase by binding to the GyrA subunit and trapping the gyrase-DNA covalent complex, which induces oxidative damage and eventually leads to bacterial cell death. This class of drugs/leads has gained a strong position in the therapy of bacterial infections with moxifloxacin currently in the phase III clinical stage and has demonstrated promising activity against both drug sensitive and drug resistant strains of *M. tuberculosis*.

Quinolones have an affinity for single stranded DNA's but have little affinity for DNA gyrase enzyme alone. [Shen L.L., *et al*., 1982]. However when DNA gyrase and double stranded DNA are both present, the quinolones make an effective, reversible and a co-operative site for binding. [Shen L.L., *et al*., 2001]. This site can bind four quinolone molecules at once. GyrA subunit has been targeted by the quinolones for inhibition and is progressing well in the field of TB drug discovery. Gatifloxacin and moxifloxacin are currently under phase III clinical trial studies for TB. Nevertheless, novel research is required in this area due to an increasing resistance to the quinolone class of drugs by TB bacteria.

The fluoroquinolones are potent, broad-spectrum antibiotics that have been used in medical practice for the treatment of severe or resistant infections since the late 1980s. As their name suggests, they are derived from the quinolone family of antibiotics; quinolones themselves are synthetic constructs, developed by modification of 1-alkyl-1,8-naphthyr- idin-4-one-3-carboxylic acid. Fluoroquinolones are potent inhibitors of bacterial type II topoisomerases, which are essential enzymes involved in key cellular processes including DNA replication [Redgrave L.S., *et al*., 2014].

The targeting of either DNA gyrase or topoisomerase IV as the primary target by fluoroquinolones varies with bacterial species and specific fluoroquinolone; however, as a broad generalisation, the key target in Gram-negative bacteria is DNA gyrase, whereas in Gram-positive microorganism's topoisomerase IV is preferentially targeted. When either DNA gyrase or topoisomerase IV induces transient double-strand DNA breaks, they first bind covalently to the DNA to form enzyme–DNA complexes before breaking the bound DNA, passing another segment of DNA through this break, and rejoining the original DNA segment [Drlica K., *et al.*, 2009]. When a fluoroquinolone is present, the complex is altered into a drug-enzyme-DNA complex (known as a ternary complex) in which the type II topoisomerase is trapped with the bound DNA. Fluoroquinolones bind to DNA gyrase or topoisomerase IV, which is then unable to re-ligate the DNA substrate; the broken segments of DNA bound to the enzyme are referred to as cleaved complexes.

The introduction of fluoroquinolones into medical practice 15 years ago raised great expectations. Because of their potent broad spectrum activity and absence of transferable mechanism of resistance or inactivating enzymes, it was hoped that clinical resistance to this useful group of drugs would not occur. However, over the years, due to intense selective

pressure and relative lack of potency of the available quinolones against some strains, bacteria have evolved at least two mechanisms of resistance [Rattan A., 1999].

(i) Alteration of molecular targets ie mutations in specified regions (quinolone resistance determining region) in genes coding for the gyrase and/or topoisomerase leads to clinical resistance. Mutations in GyrA are those the most frequently found in gram-negative bacteria, and mutations in *parC/grlA* are generally the most common in Gram-positive bacteria [Black M.T., *et al*., 2008].

(il) Resistance due to reduced drug accumulation which can probably be due to the inability of the drug to cross the bacterial cell wall (permeability barriers) or an efflux pump effective in pumping out hydrophilic quinolones.

In addition to the bacteria gaining resistance to the fluoroquinolone class of drugs, a few serious side effects such as tendonitis and tendon rupture due to collagen damage, QTc interval prolongation by blocking voltage-gated potassium channels etc associated with these classes of drugs has limited their clinical use and future progress, necessitating research into development of new antibacterial agents that lack cross-resistance mediated by mutations in the bacterial targets.

2.1.4. Drugs acting through the inhibition of DNA Gyrase B subunit

Fluoroquinolones instigate the formation of a Gyrase-DNA covalent complex, by binding to the GyrA subunit which leads to oxidative damage of the bacterial cell. This is eventually followed by cell death. Compounds such as novobiocin and coumermycin deprive the bacterial cell of its energy needs, by inhibiting the ATPase activity of the GyrB subunit. Hence the energy required for the topological maintenance of a bacterial DNA is curbed, affecting the DNA replication.

The GyrB protein comprises a 43 kDa N-terminal domain (NTD) which contains the ATPase site and dimerizes upon ATP binding. This subunit also contains a 47 kDa C-terminal domain (CTD) which consists of a coumarin drug-binding site and is involved in the interaction with the GyrA protein and DNA [Adachi T., *et al*., 1987; Mdluli K., *et al*., 2007]. ATP binding and hydrolysis is required for protein-protein interactions and recycling of the enzyme [Brino L., *et al*., 2000]. The B subunit also forms the entry site for the transfer (T) segment of DNA during the supercoiling process [Williams N.L., *et al*., 1999; Williams N.L., *et al*., 2001;

Kampranis S., *et al*., 1999]. It has also been shown to perform as an ATP-operated clamp that binds DNA during the supercoiling process [Tingey A.P., *et al*., 1996]. Most of the amino acid residues that bind ATP are in the 24-kDa NTD between residues 1-220, but two residues Gln335, and Lys337 in the CTD, residues 220-392, also make contact with the ATP molecule. These residues have been implicated in the hydrolysis of ATP and they are thought to transmit conformational changes upon ATP hydrolysis [Smith C.V., *et al*., 1998; Hu T., *et al*., 1998]. There is a loop that is thought to close the active site and it contains amino acid residues 98-118. This loop is also implicated in the binding and hydrolysis of ATP, and is composed of a number of conserved residues which are involved in the catalytic mechanism [Lee M.P., *et al*., 1994; Li W., *et al*., 1997; Tamura J.K., *et al*., 1990].

The structural details of the ATPase domain of gyrase have proved to be of great value for a number of reasons. Firstly, this information has been vital for understanding the mechanism of ATP hydrolysis, which has been established by following mechanistic and site-directed mutagenesis studies, based on this structure [Jackson A.P., *et al*., 1993; Smith C.V., *et al*., 1998]. Secondly, the ATP-driven monomer-dimer transition of this domain has endorsed the proposal for the role of this domain as an ATP-operated clamp that captures the T segment during the topoisomerase cycle [Roca J., *et al*., 1992; Roca J., *et al*., 1994]. Site-directed mutagenesis has supported the idea that DNA can be bound in the cavity during the topoisomerase reaction [Tingey A.P., *et al*., 1996]. Thirdly, this structure has proved to be valuable for understanding the action of the coumarin and cyclothialidine antibiotics and for structure-based design of other potential anti-bacterial agents, although until recently no crystal structures of Gyr B43-drug complexes were available. There is however a number of high-resolution structures of the 24-kDa N-terminal sub-domain of the ATPase fragment (GyrB24) complexed to coumarin or cyclothialidine drugs [Lewis R.J., *et al*., 1996; Holdgate G.A., *et al*., 1997; Tsai F., *et al*., 1997]. Finally, the structure of the ATPase domain of Gyr B shows homology to a number of other proteins of diverse function, which have become known as the GHKL super-family. Information about the GyrB ATPase domain has proved to be valuable in the understanding of these proteins [Mdluli K., *et al*., 2007].

Figure 2.4: Structure of the N terminal domain of GyrB (GyrB43) complexed with an ATP analogue [Wigley D.B., *et al*., 1991]; the protein is in cartoon representation with the two monomers in shades of green and shades of yellow; the nucleotide is in space-filling representation.

Fluoroquinolone resistance can be overcome by developing new and potent GyrB subunit inhibitors for TB treatment. Many natural and synthetic drug molecules designed specifically for GyrB inhibition were biologically tested but have not been promising enough to reach the fourth phase of clinical trials except novobiocin. Though it was released into the market in 1960's, it was withdrawn later due to the issues in its toxicity and permeability. [Garry M.W., *et al*., 1958; Oblak M., *et al*., 2007]. Some of the reported gyrase B inhibitors include coumarins [Lafitte D., *et al*., 2002], cyclothialidines [Angehrn P., *et al*., 2011], pyrazolothiazoles [Ronkin S.M., *et al*., 2010], pyrrolamides [Sherer B.A., *et al*., 2011], bithiazole class [Brvar M., *et al*., 2012], Aminopyrazinamides [Shirude *et al*., 2013] and Pyrrolamides [Hameed S., *et al*., 2014]. Though the research in regard to bacterial targets has been very successful, the mycobacterial GyrB as a target remains to be fully explored.

2.1.5. Potent DNA GyrB Inhibitors

Increasing prevalence of resistant bacterial strains has eroded the utility of quite successful fluoroquinolone class of drugs targeting the GyrA and ParC subunits of DNA gyrase [Reck,

F., *et al*., 2011]. Research efforts from both industry and academia that focusses on DNA gyrase inhibitors have identified many potent inhibitors belonging to the chemical class of pyrrolamides [Green O., *et al*., 2008, Sherer B.A., *et al*., 2011], N-linked aminopiperidine [Reck F., *et al*., 2011, Bax B.D., *et al*., 2010, Axten, J.M., WO004058144, 2004.], pyrazolthiazoles [Ronkin S.M., *et al*., 2010], indolinones [Oblak M., *et al*., 2005], indazoles [Boehm H.J., *et al*., 2000], pyrimidines [Lubbers T., *et al*., 2000], benzimidazole ureas [Charifson P.S., *et al*., 2008] azaindole [Manchester I.J., *et al*., 2012], bithiazoles [Brvar M., *et al*., 2012], Benzo-furans [Janupally R., *et al*., 2014], Thiazole-aminopiperidine [Jeankumar V.U., *et al*., 2013] and Isatin-hybrid analogs [Jeankumar V.U., *et al*., 2014] etc.

2.1.5.1. Aminocoumarin drug: Novobiocin

Aminocoumarin is a class of antibiotics that act by inhibiting the DNA Gyrase enzyme involved in the cell division of bacteria. They are derived from Streptomyces species. Novobiocin, belong to the aminocoumarin family. In a lot of ways, aminocoumarins are regarded as the 'cinderellas' of the gyrase inhibitors, particularly in comparison with fluoroquinolones. By measuring the ATPase activity of the GyrB43 fragment, it was demonstrated that aminocoumarins are competitive inhibitors of DNA Gyrase with respect to ATP, with one molecule of novobiocin binding to one GyrB43 monomer. Although they bind tightly to gyrase, they have still not enjoyed significant clinical success.

The classical aminocoumarins share common structural features: a 3-amino-4, 7-dihydroxycoumarin structure, an L-noviosyl sugar and an aromatic acyl component attached to the amino group of the aminocoumarin moiety (as shown in the case of novobiocin in **Figure 2.5** [Heide L., 2009]. Since 1950s it was found that the aminocoumarins inhibit gyrase by catalysed supercoiling of DNA [Gellert M., *et al*., 1976] for their inhibitory properties on nucleic acid synthesis in bacteria. It was later shown that they inhibit the gyrase ATPase reaction by competing with ATP for binding to GyrB [Mizuuchi K., *et al*., 1978; Sugino A., *et al*., 1980; Sugino A., *et al*., 1978].
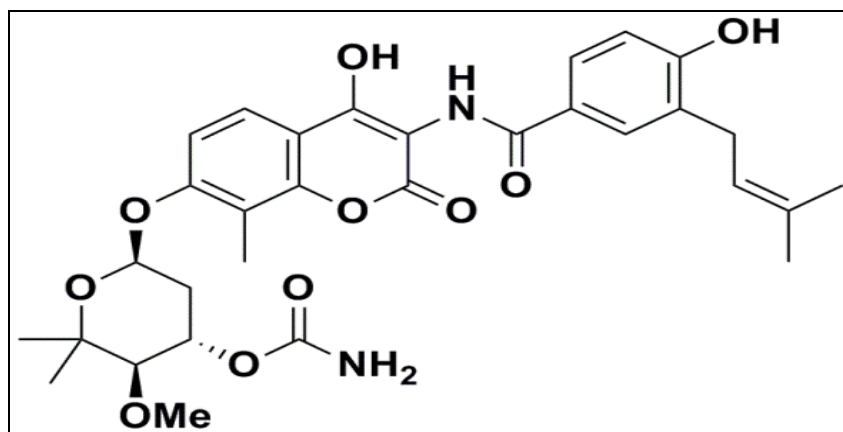
Figure 2.5: Structure of aminocoumarin antibiotic novobiocin.

The recent research efforts from Chopra *et al* [Chopra S., *et al.*, 2012] exploring the GyrB inhibitory potency of novobiocin in the mycobacterial domain have shown that, this class of drugs exert potent inhibition of mycobacterial GyrB domain as well, with both enzyme inhibition (K_i) and binding (K_d) constants in the low nanomolar range (7-15 nM). Also the ability of these molecules to inhibit DNA supercoiling was also proved *in vitro* [Glaser B.T., *et al.*, 2011]. Further they were also quite effective against the various strains of mycobacterium including the fluoroquinolone resistant strains. Novobiocin exhibited an MIC of 4 mg/L against drug sensitive *M. tuberculosis* H_{37}Rv strain and MIC's in the range of 0.62 mg/L-8 mg/L against various drug resistant strains of *M. tuberculosis* [Chopra S., *et al.*, 2012].

Though crystallising novobiocin with GyrB protein of *M. tuberculosis* or *M. smegmatis* has not been successful, it is reasonable to assume that many of the relationships found in other types of bacteria will be applicable to *M. tuberculosis* as well. In the antibacterial gyrase, the binding site of coumarins is located in the 24 kDa N-terminal part of GyrB43 (GyrB24 fragment) [Gilbert E.J., *et al.*, 1994] and the ATP-competitive mechanism was corroborated by solving the crystal structure of the Gyr B24-novobiocin complex [Gilbert E.J., *et al.*, 1994; Lewis R.J., *et al.*, 1996]. The binding site of novobiocin partially overlaps with the ATP-binding site, where the noviose sugar moiety of novobiocin and the adenine ring of ATP interact with the protein in a similar manner. This shows how aminocoumarins can be competitive inhibitors of ATP hydrolysis by gyrase despite of having limited structural resemblance to ATP.
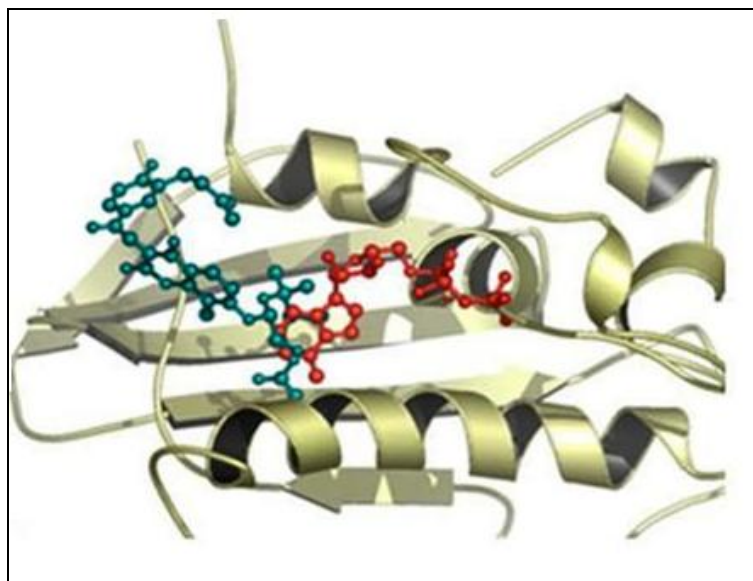
Figure 2.6: Structure of the N-terminal sub-domain of Gyr B (Gyr B24) complexed with novobiocin (blue), showing the overlap with bound ATP [Lewis R.J., *et al*., 1996].

Novobiocin forms five direct H-bonds with residues Asn46, Asp73 and Arg136. The binding is guided by additional H-bonds with Val43, Glu50, Asp73 and Thr165 residues through three crystal water molecules. The conformation of novobiocin in the binding site is further stabilized by hydrophobic interactions with residues Arg76, Ile78, Pro79, Ile94 and Val120. Furthermore, the protein structure of the Gyr B24-novobiocin complex is nearly identical to that in the complex Gyr B43- ADPNP, the only difference being observed in a loop region formed by residues A100-V120. In the Gyr B43-ADPNP dimer complex this particular loop forms a lid over the ATP-binding site, which is stabilized by the N-terminal tail of the second monomer [Wigley D.B., *et al*., 1991; Brino L., *et al*., 2000].

In the crystal structure of the GyrB24-novobiocin [Tsai F.T., *et al*., 1997; Lewis R.J., *et al*., 1996] this loop has moved away from the active site and adopts an "open" conformation, which is in contrast to the "closed" conformation observed in the GyrB43-ADPNP dimer. Therefore, it was hypothesized that the binding of ATP to GyrB causes a conformational change within the protein.

Aminocoumarins are potent inhibitors of Gyrase *in vitro*, but their poor activity against Gram-negative bacteria, mammalian cytotoxicity and poor solubility prevent them from being clinically successful drugs. Continued investigation of the coumarins could promote the development of new generations of non-quinolone, gyrase-targeted antimycobacterial agents.

2.1.5.2. Aminopyrazinamide based inhibitors

AstraZeneca Co. (AZ) identified aminopyrazinamide-based analogues as novel and specific class of mycobacetrial GyrB inhibitors using high-throughput screening (HTS) of their in house compound collection. Further optimization of the lead compound yielded more potent inhibitors with good chemical tractability, robust SAR and potent antitubercular activity. They also reported crystal structure of *M. smegmatis* GyrB in complex with one of the aminopyrazinamides (compound **6**) with a resolution of 2.20 Å (**Figure 2.7**). Crystal structure of GyrB revealed that active site contained three important sites namely site I, site II and the hydrophobic pocket considered very important in maintaining the potency. Total twenty molecules has been identified having GyrB IC_{50} of <0.002 to >50 μM and MIC of <0.5 to >32 μM. The compound **6** co-crystallized with GyrB protein which was having IC_{50} of 0.69 μM and MIC of 1 μM.

The crystal structure also revealed the presence of hydrophobic pocket; the phenyl substitutions were seen to orient towards these pockets and was considered to be responsible for their specificity observed at the enzyme activity level. This potent class of mycobacterial gyrase inhibitors with their good anti-tubercular activity *in vitro*, intracellular and in hypoxic conditions served as an ideal lead for further development of anti-tubercular drugs.
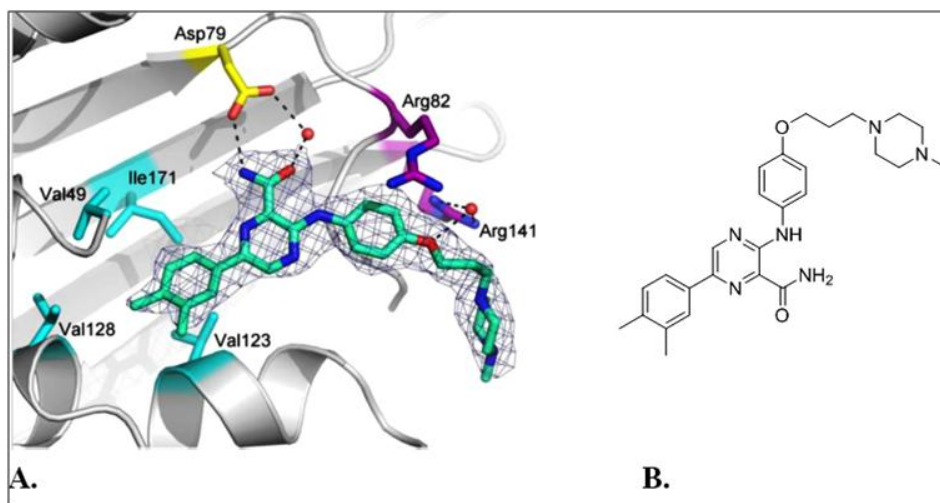
Figure 2.7: *M. smegmatis* GyrB ATPase domain double loop-deletion mutant (*M. smegmatis* GyrB-EP8) in complex with an aminopyrazinamide based inhibitor (**6**) (B). The figure shows the primary amide interacting with Asp79 (yellow); cation-pi stacking with Arg82 and water mediated interactions with Arg141 at site2 (purple) and hydrophobic pocket interactions (cyan) as described by Shirude *et al*., 2013.

2.1.5.3. Pyridothiazolyl urea based analogues

AZ [Shahul H.P., *et. al*., 2012] reported pyridothiazolyl ureas as a novel class of gyrase inhibitors with significant potency against the mycobacterial enzyme and promising anti-tubercular activity. The basic chemical skeleton belonging to this class is represented in **Figure 2.8**. These molecules also demonstrated good *in vitro* antibacterial activity against gram negative (*E.coli*) and gram positive (*S. pneumoniae*) strains.
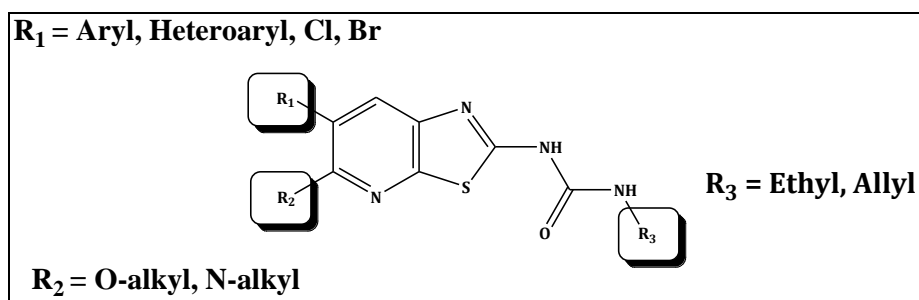
Figure 2.8: Pyridothiazolyl urea class of inhibitors.

Overall the molecules belonging to this class displayed potent inhibition of mycobacterial gyrase (a few even in the nano molar range) with promising anti-tubercular and antibacterial potency and can be considered as a useful lead in the development of newer anti-tubercular drugs.

2.1.5.4. Pyrrolamide based inhibitors

Further research efforts from AZ had identified pyrrolamide derivatives as another novel class of antibacterial DNA gyrase inhibitors using fragment-based NMR screening approach followed by a structure-guided lead identification strategy. In continuation of their research efforts in this direction a patent literature form this group reported an optimized derivative of pyrrolamide which displayed potent inhibition of *M. smegmatis* GyrB with broad spectrum antibacterial activity [Shahul H.P., *et al*., 2012]. The literature described the discovery of 22 potent pyrrolamide derivatives with *M. smegmatis* GyrB IC_{50} values in the range of 0.0026-0.030 μM, displaying excellent *in vitro* activity against *M. tuberculosis* and various gram negative and gram positive strains such as *H. influenza, S. aureus* and *S. pneumonia*.

The crystal structure of one representative compound with *M. smegmatis* GyrB protein later validated these findings, in general it was observed that the ligand occupied the ATP binding

site and retained interactions with Asp79 in *M. smegmatis* GyrB (Asp118 in *M. tuberculosis* H$_{37}$Rv GyrB) and conserved water molecule mimicking the interaction made by adenine of ATP (**Figure 2.9**) Asp79 was involved in a direct hydrogen bond interaction with the NH proton of the pyrrole and a water-mediated interaction with the carbonyl oxygen of the amide. Thr169 in *M. smegmatis* GyrB (Ser208 in *M. tuberculosis*) formed an extended hydrogen bonding network with Asp79 *via* the conserved water molecule. Arg82 in *M. smegmatis* GyrB (Arg121 in *M. tuberculosis*) was positioned above the thiazole ring making a cation-pi stacking interaction and it was held in place through extended hydrogen bonding interactions with Glu56. Arg141 in *M. smegmatis* GyrB (Arg180 in *M. tuberculosis*) bound the ligand from opposite side *via* a hydrogen bond with the pendant carboxylate group on the thiazole ring.

The most potent compound in this series showed GyrB inhibitory IC$_{50}$ of 5 nM, inhibited super coiling activity of DNA gyrase with an IC$_{50}$ < 5 nM, an MIC of 0.03 µg/mL against *M. tuberculosis* H$_{37}$Rv and an MIC < 0.25 µg/mL against 99 drug resistant, clinical isolates of *M. tuberculosis*. The best compound tested for *in vivo* efficacy in the mouse model showed 1.1 log reductions in lung CFU in the acute model and 0.7 log reductions in the chronic model. In conclusion, the reported pyrrolamide class of GyrB inhibitors offer an attractive lead for development of novel agents against both drug susceptible and drug resistant TB.
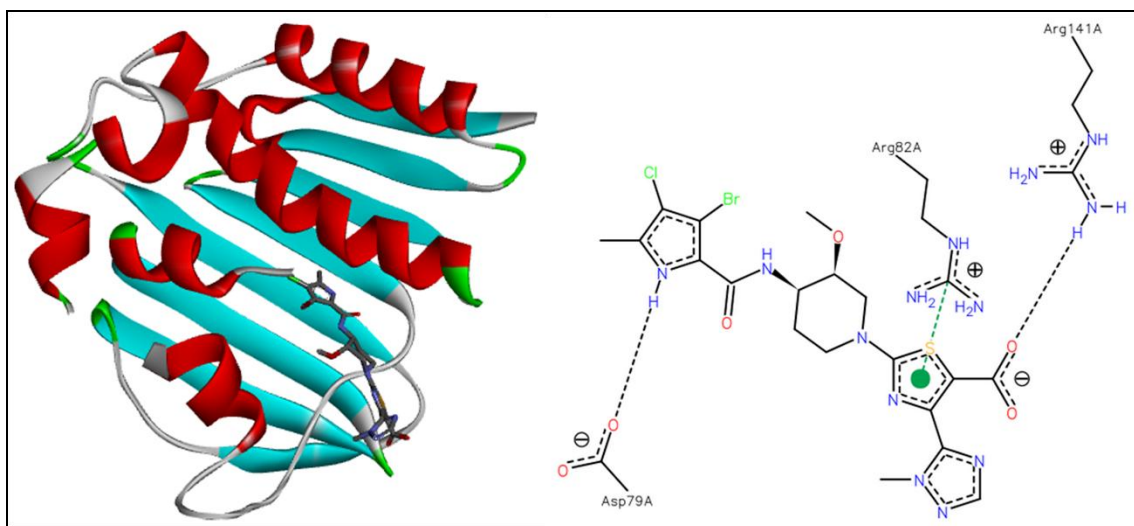
Figure 2.9: Crystal structure of *M. smegmatis* GyrB with a pyrrolamide inhibitor [Hameed S.P., *et al*., 2014].

2.1.5.5. N-linked aminopiperdine based inhibitors

Novel non-fluoroquinolone based bacterial type II topoisomerase inhibitors (NBTIs) of antibacterial DNA gyrase class of inhibitors was first discovered in the laboratories of GalxoSmithKline (GSK) and Aventis Pharma AG which produced lot of interest in the recent years. They act through a novel mechanism of action and hence were not impacted by target mutation that caused resistance to fluoroquinolones [Reck F., *et al*., 2011; Bax B.D., *et al*., 2010; Axten J.M., *et al*., 2004]. Overall the chemical structure of NBTIs though quite diverse is followed by a general topology. A bicyclic aromatic left-hand side (LHS) that stacked between two bp of the DNA in the GyrA/DNA complex linked to the right hand side (RHS) that interacted with the protein *via* a linker showed an important interaction with Asp 83 [Reck F., *et al*., 2011]. Research group from GSK were successful by extending the above antibacterial aminopiperdine class to the antimicrobial target as well with many compounds exhibiting promising inhibition of mycobacterial GyrB in the nano molar range [Barros D., 2009].

Though the N-linked aminopiperdine **(Figure 2.10)** based DNA gyrase inhibitors showed a significant progress in the recent years, their encouraging growth was found to be significantly hampered by the cardiovascular safety risk of potent hERG inhibition and QT prolongation associated with these molecules. Though various research efforts have been able to reduce the hERG liability to an extent, it still remains in the unacceptable range and requires significant improvement.
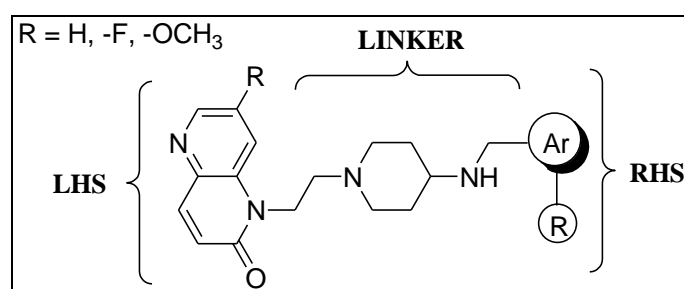
Figure 2.10: Basic skeleton of N-linked aminopiperidne based mycobacterial GyrB inhibitor.

2.1.5.6. Benzimidazole urea based inhibitors

The benzimidazole ureas are a novel class of dual targeting agents, identified in the laboratories of Vertex pharmaceuticals through a high-throughput ATPase assay targeting the

GyrB subunit, exerting their antibacterial effect *via* simultaneous inhibition of the ATPase function of gyrase and topoisomerase IV.

Later these class of compounds where also evaluated for their mycobacterial Gyr B inhibitory potency as well [Chopra S., *et al.*, 2012]. As observed, in the case of pyrrolamide class of drugs, the compounds from benzimidazole ureas also showed potent inhibition of the mycobacterial gyrase domain with GyrB inhibitory IC_{50} in the lower nM range. The study also showed that the molecule belonging to this class of drugs were effective against fluoroquinolone resistant *M. tuberculosis* strains and were efficacious in murine models of TB.

The success of benzimidazole and pyrrolamide class of mycobacterial DNA Gyrase inhibitors encouraged researchers to evaluate various other inhibitors/ leads reported for bacterial GyrB domain for their ability to inhibit the mycobacerial gyrase as well.

2.1.5.7. Thiazole-aminopiperidine hybrid analogues

A series of ethyl-4-(4-((substituted benzyl)amino)piperidin-1-yl)-2-(phenyl/pyridyl)thiazole-5-carboxylates was designed by molecular hybridization [Jeankumar V.U., *et al.*, 2013]. The compounds display unique activity against *M. tuberculosis* GyrB ATPase and promising antitubercular activity *in vitro*. Total 24 compounds have been synthesized and compound **14** was found to be most active one with an IC_{50} of 24.00±1.2 μM (**Figure 2.11**).

The present class of DNA GyrB inhibitors reported in this work provide an interesting potential for further optimization.

Most active compound 14
GyrB IC_{50}= 51.22% inhibition at 25 μM
Supercoiling IC_{50}= 43% inhibition at 25 μM
MTB MIC=28.44 μM
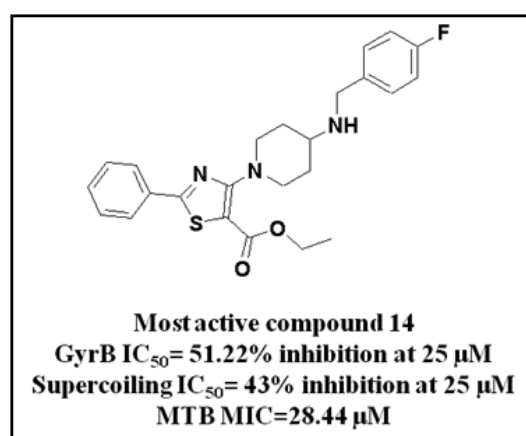
Figure 2.11: Most active analogue of thiazole-aminopiperidine hybrid derivatives.

2.1.5.8. Isatin-aminopipiridine hybrid analogs

In 2014, Jeankumar V.U., *et al.* has for the first time reported novel series of N-linked aminopiperidine analogues as highly selective inhibitors of the mycobacterial ATPase domain exhibiting promising antitubercular potency against drug-sensitive and XDR-TB strains and with an improved cardiovascular safety profile, showing no signs of arrhythmia up to 30 μM in zebra fish ether-à-go-go-related gene (zERG), which is orthologous to the hERG gene, a significant achievement compared with the previously reported cardiotoxic N- and C-linked aminopiperidine analogues. 40 molecules have been synthesized and screened for their ability to inhibit DNA supercoiling using *M. tuberculosis* DNA gyrase. All of the compounds tested showed dose-dependent inhibition. Of the 40 compounds tested, 27 compounds showed activity at an IC_{50} (50% inhibitory concentration) of ≤50 μM, including 3 compounds with an IC_{50} value of >10 μM and ≤25 μM, 2 compounds with an IC_{50} value of >5 μM and ≤10 μM and 8 compounds showing good activity with an IC_{50} value of ≤5 μM. Compounds that showed IC_{50} values of ≤50 μM in the *M. tuberculosis* DNA gyrase supercoiling activity were further evaluated in an *in vitro M. smegmatis* GyrB ATPase assay. All of the molecules inhibited GyrB ATPase activity, with IC_{50} values ranging from 10.6 ± 0.6 μM to 92 ± 1.29 μM. Compound (**17**) was found to be the most potent compound, which showed an *M. smegmatis* GyrB IC_{50} of 10.6 ± 0.6 μM with an *M. tuberculosis* DNA gyrase supercoiling IC_{50} of 3.6 ± 0.16 μM (**Figure 2.12**).
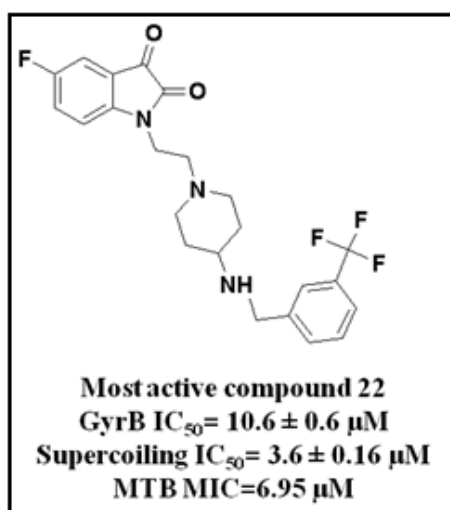
Figure 2.12: Most active analogue of isatin-aminopipiridine hybrid analogs.

2.1.5.9. Benzofuran derivatives as DNA gyrase B inhibitors

By adapting the medium throughput screening, Renuka *et al*., in 2014 discovered and optimized a series of ethyl 5-(piperazin-1-yl) benzofuran-2-carboxylate mycobacterial DNA gyraseB inhibitors, selected from their *in house* database of about 3000 molecules. These compounds were tested for their biological activity. The compound **22** emerged as the most active potent lead with an IC_{50} of 3.2 ± 0.15 µM against *M. smegmatis* DNA GyrB enzyme and 0.81 ± 0.24 µM in *M. tuberculosis* supercoiling activity, also showed moderate antibacterial activity (**Figure 2.13**). In this study they have used the previously reported, *M. tuberculosis* GyrB inhibitor as a template from their *in house* database. They have re-engineered the previously reported thiazole-amiopiperdine analogues to tailor novel inhibitor for the mycobacterial GyrB domain. Overall, they have attempted a rationalized effort to enhance the hydrophobicity of the lead molecule to facilitate the affinity towards the GyrB domain. The designed ligand (compound **2**) in the subsequent *in vitro* biological evaluation exhibited a *M. smegmatis* GyrB inhibitory IC_{50} of 6.14 ± 0.21 µM, gyrase supercoiling inhibitory IC_{50} of 3.125 ± 0.11 µM and a *M. tuberculosis* MIC of 9.18 µM. MIC value of **22** which is comparatively better than the standard drug novobiocin and equipotent to first-line anti-tubercular drug EMB. Encouraged by these promising results, they further designed and synthesized a library of twenty six compounds and consequently hit the expansion step with the goal of obtaining a lead series with tractable SAR and potencies, than the initial leads. All the molecules inhibited GyrB ATPase activity, with IC_{50} values ranging between 3.2 to 62.1µM. Most potent lead **22** showed an IC_{50} of 0.81 µM in *M. smegmatis* GyrB.

Designed compound 2
GyrB IC_{50}= 6.14±0.21 µM
Supercoiling IC_{50}= 3.12±0.11 µM
MTB MIC=4.57 µM

Most active compound 22
GyrB IC_{50}= 3.2±0.15 µM
Supercoiling IC_{50}= 0.81±0.24 µM
MTB MIC=9.18 µM
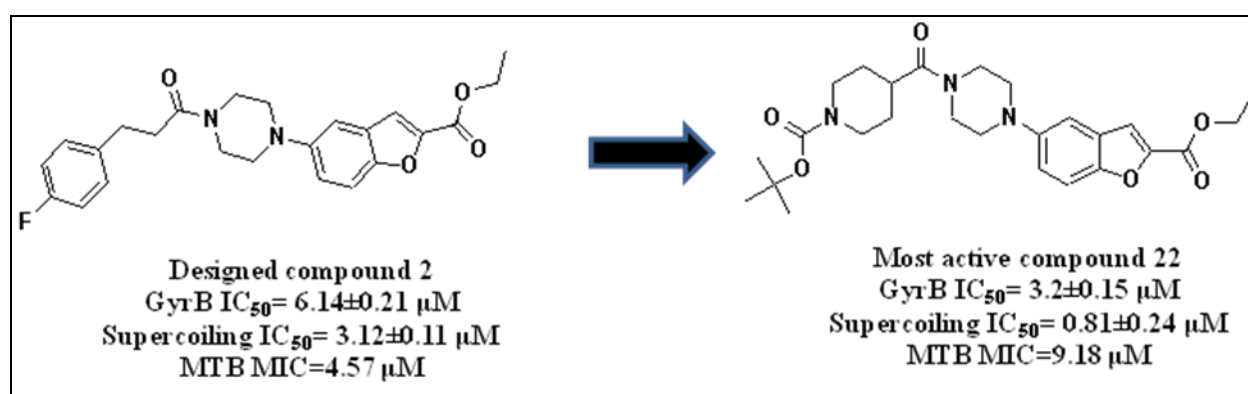
Figure 2.13: Most active analogue of benzofuran series.

2.1.5.10. Nitrothiazolyl carboxamide analogues

In 2014, Jeankumar V.U. *et al*., used the crystal structure of the *M. smegmatis* gyrase B protein co-crystallized with a ligand, was used as a structural framework for virtual screening of more than 3000 compounds of the BITS Pilani *in house* database, so as to explore new classes of GyrB inhibitor. Finally they have identified 40 compounds which were further screened through *M. smegmatis* GyrB assay and *M. tuberculosis* supercoiling assay. Among the small number of leads identified, the nitrothiazolyl carboxamides **5**, **6**, and **7** (**Figure 2.14**) emerged as the most promising compounds. The most potent compound from the virtual high-throughput screening is found to be compound **7** (GyrB IC_{50} of 1.72 ± 0.14 μM and *M. tuberculosis* supercoiling IC_{50} is 3.32 ± 0.31 μM). Later they synthesized the series of 17 compounds which selectively target mycobacterial DNA gyrase enzyme with promising activity. Three compounds were showing more activity as compared to the identified lead **7** (**Figure 2.14**). With the increasing need for new anti-TB agents, we believe that the novel DNA GyrB inhibitor class, reported in this study would provide interesting insights for further optimization.
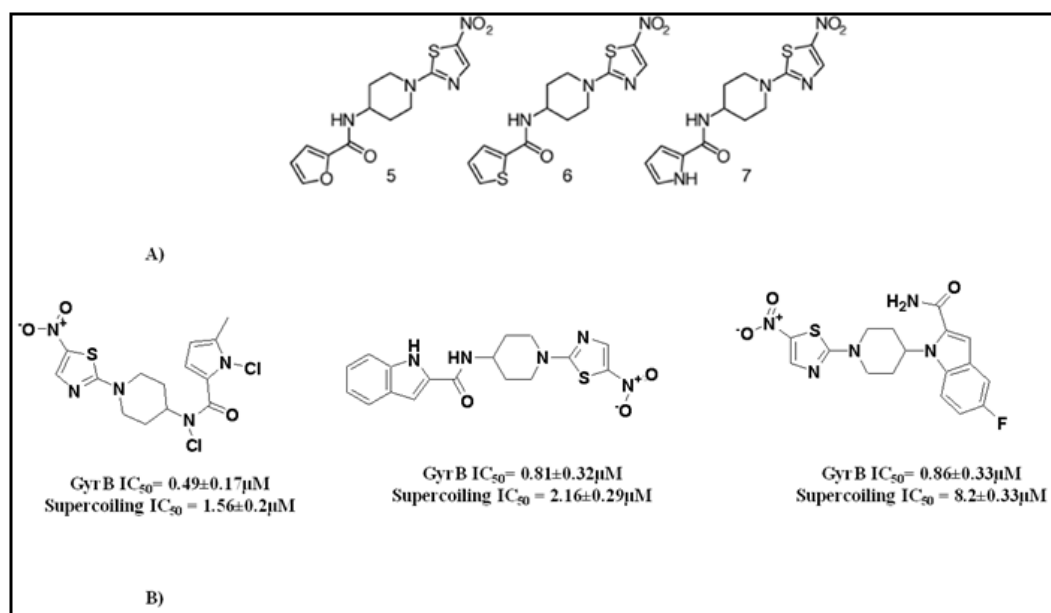
Figure 2.14: Most active analogue of nitrothiazolyl carboxamide analogues.

2.1.5.11. Benzimidazoles: Novel mycobacterial gyrase inhibitors

A scaffold hopping approach using the binding mode of novel bacterial topoisomerase inhibitors (NBTIs) led to the identification of a novel class of benzimidazoles as DNA gyrase

inhibitors with potent anti-TB activity [Hameed S.P., *et al*., 2014]. Docking of benzimidazoles to a NBTI bound crystal structure suggested that this class of compound makes key contacts in the enzyme active site similar to the reported NBTIs. This observation was further confirmed through the measurement of DNA gyrase inhibition and activity against *M. tuberculosis* strains harboring mutations that confer resistance to aminopiperidines based NBTIs and *M. tuberculosis* strains resistant to moxifloxacin. In this study compound **23** is emerged a most potent inhibitor having *M. tuberculosis* supercoiling activity 1.9μM and *M. tuberculosis* MIC in 0.12 μM. Further efforts are required to optimize PK parameters and to assess *in vivo* safety (**Figure 2.15**).

23
Mtb MIC: 0.19 μM
Mtb Gyr SC IC50:1.9 μM
hERG IC50: >33 μM
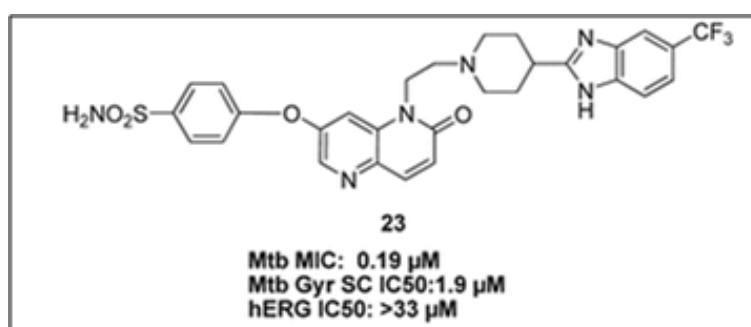
Figure 2.15: Most active analogue of benzimidazoles series.

2.1.5.12. Thiazolopyridone ureas as DNA gyrase B inhibitors

Scaffold hopping from the thiazolopyridine ureas led to thiazolopyridone ureas with potent antitubercular activity, acting through inhibition of DNA GyrB ATPase activity [Kale R.R., *et al*., 2014]. In this study they introduced structural diversity by extension of substituents from thiazolopyridone at N-4 position. Total thirty two compounds has been synthesized which showed *M. smegmatis* GyrB IC_{50} ranging from 2 nM to 2870 nM. Further optimization led to the identification of two most potent inhibitors (IC_{50} 2 nM) along with potent cellular activity (MIC = 0.1 μM) against *M. tuberculosis*. Efficacy was also demonstrated in an acute mouse model of tuberculosis on oral administration (**Figure 2.16**).
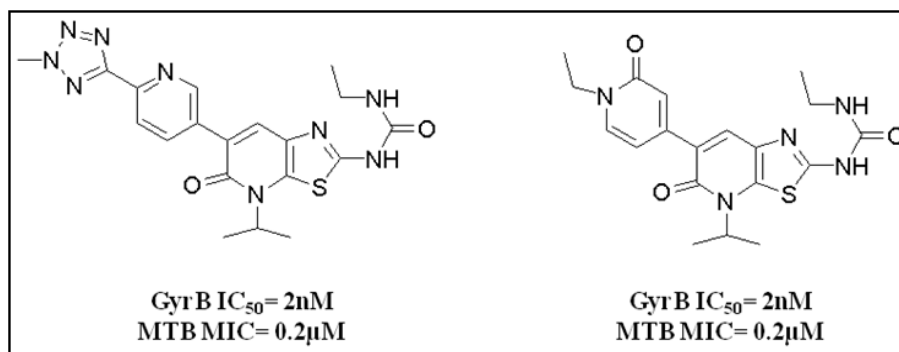
Figure 2.16: Most active analogue of the thiazolopyridine urea series.

2.1.5.13. Extended N-linked aminopiperidine class

A series of 1-(2-(4-aminopiperidin-1-yl)ethyl)-1,5-naphthyridin-2(1H)-one derivatives were designed by molecular hybridization strategy [Bobesh K.A., *et al*., 2014]. Total 40 compounds has been synthesized and tested against *M. tuberculosis* DNA gyrase enzyme. All the 40 compounds synthesized have showed good activity and among these compounds1-(4-fluorophenyl)-3-(1-(2-(7-methoxy-2-oxo-1,5-naphthyridin-1(2H)-l)ethyl)piperidin-4-yl) urea (**35**) emerged as the most promising inhibitor with an IC_{50} of 78 nM against *M. tuberculosis* DNA gyrase enzyme, with *M. tuberculosis* MIC of 0.62 nM (**Figure 2.17**).
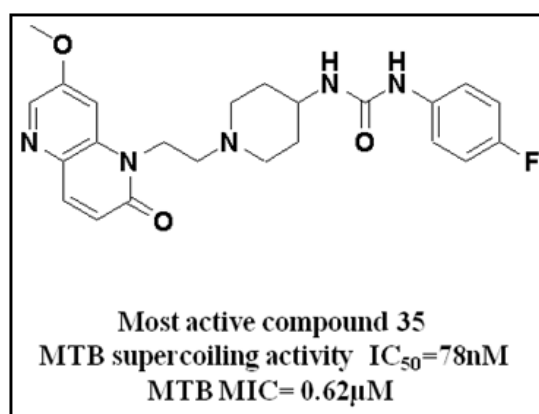
Figure 2.17: Most active compound from extending N-linked aminopiperidine class.

With recent data suggesting that incorporating fluoroquinolones in first-line anti-TB drug cocktails may shorten the required length of drug treatments, it is important to begin the development of backup drugs to replace fluoroquinolones when resistance for that class of drugs becomes prevalent. The data generated with the above class of drugs suggest that drugs targeting GyrB may be a viable alternative to include in first-line anti-TB drug cocktails.

2.2. M. tuberculosis L-AlaDH as a drug target

M. tuberculosis is a pathogen capable of causing both an acute disease and an asymptomatic latent infection. In the latent infection, dormant tubercle bacilli persist for years before reviving and resulting in reactivation of tuberculosis. Our current arsenal of drugs for treating active tuberculosis is relatively ineffective against the latent form. During the normal sporulation, L-AlaDH is known to be required for *Bacillus subtilis* which is one of the Bascilli species which utilizes the alanine as a sole carbon and nitrogen source [Siranosian K.J., et *al*., 1993].

To known the molecular mechanisms of oxygen depletion-induced dormancy *M. smegmatis* is used as a fast-growing non-pathogenic model [Hutter B., *et al*., 1998]. The present knowledge of the machinery involved in dormancy is limited. One of the major questions is that, how does bacilli recycle NADH derived from their catabolic activities under oxygen limiting conditions. *M. tuberculosis* L-AlaDH (EC 1.4.1.1) is a 40-kDa antigen catalyses the reductive amination of pyruvate to alanine under physiological pH. They report that the activity of alanine dehydrogenase was increased during dormancy development. They also proposed that the enzyme function is the generation of alanine for protein and peptidoglycan synthesis which may play an additional role in maintaining the NAD^+ pool under oxygen limiting conditions. As alanine synthesis is coupled to NADH oxidation, it was proposed that the induction of alanine dehydrogenase activity might also support the maintenance of the NAD^+ pool when oxygen as a terminal electron acceptor becomes limiting. Mycobacterium L-AlaDH belongs to the AlaDH/PNT family and it is a 40 kDa protein secreted from short term culture of *M. tuberculosis*; which may play a role in cell wall synthesis as L-alanine. It is an important constituent of the peptidoglycan layer [Andersen A.B., *et al*., 1992]. As L-alanine is frequently occurring in all known proteins, it is supposed that enzyme may play an important role in protein synthesis within the cytoplasm of the bacteria. Moreover, the enzyme may be active in the synthesis of the cell wall skeleton as, L-alanine is one of the three amino acids constituting the repeating peptide subunit of the peptidoglycan layer.

Research with *M. tuberculosis* has described a pathogen uniquely adapted to the wide range of harsh environments presented by the host. Much of this work has focused on the microbe's metabolism, with the idea of identification of novel enzymes or pathways to target for drug development.

M. tuberculosis is able to evade in the immune system and survive in human host for decades in a persistent state [Wayne L.G., *et al*., 1996], when the pathogens were under anaerobic growth conditions or nutrient starvation regimes, one of genes, Rv2780 encoding L-alanine dehydrogenase (L-AlaDH), was found to be up-regulated in this condition. The production and activity of this enzyme were observed to increase in *M. tuberculosis* [Starck J., *et al*., 2004] and alanine dehydrogenase is therefore a potential target for pathogen control by antibacterial compounds.

2.2.1. Mechanism of L-AlaDH

The mechanism of L-AlaDH follows the reversible oxidative deamination of l-alanine to pyruvate and ammonia through the catalysis of NADH-dependent reaction and is involved in microbial carbon and nitrogen metabolism. The reversible catalytic mechanism is as follows

$$l\text{-Alanine} + NAD^+ + H_2O \rightleftharpoons Pyruvate + NADH + H^+ + NH_4^+$$
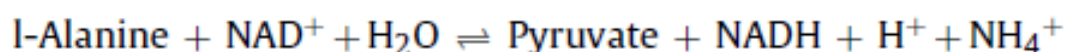
Kinetic and mechanistic studies of L-alanine dehydrogenases from several species showed that the enzyme predominantly follows ordered mechanisms with coenzyme binding, with NAD^+ and NADH binding occurring first in the oxidative deamination and then in reductive amination, respectively [Agren D., *et al*., 2008]. The NADH binds first in the oxidative deamination while the NAD^+ binding occurs first in the reversible reductive amination. However, the binding or releasing order of ammonia and pyruvate varies with different enzymes. L-AlaDH is known to be involved in the generation of pyruvate from alanine during sporulation [Siranosian K.J., *et al*., 1993].

2.2.2. Regulation of Ald gene in pathogenic mycobacteria

Alanine dehydrogenase encoded by gene *Ald* from *M. tuberculosis* and *M. smegmatis* have similar reductive aminase activity. The enzyme catalyses glyoxylate to glycine but not the reverse reaction, in which glycine is converted to glyoxylate by oxidative deamination with the help of glyciene dehydrogenases. [Jeong J.A., *et al*., 2013] reported that *ald* gene was up-regulated in *M. tuberculosis* in many conditions like,

- Nutrient starvation condition
- Energy limiting conditions

[Chan K., *et al*., 2002] also found that, *ald* gene expression is up-regulated in long-term granulomatous infection in *M. marinum*. The activity of *ald* gene was shown to be induced more when the pathogenic bacteria *M. tuberculosis* shifted from aerobic to hypoxic conditions. [Jeong J.A., *et al*., 2013] shows that DevSR two component system is the major regulatory system responsible for hypoxic induction of gene expression in bacteria. In-order to identify the regulatory systems other than two component system, [Jeong J.A., *et al*., 2013] performed some mutational studies and identified three proteins,

- L-alanine dehydrogenase (*ald*),
- glyceraldehyde-3-phosphate dehydrogenase (*gap*)
- D-3-phosphoglyceraldehyde dehydrogenase (*SerA*).

Among the three proteins, synthesis of alanine dehydrogenase was increased the most (11.8-fold) under hypoxic condition. They also proved that expression of *ald* gene was strongly induced under limited time period of hypoxic condtions. But still the mechanism of *ald* gene in hypoxic conditions is undetermined. They also found that, the expression of *ald* gene was more induced by exogenous L-alanine than by hypoxic stress and intracellular level of L-alanine was increased in the cells grown under hypoxic conditions that grown aerobically. These findings led us to hypothesize that the hypoxic induction of *ald* in *M. smegmatis* is mediated through an increase in alanine levels in the cells under hypoxic conditions.

2.2.3. Importance of AlaDH in pathogenesis

It is interesting that alanine dehydrogenase is important in other bacteria that have specialized persistence programs, such as sporulation. The *ald* mutant of *Bacillus subtilis* was defective for sporulation. This was partially complemented by the addition of pyruvate, suggesting that the role of alanine dehydrogenase is to provide pyruvate as an energy source. The *ald* gene of *M. bovis* contains a single nucleotide deletion and therefore lacks this enzyme. Also absent due to a point mutation is pyruvate kinase, suggesting there are major differences in central metabolism between *M. bovis* and *M. tuberculosis*. *M. bovis* BCG expressing the *M. tuberculosis ald* showed similar survival in both macrophages and mice [Giffin M.M., *et al*., 2012]. AlaDH is probably not essential for pathogenesis in *M. tuberculosis* but may still play an important role.

2.2.4. Structure information of AlaDH

The reported crystal structures of apo enzyme complex with NAD^+ and pyruvate, demonstrates that the enzyme consists of a NAD binding domain made up largely of the C-

terminus residues and a catalytic domain which binds to pyruvate. Both domains are separated by a cleft [Tripathi S.M., *et al*., 2008]. The NAD binding domain consists of residues 130-310 while the catalytic domain consists of residues 1-129 and 311-371. There are a total of 13 α-helices and 15 β-strands in the subunit. Like the *apo* and *holo* enzyme crystals, the individual subunits form a hexamer with the catalytic domains on the outside. The fact that the structures have an open and a closed conformation, claims that the domain rearrangement step occurs during the reaction and not during the changes in the inter subunit interactions. The structural analysis has led to the identification of a water molecule which is hydrogen bonded to the active site His96 and probably drives the conversion of the iminopyruvate intermediate to a carbinolamine. Most of the active site residues are clustered around a cleft between the two domains. The accessible surface area of the subunit in the *apo* and *holo* enzyme forms is 15,785 and 15,056 Å respectively. Asp270 and His96 are presumably the active site catalytic residues in *M. tuberculosis* ALD as seen from the crystal structures. NAD interacts extensively with the enzyme and includes polar interactions with Met301, Asn300, Asp270, Ile 267, Val239, Ser134, Thr178, Ala179, Ala240, Asp 198, Gly177 and Lys203. Most dehydrogenases have been studied to have similar mode of binding. The interaction of the carboxyl group with Arg15 stabilizes the pyruvate moiety. The other interaction includes those with Lys75 and Wat53. The latter water molecule interacts with His96 and Glu76 also. The pyruvate is about 4.1 Å from the nicotinamide moiety and about 3.8 Å from Asp270, an important active site residue. The reported work backs several aspects of the reaction and sketches an outline for structure aided inhibitor design to further explore and understand its potential as a novel anti-TB target.
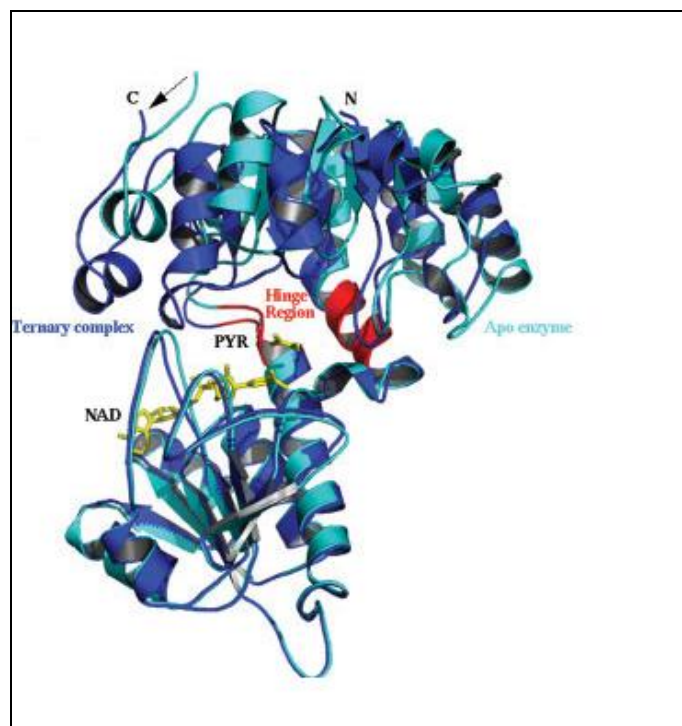
Figure 2.18: Crystal structure of *M. tuberculosis* L-AlaDH [Tripathi S.M., *et al*., 2008].

His96 and Asp270 conserved active site residues were identified as the potential acid/base catalysts in a reaction by their crystal structures. The essentiality of these amino acids in enzymatic reaction mechanisms has been highlighted through replacement of the amino acid by directed mutagenesis which led to inactive mutants [Agren D., *et al*., 2008].

The AlaDH enzyme of *M. tuberculosis* has been shown to have two conformations as shown by the structural analysis of *apo* and *holo* forms. The conformation observed in the presence of the coenzymes NAD^+ and NADH, respectively, is characterized by (i) a feasible hydride transfer and active site inaccessibility to solvent molecules due to domain closure (ii) Interaction of conserved residues with the active site of the substrate and its participation in catalysis. Furthermore, the closed conformation ensures proper orientation of the nicotinamide ring and the substrate suitable for hydride transfer. Small nucleophiles like water and ammonia approaching to the reaction intermediates is possible only through conformational changes of the substrate making the active site, easily accessible.
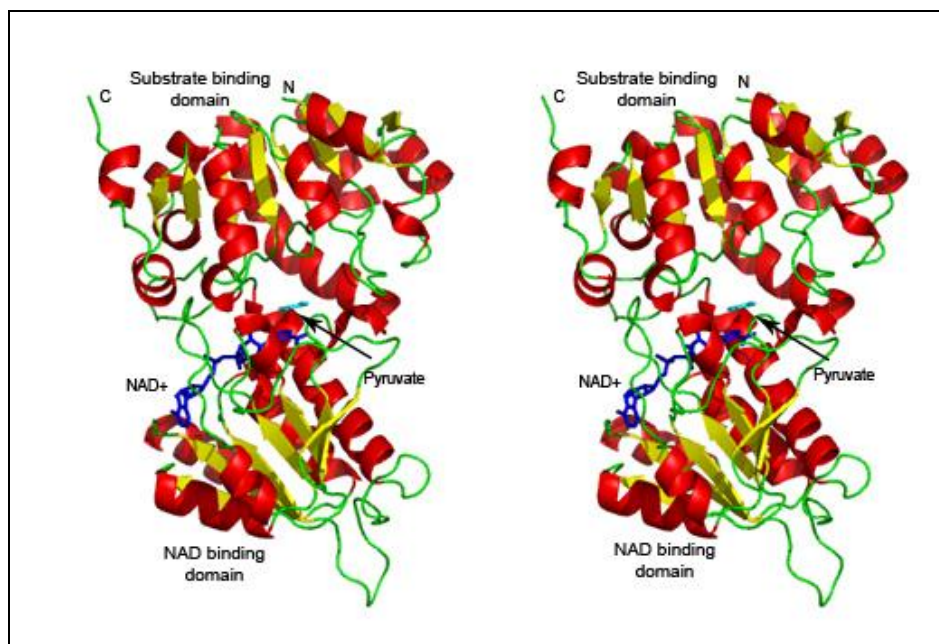
Figure 2.19: Molecular architecture of L-AlaDH from *M. tuberculosis* [Agren D., *et al.,* 2008].

The molecular dynamic simulations were performed, based on the crystal structures of the enzyme; to investigate the conformational changes of *M. tuberculosis* L-AlaDH induced by coenzyme NADH [Ling B., *et al.*, 2012]. Presence of NADH in the binding domain affects the distribution of *M. tuberculosis* L-AlaDH and restricts its motion as well. There are two loops (residues 94-99 and 238-251) playing important roles for the binding of NADH, while another loop (residues 267-293) is responsible for the binding of substrate. The conformational changes of *M. tuberculosis* L-AlaDH induced by NADH are closely related to the opening/closing and twisting motions of the two domains. The crystal structures of *M. tuberculosis* L-AlaDH from *M. tuberculosis* show that the enzyme contains two distinct domains, namely a NAD binding domain and a substrate-binding domain, which are separated by a cleft as discussed in the previous section. The closed structure of the enzyme (*holo-M. tuberculosis* L-AlaDH), is stabilized by the coenzyme while the substrate binding domain rotates by 16° toward the dinucleotide binding domain as compared to its open structure (*apo-M. tuberculosis* L-AlaDH). Hitherto, detailed studies of the conformational changes of the protein due to the binding of NADH have not been done. Also the mode of motion and the driving force for a conformational change is not yet clear. To investigate the conformational changes of *M. tuberculosis* L-AlaDH upon coenzyme binding at the atomic level, molecular dynamics (MD) simulations were performed.
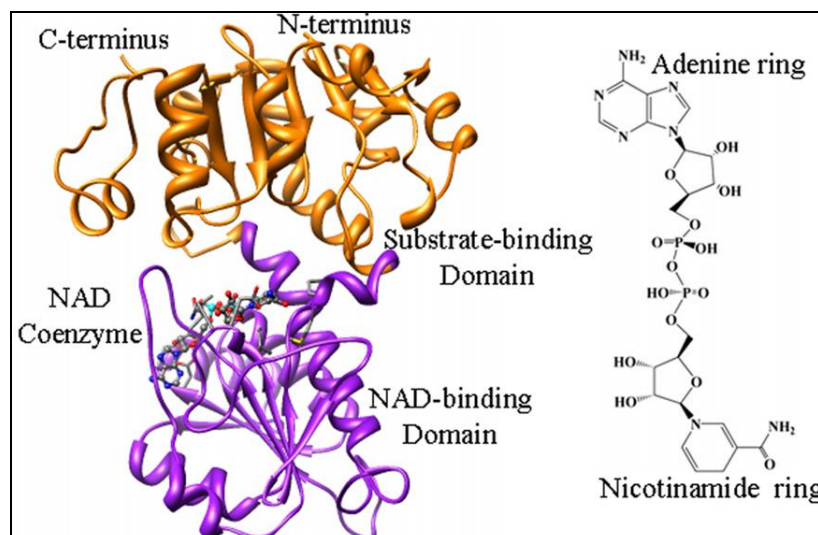
Figure 2.20: The x-ray crystal of *holo- M. tuberculosis* AlaDH (PDB code: 2VOJ, Chain A) and the structure of NADH. The protein is represented by ribbon model with the substrate-binding domain in orange and NAD-binding domain in purple, and the coenzyme NADH is shown in ball and stick model [Ling B., *et al.*, 2012].

The 3D X-ray crystal structures of *M. tuberculosis* L-AlaDH was used for this study, the opened (*apo*-form) and closed structure (*holo*-form) structure of the enzymes were used in this study (PDB code: 2VOE with resolution of 2.60 Å and 2VOJ with 2.60 Å). Apart from this the hybrid structure which has complexed with co-enzyme but without the conformational changes was also used [2VHW with 2.0 Å resolutions].

MD simulation shows that the conformation of *M. tuberculosis* L-AlaDH in the systems keeps stable after 23 ns. PCA suggests that the presence of NAD restricts the flexibility and motions of *M. tuberculosis* L-AlaDH. The conformational change in *M. tuberculosis* L-AlaDH is because of the opening/closing and twisting motions. The conformational change in proteins from a closed state to an open state facilitates the release of products, in *holo-M. tuberculosis* L-AlaDH system. Additionally, loop1 and loop3 plays an important role in NAD$^+$ binding while loop4 is important for binding the substrate. Summarizing these facts, we conclude that, the NAD binding induces a structural rearrangement of residues in active site, while the substrate-binding domain moves toward the NAD$^+$ binding domain. Conversely the open state converts to the closed state upon binding NAD$^+$ to facilitate the enzymatic catalysis, while the closed state changes to the open state to assist the releasing of the products.

The experiment has verified that amino acid replacement of the conserved active-site residues which have strong stability and no great changes in biological evolutionary process, such asHis96 and Asp270, could lead to inactive mutants [Agren D., *et al*., 2008]. However, the role of these conserved residues in catalytic reaction still remains unclear. So based on the crystal structure of AlaDH, a series of mutant structures were constructed to investigate the role of the conserved residues in enzymatic reaction by using MD simulations to investigate the effect of conserved residues on the structure and activity of *M. tuberculosis* L-AlaDH [Ling B. *et al*., 2014].

The results of this study showed that whatever the conserved residues were mutated, the protein can still convert its conformation from open state to closed state as long as NADH is present in active site. Asp270 maintains the stability of nicotinamidering and ribose of NADH through hydrogen bond interactions, and His96 is helpful to convert the protein conformation by interactions with Gln271, whereas, they would lead to the structural rearrangement in active site and lose the catalytic activity when they were mutated. Additionally, Met301plays a major role in catalytic reaction due to fixing the nicotinamide ring of NADH to prevent its rotation, and it was proposed that Met301 would be mutated to the hydrophobic residue with large steric hindrance in side chain to test the activity of the protein in future experiments. Since the crystal structure of human L-AlaDH has not been solved, L-AlaDH from *M. tuberculosis* was used in this study, which is a secretory antigen associated with bacterial persistence during infection. Argen D. *et al*. have proposed possible catalytic mechanism and identified the conserved active site residues as potential catalysts in the reaction by site-directed mutagenesis. The experimental results revealed that amino acid replacement by mutation led to inactive mutants, however, no obvious structural difference was observed in the position of active site residue or the bound NADH. The results of MD simulations show that the protein still changes conformations from open state to closed state whether either or both of the two residues are mutated in active site, in other words, the presence of coenzyme NADH indeed induces the protein to convert its conformations. However, when the conserved residues were mutated, the nicotinamide ring and ribose of NADH would rotate with the loss of interactions of NADH with Asp270, and Gln271 loses the interactions with His96 in another domain and is flipped out of the active site. Thereby, a series of sequential structural rearrangement in active site takes place to make the residues locate in unsuitable positions and lose the activity of protein.

Chapter **3**

OBJECTIVES AND PLAN OF WORK

3.1. Objectives

Despite the availability of a cheap and effective treatment, TB still accounts for millions of cases of active disease and deaths worldwide. The global epidemic of drug sensitive TB as well as the increasing threat from various drug resistant forms of TB drives for newer, safer, more effective TB treatment options. Due to the emergence of MDR-TB, high incidence of HIV/TB co-infection and lack of new anti-tubercular drugs, TB has declared a global health emergency. Currently available anti-tubercular drugs were found to be ineffective to treat dormant *M. tuberculosis*; thus there is an urgent need for a new anti-tubercular drug to cure active as well as dormant TB. A thorough review of the various literatures available enlightened the importance of *M. tuberculosis* L-AlaDH in dormant form of TB, while the second target DNA GyrB is a validated target for antibacterial chemotherapy. It is a member of DNA topoisomerase family of enzymes which are responsible for maintaining and manipulating the topological state of DNA and catalyze the essential function of introducing negative supercoils in an ATP-dependent manner.

The main objective of the proposed work is to:

1. Design and identification of novel *M. tuberculosis* DNA GyrB inhibitors and *M. tuberculosis* L-AlaDH inhibitors using structure based and ligand based drug design in view of understanding the pharmacophoric requirements for antimycobacterial activity.

   a. To evaluate the inhibitory potency of the identified GyrB inhibitors by (i) GyrB ATPase assay and (ii) DNA Supercoiling assay.

   b. To evaluate the inhibitory potency of the identified *M. tuberculosis* L-AlaDH leads by AlaDH enzymatic assay.

2. To evaluate the protein-inhibitor binding using biophysical characterization techniques.

3. To carry out *in vitro* antimycobacterial screening of the identified compounds for GyrB and L-AlaDH.

4. To perform the cytotoxicity studies of all the identified and synthesized compounds.

3.2. Plan of work

The plan of work was classified into the following categories.

3.2.1. Designing the inhibitor for mycobacterial GyrB and L-AlaDH

We have utilized two strategies for designing the inhibitors.

3.2.1a. Structure based drug design approach

The available crystal structure of mycobacterial GyrB and AlaDH protein bound to inhibitor and substrate was utilized as a structural framework for virtual screening of a commercially available database (Asinex) and BITS *in house* compounds collection to identify new leads.

3.2.1b. Ligand based drug design approach

The development of a quantitative pharmacophore model was generated using CATALYST/HypoGen software for structurally diverse set of mycobacterial GyrB inhibitors with an aim to obtain 3D-pharmacophore model that could provide a rational hypothetical model based on the primary chemical features responsible for GyrB inhibitory activity. The model provided useful knowledge for developing new potentially active candidates for TB.

3.2.2. Cloning, expression and purification of mycobacterial GyrB and L-AlaDH protein

3.2.2a: Cloning, expression and purification of mycobacterial GyrB protein

The Rv3290c gene was amplified from *M. tuberculosis* H37Rv genomic DNA. Clones were screened by restriction digestion and the resulting construct was transformed in to expression vector pQE2 (Qiagen) with a 6-His-tagged cloned vector and was then transformed into BL21 (DE3) pLysS cells.

3.2.2b: Cloning, expression and purification of mycobacterial L-AlaDH protein

AlaDH gene (Rv2780) was amplified from *M. tuberculosis* H37Rv genomic DNA by standard PCR techniques and was transformed into *Escherichia coli* C41 (DE3).The crude obtained after the cell lysis was purified and the protein obtained was further tested for its activity.

3.2.3. Biological assessment of the mycobacterial GyrB and L-AlaDH protein with designed inhibitors

3.2.3a. *In vitro* GyrB inhibitory potency

The identified GyrB analogues were further evaluated for their GyrB inhibitory potency in *M. smegmatis* GyrB protein and *M. tuberculosis* GyrA protein

3.2.3b. *In vitro* L-AlaDH inhibitory potency

The identified *M. tuberculosis* L-AlaDH analogues will be further evaluated for their MTB L-AlaDH inhibitory potency using an assay based on the spectrophotometric determination of the oxidative deamination of L-alanine to pyruvate and ammonia adapted to 96-well plate format.

3.2.4. Synthesis and characterization

The designed molecules were further synthesized in our laboratory utilizing novel/previously reported methodology available in literature for structurally related molecules. All reactions were monitored using thin layer chromatography and LCMS. The synthesized compounds were fully characterized using modern analytical techniques. LCMS, ^{1}H-NMR and ^{13}C NMR were recorded and analyzed to confirm the structure of the compounds. Purity of the compounds was evaluated by elemental analysis and HPLC.

3.2.5. Evaluation of protein-inhibitor binding affinity using biophysical technique

Binding affinity of the potent GyrB and L-AlaDH analogues was evaluated by differential scanning fluorimetry experiment using real time PCR.

3.2.6. *In vitro M. tuberculosis* screening

3.2.6a. *In vitro* active *M. tuberculosis* model

All molecules were further screened for their *in vitro* antimycobacterial activity against *M. tuberculosis* $H_{37}Rv$ by microplate alamar blue assay method.

3.2.6b. *In vitro* dormant *M. tuberculosis* model

Estimation of the test compounds activity against dormant *M. tuberculosis* forms for *M. tuberculosis* L-AlaDH inhibitors was performed tested by most probable number (MPN) assay.

3.2.7. *In vitro* cytotoxicity screening

All the compounds were also tested for *in vitro* cytotoxicity against RAW 264.7 cells at 50 µM concentration using MTT assay to evaluate their selectivity index and toxicity profiles.

Chapter 4

MATERIALS AND METHODS

4.1. Identification of novel inhibitors targeting M. tuberculosis acting through the inhibition of GyrB and M. tuberculosis L-AlaDH protein

4.1.1. Identification of novel inhibitors targeting the mycobacterial GyrB protein

4.1.1.1. Design of novel inhibitors for mycobacterial GyrB protein

In the case of mycobacterial GyrB domain, we utilized two important design strategies for developing novel inhibitors, as described below.

4.1.1.1.1. Structure based drug design approach

In the case of mycobacterial GyrB domain, we describe here a novel protocol for generating energy-optimized pharmacophore (e-pharmacophore) based on mapping of the energetic terms from the Glide XP scoring function onto atom centers. Beginning with a ligand-receptor complex we refined the ligand pose, computed the Glide XP scoring terms, and mapped the energies onto atoms. Then, pharmacophore sites were generated, and the Glide XP energies from the atoms that comprised each pharmacophore site were summed. The sites are then ranked based on these energies, and the most favorable sites were selected for the pharmacophore hypothesis [Salam N.K., *et al*., 2009]. Finally, these e-pharmacophores were used as queries for virtual screening.

4.1.1.1.1a. Protein target

In the present study, crystal structures of *M. smegmatis* GyrB in complex with aminopyrazinamides (PDB code: 4B6C) and pyrrolamides inhibitor complex (PDB entry 4BAE) were retrieved from protein data bank (PDB) and were utilized for structure-based drug design [Shirude P.S., *et al*., 2013; Hameed S.P., *et al*., 2014]. Hydrogen atoms, bond orders and formal charges were added using the protein preparation wizard of the maestro software package. Water molecules were removed from the atomic co-ordinates, but in case

of *M. smegmatis* GyrB protein the inhibitor was found to be involved in water mediated hydrogen bonding interactions with the protein, thus while preparation of protein, these water molecules were retained. The resulting structure was energy minimized. Interactions of the ligand with the protein residues in the active site were visualized using ligand interaction diagram in Schrodinger suite version 9.3.

4.1.1.1.1b. Protein and ligand preparation

The protein files were prepared using protein preparation wizard and impact energy minimization was performed using 500 cycles of steepest descent (SD) and 5000 cycles of conjugate gradient (CG) methods. The optimized potential for liquid simulations (OPLS) 2005 force field was attained. The active site of the proteins was defined and grid files were generated using receptor grid generation panel. The reference ligand structure of both the proteins were downloaded from PDB and minimized using impact energy minimization with 100 cycles of SD and 500 cycles of CG. The three dimensional structure of the compounds were retrieved from Asinex and *in house* database were employed for the virtual screening. The database compounds were energy minimized and used as a single file using LigPrep (LigPrep v2.2, Schrodinger, LLC, New York, NY) module.

4.1.1.1.1c. Glide XP (Extra-Precision) docking

The generated grid files from the prepared proteins were used for Glide XP docking calculations. The minimized conjugate gradient output of the reference ligand was used. The "Write XP descriptor information" option and "Compute RMSD" option were enabled and the settings were kept default for the rest of the parameters. The XP Glide scoring function was used to order the best ranked compounds and the specific interactions like *pi-cation* and *pi-pi* stacking were analyzed using XP visualizer in Glide module. The input RMSD of the ligand was also ascertained.

4.1.1.1.1d. E-pharmacophore generation

The pharmacophore hypotheses were created for the reference ligands of both proteins by using the Xpdes file of the Glide XP output in the docking post processing tool of the scripts module by using default settings for refinement and scoring. Starting with the refined crystal ligands, pharmacophore sites were automatically generated with Phase using the default set of six chemical features: hydrogen bond acceptor (A), hydrogen bond donor (D), hydrophobic (H), negative ionizable (N), positive ionizable (P), and aromatic ring (R).

Hydrogen bond acceptor sites were represented as vectors along the hydrogen bond axis in accordance with the hybridization of the acceptor atom. Hydrogen bond donors were represented as projected points, located at the corresponding hydrogen bond acceptor positions in the binding site. Projected points allowed the possibility for structurally dissimilar active compounds to form hydrogen bonds at the same location, regardless of their point of origin and directionality [Singh K.D., *et al*., 2012]. The reference ligands were docked with Glide XP and the docked pose was refined and the Glide XP scoring terms were computed to map energies onto the atoms. The pharmacophore sites were generated, and the Glide XP energies from the atoms that comprised each pharmacophore sites were summed up. These sites were then ranked based on the individual energies, and the most favorable sites were selected for the pharmacophore hypotheses.

4.1.1.1.1e. Enrichment calculations

Enrichment factor (EF) was employed for the fraction of known actives recovered when a fraction of database was screened. EF may be defined as the ratio of number of actives retrieved relative to the number of database molecules tested. EF was often described with respect to a given percentage of the database screened [Venkatraman V., *et al*., 2010]. Decoy set consisted of 1000 molecules with an average molecular weight of 400 kDa was used. Ligand decoy sets were available for download (http://www.schrodinger.com/glidedecoyset). In decoy set 48 known active molecules of *M. smegmatis* inhibitors were included for validation. For this, we focused primarily on EF (1%), the enrichment in the top 1% of the decoys, second enrichment metrics, the Boltzmann-enhanced discrimination of receiver operating characteristic (BEDROC) was also used as a way to ensure that the results and conclusions were significant. EF, goodness of fit (GH), % Actives, and % Yield were calculated using the following equations.

$$EF = \frac{(H_a \times D)}{(H_t \times A)} \tag{1}$$

$$GH = \left(\left(\frac{H_a}{4H_t A} \right) \times (3A + H_t) \right) \times \left(1 - \left(\frac{H_t - H_a}{D - A} \right) \right) \tag{2}$$

$$\% \text{ Yield} = \left[\left(\frac{Ha}{Hb} \right) \times 100 \right] \tag{3}$$

$$\%A = \left[\left(\frac{Ha}{A} \right) \times 100 \right] \tag{4}$$

Where

'H_t' was total number of compounds in the hit list

'H_a' was the total number of active molecules in the hit list

'A' was the total number of actives in the decoy set

'D' was the total number of molecules in the decoy set

4.1.1.1.1f. Preparation of commercial database

Asinex database containing 500000 unique structures and BITS *in house* database of 2500 compounds were used in this study. Database molecules were prepared using LigPrep and Epik to expand protonation and tautomeric states at pH 7.0. Conformational sampling was performed for all molecules using the ConfGen search algorithm. We employed ConfGen with the OPLS_2005 force field and a duplicate pose elimination criterion of 1.0Å RMSD to remove redundant conformers. A distance-dependent dielectric solvation treatment was used to screen electrostatic interactions. A maximum relative energy difference of 10.0 kcal/mol was chosen to exclude high energy structures. Using Phase, the database was indexed with the automatic creation of pharmacophore sites for each conformer to allow rapid database alignments and screening

4.1.1.1.1g. High-throughput virtual screening and docking studies

For the e-pharmacophore approach, explicit matching was required for the most energetically favourable site (scoring better than 1.0 kcal/mol) that finds matching pharmacophores in the ligands. For filtering the database molecules, a minimum of 4-5 sites were required to match for hypotheses with 5-7 sites. The above criterion was followed in the present work to screen the Asinex database. In order of their fitness score, database hits were ranked to measure how well the aligned ligand conformer matched the hypothesis based on RMSD, site matching, vector alignments and volume terms. Database ligands after e-pharmacophore filter were docked into the binding sites of the protein utilizing high-throughput virtual screening (HTVS) scoring function to estimate protein-ligand binding affinities. Ligands filtered from HTVS were subjected to Glide SP (standard precision) docking. The centre of the Glide grid was defined by the position of the co-crystallized ligand. Default settings were used for both the grid generation and docking. Post docking minimization was implemented to optimize the ligand geometries. Compounds with best docking and Glide scores were then subjected to Glide XP (extra precision) docking. Final short listing of possible hit compounds was based

on visual inspection of the important amino acid residues in the active site cleft involved in binding and the hydrophobic interactions.

4.1.1.1.1h. Molecular docking using GOLD

In order to check the accuracy and validity of the ligand-based and structure-based approaches, the molecular docking studies were carried out to understand the binding modes of the GyrB inhibitors using the Genetic Optimisation for Ligand Docking (GOLD 5.2) software on a Windows-based PC, which allowed partial flexibility of the protein and full flexibility of the ligand. The reported crystal structure of aminopyrazinamides and pyrrolamides bound GyrB ATPase protein (PDB ID: 4B6C and 4BAE) was downloaded from the PDB. Initially, the protein was considered without the ligand for the purpose of docking studies. The proteins were minimized up to a gradient of 0.01 kcal/mol Å and hydrogens were added using the CHARMm force field available in the Discovery studio 3.5 software. The energy-minimized structure was used for further docking analysis. In the GOLD docking software, the default parameters were: population size (100); selection-pressure (1.1); number of operations (10,000); number of islands (1); niche size (2); and operator weights for migrate (0), mutate (100) and crossover (100) were applied. The active site was defined within 10Å and the ligand-binding interactions were analyzed using scoring functions: Goldscore (GS) and Chemscore (CS).

4.1.1.1.1i. QikProp analysis

The selected compounds after virtual screening were further selected for in-silico prediction of absorption, distribution, metabolism, excretion and toxicity using Quick-pro module of Schrodinger. QikProp efficiently evaluated pharmaceutically relevant properties for over half a million compounds per hour, making it an indispensable lead generation and lead optimization tool. Accurate prediction of absorption, distribution, metabolism, elimination (ADME) properties prior to expensive experimental procedures, such as HTS, could eliminate unnecessary testing on compounds that would ultimately fail; ADME prediction can also be used to focus lead optimization efforts to enhance the desired properties of a given compound. The ADME properties of the synthesized compounds were also predicted using QikProp. The compounds prepared were subjected to druglikeness filter. The criteria of the filter included molecular weight 160-480, number of heavy atoms 20-70, lipophilicity 40-

130, number of hydrogen bond donors 4-7, number of hydrogen bond acceptors 8-12, percentage of human oral absorption, solubility, cell permeability etc.

4.1.1.1.2. Ligand based drug design approach

The ligand-based drug design relied on knowledge of other molecules that bind to the biological target of interest. These other molecules may be used to derive a pharmacophore which defined the minimum necessary structural characteristics a molecule must possess in order to bind to the target. In other words, a model of the biological target may be built based on the knowledge of what binds to it and this model in turn may be used to design new molecular entities that interact with the target. The 2D and 3D QSARs, molecular similarity search and pharmacophore modeling etc. are the ligand based design techniques.

4.1.1.1.2a. Pharmacophore generation in Catalyst

The CATALYST software packages was launched in 1992 by BioCAD (now Accelrys) as a tool for automated pharmacophore pattern recognition in a collection of compounds based on chemical features correlation with 3D molecular structures and biological activity data. The catalyst models (hypotheses) consisted of sets of abstract chemical features arranged at certain positions in the three-dimensional space. The feature definitions were designed to cover different types of interactions between ligand and target, e.g. hydrophobic (HY), Hydrogen bond donor (HBD), Hydrogen bond acceptor (HBA), positive ionizable (PI), negative ionizable (NI) (**Figure 4.1**). Different chemical groups that lead to the same type of interaction, and thus to the same type of biological effect, were handled as equivalent, except in some special cases. The directions of the H-bonds were usually determined and were given by vectors. These models could be used directly as three-dimensional database search queries in the Catalyst environment. The pharmacophore identification process as implemented in the Catalyst package involved 3D structure generation, followed by conformational search and definition of the pharmacophore points consistent with the training set.
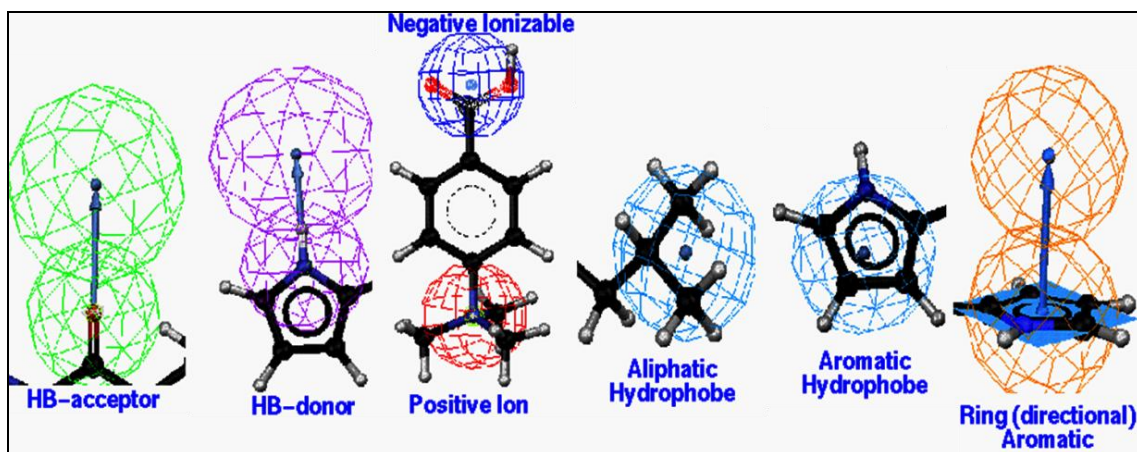
Figure 4.1: The common pharmacophoric features. (As defined in software Catalyst, www.accelrys.com)

4.1.1.1.2b. Computational methodology

All compounds were built using Chemdraw 8.0, imported to Accelry's Discovery Studio window, and optimized using CHARMm force field. The CATALYST module treated molecular structures as templates consisting of strategically positioned chemical functions that would bind effectively with receptor. The biologically most important binding functions are deduced from a small set of compounds that covered a broad range of activity. CATALYST generated conformational models for each compound using the Poling algorithm. Diverse conformational models for each compound were generated such that the conformers covered accessible conformational space defined within 20 kcal/mol of the estimated global minimum. Among the two types; fast and best quality of conformational analyses provided in the CATALYST, the best option was used specifying 255 as maximum number of conformers and 20 kcal/mol as energy cutoff. The generated diverse conformations for molecules were submitted to CATALYST for hypothesis generation using Hip-Hop algorithm or HypoGen algorithm (**Figure 4.2**).
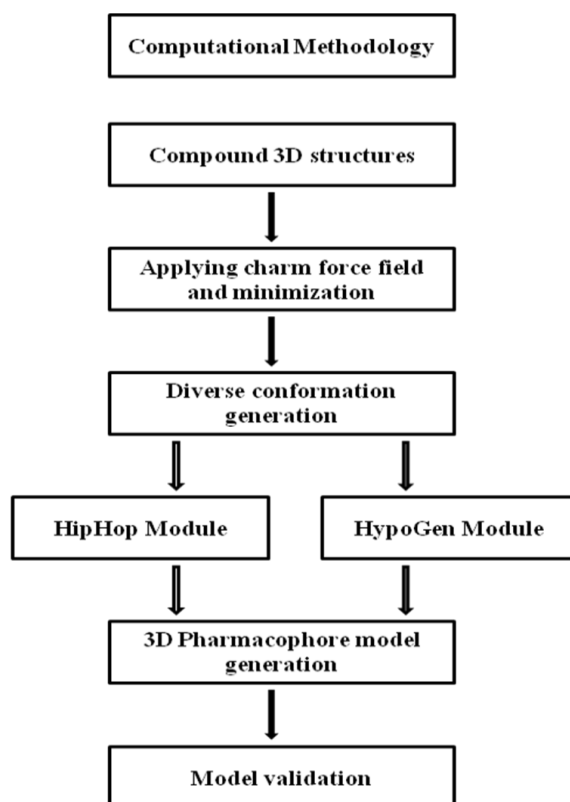
Figure 4.2: Flow Diagram of computational methodology used in ligand based drug design.

4.1.1.1.2c. Collections of data set

A total set of 61 GyrB *M. smegmatis* inhibitors with an activity range of 3.97 order of magnitude (IC$_{50}$ 0.0026 to 24.67 μM) was used for pharmacophore modeling studies [Sandeep, R.G., *et al*., 2009 and Shahul H.P., *et al*., 2012]. Pharmacophore modelling was carried out using the HypoGen module implemented in Catalyst software.

4.1.1.1.2d. Generation and validation of pharmacophore hypotheses

The 10 best pharmacophore models were generated from the structures of the training set compounds and their experimentally determined inhibitory activities against *M. smegmatis* GyrB inhibition using the HypoGen module implemented in Discovery Studio 3.5 using a default uncertainty value of 3 (defined by Catalyst as the measured value being within three times higher or three times lower of the true value). During the hypothesis generation, Catalyst considered and discarded thousands of models in an attempt to minimize a cost function consisting of two terms. Analysing the cost values would help us in understanding the validity of generated pharmacophore hypotheses. Three cost values named fixed cost, total cost and null cost were generated by HypoGen during pharmacophore generation

process. Every single pharmacophore generation run produced maximum of ten pharmacophore hypotheses, fixed and null cost values which were normally used to determine the quality of any pharmacophore hypothesis. To validate the best pharmacophore hypothesis, a test set and Fisher test was used.

4.1.1.1.2e. Database searching

The validated pharmacophore hypothesis was used as a 3D structural query for searching potent compounds from *in house* 3D database consisting of 2500 compounds. Virtual screening of databases was used to identify compounds that fit well on the pharmacophore hypothesis and thereby could act as potential virtual leads in GyrB *M. smegmatis* inhibitors design. Database screening was performed using the pharmacophore mapping protocol with fast/flexible search option as available in Discovery studio 3.5. The top hits from the screening were selected based on pharmacophore fit value and mapping.

4.1.1.2. Synthesis and characterization

The top active lead compound identified by the above mentioned strategies were taken up for further lead optimization through synthesis. Hit expansion of the various lead identified were achieved using the following synthetic protocols.

4.1.1.2.1. Synthetic protocol adopted for hit expansion of the leads obtained from structure based virtual screening.

Reagents & Conditions: a:Morpholine, Sulphur powder, EtOH, rt, 7 h; b: Dry HCl gas, THF, 0 c, 2h; c: R-NCO/R-NCS, Microwave, 100 C, 20 min; c: R-COCl, Et₃N, DCM, rt, 4 h;
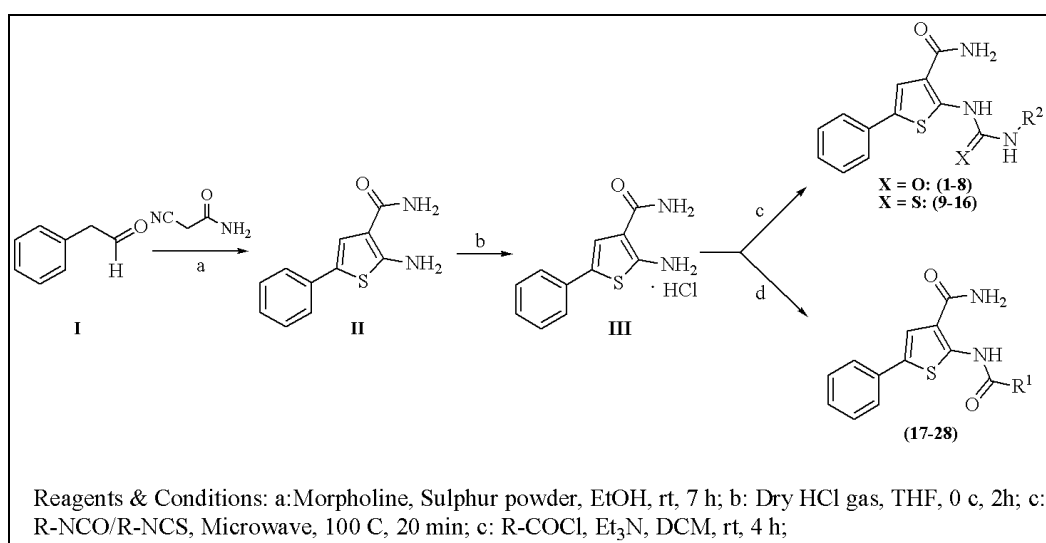
Figure 4.3: Synthetic pathway used to achieve the target compounds **S1-28**.

All commercially available chemicals and solvents were used without further purification. TLC experiments were performed on alumina-backed silica gel 40 F254 plates (Merck, Darmstadt, Germany). The homogeneity of the compounds was monitored by thin layer chromatography (TLC) on silica gel 40 F254 coated on aluminum plates, visualized by UV light and $KMnO_4$ treatment. Purifications were done on Biotage Isolera purification system on silica gel (MPLC grade) by using either hexane: ethylacetate or dichloromethane: methanol as eluent. All ^1H and ^{13}C NMR spectra were recorded on a Bruker AM-300 (300.12 MHz, 75.12 MHz) NMR spectrometer, BrukerBioSpin Corp. Germany. Chemical shifts are reported in ppm (δ) with reference to the internal standard TMS. The signals were designated as follows: s, singlet; d, doublet; dd, doublet of doublets; t, triplet; m, multiplet. Molecular weights of the synthesized compounds were checked by LCMS 6100B series Agilent Technology. Elemental analyses were carried out on an automatic Flash EA 1112 Series, CHN Analyzer (Thermo). The purity of the final compounds was examined by HPLC (Shimadzu, Japan, (on Phenomenex C8 (150 * 4.6 mm, 5µm, 100 Å) double end-capped RP-HPLC column)) and was greater than 95% and by elemental analysis.

4.1.1.3. *In vitro* biological and biophysical evaluation

All the identified leads and the synthesized analogues were evaluated for *in vitro* gyrase inhibitory potency using a GyrB *in vitro* ATPase assay and GyrA *in vitro* DNA supercoiling assay. The binding affinities of the potent ligands were evaluated by biophysical differential scanning flourimetry experiments (DSF). Furthermore, all the compounds were also evaluated for antimycobacterial potency against *M. tuberculosis* $H_{37}R_V$ strain using MABA assay [Sriram D., *et al*., 2005] and cytotoxicity against RAW 264.7 celline using MTT assay [Sriram D., *et al*., 2005].

4.1.1.3.1. Cloning and purification

Cloning of *M. smegmatis* GyrB was done by amplifying the gene from mc^2155 genomic DNA using the specific forward and reverse primers 5' CACCCATATGGTGGCTGCCCAGAAGAACAA 3' (NdeI), and 5' AGCTAAGCTTTTAAACATCCAGGAAGCGAA 3' (Hind III) respectively. The final PCR amplicons were cloned in expression vector pQE2 (Qiagen) with a 6-His-tagged cloned vector and then transformed into *BL21 (DE3) pLysS* cells. The transformed cells were later grown at 37 ºC in LB broth containing 50 µg/mL ampicillin to an optical density (OD) of 0.6

(A595). Further bacterial cells were induced with isopropyl-β-D-thiogalactopyranoside at a final concentration of 0.2 mM while the cells were in exponential growth phase and the cell growth was further continued for another 12 h at 18°C. The bacterial cells were then centrifuged at 10,000 g at 4ºC for 15 min. The cell pellet was resuspended in PBSG buffer (PBS containing 5% glycerol) further lysed using sonicator (20 sec pulse and 45 sec halt) and centrifuged the crude lysate at 8000 rpm at 4ºC for 10 min, subsequently centrifugation was repeated for the supernatant of previous step at 10000 rpm at 4ºC for 35 min for a clear supernatant. The cell extract was later applied to Ni-NTA column (Bio-Rad), the column was washed with wash buffer (5% glycerol in PBS and 500 mM NaCl) and the protein was eluted using different concentration of imidazole ranging from 10 mM to 200 mM in the elution buffer (5% Glycerol, 140mM NaCl in 25 mM Tris-Cl (pH 8.0)). Fractions containing the desired GyrB subunit was identified by sodium dodecyl sulphate-polyacrylamide gel electro-phoresis (SDS-PAGE), later pooled the 100 mM and 200 mM fractions and dialyzed against the dialyses buffer (15% Glycerol, 140 mM NaCl in 25 mM Tris-HCl (pH 7.4)), frozen in liquid nitrogen and stored at -80ºC.

4.1.1.3.2. Enzyme kinetics of GyrB ATPase activity

The ATPase activity of DNA GyrB enzyme concentration followed greater than first order kinetics, as a result the GyrB ATPase activity of *M. smegmatis* did not follow Michaelis-Menten kinetics; however, at a constant optimized enzyme concentration of 15 μM there was a hyperbolic dependence of rate of the reaction on substrate (ATP) concentration [Ali J.A., *et al.*, 1993].

4.1.1.3.3. *In vitro* GyrB ATPase assay

The ATPase assay was performed as per published method [Shirude P.S., *et al.*, 2013] on *M. smegmatis* protein. The ATPase activity of GyrB protein from *M. tuberculosis* was found to be very low compared with *M. smegmatis* [Shirude P.S., *et al.*, 2013]. It was carried out in 30 μL reaction volumes for 2 h at 25°C in reaction buffer containing 60 mM HEPES-KOH pH 7.7, 250 mM potassium glutamate, 200 mM KCl, 2 mM magnesium chloride, 1 mM DTT, 2% glycerol, 4% DMSO, 0.001% BriJ-35, 0.65 mM ATP, 40 nM GyrB. All the test compounds were diluted in DMSO at 30 times the final assay concentrations. Assay was performed in 96 well plates (Polystyrene untreated) flat bottomed plates. Initially 1 μL of test compound was placed in the assay well, which was followed by 15 μL of 2x assay buffer

containing purified GyrB enzyme and substrate mix, later the enzyme reaction was initiated by adding 14 µL of MgCl$_2$ solution. Then the reaction was allowed to proceed for 2 hrs at room temperature. Subsequently, the reaction was quenched by adding malachite green reagent (Bioassay systems). Inorganic phosphates (Pi) released during the reaction was measured at 635 nm after 20 min.

4.1.1.3.4. *In vitro* supercoiling assay

The supercoiling assay was performed using Inspiralis kit (Inspiralis Limited, Norwich). The assay was performed in 30 µL reaction volume for 30 min at 37 ºC in assay buffer containing 50 mM HEPES. KOH (pH 7.9), 6 mM magnesium acetate, 1mM ATP, 4 mM DTT, 2 mM spermidine, 100 mM potassium glutamate, and 0.05 mg/mL of albumin. During the assay 1U of DNA Gyrase was incubated with 0.5 µg of relaxed pBR322 in assay buffer for 30 min followed by brief vortexing, centrifugation and later quenched by addition of equal volume of chloroform: isoamylalcohol (24:1), 30 mL STEB (40% sucrose, 100 mM Tris-HCl (pH 8.0), 100 mM EDTA and 0.5 mg/mL bromophenol blue). Subsequently, the products were analysed by electrophoresis on 1% agarose gel and stained with ethidium bromide and destaing it in 1X TAE buffer. Image lab software (Bio-Rad) was used to measure and analyse the enzyme inhibition.

4.1.1.3.5. Biophysical characterization using DSF

The binding affinities of the most potent ligand was evaluated by measuring the fluorescence of the native protein and protein-ligand complex in presence of a fluorescent dye whose fluorescence increased when exposed to non polar residues of the protein and reached the maximum when the protein denatured [Brvar M., *et al*., 2012; Niesen F.H., *et al*., 2007]. In brief, firstly native protein (7.5 µl of protein (1.5 mg/mL) + 3.5 µl of buffer (50 mM Tris pH 7.4, 1 mM EDTA, 5 mM DTT)) was subjected to stepwise heating in a PCR instrument (Bio-Rad) from 25 ºC to 100 ºC with an increment of 0.6 ºC /min in presence of the fluorescent dye SYPRO orange (2.5 µl, (1:100) (Sigma)). As the temperature was increased the stability of the protein decreased and is zero at equilibrium, where the concentrations of folded and unfolded protein were equal. This temperature was noted as the melting temperature (T$_M$). The dye exhibited the maximum fluorescence at this point as it was exposed to hydrophobic portion of the protein as a result of protein denaturing. A higher or positive shift of melting temperature (T$_M$) of protein-ligand complex compared to the native protein T$_M$ signified a

better stabilization of the protein-ligand complex, which in turn was a reflection of the inhibitor binding.

4.1.1.3.6. *In vitro* antitubercular screening

In this technique, the minimal inhibitory concentration (MIC) value of all the identified compounds against *M. tuberculosis* H37Rv in 90% was determined using alamar blue as a fluorescent vital dye. In brief, the inoculum was prepared from fresh LJ medium re-suspended in 7H9-S medium (7H9 broth, 0.1% casitone, 0.5% glycerol, supplemented oleic acid, albumin, dextrose, and catalase [OADC]), adjusted to a McFarland tube No. 1, and diluted 1:20; 100 µl was used as inoculum. Each drug stock solution was thawed and diluted in 7H9-S at four-fold the final highest concentration tested. Serial two-fold dilutions of each drug were prepared directly in a sterile 96-well microtiter plate using 100 µl 7H9-S. A growth control containing no antibiotic and a sterile control were also prepared on each plate. Sterile water was added to all perimetre wells to avoid evaporation during the incubation. The plate was covered, sealed in plastic bags and incubated at 37ºC in normal atmosphere. After 7 days incubation, 30 mL of alamar blue solution was added to each well, and the plate was re-incubated overnight. A change in colour from blue (oxidised state) to pink (reduced) indicated the growth of bacteria, and the MIC was defined as the lowest concentration of drug that prevented this change in colour [Sriram D., *et al*., 2005].

4.1.1.3.7. *In vitro* cytotoxicity screening

The compounds displaying good *in vitro* potency in the GyrB ATPase assay were further examined for toxicity in a RAW 264.7 cell line at 100 µM concentration. After 48 h of exposure, viability was assessed on the basis of cellular conversion of MTT into a formazan product using the Promega Cell Titer 96 non-radioactive cell proliferation assay. Mouse macrophages cell lines (RAW 264.7) were grown in RPMI medium supplemented with 10% fetal bovine serum (FBS), 10,000 units penicillin and 10 mg streptomycin per mL in T25 flasks to attain 80-90% confluency. Cells were scraped and seeded into wells i.e 5,000 cells per well in poly-L-lysine coated plates. The microtiter plates were incubated at 37ºC, 5% CO_2, 95% air and 100 % relative humidity for 24 h prior to addition of experimental drugs. The test compounds at 100 µM concentrations were then added to cells and incubated at 37 °C for 48 h. Later 10 µL of 10 mg/mL concentration of MTT was added and incubated for 3 h at 37ºC. At the end of incubation period formazon crystals were formed, the plates were then

centrifuged and the media from microtiter plates were removed. Later, plates were air dried. The bound crystals were subsequently dissolved by adding 100 μL DMSO. The absorbance was then read on ELISA plate reader at a wavelength of 595 nm. Relative to the control wells the percent growth was calculated for each well. The percentage of cells killed was obtained from the formula [Sriram D., *et al.*, 2005].

$$\text{Percentage of cells killed} = \frac{100 - \text{mean OD sample}}{\text{mean OD day 0}}$$

4.1.2. Identification of novel inhibitors targeting the *M. tuberculosis* L-AlaDH protein

4.1.2.1. Design of novel inhibitors for *M. tuberculosis* L-AlaDH protein

In the case of *M. tuberculosis* AlaDH domain, we utilized the computational structure based drug design strategy similar to the one utilized for the GyrB domain. The ligand based drug design concept was not utilized in the case of *M. tuberculosis* AlaDH due to lack of *M. tuberculosis* L-AlaDH inhibitors in literature. In the present study we utilized the two crystal structure of the *M. tuberculosis* L-AlaDH complexed with substrate NAD^+ and N_6-mehyl adenosine as template for energy-based pharmacophore (e-pharmacophore) modeling and in-silico docking to identify drug like compounds as putative active site ligands [PDB ID: 2VHW and 4LMP]. The generated e-pharmacophore was then utilized for the virtual screening of BITS *in house* compound collection and a commercial database (Asinex) using same protocol used for DNA GyrB. The hits have been identified through structure based design and further top lead molecules from virtual screening were taken for synthesis using the protocol described below.

4.1.2.2. Synthesis and characterization

Two lead molecules were further synthesized and hit expansions of the both leads identified were achieved using the following synthetic protocols. A library of 30 molecules, comprising of fifteen iminothiazolidine-4-one derivatives (compound **4a-o**) based on **Lead 1** and another fifteen 4,5,6,7-tetrahydrothieno[2,3-c]pyridine-3-carboxamide derivatives (compound **11-25**) based on **Lead 2** were synthesised as shown in **Figure 4.4** and **4.5** respectively.

4.1.2.2a. Synthetic protocol adopted for hit expansion of the leads obtained by virtual screening.
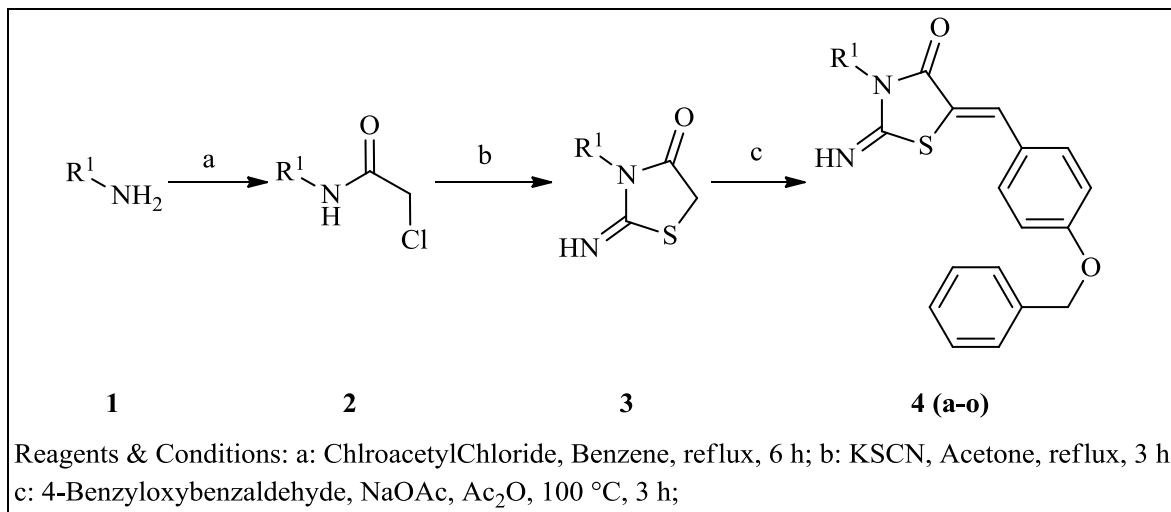
Figure 4.4: Synthetic protocol of compounds **4a-o.**
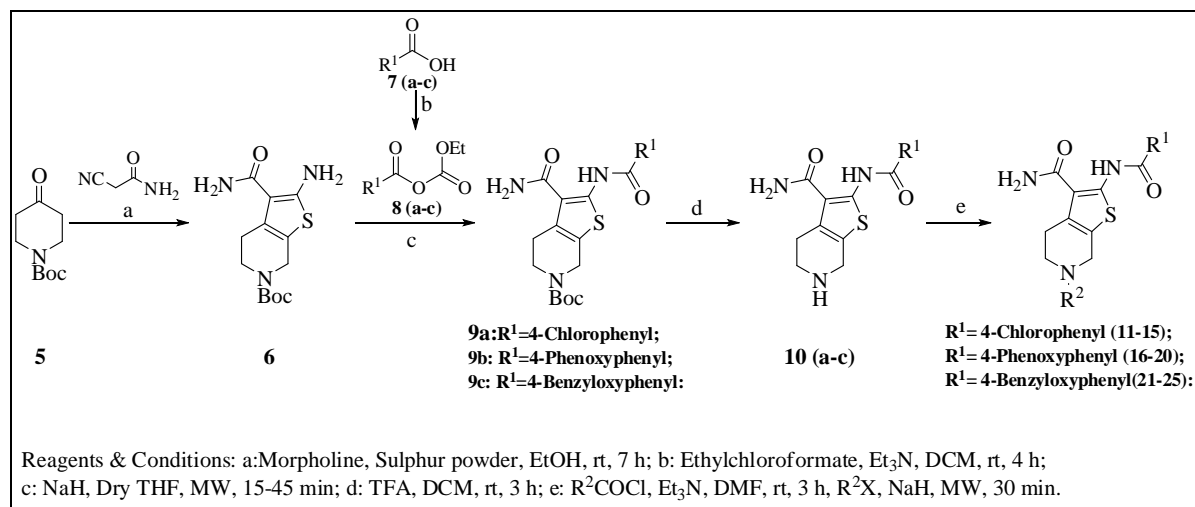
Figure 4.5: Synthetic protocol of compounds **11-25.**

The characterization of all the compounds was done as previously mentioned for GyrB compounds synthesis (Section 4.1.1.2.1).

4.1.2.3. *In vitro* biological and biophysical evaluation

4.1.2.3.1. Cloning and purification of *M. tuberculosis* L-AlaDH

Gene encoding *M. tuberculosis* L-AlaDH was amplified from H37Rv genomic DNA by using the forward primer (5'CCCAAGCTTATGCGCGTCGGTATTCCGACCGAG3') and the reverse primer (5'CCCAAGCTTTCAGGCCAGCACGCTGGCGGGCTCGGT') flanked with Hind-III site. The amplified PCR products were digested with Hind-III and cloned at Hind-III restriction enzyme site of the pET-28a (Novagen) expression vector to generate the pET-28a-ADH construct. Further, this clone was transformed into C41(DE3) cells (Lucigen). Transformants were grown in LB broth at 37 °C with constant aeration in the presence of 50 μg/mL kanamycin. Exponentially growing cultures (A600 of ~0.6) were induced with 0.2 mM IPTG and further grown for 12-16 h at 18 °C. Cells were then harvested and lyzed by sonication in lysis buffer. The cell lysate containing His6-fusion proteins were mixed with equilibrated Ni-NTA affinity resins and the tagged proteins were eluted with buffer containing 500 mM imidazole.

4.1.2.3.2. Enzyme kinetics of *M. tuberculosis* L-AlaDH

M. tuberculosis L-AlaDH enzyme assay was performed in 100 μl reaction in 96 well microtitre plate containing 125 mM glycine-KOH buffer (pH-10.2), 1 mM NAD^+, 50 mM of L-alanine as substrate and various concentrations of *M. tuberculosis* L-AlaDH for 20 min at 37 °C. The *M. tuberculosis* L-AlaDH enzyme activity was continuously monitored and the end product NADH was observed at 340 nm [Agren D., *et al*., 2008]. Concentration of enzyme was later determined based on the range finding experiments. In order to determine the kinetic parameters K_m and V_{max}, the substrate L-alanine was varied from 1 mM to 200 mM, similarly NAD^+ concentrations were also varied from 0.1 mM to 1 mM and K_m and V_{max} were determined using non-linear regression analysis from GraphPad prism software.

4.1.2.3.3. *In vitro M. tuberculosis* L-AlaDH enzyme inhibition assay

The enzyme inhibition studies were performed in microtitre plate containing desired substrate and enzyme concentration as explained above. The spectrophotometric determination of the reaction product NADH that accompanied the conversion of L-alanine into pyruvate in the oxidative deamination was measured at 340 nm in heat controlled microplate reader PerkinElmer Victor X3 instrument. The synthesized compounds were added to the plate with different concentrations from 25 μM to 0.5 μM in order to determine IC_{50} values for the all the compounds. The reaction mixture except *M. tuberculosis* L-AlaDH was added and

background reactions were measured. Further the IC_{50} values were calculated using GraphPad Prism analysis software.

4.1.2.3.4. In *vitro M. tuberculosis* screening

4.1.2.3.4a. *In vitro* dormant *M. tuberculosis* model

Culture of *M. tuberculosis* H37RV were grown in Middlebrook 7H9 medium supplemented with OADC (nutrient rich medium) and was pelleted and washed twice with PBS (Phosphate Buffer Saline, HiMedia Laboratories). The pellet was re suspended in PBS in sealed bottles and was incubated at 37°C for 6 weeks. Six week starved cultures were treated with standard drugs like INH, RIF and moxifloxacin along with test drugs for 7 days at a concentration of 10 µg/ml. The treated cell suspensions were diluted 10-fold up to 10^{-6} using Middlebrook 7H9 medium supplemented with OADC and 100 µl of each dilutions were plated in 48 well plates in triplicates along with 900 µl of Midllebrook 7H9 medium (HiMedia Laboratories) supplemented with OADC (HiMedia Laboratories). The microplates were incubated at 37°C for 28 days without agitation wells with visible bacterial growth were counted as positive, and MPN values were calculated using standard statistical methods.

4.1.2.3.4b. *In vitro* active *M. tuberculosis* model

The test compounds were further examined for its activity in active model of *M. tuberculosis* similar to the protocol described in section 4.1.1.3.6.

4.1.2.3.5. *In vitro* cytotoxicity screening

The synthesized compounds were further examined for its cytotoxicity in mouse macrophage cell line (RAW 264.7) at 50 µM concentration similar to the protocol described above for GyrB (section 4.1.1.3.7).

4.1.2.3.6. Biophysical characterization

A thermal shift assay, also called DSF was a thermal-denaturation assay that measured the thermal stability of a target protein and a subsequent increase in protein melting temperature upon binding of a ligand to the protein [Joanna C., *et al*., 2002]. It used a Sypro Orange dye (Sigma-aldrich) in a Real time PCR instrument (Bio-Rad iCycle5), which bind to exposed core residues of a denatured protein and resulted in an increased fluorescence signal. The

instrument was programmed to equilibrate the samples at 25°C for 3 min and further rise in temperature till 95°C, with every 0.1°C rise using a LED/Photodiode set matched with dye excitation and emission wavelengths. Required concentration of MTB L-AlaDH and dye were determined by varying different concentrations of protein and dye in analysis buffer containing 100 mM HEPES-NaOH, pH-7.8. The selected top active compounds were diluted in <10% DMSO. Later, in a 96 well PCR plate, 20 µl of reaction volume containing 10 µl of MTB L-AlaDH (100 µg/ml) in analysis buffer, 6 µl of 15X dye (Diluted from 5000X stock with sub-stock of 50X in DMSO) were taken. Based on their dilutions, the compounds were diluted and added to the subsequent wells. The melting temperature of the protein and protein complexed with ligand was determined as the lowest point of first derivative plot and calculated by the software provided with the instrument.

Chapter 5

RESULTS AND DISCUSSIONS

5.1. DEVELOPMENT OF DNA GYRASE B INHIBITORS AS POTENTIAL ANTI-TUBERCULAR AGENTS

Bacterial DNA gyrase (EC 5.99.1.3) is a validated target for antibacterial chemotherapy. It is a member of DNA topoisomerase family of enzymes which are responsible for maintaining and manipulating the topological state of DNA and catalyze the essential function of introducing negative supercoils in an ATP-dependent manner. The enzyme is present in all prokaryotes and this is the only type II topoisomerase enzyme in *M. tuberculosis*. This lack of redundancy makes it an attractive target for discovering novel drugs against TB. It is the only Type II topoisomerase and sole target for quinolones in *M. tuberculosis*, and pharmaceutically effective target for drug discovery against this important pathogen. Quinolones preferably targets GyrA subunit; and has made quite successful progress in TB drug discovery pipeline with gatifloxacin and moxifloxacin, which is currently in phase 3 clinical trials for the treatment of TB. However the emergence of quinolone resistant strains and the occurrence of some serious side effects call for novel research in this field. The ATPase activity of bacterial DNA Gyrase that resides in the GyrB subunit remains pharmaceutically under-exploited. Inhibitors of GyrB subunit competitively inhibit the ATPase activity conferred by the DNA GyrB subunit and thereby abolishes the energy-dependent reactions catalyzed by DNA Gyrase. Developing novel inhibitors that target the GyrB subunit offers an excellent opportunity to address fluoroquinolones resistance and to develop an effective treatment for TB. In the present study we explore the pharmaceutically underexploited mycobacterial gyrase ATPase domain (GyrB) as a template to discover newer inhibitors targeting *M. tuberculosis*.

5.1.1. Design and identification of DNA GyrB inhibitors

In the present study we utilized two important computational strategies for developing novel inhibitors targeting the GyrB domain. The first approach employed the structure based virtual screening protocol described in the material and method section, to identify newer scaffolds

as potential mycobacterial GyrB leads. The second strategy utilized the ligand based pharmacophore modeling to develop newer leads.

5.1.1a. Inhibitors developed using structure based drug design approach

Structure-based drug design relies on the knowledge of the three dimensional structure of the biological target obtained through methods such as x-ray crystallography or NMR spectroscopy [McCarthy J.D., 1999]. Using the structure of the biological target, candidate drugs that are predicted to bind with high affinity and selectivity to the target may be designed using interactive graphics and the intuition of a medicinal chemist. Alternatively various automated computational procedures are used to suggest new drug candidates. The receptor-based (direct) approach to CADD can be used when a reliable model of the receptor (preferentially complexed with a ligand) is available from x-ray diffraction. If the receptor structure is available, a primary challenge in lead discovery and optimization is to predict both the ligands orientation and binding affinity; the former is often referred to as 'molecular docking' while the latter is known as 'scoring' [Taylor R.D., *et al.*, 2002]. Aminopyrazinamides and pyrrolamides are the recent class of mycobacterial DNA GyrB inhibitors that were derived by scaffold hopping efforts of their antibacterial counterparts. These classes of drugs were also found to be effective against both drug sensitive and drug resistant clinical isolates of *M. tuberculosis*. Potent analogues from both series 6-(3,4-dimethylphenyl)-3-[4-[3-(4-methylpiperazin-1-yl)propoxy]phenyl]amino]pyrazine-2-carboxamide & 2-[4-(3-bromo-4-chloro-5-methyl-1H-pyrrole-2-amido)-3-methoxypiperidin-1-yl]-4-(1-methyl-1H-1,2,4-triazol-5-yl)-1,3-thiazole-5-carboxylic acid were co-crystallized with *M. smegmatis* GyrB domain. Bacterial DNA gyrase protein is heterotetramer protein, composed of two GyrA and two GyrB chains. Within the heterotetramer, GyrA contains the active site tyrosine that forms a covalent intermediate with the DNA, while GyrB contributes the cofactor binding sites and catalyzes ATP hydrolysis. The structure of *M. smegmatis* GyrB ATPase domain in complex with an aminopyrazinamide revealed two chains A and B and the aminopyrazinamides was found to bind to the both the chains of ATPase domain with *M. smegmatis* GyrB IC_{50} of 3 nM. Similarly the pyrrolamide inhibitor was bound in the 22.7 kDa N-terminal fragment *of M. smegmatis* GyrB ATPase domain, referred to as *M. smegmatis* GyrB EP6 and with *M. smegmatis* GyrB IC_{50} of 3 nM. In the present study both the crystal structures of *M. smegmatis* Gyrase B protein co-crystallized with ligands [PDB: 4BAE, Shahul H.P., *et al.*, 2014] and [PDB: 4B6C, Shirude P.S., *et al.*, 2014] were retrieved

from the protein data bank and were utilized as a structural framework for structure based virtual screening of a commercial database of Asinex to explore newer class of GyrB inhibitors.

5.1.1a.1. Design and development of GyrB inhibitor based on aminopyrazinamides inhibitor bound protein (PDB ID: 4B6C)

5.1.1a.1.1. Designing of inhibitors

5.1.1a.1.1a. Protein preparation and active site validation

The crystal structure of *M. smegmatis* GyrB in complex with aminopyrazinamide was retrieved from protein data bank and used for structure-based pharmacophore modeling. The asymmetric unit of *M. smegmatis* protein consisted of two chains and the inhibitor was bound in the ATPase binding domain. The reference inhibitor showed two key interactions at site 1 and site 2. First, the primary carboxamide at site 1 was involved in two hydrogen bond interactions with Asp79, one directly and a second *via* water. Second, the phenyl group at site 2 formed *pi-pi* stacking interactions with Arg82. For the validation of active site cavity, inhibitor bound to the protein was removed and prepared using Ligprep and redocked with the active site residues of the *M. smegmatis* protein. The re-docked ligand exhibited Glide score of -11.42 kcal/mol and was found in the vicinity of important amino acids like Pro85, Asp97, Val98, Arg82, Glu56, Ala53, Asp79, Asn52, Ile171, Val49, Val128, Gly48, Ser126, Val123, Gln102, Ile84, Gly83, Arg141 and Val99. Thus the re-docking results showed that the ligand exhibited similar interactions as that of the original crystal structure with RMSD of 0.567Å (**Figure 5.1**).
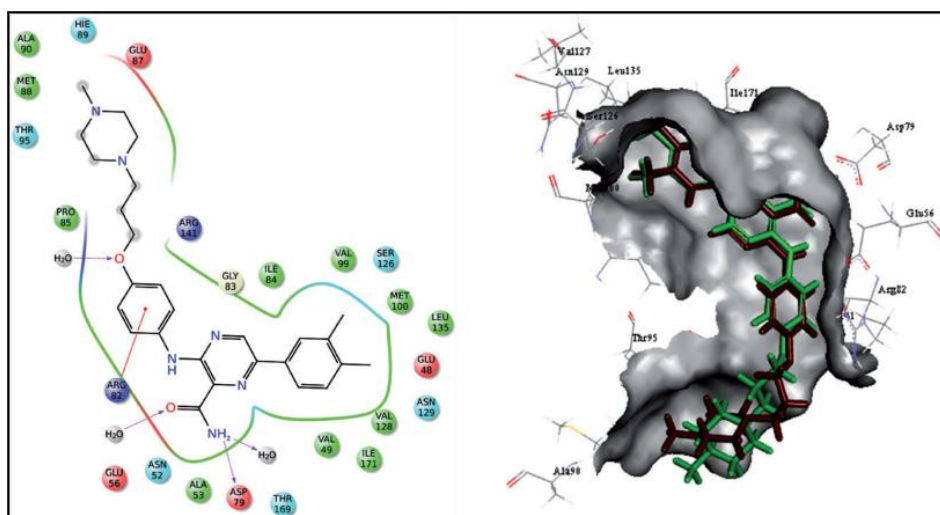
Figure 5.1: Interactions of reference inhibitor with the active site residues of *M. smegmatis* protein and superimposition of docked pose of the reference inhibitor to the original pose of the inhibitor.

5.1.1a.1.1b. E- pharmacophore generation

The e-pharmacophore methods which combine the aspects of structure-based and ligand-based techniques were explored for the *M. smegmatis* protein in this study. The binding mode of the inhibitor bound to the *M. smegmatis* protein was defined by the interaction pattern of its pharmacophore. Pharmacophore hypotheses were developed by mapping Glide XP energetic terms onto pharmacophore sites, which was calculated based on the structural and energetic information between the protein and the ligand using Phase module having the default set of chemical features. Hydrogen-bond donors (D) were represented as projected points, located at the corresponding hydrogen-bond acceptor (A) positions in the binding site. The initial number of pharmacophoric sites was set up to 10 for the crystal structure. Docking results (Xpdes) were then imported to find the structure-based pharmacophoric features, which would help in finding the best featured functional groups. The maximum number of pharmacophoric sites derived for the reference inhibitor was seven points with two acceptors (A), three ring aromatic ring (R) and two donors (D) (**Figure 5.2**). The important sites obtained in e-pharmacophore model such as D5, D6, were found to correspond to the important amino acid residue Asp79, while A3 and A4 corresponded to water molecules and R15 was directly involved in *cation-pi* interaction with Arg82, while R13 and R14 was not involved in any interaction but these features were inserted into the hydrophobic cavity which was considered to be very crucial for retaining the activity. Energy score of all the seven

point features is represented in **Table 5.1**. As shown in the **Table 5.1** A3 and D5 features showed high energy scores which indicated that these features were not much contributing to the activity, while the other features such as A4, D6, R13, R14 and R15 showed good energy score. On an average, there were 7 sites per hypothesis, many of which did not even appear to be directly involved in protein-ligand interactions. Each pharmacophore point of the hypothesis were made into combinations of pharmacophores having 6, 5, 4 and 3 point features totalled to 33 combination represented in **Table 5.2**

Table 5.1: Energy scores of hypothesis in e-pharmacophore.

Rank	Feature label	Score	Type
1	A4	-0.62	A[a]
2	D6	-0.57	D[b]
3	D5	-0.31	D
4	A3	-0.19	A
5	R13	-0.95	R[c]
6	R15	-0.81	R
7	R14	-0.72	R

[a] Acceptor
[b] Donor
[c] Ring Aromatics
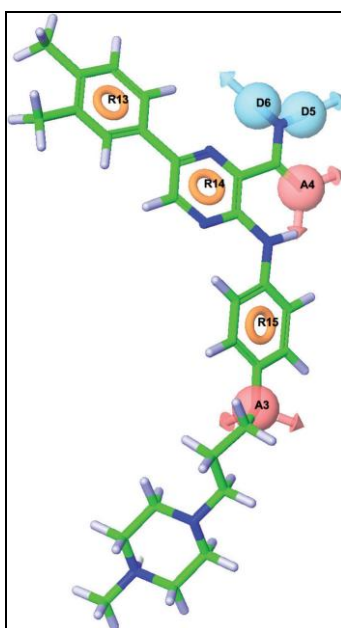
Figure 5.2: The energy based pharmacophoric features of inhibitor bound to the *M. smegmatis* protein.

5.1.1a.1.1c. Validation of constructed pharmacophore models

The enrichment results for all the 33 pharmacophoric hypotheses were compared based on enrichment factor (EF), BEDROC ($\alpha=20.0$) and % of active based on recovery rate of actives against the ranked decoy database as shown in **Table 5.2**. This not only helped us to eliminate the pharmacophore sites which lacked significant interactions but also prioritized the sites for further virtual screening. Hence, from this methodology we obtained both good enrichment as well as diversity in our hits. The energy contribution between the ligand and every amino acid in the binding site always were key things in the ligand-receptor complex. The enrichment factor reflected the capability of a screening application to detect active ligands (true positives) compared to random selection. Thus, its value was expected always to be greater than 1 and the higher it was, the better the enrichment performance of the virtual screening. A second enrichment metric, the Boltzmann-enhanced discrimination of receiver operating characteristic (BEDROC) was also used as a way to ensure that the results and conclusions were significant and generalized the receiver operating characteristic (ROC) that addressed the "early scoring problem" by Boltzmann weighting the hits based on how early they were retrieved. Based on the recovery rate of actives against the total 1048 compounds in which 48 were known inhibitors of mycobacterial GyrB inhibitors and 1000 were the decoy set which represented inactives.

The results are as shown in **Table 5.2**, where 5 point (R13, R14, R15, A3, D6), 4 point (R13, R14, R15, D6) and 3point (R15, A4, D5) pharmacophore models showed the highest enrichment at 1% (EF1%) and BEDROC values. Also, the overall % active, and % yield obtained as output and goodness of fit (GH) were better for all the selected pharmacophores (**Figure 5.3**).
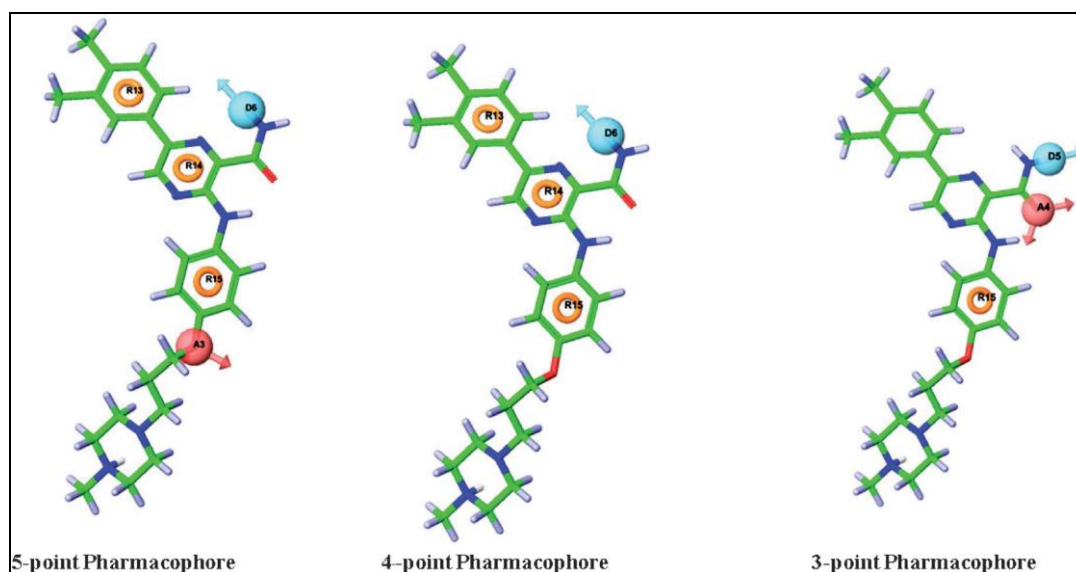
Figure 5.3: E-pharmacophore models of reference inhibitor after validations.

Table 5.2: Validation of e-pharmacophore models.

E-pharm features[a]	GH[b]	%active (s/w)[c]	EF(s/w) 1%[d]	EF (manual)[e]	% yield[f]	%A[g]	BEDROC (α=20)[h]
R13, R14,R15,A3,A4,D5,D6	0.060	10.4	2.2	1.09	5.49	10	0.17
R14,R15,R16,A4,D5, D6	0.070	6.2	0	0.93	4.65	24	0.094
R13, R14,R15,A4,D6	0.082	12.5	4.4	1.15	5.76	74	0.15
R13, R14,R15,A4,D5	0.091	14.6	0	1.18	5.94	70	0.017
R13, R14,R15,A3,D6	0.102	16.7	6.5	1.25	6.26	64	0.41
R13, R14,R15,A3,D5	0.114	20.8	0	1.36	6.84	62	0.0164
R13,R14,R15,A3,A4	0.100	12.5	0	1.26	6.34	72	0.102
R13,R14,R15,D5,D6	0.057	8.3	2.2	0.71	3.55	34	0.203
R13,R14,A4,D5,D6	0.084	6.2	0	1.15	5.76	72	0.045
R14,R15,A4,D5,D6	0.116	10.4	2.2	1.41	7.05	72	0.053
R13,R15,A4,D5,D6	0.084	6.2	2.2	1.16	5.80	74	0.096
R13, R14,R15,A4	0.038	6.2	2.2	0.53	2.66	12	0.028
R13, R14,R15,D6	0.028	10.4	8.7	0.38	1.92	10	0.46
R13, R14,R15,D5	0.055	10.4	6.5	0.89	4.47	12	0.16
R13,R15,A4, D6	0.062	10.4	2.2	0.78	3.94	24	0.103

E-pharm features[a]	GH[b]	%active (s/w) [c]	EF(s/w) 1%[d]	EF (manual) [e]	% yield[f]	%A[g]	BEDROC (α=20) [h]
R13,R14,A4, D6	0.061	4.2	4.4	0.74	3.72	32	0.047
R14,R15,A4, D6	0.104	6.2	0	1.25	6.28	60	0.05
R14,A4,D5, D6	0.135	2.1	0	1.65	8.28	54	0.063
R15,A4,D5, D6	0.077	6.2	0	1.00	5.03	28	0.108
R13,A4,D5, D6	0.144	8.3	0	1.78	8.91	56	0.05
R13,R15,A4	0.043	6.2	0	0.54	2.74	28	0.136
R13,R14,A4	0.071	12.5	6.5	1.07	5.38	74	0.18
R14,R15,A4	0.057	2.1	0	0.92	4.64	66	0.136
R13,A4, D6	0.076	18.8	4.4	1.12	5.62	76	0.4
R14,A4, D6	0.058	6.2	4.4	1.03	5.19	78	0.3
R15,A4, D6	0.082	41.7	2.2	1.16	5.82	76	0.017
R14,A4, D5	0.060	0	0	1.04	5.23	78	0.01
R15,A4, D5	0.088	45.8	15	1.22	6.10	78	0.45
R13,A4, D5	0.078	10.4	0	1.11	5.55	72	0.063
R14,D5,D6	0.110	2.1	0	1.32	6.62	62	0.009
R15,D5,D6	0.075	6.2	0	0.92	4.61	34	0.03
R13,D5,D6	0.116	2.1	0	1.38	6.91	60	0.017
A4,D5,D6	0.157	6.2	0	1.84	9.24	76	0.043

[a] Pharmacophore features combination obtained from structure based approach.

[b] Goodness of fit.

[c] % of active at 10% of the decoy data set.

[d] Enrichment factor at 1% of the decoy data set.

[e] Overall enrichment factor.

[f] % yield of actives.

[g] Overall % of active retrieved from the decoy data set.

[h] Boltzmann-enhanced discrimination of receiver operating characteristic.

As shown in **Figure 5.4a** the graph represents the correlation between the pharmacophore features and EF. The results showed that the 5 point pharmacophore feature (R13, R14, R15, A3, D6), 4 point (R13, R14, R15, D6) and 3point (R15, A4, D5) pharmacophore models showed the highest enrichment at 1% (EF1%), while **Figure 5.4b** represented the correlation between the pharmacophore features and % of actives retrieved by each pharmacophore model. It also indicated that the 5 point (R13, R14, R15, A3, D6), 4 point (R13, R14, R15,

D6) and 3point (R15, A4, D5) as well as another 3 point (R15,A4, D6) pharmacophore were able to predict the actives, with a recovery rate of the known actives close to 70% in the total ranked decoy database. We also found a good correlation value of 0.7432 for EF1% versus BEDROC (α=20). **Figure 5.5** represents the correlation between EF1% and the BEDROC value.
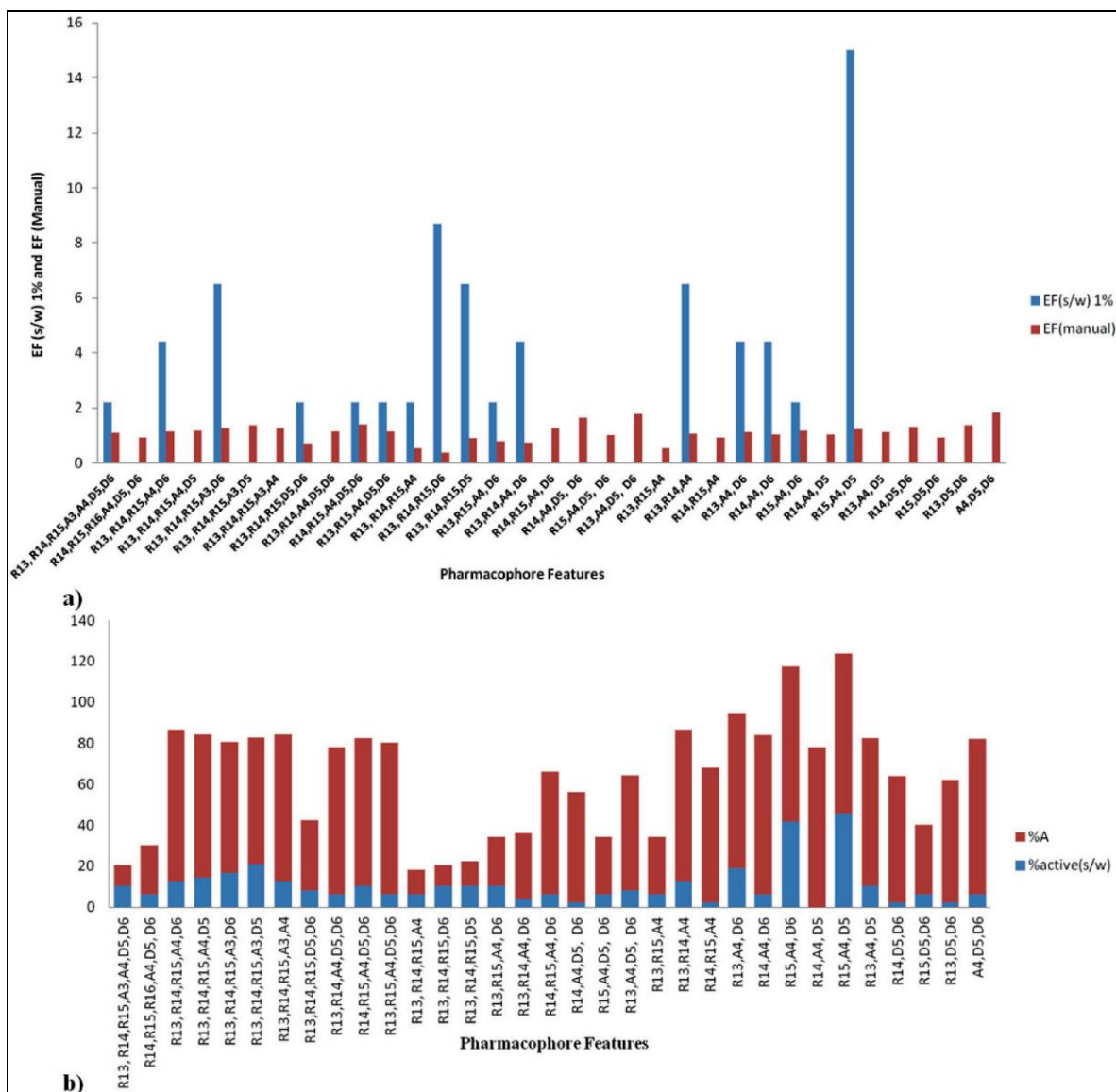
Figure 5.4: a) Enrichment values (EF1%) for the each pharmacophore model. **b)** The recovery rate of known actives from the constructed decoy database versus the Pharmacophore features.
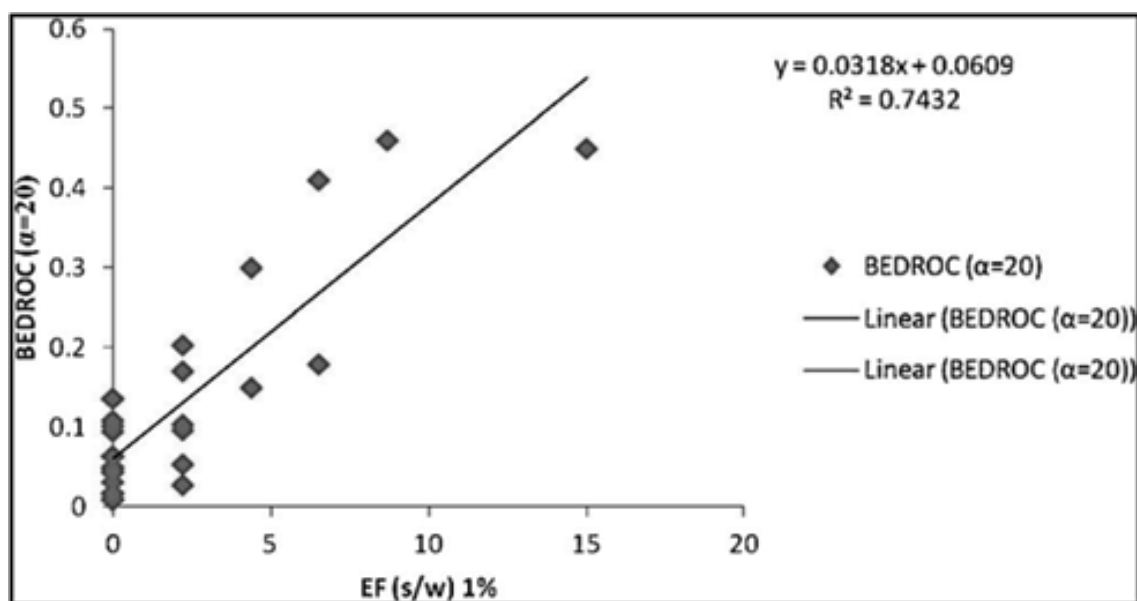
Figure 5.5: Correlation between EF1% and the BEDROC (α=20) value.

The overall results indicated that the three pharmacophore models generated from the crystal structures of *M. smegmatis* protein could differentiate the actives from the inactives. Based on the validation results, these pharmacophore models were further employed for thoroughly identifying potential hits.

5.1.1a.1.1d. Virtual screening

The basic goal of any virtual screening protocol would be to reduce enormous virtual chemical space of small organic molecules to a manageable number of compounds that could inhibit the protein. The top three pharmacophore models after validation were subjected to virtual screening of commercially available database (Asinex) following a protocol as summarized in **Figure 5.6.**
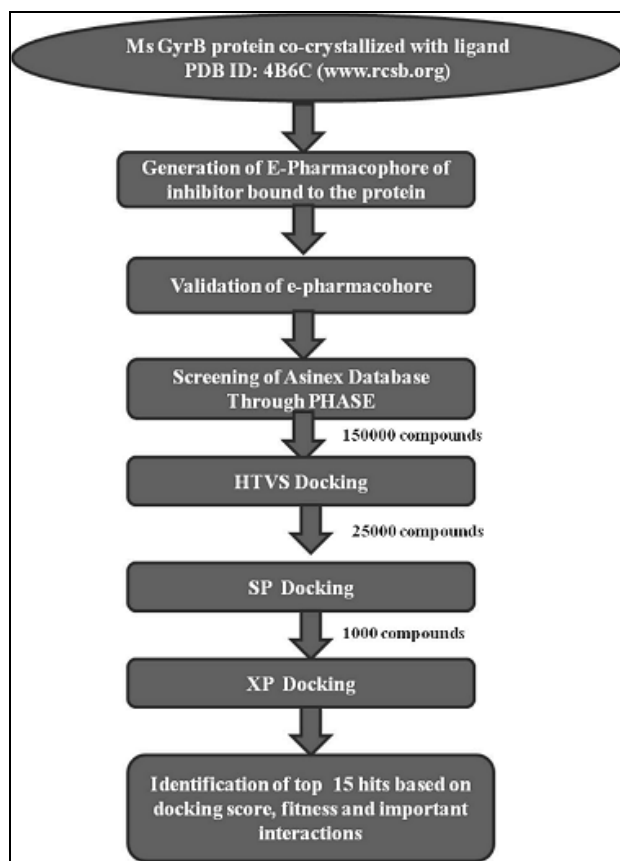
Figure 5.6: Virtual screening workflow.

The option implying "find matches" to the hypothesis in Maestro was employed for this step. Compounds retrieved by each e-pharmacophore models using phase with a fit value of above 1.5 were regarded as potential hits. Totally 150000 compounds from 500000 compounds were selected in this step. Further these compounds were carried forward for HTVS and top 25000 compounds were selected and were subjected to another round of docking by Glide SP. Finally top 1000 compounds from this screen resulting in a score of $\geq$ -6.0 kcal mol^{-1} with one or two hydrogen bonds were subjected to another round of docking by Glide XP. Glide XP combined accurate, physics-based scoring terms with thorough sampling, and the results gave scores ranging from -8.53 to -11.10 kcal mol^{-1}. Final short listing of possible lead compounds were based on visual inspection of the important amino acid residues involved in binding that included hydrogen bonding with Asp79 and *pi-stacking* with Arg82; analogous to the one observed with the crystal ligand and also hydrophobic interactions with Val123, Ile84, Val99, Pro85, and Phe199 amino acid residues were also preferred. In order to understand how these ligands bind to the enzyme, final hit molecules obtained from Glide XP were further evaluated with GOLD 5.1.2 program to confirm their potency. Further the top 50 hits were filtered based on drug-likeliness filter by using Qikprop module and the results are

presented in the **Table 5.3**. All the selected compounds passed the drug-likeliness filter having good permeability, solubility, absorbtion and these compounds were not violating the rule of five. Thus we had selected top fifteen compounds from the Glide XP docking study with no violations of drug likeliness properties with the best Glide scores (-8.00 to -11.23 kcal mol^{-1}) and GOLD scores (51.3-66.69), suggesting strong protein-ligand interactions. The chemical structures of these fifteen compounds are illustrated in **Figure 5.7**. All these top fifteen hits showed good docking score and interaction with important amino acids such as Asp79, Arg82 and also hydrophobic interaction with Val123, Ile84, Val99, Pro85, and Phe199 amino acid residues and were well fit in the active site cavity of the protein. The docking score, H-bond and important interactions of these hits can be seen in **Table 5.4**. Predicted binding pose of the all the identified hits with key interactions in the binding site of GyrB is represented in **Figure 5.8**.
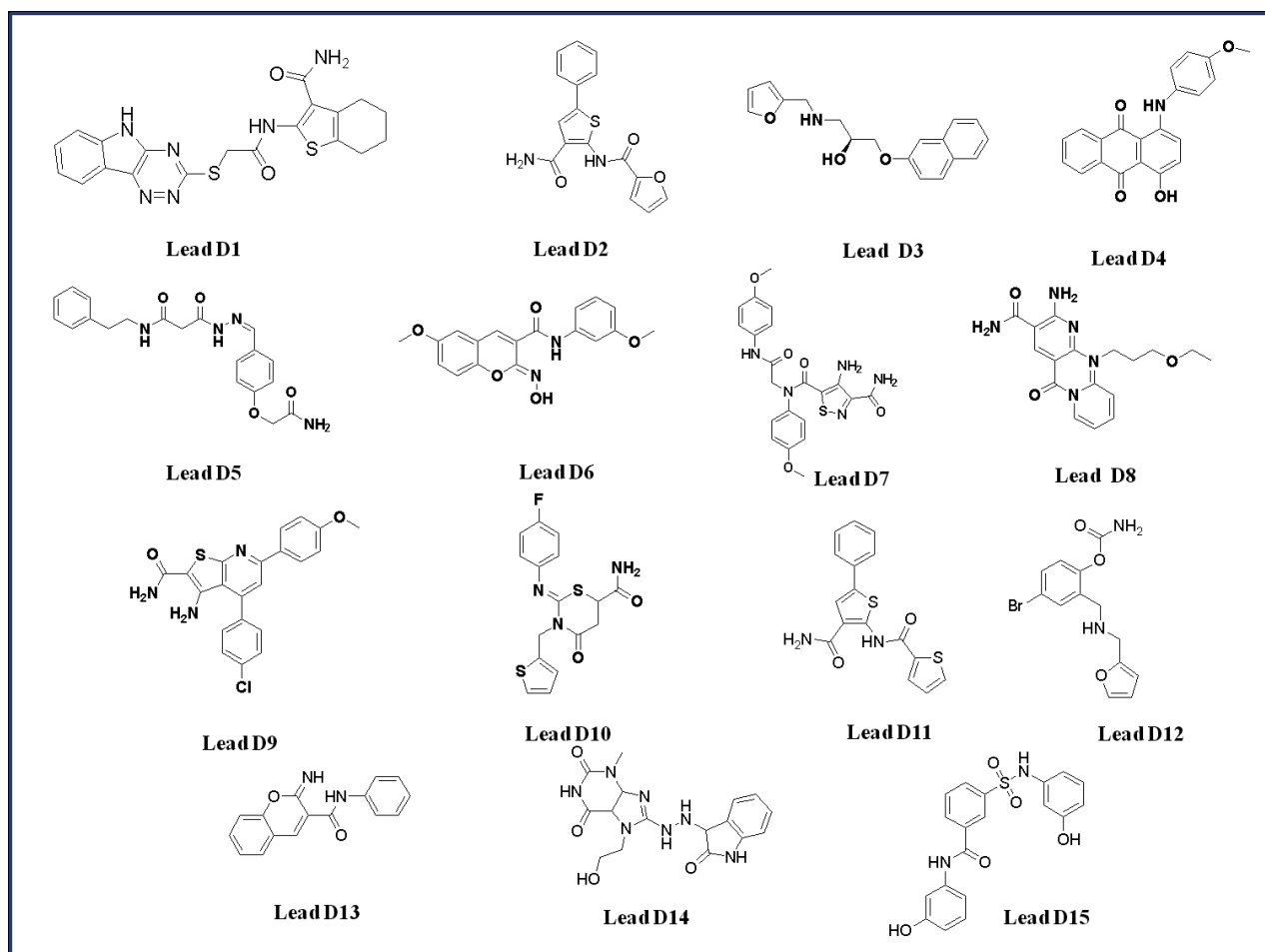
Figure 5.7: 2D chemical structures of top fifteen compounds.
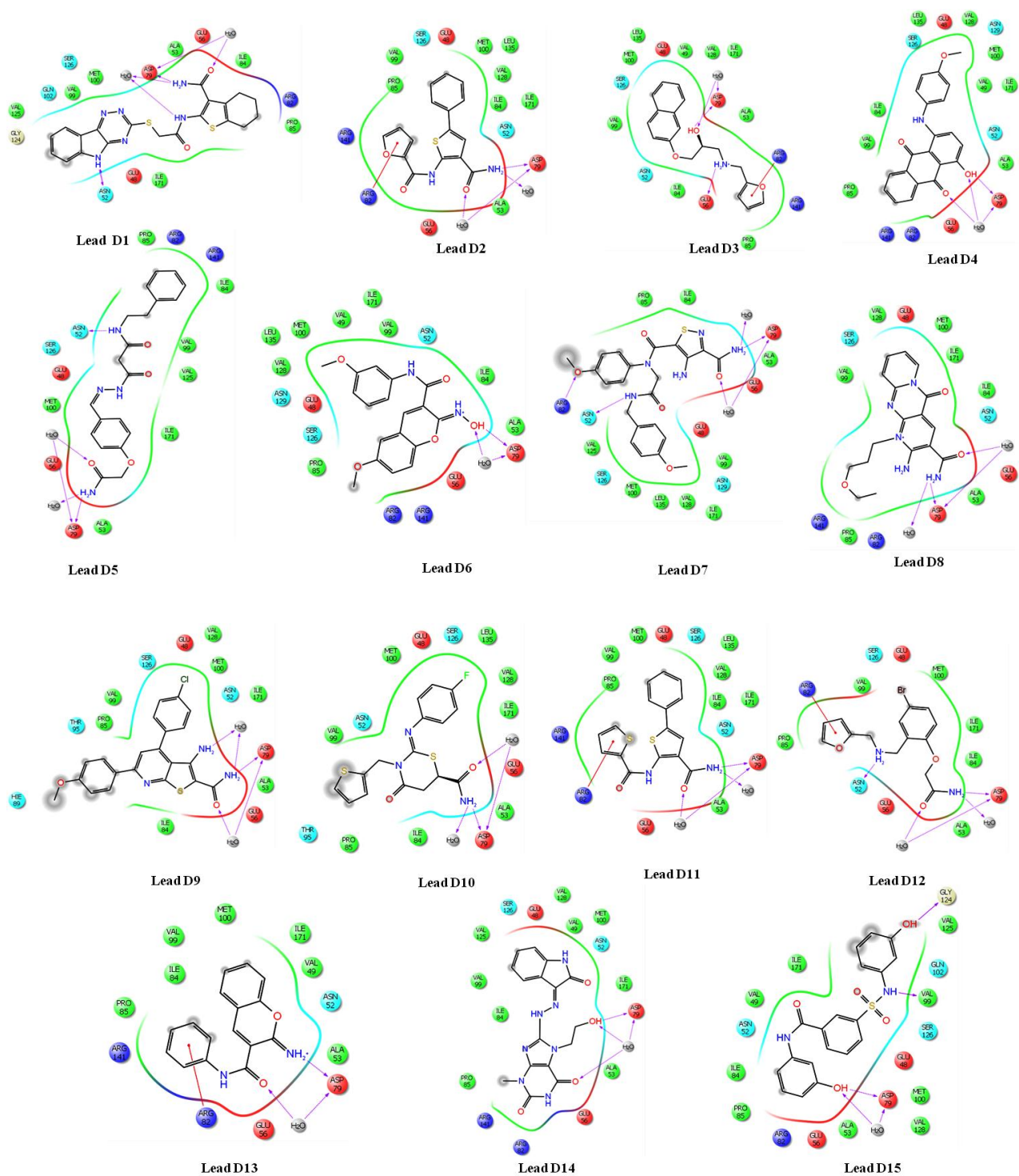
Figure 5.8: Ligand-protein interactions of all the hit with the active site residues of *M. smegmatis* protein.

Table 5.3: A QikProp analysis of the ADMET properties of the hits.

Properties	1	2	3	4	5	6	7	8	9	10	11	12	13	14	15	Range
QPPCaco	129.17	376.79	645.27	652.44	529.27	725.44	100	254.60	105.48	233.04	436.11	115.05	376.77	42.26	68.82	<25 poor, >500 great
QPlogBB	-1.62	-0.99	-0.11	-0.83	0.092	-0.99	-2.20	-1.52	-0.54	-0.79	-0.82	-0.23	-0.99	-2.15	-2.27	-3.0 to 1.2
QPlogpo/w	-2.95	2.69	3.11	-3.66	3.53	-2.30	0.95	-1.85	3.71	2.16	3.23	1.05	-2.69	0.022	1.55	−2.0 to 6.5
QPlogS	-5.0	-4.39	-3.28	-4.54	-3.6	-4.23	-2.98	-3.86	-4.93	-3.19	-4.93	-0.53	-4.01	-2.95	-4.28	<5.0
Percentage of human oral absorption	82.04	88.83	95.64	100	96.38	91.63	50.50	80.12	84.92	82.04	93.13	79.98	100	53.26	68.95	>80% high <25% poor
Rule of five violations	0	0	0	0	0	0	0	0	0	0	0	0	0	1	0	Concern above 1

Parameter range indicating value desired for drug like compound: **QPPCaco** – Predicted apparent Caco-2 cell (model for gut-blood barrier) permeability in nm/s. **QPlogBB** – Predicted brain/blood partition coefficient. **QPlogpo/w**- Predicted octanol/water partition co-efficient log p. **QPlogS-**- Predicted solubility. **Rule of 5 violations** – an orally active drug has no more than one violation of the rule of 5 criteria**.** Range indicates the values desired for drug-like compound.

Table 5.4: The docking score, fitness, hydrogen bond interaction and GOLD score of best fit ligands.

Compound Name	Docking score	Interactions	Fit value	GOLD Score
Lead D1	-10.36	Asp79, Asn52	1.79	66.69
Lead D2	-10.32	Asp79	2.18	62.83
Lead D3	-11.733	Asp79,Glu56	2.00	62.48
Lead D4	-9.91	Asp79	1.79	66.05
Lead D5	-10.33	Asp79, Asn52	1.95	60.1
Lead D6	-11.27	Asp79	1.79	55.9
Lead D7	-10.16	Asp79, Asn52, Arg82	1.98	58.34
Lead D8	-10.04	Asp79	1.60	66.87
Lead D9	-8.53	Asp79	1.28	58.26
Lead D10	-9.99	Asp79	1.74	65.23
Lead D11	-10.30	Asp79	2.11	62.12
Lead D12	-11.10	Asp79,Asn52	1.11	51.3
Lead D13	-9.11	Asp79	1.26	60.12
Lead D14	-9.37	Asp79,Gly83	1.77	61.12
Lead D15	-9.15	Asp79,Val99,Gly124	1.56	57.12

5.1.1a.1.2. Experimental validation of the virtual screening hits

The selected hits retrieved from the Asinex database were experimentally screened at a compound concentration of 50 µM against *M. smegmatis* GyrB as described in the material and method section. Compounds that displayed > 50% inhibition at 50 µM concentrations were re-screened at 25 µM inhibitor concentration. Out of 15 compounds five compounds exhibited promising activity at less than 10 µM and were studied in more detail in a dose response manner and further evaluated for biophysical evaluation using DSF technique.

5.1.1a.1.2a. Sequence similarity between GyrB of *M. tuberculosis* and *M. smegmatis*

The *M. tuberculosis* GyrB and GyrA proteins shared 63% and 69% similarity with the *E. coli* enzymes respectively [Reck F., *et al.*, 2011]. GyrB of *M. tuberculosis* shared 87.4% similarity with *M. smegmatis*; hence we used *M. smegmatis* as surrogate organism for *M. tuberculosis*.

The sequence alignment of the *M. smegmatis* (MYCSM) and *M. tuberculosis* (MYCTU) DNA GyrB have been done using CLUSTALW tool and the similarity score was 87.42.

The important amino acids responsible for the activity were Asp 79(D) and Arg 141(R) along with Arg 82 in *M. smegmatis*; these amino acids interact with the ligand directly *via* hydrogen bonding and cation *pi* stacking interactions respectively [Shirude P.S., *et al.*, 2013] (**Figure 5.9**). All these amino acids were conserved within the mycobacterium species ensuring that the *M. smegmatis* GyrB ATPase domain and *M. tuberculosis* GyrB ATPase domain were highly conserved and thus *M. smegmatis* DNA GyrB can be used as a surrogate enzyme for *M. tuberculosis* DNA GyrB. The other parameter which was included was the sequence similarity of the two organisms, DNA GyrB ATPase binding pockets. As per the DNA sequence information, recently the GyrB genes among the *M. tuberculosis* isolates showed an almost 99.9% homology with almost no changes in sequence, which further signified its applicability between the organisms.

The reason for the lower activity of *M. tuberculosis* GyrB could be because of the slow-growing mechanism of *M. tuberculosis* compared with *M. smegmatis*. Whilst performing the assay, we considered novobiocin as a standard inhibitor; furthermore, it gave a correlation of 3-5 fold variation in IC_{50} between the ATPase activity of *M. smegmatis* and the supercoiling activity of *M. tuberculosis*, and this had given us enough confidence to use *M. smegmatis* as a surrogate enzyme for DNA GyrB ATPase activity. [Jeankumar V.U., *et al.*, 2013].

```
sp|P0C559|GYRB_MYCSM    MAAQKNNAPKEYGADSITILEGLEAVRKRPGMYIGSTGERGLHHLIWEVVDNAVDEAMAG  60
sp|P0C5C5|GYRB_MYCTU    MAAQKKKAQDEYGAASITILEGLEAVRKRPGMYIGSTGERGLHHLIWEVVDNAVDEAMAG  60
                        *****::* .**** .*********************************************

                                          79  82
sp|P0C559|GYRB_MYCSM    FATRVDVKIHADGSVEVRNDGRGIPVEMHATGMPTIDVVMTQLHAGGKFDGETYAVSGGL  120
sp|P0C5C5|GYRB_MYCTU    YATTVNVVLLEDGGVEVANDGRGIPVATHASGIPTVDVVMTQLHAGGKFDSDAYAISGGL  120
                        :** *:* :   **.*** .******* **.*:**.************:.::**.****

                                      141
sp|P0C559|GYRB_MYCSM    HGVGVSVVNALSTRLEATVLHDGYEWFQYYDRSVPGKLKQGGETKETGTTIRFWADPEIF  180
sp|P0C5C5|GYRB_MYCTU    HGVGVSVVNALSTRLEVEIKHDGYEWSQVYEKSEPLGLRQGAPTKKTGSTVRFWADPAVF  180
                        ****************. : ****** * *.;:* *  ****. **:**:*;****** ;*

sp|P0C559|GYRB_MYCSM    ETTDYNFETVARRLQEMAFLNKGLTIELTDERVTAEEVVDDVVKDTAEAPKTADEKAAEA  240
sp|P0C5C5|GYRB_MYCTU    ETTEYDFETVARRLQEMAFLNKGLTINLTDERVTQDEVVDEVVSDVAEAPKSASERAAES  240
                        ***.*:.*****************;.****** ;****;**.*.*****;*.*;***;

sp|P0C559|GYRB_MYCSM    TGPSKVKHRVFHYPGGLVDYVKHINRTKTPIQQSIIDFDGKGPGHEVEIAMQWNAGYSES  300
sp|P0C5C5|GYRB_MYCTU    TAPHKVKSRIFHYPGGLVDFVKHINRTKNAIHSSIVDFSGKGTGHEVEIAMQWNAGYSES  300
                        *.* *** *.*********;*******..*:.**;**.***.*****************

sp|P0C559|GYRB_MYCSM    VMTFANTINTHEGGTHEEGFRAALTSVVNRYAKDKKLLKDKDPNLTGDDIREGLAAVISV  360
sp|P0C5C5|GYRB_MYCTU    VMTFANTINTHEGGTHEEGFRSALTSVVNRYAKDRKLLKDKDPNLTGDDIREGLAAVISV  360
                        *********************:************:*************************

sp|P0C559|GYRB_MYCSM    KVAEPQFEGQTKTKLGNTEVKSFVQKICNEQLQHWFEANPAEAKTVVNKAVSSAQARIAA  420
sp|P0C5C5|GYRB_MYCTU    KVSEPQFEGQTKTKLGNTEVKSFVQKVCNEQLTHWFEANPTDAKVVVNKAVSSAQARIAA  420
                        **;***********************:***** ******:;**.*************

sp|P0C559|GYRB_MYCSM    RKARELVRRKSATDIGGLPGKLADCRSTDPSKSELYVVEGDSAGGSAKSGRDSMFQAILP  480
sp|P0C5C5|GYRB_MYCTU    RKARELVRRKSATDIGGLPGKLADCRSTDPRKSELYVVEGDSAGGSAKSGRDSMFQAILP  480
                        ****************************** *****************************

sp|P0C559|GYRB_MYCSM    LRGKIINVEKARIDRVLKNTEVQSIITALGTGIHDEFDISKLRYHKIVLMADADVDGQHI  540
sp|P0C5C5|GYRB_MYCTU    LRGKIINVEKARIDRVLKNTEVQAIITALGTGIHDEFDIGKLRYHKIVLMADADVDGQHI  540
                        ***********************;**************;*********************

sp|P0C559|GYRB_MYCSM    STLLLTLLFRFMKPLVENGHIFLAQPPLYKLKWQRSEPEFAYSDRERDGLLEAGRAAGKK  600
sp|P0C5C5|GYRB_MYCTU    STLLLTLLFRFMRPLIENGHVFLAQPPLYKLKWQRSDPEFAYSDRERDGLLEAGLKAGKK  600
                        ************;**;****;***************.*****************   ****

sp|P0C559|GYRB_MYCSM    INVDDGIQRYKGLGEMDAKELWETTMDPSVRVLRQVTLDDAAAADELFSILMGEDVEARR  660
sp|P0C5C5|GYRB_MYCTU    INKEDGIQRYKGLGEMDAKELWETTMDPSVRVLRQVTLDDAAAADELFSILMGEDVDARR  660
                        ** ;**********************************************************;***

sp|P0C559|GYRB_MYCSM    SFITRNAKDVRFLDV  675
sp|P0C5C5|GYRB_MYCTU    SFITRNAKDVRFLDV  675
                        ***************
```

Figure 5.9: The sequence alignment of the *M. smegmatis* (MYCSM) and *M. tuberculosis* (MYCTU) DNA GyrB.

5.1.1a.1.2b. Enzyme kinetics of GyrB ATPase activity

Initially the rate at which the *M. smegmatis* DNA GyrB enzyme works was measured. The ATPase activity of enzyme generally followed greater than first-order kinetics. However at a constant enzyme concentration of 15 μM there was a hyperbolic dependence of rate on substrate (ATP) concentration because the GyrB ATPase activity of *M. smegmatis* did not follow Michaelis-Menten kinetics. The apparent KM_{app} and $Vmax_{app}$ determined experimentally were 300 μM and 2.1 μmol/s respectively (**Figure 5.10**).
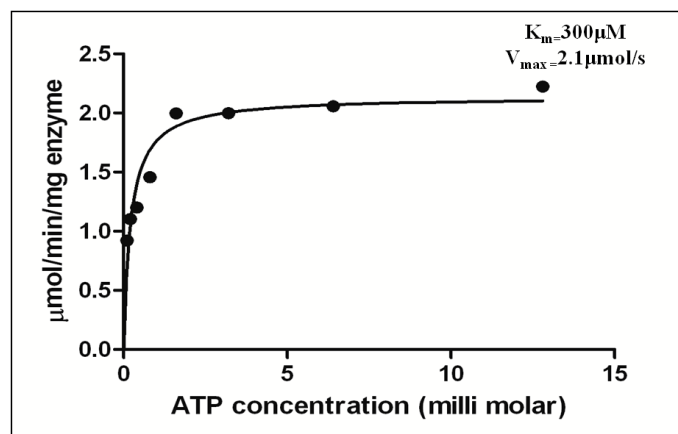
Figure 5.10: Enzyme kinetics of *M. smegmatis* GyrB protein.

5.1.1a.1.2c. *M. smegmatis* GyrB ATPase assay

To prove the design concept, the final hits were procured from Asinex database, and subjected to *in vitro M. smegmatis* GyrB ATPase assay. In this assay, novobiocin was used as a standard inhibitor which correlated with 3-5 fold variation in IC_{50} between the ATPase activity of *M. smegmatis* and the supercoiling activity of *M. tuberculosis*, and this had given us enough confidence to use *M. smegmatis* as a surrogate enzyme for DNA GyrB ATPase activity. The other parameters that were considered were sequence alignment between *M. smegmatis* and *M. tuberculosis* gyrase proteins, in which we found almost 87% identities that proved a higher degree of conservation in the ATP binding pocket of the two organisms. All of the fifteen compounds inhibited GyrB ATPase activity, with IC_{50} values ranging from 1.5-45.5 μM. The lead compound **D11** emerged as the most potent one with an IC_{50} of 1.5± 0.12 μM. Dose-response curves were plotted for the inhibitor **D11** using Graph Pad Prism software (Graph Pad Software Inc., La Jolla, CA) by taking log (inhibitor concentration) on the x-axis and response (% inhibition) on the y-axis as shown in **Figure 5.11**. The IC_{50}s of all the fifteen compounds against *M. smegmatis* GyrB ATPase assay is presented in **Table 5.5**.
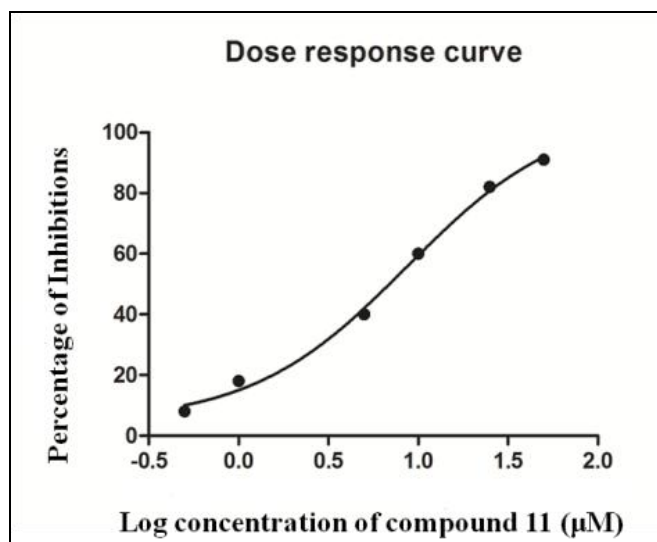
Figure 5.11: Dose response curve of most active compound **D11**.

5.1.1a.1.2d. *In vitro M. tuberculosis* **supercoiling assay**

All the fifteen compounds were further evaluated for their supercoiling inhibition. The supercoiling assay was an indirect measurement of their GyrB inhibitory potency as any inhibition of ATPase activity conferred by the DNA GyrB subunit should also inhibit the supercoiling activity performed by GyrA domain. Novobiocin was used as a positive control in these assays as it was shown to be a potent inhibitor of DNA supercoiling of mycobacterial DNA gyrase. Out of the 15 compounds tested, five compounds showed >40% inhibition in *M. tuberculosis* DNA gyrase supercoiling assay at 10 μM concentration. The most potential lead compound **D11** emerged as the most potent inhibitor having IC_{50} of 1.16±0.25 μM. The IC_{50} of the standard compound novobiocin was found to be 46±10 nM. The inhibitory profile of *M. tuberculosis* DNA gyrase supercoiling activity by lead compound **D11** is provided in **Figure 5.12**.
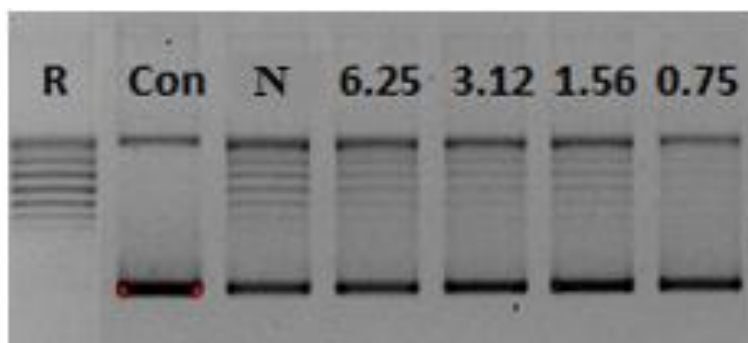
Figure 5.12: Inhibitory profile of *M. tuberculosis* DNA gyrase supercoiling activity by lead **D11**. A representative gel obtained from the analysis of the inhibition of DNA gyrase supercoiling activity as shown above. (R) represented relaxed closed circular DNA; (C) represented the supercoiled DNA in the presence of gyrase enzyme; novobiocin (N) shown as positive standard.

Table 5.5: Activity table showing the IC_{50} value of all the fifteen top hits obtained through virtual screening.

Compound Name	IC_{50} GyrB assay(µM)	IC_{50} Supercoiling assay(µM)
Novobiocin	**0.18±3.9**	**0.046±0.45**
Lead 1	51.4±1.42	13.9±0.36
Lead 2	6.7±0.23	4.92±0.55
Lead 3	8.6±0.44	11.9±0.47
Lead 4	44.87±0.94	>25
Lead 5	19.8±0.77	19±0.32
Lead 6	32.3±0.52	23.3±0.44
Lead 7	27±0.41	14.6±0.54
Lead 8	2.66±0.22	11.1±0.21
Lead 9	>50	>25
Lead 10	45.5±1.82	>25
Lead 11	1.5± 0.12	1.16±0.25
Lead 12	36.19±0.92	>25
Lead 13	>50	>25
Lead 14	6.3±0.33	3.125±0.24
Lead 15	>50	>25

5.1.1a.1.2e. Biophysical characterization

The interaction of the most potent analogue lead **D11** with the enzyme was further evaluated by measuring the thermal stability of the protein-ligand complex using biophysical DSF experiments. DSF measured the thermal stability of a target protein and a subsequent increase in protein melting temperature was due to the binding of a ligand to the protein. Positive shift of T_M corresponding to native protein indicated that stability was increased due to inhibitor binding. **Figure 5.13** shows the melting curve of compound **D11**. *M. smegmatis* protein showed a melting temperature of 46°C, whereas along with compound **D11** the corresponding T_M was found to be 49°C. A higher or positive shift of melting temperature (T_M) of protein-ligand complex compared to the native protein T_M signified a better stabilization of the protein-ligand complex, which in turn reflected on the inhibitor binding. The most potent analogue from the screening, compound **D11** displayed a Tm shift of 3°C which further was re-ascertained for its interaction with the GyrB protein and correlated with its GyrB IC_{50} of 1.5± 0.12 µM.
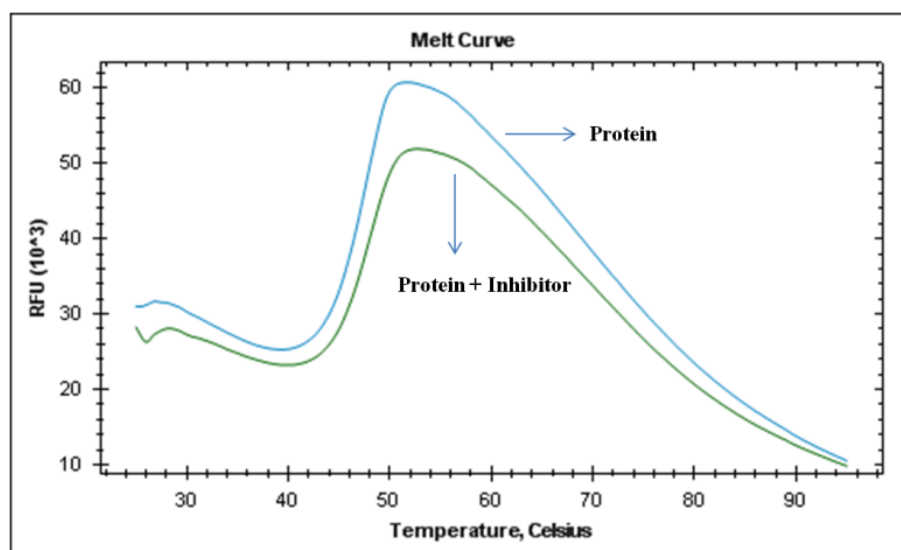
Figure 5.13: DSF experiment for compounds **D11** showing an increase in thermal stability between the native *M. tuberculosis M. smegmatis* protein (blue) and *M. tuberculosis M. smegmatis* protein-compounds complex (green).

5.1.1a.1.3. Highlights of the study

In this study, structure-based e-pharmacophore modeling was employed to identify structurally diverse, small molecule inhibitors of mycobacterial DNA GyrB using

aminopyrazinamide bound crystal structure of the protein. Fifteen compounds were identified, out of which, five molecules showed IC$_{50}$ in the range of <10 μM in *M. smegmatis* GyrB assay and in *M. tuberculosis* supercoiling activity seven compounds were found in the range of <15 mM. The best compound was found to be lead **D11** having IC$_{50}$ of 1.5±0.12 μM in *M. smegmatis* GyrB and 1.16±0.25 μM in *M. tuberculosis* supercoiling assay (**Figure 5.14**). Further their tight binding with the protein was biophysically confirmed by DSF. It was satisfying to see that the best inhibitory compound **D11** also showed a positive shift in DSF, indicating an increase in thermal stability of the inhibitor-protein complex that matched with its *in vitro* mycobacterial DNA gyrase B enzyme activity as well.
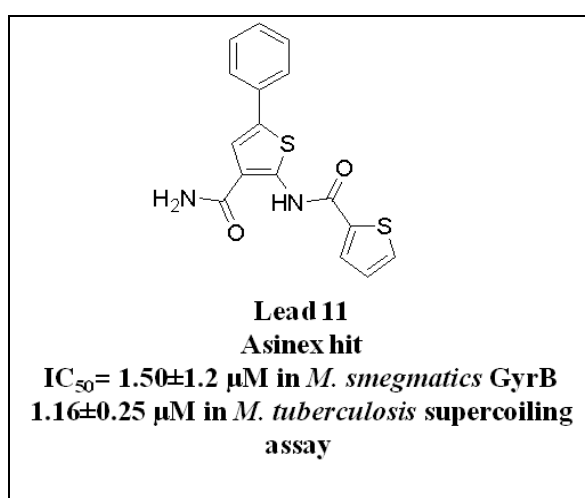
Figure 5.14: Identified most active **D11**.

5.1.1a.2. Design and development of GyrB inhibitor based on pyrrolamide bound protein (PDB ID: 4BAE)

5.1.1a.2.1. Design of inhibitors

In this study, we have again explored the e-pharmacophore approach, that efficiently utilized the aspects of energy based and the ligand based techniques to identify putative ligands that bind to the active site of mycobacterial ATPase domain using the crystal structure of the pyrrolamide (PDB entry 4BAE) bound to *M. smegmatis* GyrB ATPase as template[Hameed S.P., *et al.;* 2014]. An initial validation of the active site pocket was performed by re-docking the crystal 2-[4-(3-bromo-4-chloro-5-methyl-1H-pyrrole-2-amido)-3-methoxypiperidin-1-yl]-4-(1-methyl-1H-1,2,4-triazol-5-yl)-1,3-thiazole-5-carboxylic acid, with the active site residues of the *M. smegmatis* GyrB protein. Re-docking results showed that the compound

exhibited similar interactions as that of the original crystal structure which was further confirmed with RMSD of 1.45Å with a Glide score of -7.68 kcal/mol and was found in the vicinity of amino acids Asn52, Ile84, Val98, Val99, Asp79, Pro85, Glu56, Ala53, Ile17, Arg82, Arg141 and Gly83 amino acid residues (**Figure 5.15**).
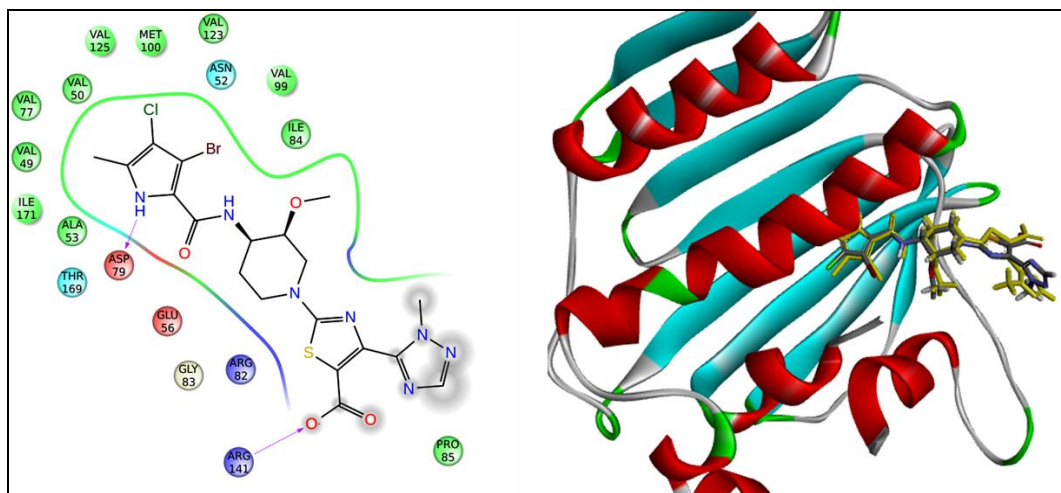
Figure 5.15: Interactions of reference inhibitor with the active site residues of *M. smegmatis* protein (4BAE) and superimposition of docked pose of the reference inhibitor to the original pose of the inhibitor.

The output file was used to identify a pharmacophore hypotheses to be further utilized for screening database compounds of Asinex. The pharmacophore hypotheses based on mapping of the energetic terms from the XP Glide scoring function (Glide, version 5.7, Schrödinger, LLC, New York, NY, 2011) onto atom centers was employed to derive pharmacophore sites. These were based on the structural and energy information between the protein and the ligand using phase (Phase, v3.3, Schrödinger, LLC, New York, NY). The initial number of pharmacophore sites was set up to 10. The docking result (Xpdes) was then imported to find the structure-based pharmacophoric features, which would help in finding the best featured functional groups. The results of the e-pharmacophore generation of the reference ligand used to identify the best pharmacophoric features are given in **Table 5.6**.

Table 5.6: Energy scores of hypothesis in e-pharmacophore.

Rank	Feature label	Score
1	N13[a]	-1.64
2	D6 [b]	-0.35
3	R15 [c]	-0.97
4	R16	-0.63

[a] Negative ionizable
[b] Donor
[c] Ring Aromatics

The maximum number of pharmacophore sites derived for the reference ligand was four with two R, one N, and D (**Figure 5.16**). The energy contribution for binding of ligand to the protein was the key to derive pharmacophoric features in structure-based design. On the basis of their energy scores, the least energy score feature (D) was removed and further utilized for the virtual screening of a commercial database (Asinex). Finally both 4-features (2R, 1N and 1 D) and 3- (2R and 1N) feature pharmacophore were utilized for virtual screening.
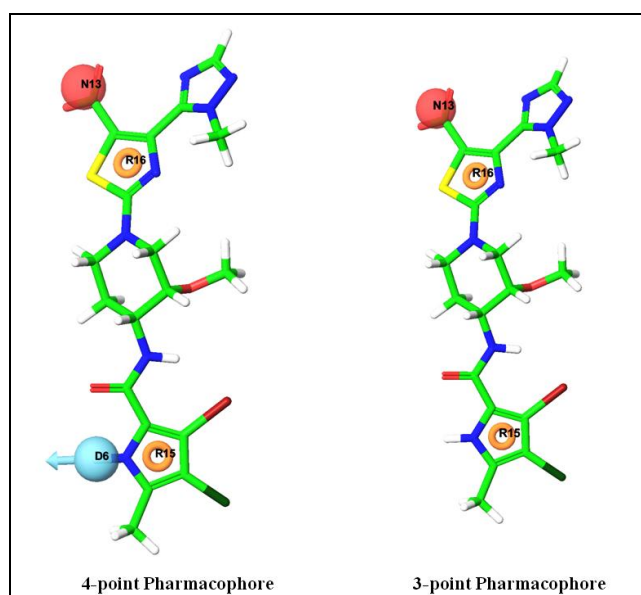
Figure 5.16: The energy based pharmacophoric features of the reference ligand bound to the protein.

Compounds retrieved by the e-pharmacophore model using phase with a fit value above 1.0 were regarded as potential hits and were carried forward for high-throughput virtual screening. Top compounds from this screen resulting in a score of $\geq$ -5.0 kcal mol^{-1} and

docked with one or more hydrogen bonds were subjected to another round of docking by Glide XP. The Glide XP combined accurate, physics-based scoring terms and thorough sampling, and the results gave scores ranging from -9.15 to -6.50 kcal mol^{-1}. Final short listing of possible hit compounds was based on visual inspection of the important amino acid residues in the active site cleft involved in binding that included hydrogen bonds to Asp79, Arg141, and Arg82. Top 10 hits were finally selected and presented in **Table 5.7** and **Figure 5.18**. Further the top hits were subjected to drug-likeliness filter by using Qikprop module because the molecular properties for absorption, distribution, metabolism, and excretion (ADME) were crucial for drug design. For oral administration, a drug must pass through intestinal cell membranes *via* passive diffusion, carrier-mediated uptake, or active transport processes before reaching the systemic circulation. The development of many potential drugs has been discontinued because of their poor absorption, thus we have checked the ADME properties of selected hits and results are presented in the **Table 5.8**. As shown in Table 5.8 all the molecules were passed the drug-likeliness filter having good permeability, solubility and absorption. Thus we selected top ten compounds from the Glide XP docking study with the best Glide scores (-9.15 to -7.15 kcal mol^{-1}) suggesting strong protein-ligand interactions. All the top ten hits showed good docking score and interaction with important amino acids such as Asp79, Arg141 and Arg82 (**Table 5.7**). The 2D representation of all the top hits is represented in **Figure 5.17**. These compounds were well fit in the active site cavity of the protein; the binding mode of all the identified compounds was represented in **Figure 5.18**. Further to prove the design concept, the final hits were procured from Asinex database, and screen against mycobacterial *M. smegmatis* enzyme activity.

Table 5.7: Shows the docking score, fitness, hydrogen bond interactions and GOLD score of best fit ligands.

Ligand	Fitness	Docking score	H-Bond	Interactions	Gold Score
Lead G1	1.82	-8.39	2	Asp79, Arg141	65.12
Lead G2	1.80	-7.61	2	Asp79, Arg141	60.67
Lead G3	1.78	-7.85	2	Asp79, Arg141	63.67
Lead G4	1.87	-7.15	3	Arg141,Gly83,Arg82	60.34
Lead G5	1.67	-7.93	3	Arg141,Gly83,Thr169	59.12

Contd.

Ligand	Fitness	Docking score	H-Bond	Interactions	Gold Score
Lead G6	1.56	-7.73	4	2Arg141,Arg82,Gly83	58.45
Lead G7	1.77	-7.47	2	Asp79, Arg141	67.23
Lead G8	1.71	-9.15	3	2Asp79,Gly83	65.12
Lead G9	1.77	-7.55	3	Asp79, Arg82,Gly83	61.45
Lead G10	1.56	-8.13	2	Asp79, Arg141	56.45
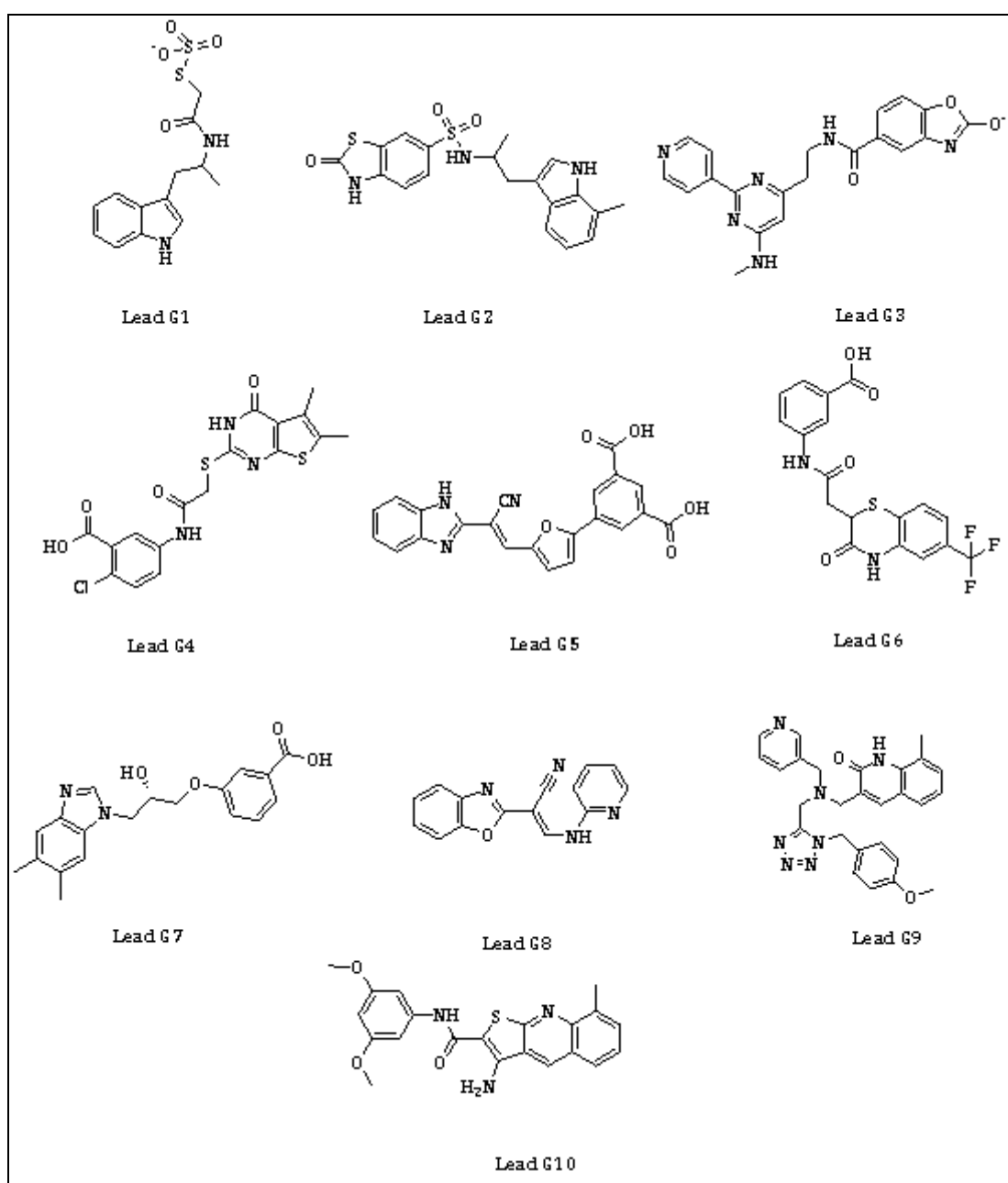
Figure 5.17: 2D chemical structures of top ten compounds.
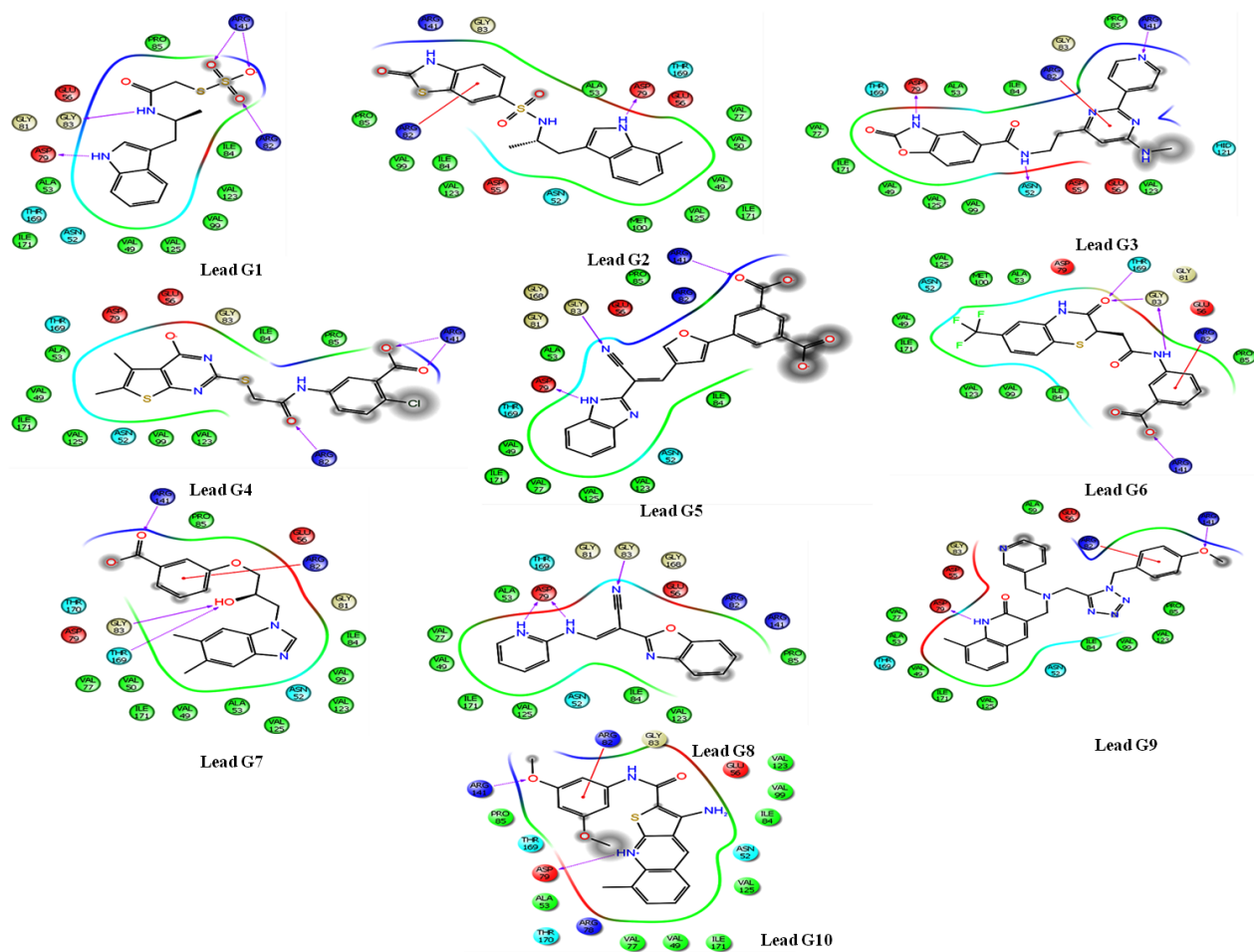
Figure 5.18: Binding mode of all the identified ten compounds in the active site of *M. smegmatis* protein.

Table 5.8: A QikProp analysis of the ADMET properties of the hits.

Properties	1	2	3	4	5	6	7	8	9	10	Range
QPPCaco	113.46	141.28	84.68	152.44	129.27	225.44	65	254.60	163.34	325.50	<25 poor, >500 great
QPlogBB	-1.91	-1.47	-2.14	-1.98	1.60	-0.84	-2.20	-1.52	-0.84	-0.22	-3.0 to 1.2
QPlogpo/w	-1.42	2.48	1.59	-2.80	2.82	-2.82	3.30	-3.30	3.35	3.84	−2.0 to 6.5
QPlogS	-2.75	-4.65	-4.69	-4.54	-3.6	-4.9	-4.78	-3.86	-4.93	-4.93	<5.0
Percentage of human oral absorption	85.51	79.90	70.97	80	96.38	91.63	78.50	80.12	86.12	94.50	>80% high <25% poor
Rule of five violations	0	0	0	0	0	0	0	0	0	0	Concern above 1

Parameter range indicating value desired for drug like compound: **QPPCaco** – Predicted apparent Caco-2 cell (model for gut-blood barrier) permeability in nm/s. **QPlogBB** – Predicted brain/blood partition coefficient. **QPlogpo/w**- Predicted octanol/water partition co-efficient log p. **QPlogS**-- Predicted solubility. **Rule of 5 violations** – an orally active drug has no more than one violation of the rule of 5 criteria. Range indicates the values desired for drug-like compound.

5.1.1a.2.2. Experimental validation of the virtual screening hits

The selected hits retrieved from the Asinex database were experimentally screened at a compound concentration of 50 μM against *M. smegmatis* GyrB as described in the materials and method section. Compounds that displayed > 50% inhibition at 50 μM concentration were re-screened at 25 μM inhibitor concentration. Out of ten compounds, five compounds exhibited promising inhibition and their IC_{50} was calculated and found to be in the range of 4.61± 0.1μM to 73.67±0.4μM.

5.1.1a.2.2a. *M. smegmatis* GyrB ATPase assay

All the ten compounds were experimentally screened for the GyrB inhibitory potency against *M. smegmatis* GyrB protein using the malachite green assay by the protocol described in the material and methods section. The IC_{50} of all the ten compounds in the *M. smegmatis* GyrB assay was found in the range of 4.61± 0.1 μM to 73.67±0.4 μM.The most promising compound from the *in vitro* GyrB assay was 5-{5-[(1E)-2-(1H-1,3-benzodiazol-2-yl)-2-cyanoeth-1-en-1-yl]furan-2-yl}benzene-1,3-dicarboxylicacid (**Lead G5**) having IC_{50} of 4.61 ± 0.1μM in *M. smegmatis* GyrB assay.
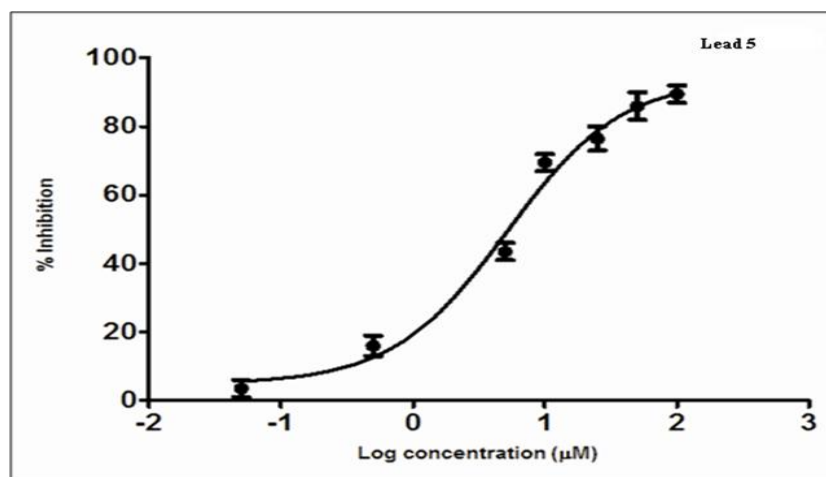
Figure 5.19: Dose-response curve of Lead **G5**.

5.1.1a.2.2b. *In vitro M. tuberculosis* supercoiling assay

Later these molecules were also evaluated for their *in vitro M. tuberculosis* supercoiling assay. In general a good correlation was observed between the *in vitro* GyrB potency and *in*

vitro supercoiling activity. The IC_{50} of all the ten compounds in the *M. tuberculosis* supercoiling assay was found in the range of 5.1 ± 0.2 µM to 73.67 ± 0.4 µM (**Table 5.9**).The most potent compound in the GyrB assay **G5** showed a well synchronizing supercoiling inhibitory IC_{50} of 5.1 ± 0.2 µM (**Figure 5.20**); reconfirming our earlier findings, as any inhibition of ATPase activity conferred by the DNA GyrB subunit should also inhibit the supercoiling activity performed by GyrA domain.
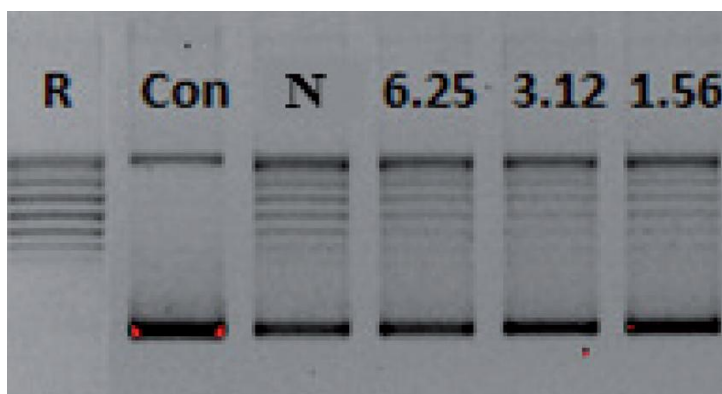
Figure 5.20: The inhibitory profile of *M. tuberculosis* DNA gyrase supercoiling activity by lead compound **G5.**

Table 5.9: Activity table showing the IC_{50} value of all the top hits obtained through virtual screening.

Compound Name	IC_{50} GyrB assay(µM)	IC_{50} Supercoiling assay(µM)
Novobiocin	**0.18±3.9**	**0.046±0.45**
Lead G1	7.32±1.3	8.12±1.3
Lead G2	6.71±0.8	7.12±0.12
Lead G3	10.61±0.5	12.12±0.4
Lead G4	6.81±0.1	7.12±0.8
Lead G5	4.61±0.1	5.1 ± 0.2 µM
Lead G6	9.32±0.1	10.12±1.3
Lead G7	73.67±0.4	>25
Lead G8	70.12±0.5	>25
Lead G9	45.12±0.7	>25
Lead G10	55.0±1.5	>25

5.1.1a.2.2c. Biophysical Characterization

Furthermore, the binding affinity of the most potent analogue was evaluated by measuring the thermal stability of the protein-ligand complex using biophysical differential scanning fluorimetry experiments (**Figure 5.21**). Compound **G5** displayed a T_M shift of 2.5°C (T_M = 48.5°C) compared with the native protein (T_M = 46°C), a repercussion of strong binding of the ligand to the protein and highly correlated with its GyrB IC_{50} of 4.61 ± 0.1 µM.
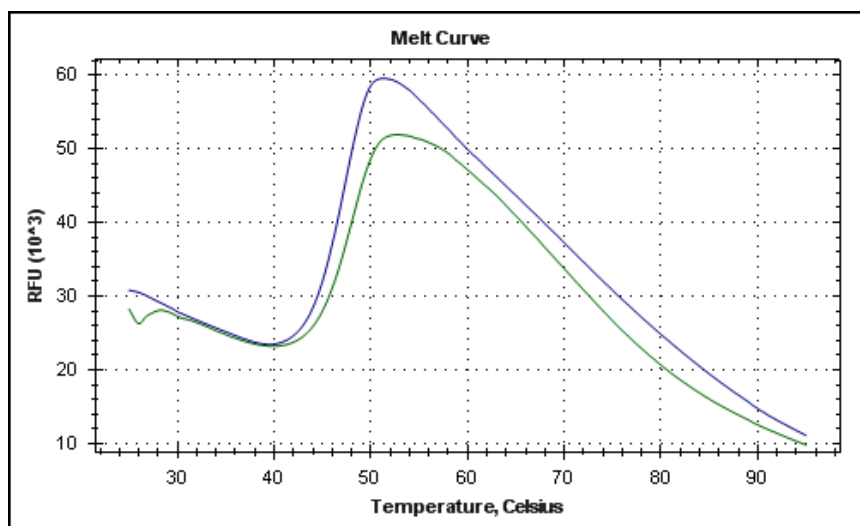
Figure 5.21: DSF experiment for compound **G5** showing an increase in thermal stability between the native *M. smegmatis* protein (green) and *M. smegmatis* protein-ligand complex (blue).

5.1.1a.2.3. Highlights of the study

In this study, structure based e-pharmacophore modeling was used as a template to identify diverse small molecule inhibitors of mycobacterial DNA gyrase B using crystal structure of the pyrrolamides (PDB entry 4BAE) bound to *M. smegmatis* GyrB ATPase as template. Ten compounds were identified, out of which, five molecules showed IC_{50} in the range of <10 µM in *M. smegmatis* GyrB assay and in *M. tuberculosis* supercoiling activity six compounds were found in the range of <15 µM. The best compound was found to be lead **G5** having IC_{50} of 4.61 ± 0.1 µM µM in *M. smegmatis* GyrB and 5.1 ± 0.2 µM in *M. tuberculosis* supercoiling assay (**Figure 5.22**). Further their tight binding with the protein was biophysically confirmed by DSF.
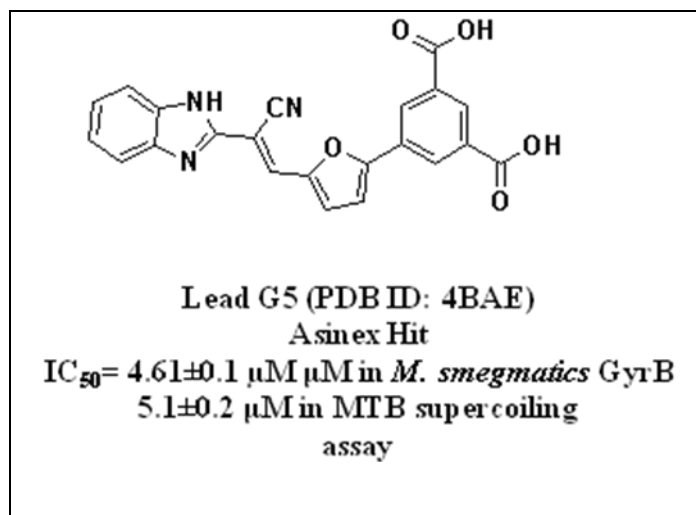
Figure 5.22: Identified most active lead **G5**.

5.1.1b. Inhibitors developed using ligand based drug design approach

The development of a quantitative pharmacophore model using CATALYST/HypoGen software for structurally diverse set of reported GyrB inhibitors with an aim to obtain 3D-pharmacophore model that could provide a rational hypothetical model based on the primary chemical features responsible for GyrB inhibitory activity was attempted. A total set of 61 GyrB *M. smegmatis* inhibitors with an activity range of 3.97 order of magnitude (IC$_{50}$ 0.0026 to 24.67 µM) were used for pharmacophore modeling studies. The term "pharmacophore" has become one of the most popular word in medicinal chemistry. Many authors use the term "pharmacophores" to define functional or structural elements possessing biological activity. This does not correspond to the official definition elaborated by an IUPAC working groups and published in 1998 which states that a pharmacophore is the ensemble of steric and electronic features that is necessary, to ensure the optimal supra molecular interactions with a specific biological target structure and to trigger (or to block) its biological response. A pharmacophore can be considered as the highest common denominator of a group of molecules exhibiting a similar pharmacological profile, through interactions at the same site of the target protein.

5.1.1b.1. Collections of data set and molecular modeling

A total set of 61 GyrB *M. smegmatis* inhibitors with an activity range of 3.97 order of magnitude (IC$_{50}$ 0.0026 to 24.67 µM) was used for pharmacophore modeling studies [Sandeep R.G., *et al*., 2009 and Shahul H.P., *et al*., 2012]. This dataset was divided into

training set of 19 compounds and test set of 42 compounds. Pharmacophore modelling was carried out using the HypoGen module implemented in Catalyst software.

5.1.1b.2. Training and test set selection and conformational models

In the selection of the training set, some basic requirements namely the activity range in the total set (3-4 orders of magnitude) and the presence of maximum structural information were considered. Thus, the most active, moderately active, and some inactive compounds were included in the training set in order to obtain critical information on pharmacophoric requirements. The training set of 19 compounds (**Figure 5.23**) with IC_{50} of 0.0026 to 24.67 μM was used to generate HypoGen hypotheses featuring quantitative predictive character. The test set of the remaining 42 compounds (**Figure 5.24**) was used to validate the statistically best pharmacophore model. All the structures were minimized to the closest local minimum using the CHARMm force field and the conformational analysis for each molecule was performed using the poling algorithm, in which the number of conformers was limited to a maximum value of 255 using 'best conformers generation' option with 20 kcal/mol energy cutoff. The compounds associated with their conformational models were then submitted to Catalyst for generation of hypotheses.
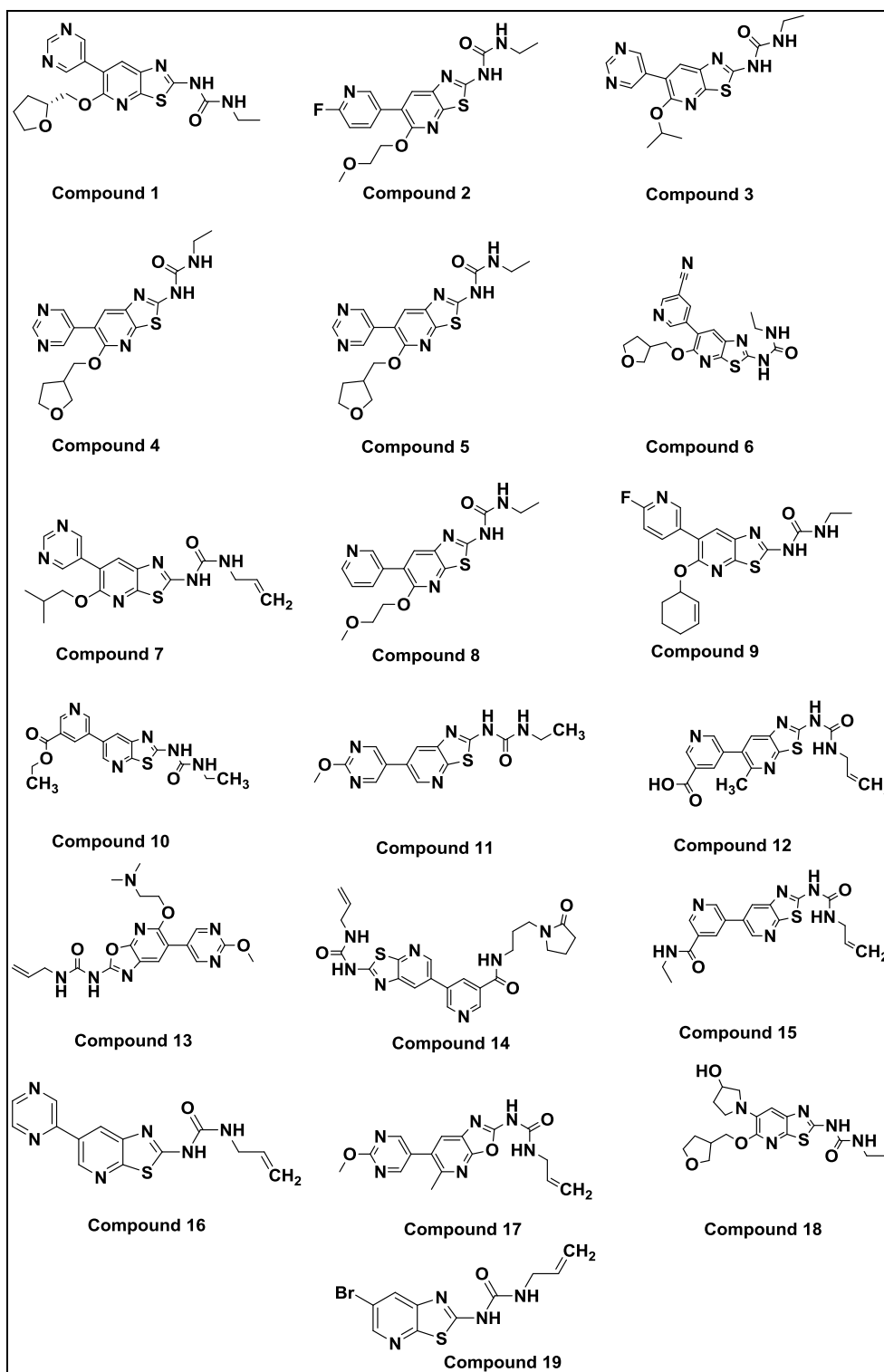
Figure 5.23: Chemical structures of the 19 training set compounds.
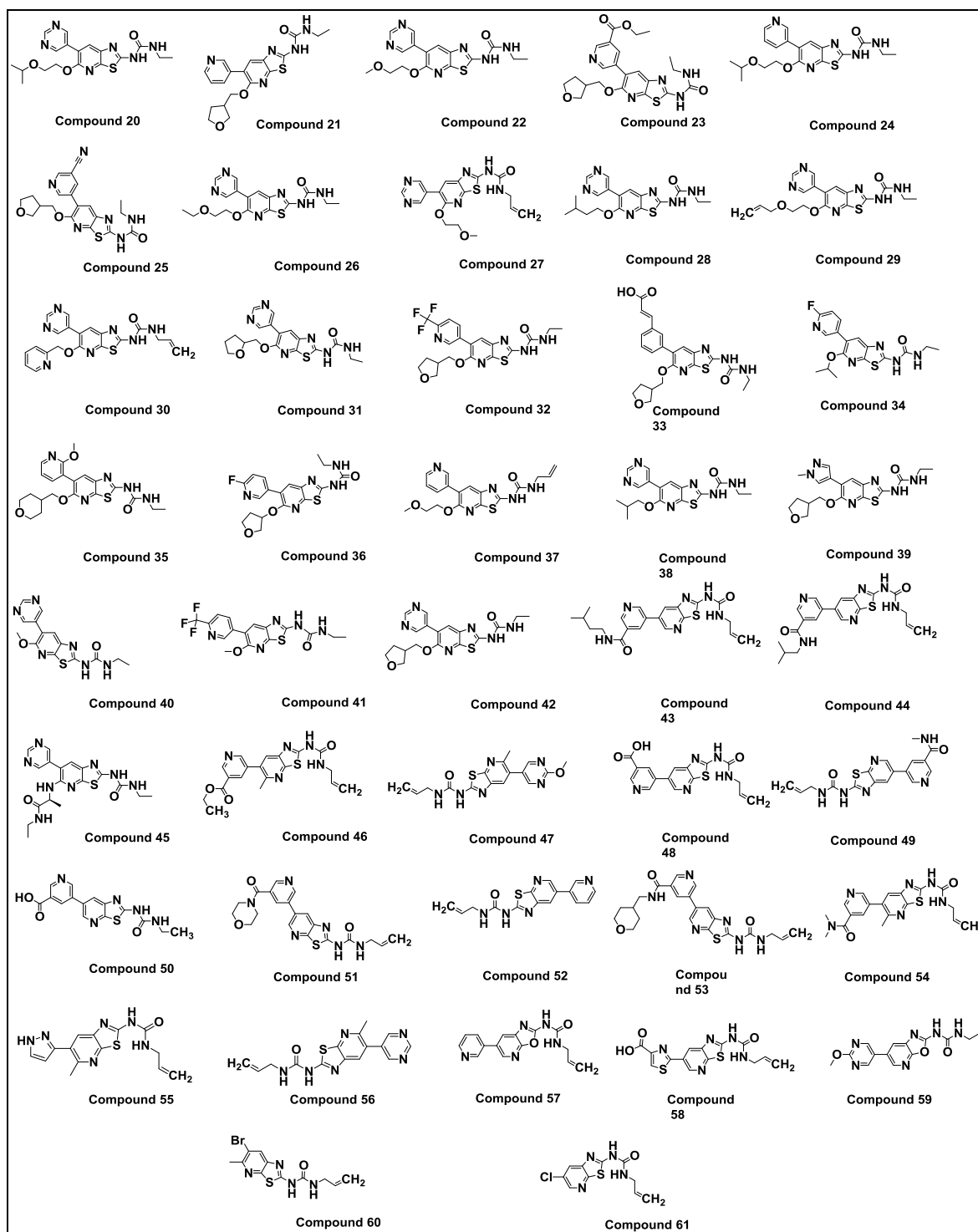
Figure 5.24: Chemical structures of the 42 test set compounds.

5.1.1b.3. Pharmacophore modelling

A set of 10 pharmacophore hypotheses were generated using the training set of 19 compounds. All the 10 generated hypotheses were found to have four features comprising one or two HBA, HBD, RA and HY-AR features. The top ranked pharmacophore hypotheses (Hypo-1 and 2) were characterized with high cost difference (23.43), low RMSD (0.665), along with highest correlation coefficient (0.952). Both the hypotheses (Hypo-1 and 2) also showed good prediction of the 42 test set compounds (Q_2 pred =0. 639 and 0.699) respectively. Finally based on the chemical feature similarities, statistical significance and predictive values for test set, Hypo-2 was considered further to be utilized in database screening. Among the generated pharmacophore models, based on the training set of 19 compounds (**Figure 5.25**), Hypo-2 consisted of five pharmacophoric features including two HBA, one RA and one HY-AR (**Figure 5.25**). The results of the top 10 pharmacophore models are summarized in **Table 5.10**.
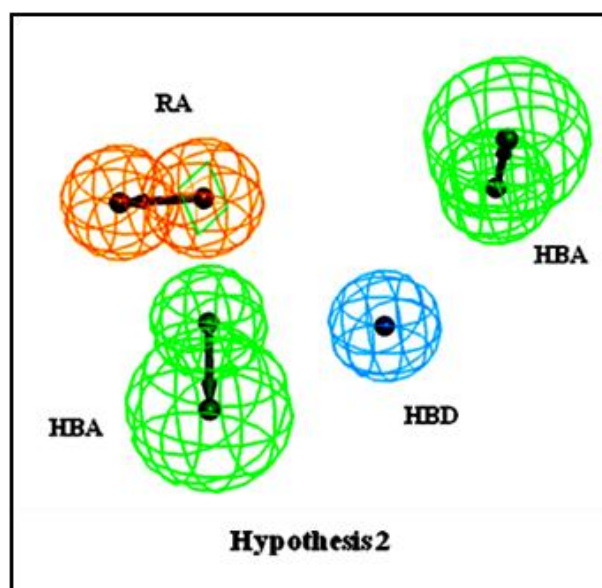
Figure 5.25: The best hypothesis model Hypo 2 produced by the HypoGen module in Catalyst 3.5 software. Pharmacophore features consisting of two HBA, RA, HY-AR.

Table 5.10: Information of statistical significance and predictive power of top 10 hypotheses of training set compounds.

Hypothesis	Features[a]	Total cost	Δ-cost	RMS[b]	Correlation (r)
1	2HBA, RA, HY-Ar	85.7946	23.432	0.6651	0.9524
2	2HBA,RA, HY-Ar	85.9538	23.273	0.6696	0.9519
3	HBA, HBD, RA, HY- Ar	86.3791	22.848	0.7097	0.9457
4	2HBA,RA, HY- Ar	86.6081	22.619	0.7258	0.9431
5	HBA, HBD, RA, HY- Ar	86.7805	22.447	0.7378	0.9412
6	2HBA, HBD, HY- Ar	86.98	22.247	0.7462	0.9399
7	2HBA, HBD, HY- Ar	87.3456	21.881	0.7548	0.9387
8	HBA, HBD, RA, HY- Ar	87.3851	21.842	0.7692	0.9361
9	HBA, HY- Ar, HY, RA	87.4626	21.764	0.7790	0.9343
10	HBA, 2HY, RA	87.5369	21.690	0.7885	0.9326

Null cost 109.227; fixed cost 81.5902; configuration cost 16, Cost difference (Δ-cost) = null cost- total cost, [a] HBA, hydrogen-bond acceptor; HBD, hydrogen-bond donor; HY, hydrophobic group; RA, ring aromatic, [b] RMS (root mean square), the deviation of the log (estimated activities) from the log (measured activities) normalized by the log (uncertainties)

All the training and test set compounds were classified based on their activity as high ($\leq$0.0025µM), moderate (0.0025-2.18 µM) and less active (>2.18 µM) in order to verify the predictive ability of Hypo-2. The ability of the selected pharmacophore hypothesis to distinguish the active compounds from the inactive ones was analyzed using the experimental and estimated activities of the training set compounds. The experimental and the estimated activity values of the training set compounds are given in **Table 5.11**. The results showed that, all compounds in the training set were estimated within their activity scale. All the high active compounds were predicted as high active, and all 12 moderate active compounds were predicted as moderate active whereas the last one inactive compound was predicted as less active. The correlation graph between experimental and estimated activity of all the 19 training set compounds were shown in **Figure 5.26**.

Table 5.11: Experimental and estimated IC_{50} values of the training set compounds based on the pharmacophore model Hypo-2.

Compound	Experimental activity IC_{50} (µM)	Estimated activity IC_{50} (µM)	Error[a]	Fit value[b]	Status
1	0.0026	0.0066	+2.5	6.82	active
2	0.0045	0.0042	-1.1	7.02	active
3	0.0052	0.0085	+1.6	6.72	active
4	0.0075	0.0078	+1	6.75	active
5	0.0098	0.0078	-1.3	6.75	active
6	0.014	0.012	-1.1	6.55	active
7	0.018	0.0059	-3.1	6.88	active
8	0.025	0.0091	-2.8	6.68	moderately active
9	0.029	0.022	-1.3	6.30	moderately active
10	0.051	0.22	+4.3	6.50	moderately active
11	0.14	0.49	+3.5	4.95	moderately active
12	0.17	0.22	+1.4	5.29	moderately active
13	0.22	0.42	+1.9	5.02	moderately active
14	0.3	0.32	+1.1	5.13	moderately active
15	0.4	0.33	+1.2	5.13	moderately active
16	0.84	0.5	-1.7	4.95	moderately active
17	1.6	2.4	+1.5	4.27	moderately active
18	2.1	0.71	-3	4.79	moderately active
19	25	10	-2.5	3.64	Inactive

[a] (+) indicated that predicted IC_{50} was higher than experimental IC_{50}; (-) indicated that predicted IC_{50} was lower than experimental IC_{50}.

[b] Fit value indicated how well feature of the pharmacophore (Hypo-1) overlapped the chemical feature in the compound.
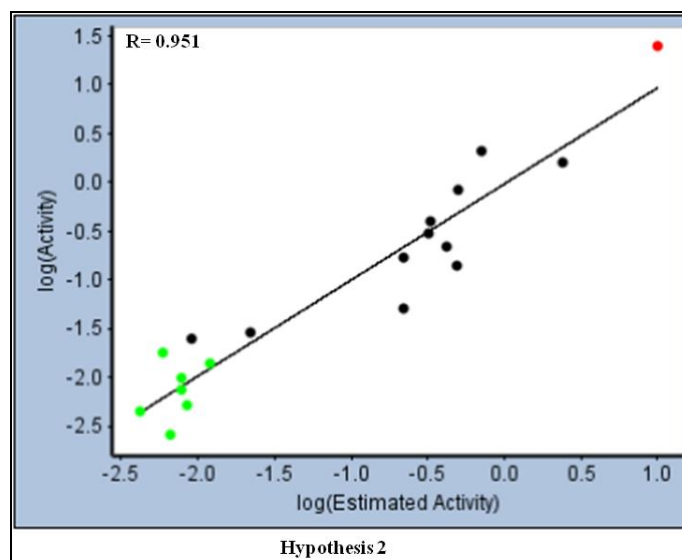
Figure 5.26: Correlation between experimental and estimated activity of 19 training set compounds based on Hypo-2.

5.1.1b.4. Cost analysis

In this study the cost difference between the fixed cost and total cost values of Hypo-2 was found to be 4.2, whereas between the null cost and the total cost value of Hypo-2 was 23.27. A good pharmacophore hypotheses should also have the configuration cost <17 and it was 16.55 for the selected pharmacophore hypothesis Hypo-2. The RMSD represented quality of the correlation between the estimated and the experimental activity data and the ideal value should be <1. For Hypo-2 the RMSD value was found to be 0.665 which indicated a good correlation between the estimated and the experimental activities. High correlation with good cost difference, low RMSD and configuration cost demonstrated a reliable pharmacophore hypothesis with high predictive ability. **Figure 5.25** presents the best pharmacophore hypotheses Hypo-2.

As the error ratio between the experimental and estimated GyrB *M. smegmatis* activities was less than 10 (**Table 5.11**), which was within the acceptable range. Positive error value would be obtained if the estimated activity was greater than the experimental activity and negative value would be obtained if the estimated activity was lesser than the experimental value. In our study, Hypo-2 was found to have predicted all the training set compounds with error values less than 10 and thus showed that Hypo-2 was able to predict the training set compounds accurately.

Overlay of the most active and the least active compounds in the training set on Hypo-2 is presented in **Figure 5.27**. The most active compound **1** mapped correctly on all the four pharmacophoric features of Hypo-2 whereas the least active compound **19** showed feature mapping only on two out of four features. The most active compound showed good fitness with all features of the pharmacophore hypothesis Hypo-2. In the least active compound **19**, it was observed that one RA and one HBA group were missing. Based on these results, it was concluded that the RA and HBA features were important for GyrB *M. smegmatis* inhibitory activity.

A) Most Active compound 1 in the training set   **B) Inactive compound 19 in the training set**
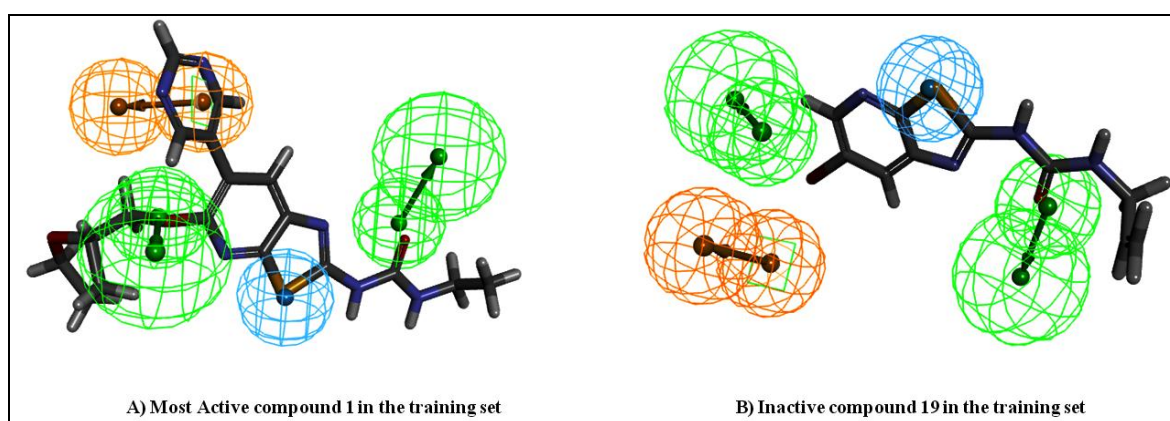
Figure 5.27: Hypo-2 mapped, on the most active compound, 1 (IC_{50}=0.0026 µM), and on the least active compound, 19 (IC_{50}=24 µM), in the training set. Pharmacophore features: hydrogen bond acceptor (HBA); ring aromatics (RA); hydrophobic aromatics (HY-AY).

5.1.1b.5. Validation of pharmacophore hypotheses

5.1.1b.5.1. Test set

In order to determine whether the hypothesis could be utilized for predicting the activity of compounds that were structurally distinct from those included in the training set, an internal test set of 42 compounds was used to check the predictive ability of the Hypo-2. Experimental and estimated activities of the test set compounds are shown in the **Tables 5.12**. The best pharmacophore model Hypo-2 performed well in classifying active and inactive compounds correctly, with a significant predictive R^2 [$R^2_{pred\ test}$] value of 0.7833 for the 42 test set compounds. The test set compounds were mapped onto the best pharmacophore hypotheses (Hypo-2). The predictive ability of Hypo-2 was very impressive with a correlation coefficient value (R^2=0.7833).

Table 5.12: Experimental and estimated IC_{50} values of the test set compounds based on the pharmacophore model Hypo-2.

Compound	Experimental activity IC_{50} (μM)	Estimated activity IC_{50} (μM)	Error[a]	Fit value[b]
20	0.028	0.0075	-3.68	6.7628
21	0.0048	0.0076	+1.5	6.7602
22	0.0175	0.0083	-2.08	6.7195
23	0.0266	0.0085	-3.11	6.7112
24	0.0091	0.0086	-1.05	6.7071
25	0.0124	0.0091	-1.35	6.6813
26	0.02	0.0092	-2.16	6.6778
27	0.0603	0.0093	-6.43	6.6711
28	0.0117	0.0093	-1.25	6.6700
29	0.0171	0.0095	-1.793	6.6623
30	0.0280	0.0096	-2.91	6.6588
31	0.0048	0.0104	+2.14	6.6249
32	0.0069	0.0104	+1.51	6.6234
33	0.0352	0.0106	-3.30	6.6153
34	0.01	0.0107	+1.07	6.6121
35	0.0047	0.0109	+2.30	6.6046
36	0.0035	0.0109	+3.10	6.6027
37	0.0465	0.0119	-3.88	6.5639
38	0.0043	0.0131	+2.99	6.5244
39	0.0249	0.0141	-1.76	6.4922
40	0.0215	0.0258	+1.19	6.2309
41	0.0029	0.0283	+9.77	6.1903
42	0.0077	0.0421	+5.43	6.0181
43	0.5834	0.3378	-1.72	5.1142
44	0.3945	0.3595	-1.09	5.0871
45	0.0158	0.12	+7.56	5.0752
46	0.1505	0.4792	+3.18	4.9624
47	0.2392	0.5458	+2.28	4.9059
48	0.1853	0.5460	+2.94	4.9058

Contd.

Compound	Experimental activity IC_{50} (μM)	Estimated activity IC_{50} (μM)	Error[a]	Fit value[b]
49	0.3234	0.5462	+1.68	4.9056
50	0.1585	0.5693	+3.59	4.8876
51	1.442	0.5695	-2.53	4.8874
52	0.0880	0.5806	+6.59	4.8791
53	0.2589	0.6034	+2.33	4.8623
54	0.6439	0.6129	-1.05	4.8555
55	1.836	0.6838	-2.68	4.8080
56	0.1507	0.7791	+5.17	4.7513
57	2.005	2.9266	+1.45	4.1766
58	8.94	3.2168	-2.77	4.1355
59	10.89	9.9788	-1.09	3.6439
60	2.18	11.8518	+5.43	3.5692
61	0.1907	1.2	+6.44	3.5615

[a] (+) indicated that predicted IC_{50} was higher than experimental IC_{50}; (-) indicated that predicted IC_{50} was lower than experimental IC_{50}, [b] Fit value indicated how well feature of the pharmacophore (Hypo-1) overlap the chemical feature in the compound.

Figure 5.28 show the correlation between experimental and estimated activities of the 42 test set compounds. Another validation method used to characterize the quality of hypothesis was represented by error ratio, which was the difference between estimated activity and experimental activity values. An error ratio ≤10 would mean more than one order difference between the estimated and experimental activity. In the case of Hypo-2, all the 42 compounds showed an error value ≤10.
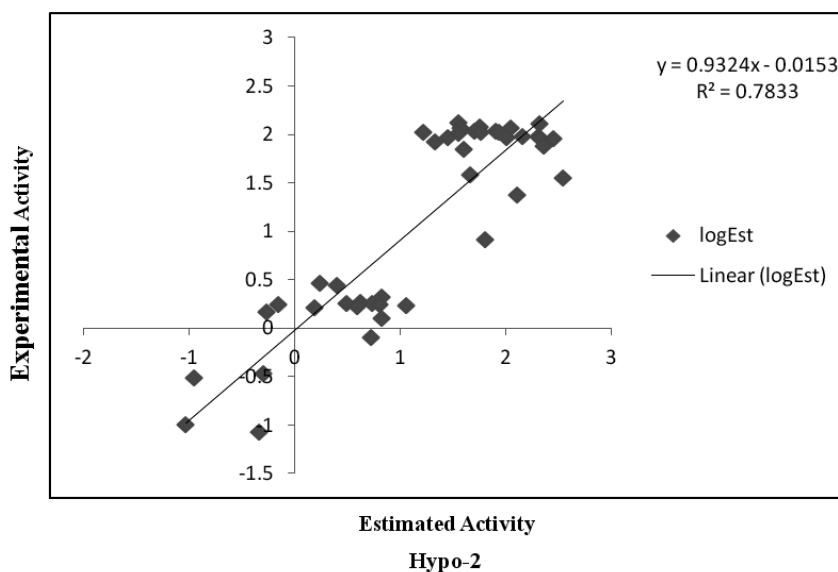
Figure 5.28: Correlation between experimental and estimated activity of 42 test set compounds based on Hypo-2.

The most potent compound **41** and inactive compound **59** of the test set was mapped with Hypo-2 (**Figure 5.29**). The best pharmacophore model Hypo-2 matched very well with the chemical features of these compounds and estimated the IC_{50} values of 0.0160938 and 0.0283598 µM respectively with the error value less than 10. The most active compound well matched to all chemical features with good fitness value of 6.1903 whereas inactive compound missed one RA group and one HBA group. Based on these results, again it was concluded that the RA and HBA features were important for *M. smegmatis* GyrB inhibitory activity. Pharmacophore mapping of the most active compound **41** and inactive compound **59** of the test set on the best pharmacophore hypotheses Hypo-2 is represented in **Figure 5.29**.

A) Most Active Compound 41 in the test set **B) Inactive Compound 59 in the test set**
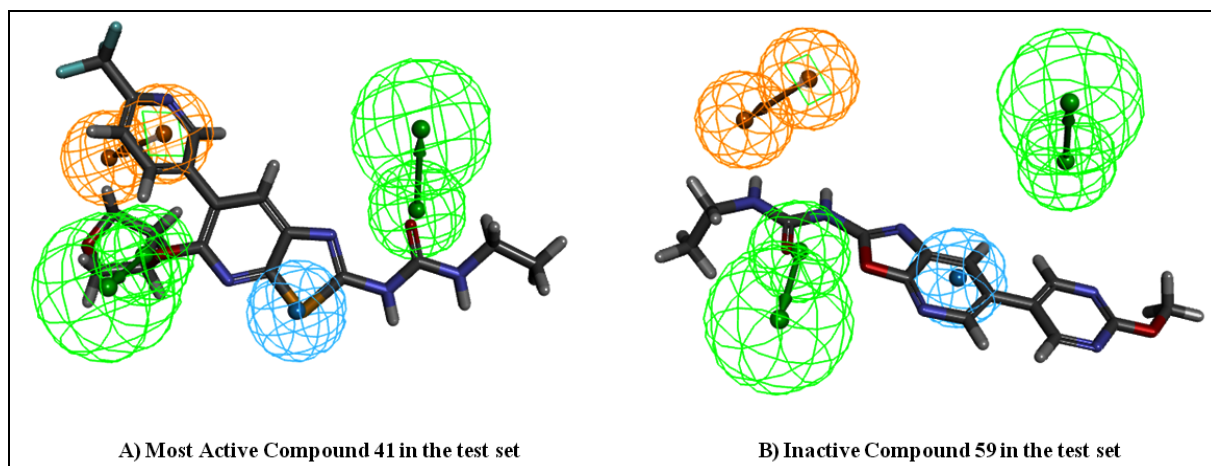
Figure 5.29: Hypo-2 mapped, on the most active compound, **41** (IC$_{50}$=0.0029 µM) and inactive compound **59** (IC$_{50}$=10 µM), in the test set. Pharmacophore features: hydrogen bond acceptor (HBA); ring aromatics (RA); hydrophobic aromatics (HY-AY).

5.1.1b.5.2. Fischer's randomization method

Fischer's randomization was used to evaluate the statistical significance of Hypo-2. Validation was done by generating random spreadsheets for training set molecules, which were randomly reassigned activity values to each compound and subsequently generated the hypotheses using the same features and parameters originated for Hypo-2. To achieve the confidence level of 95%, 19 random spreadsheets (random hypotheses) were generated. The significance of the hypotheses was calculated using the following formula:

$[1 - (1 + X)/Y]* 100$

Where X represented, total number of hypotheses having a total cost lower than Hypo.

X and Y represented, total number of Hypogen runs (initial+ random runs).

Here, $X = 0$ and $Y = (19 + 1)$, $S = [1 - ((1+0)/ (19 + 1))] * 100\% = 95\%$.

The results of top 10 random spreadsheets along with Hypo-2 are presented in **Table 5.13**. None of the top 10 randomly generated hypotheses scored a total cost lower than the original hypothesis and correlation cost higher than the Hypo-2. The statistics of Hypo- 2 was far more superior to the top 10 random hypotheses. This cross validation results clearly showed that the Hypo-2 was not generated by chance, and had strong confidence to represent a true correlation in the training set.

Table 5.13: Fischer's randomization test results of the pharmacophore hypothesis Hypo-2.
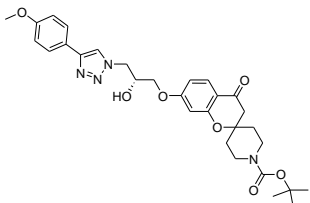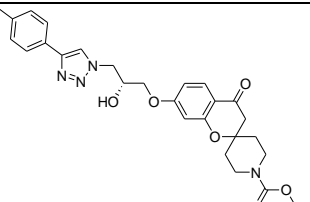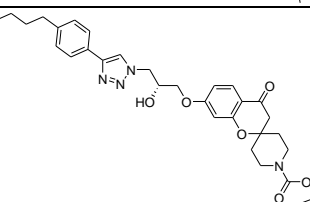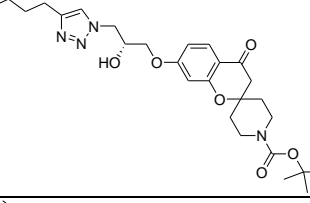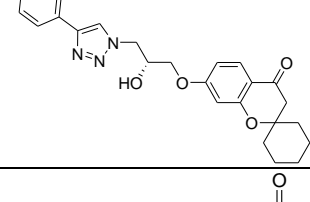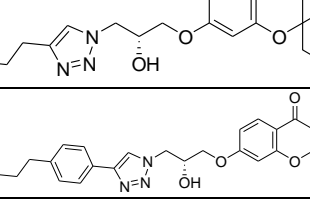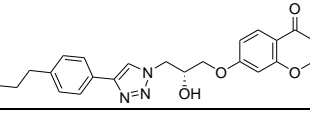
Hypothesis	Cost Value	Correlation
Hypo-2	**85.9538**	**0.951969**
Random-1	107.573	0.602635
Random-2	104.029	0.739856
Random-3	106.98	0.650065
Random-4	99.9792	0.803079
Random-5	101.857	0.770008
Random-6	95.5989	0.838618
Random-7	103.974	0.700719
Random-8	106.304	0.64776
Random-9	97.8725	0.777945
Random-10	98.9728	0.775268
Random-11	101.116	0.753624
Random-12	97.4731	0.791232
Random-13	102.983	0.74884
Random-14	108.678	0.604166
Random-15	103.32	0.718135
Random-16	107.176	0.657503
Random-17	109.227	0
Random-18	107.648	0.592711
Random-19	96.0014	0.839754

5.1.1b.6. Virtual screening
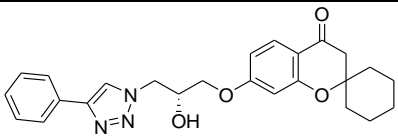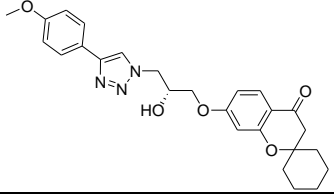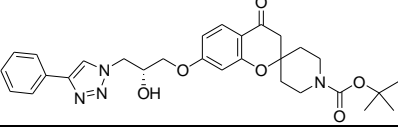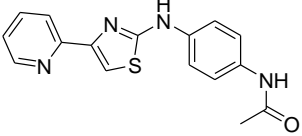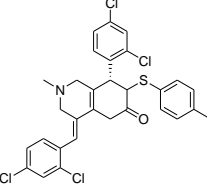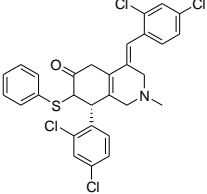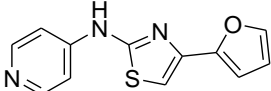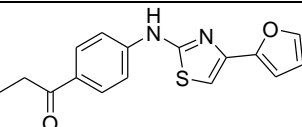
The validated pharmacophore hypothesis Hypo-2 was used as a 3D structural query for retrieving potential *M. smegmatis* GyrB inhibitors from our in house database. As a result, 150 hits from in house database showed very good mapping on Hypo-2. To refine these retrieved hits, the estimated activity value of 150 hit compounds based on the selected pharmacophore hypothesis, Hypo-2, were considered and finally 15 hit compounds with the

estimated activity value <1μM were chosen for *in vitro* enzyme inhibition studies. The 2D structure of all the selected 15 hits and their fitness values with estimated activities are presented in **Table 5.14**.

Table 5.14: Identified 15 hits through *in house* database search along with their fit value, estimated activity.

Compound Name	Structure	Estimated Activity (μM)	Fit value
Ex-355		0.067	6.8457
Ex-361		0.097	6.84485
Ex-362		0.114	6.79827
Ex-360		0.143	6.7776
Ex-359		0.158	6.77003
Ex-348		0.217	6.76409
Ex-363		0.237	6.734

Compound Name	Structure	Estimated Activity (µM)	Fit value
Ex-358		0.245	6.7038
Ex-352		0.264	6.47572
Ex-356		0.280	6.36168
TC7		0.883	5.35566
PTA7		0.510	5.93506
PTA3		0.530	5.91836
TA6		1	5.06926
TA7		1.5	5.012

5.1.1b.7. *In vitro M. smegmatis* GyrB assay

The assay was performed in a 96 well plate, each well constituted 20µl of assay buffer with 100 nM of the *M. smegmatis* GyrB protein, 0.6µM of ATP. Compounds were added to the plates and incubated for 2 hrs at 37^0 C, after the incubation 20 µl of malachite green reagent was added and the reading was observed at 520 nm. The blank was considered without the protein and a positive control novobiocin was employed. The selected molecules selectively inhibited mycobacterial GyrB and were not active against *S. aureus* GyrB. The fifteen most

promising compounds exhibiting % inhibition values in the range of 5.32 to 50.2, and out of these fifteen compounds six of them showed inhibition more than 40% at 30 μM concentration. The % inhibition of all the fifteen compounds with respect to standard compound novobiocin is presented in **Table 5.15**.

5.1.1b.8. *M. tuberculosis s*upercoiling assay

For the six compounds (Ex-355, Ex-359, Ex-363, Ex-358, Ex-356, and TC7) which showed 40% inhibition in *M. smegmatis* GyrB ATPase activity, we screened for the DNA supercoiling using DNA gyrase from *M. tuberculosis* (Inspiralis, Norwich). Novobiocin was used as positive control in these assays. Each of the compounds tested showed dose-dependent inhibition. At 30 μM concentration, two compounds showed more than 50% inhibition. The standard compound novobiocin showed 100% inhibition and showed IC_{50} of 0.046±0.45 μM. These molecules did not inhibit DNA supercoiling activity of *S. aureus, E. coli* and *P. aeruginosa* DNA gyrases. The % inhibition of all the six compounds in supercoiling assay with respect to standard compound novobiocin is presented in **Table 5.15**.

Table 5.15: Activity table showing the IC_{50} value of all the fifteen top hits obtained through ligand based virtual screening.

Compound Name	GyrB assay % inhibition at 30 μM	Supercoiling assay% inhibition at 30 μM
Novobiocin	0.18±3.9 μM	0.046±0.45 μM
Ex-355	50.00%	54%
Ex-361	34.3%	NA
Ex-362	28.2%	NA
Ex-360	30.4%	NA
Ex-359	43.17%	47%
Ex-348	10.55%	NA
Ex-363	40.14%	46%
Ex-358	50.2%	68%
Ex-352	5.32%	NA
Ex-356	42.06%	51%

Contd.

Compound Name	GyrB assay % inhibition at 30 μM	Supercoiling assay% inhibition at 30 μM
TC7	44.11%	51%
PTA7	20.8%	NA
PTA3	37.25%	NA
TA6	37.7%	NA
TA7	20.8%	NA

5.1.1b.9. Highlights of the study

In the present study, the best 3D pharmacophore model (Hypo-2) was developed based on a series of pyrrolamide and pyridothiazole derivatives with activity range of 3.97 order of magnitude (0.0026 to 24.67 μM) using the HypoGen module in Catalyst software. This model consisting of four chemical features i.e. two HBA, one RA, and one Ar-HY with a correlation coefficient (r) value of 0.951 and was validated on 42 test set compounds with significant predictive $R^2[R^2pred]$ value of 0.7833. The model performed well in classifying the active and inactive compounds correctly. Furthermore, use of Hypo-2 as a 3D query for screening small databases of *in house* led to the selection of fifteen compounds as potent *M. smegmatis* inhibitors based on the fitness and estimated activity. Furthermore, *in vitro* enzymatic inhibition studies were performed for these fifteen most promising candidates and these compounds were found to exhibit inhibition at 30 μM and out of these fifteen compounds six of them showed inhibition more than 40% at 30 μM concentration. Thus, the overall analysis suggested that the 3D pharmacophore model may provided useful information required for proper understanding of the important structural and physicochemical features for designing novel *M. smegmatis* DNA gyrase inhibitors.

5.1.2. Hit expansion and lead optimization of the most active lead obtained from virtual screening

In the case of compounds shortlisted from asinex database through structure based virtual screening, total 25 compounds were screened against *M. smegmatis* GyrB ATPase and *M. tuberculosis* supercoiling assay. All the 25 molecules showed IC_{50} in the range of *M. smegmatis* GyrB IC_{50} of 1.5±0.12 to 73.67±0.4 μM and *M. tuberculosis* supercoiling assay activity in the range of 1.16±0.25 to >25 μM with **lead D11** (**Figure 5.30**) emerges the most

potent inhibitor with an IC$_{50}$ of 1.5±0.12µM and 1.16±0.25 µM. In case of ligand based virtual screening none of the compound showed promising activity as this **lead D11**. Thus for lead optimization we have taken most active compound from structure based virtual screening.
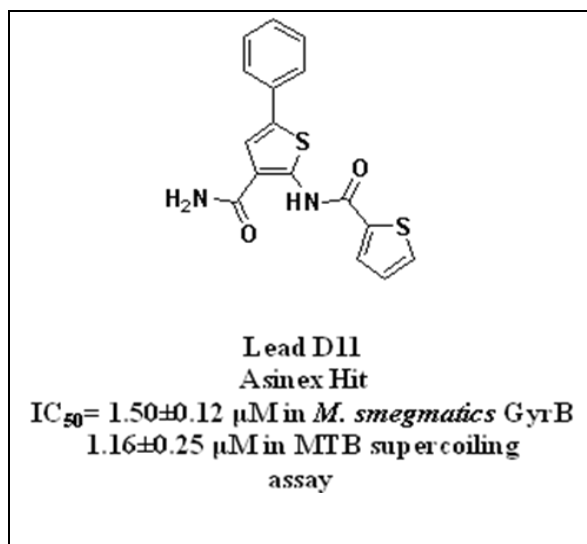
Figure 5.30: Most active compound **D11** obtained from virtual screening.

5.1.2.1. Development of 2-amino-5-phenylthiophene-3-carboxamide derivatives as potential *M. tuberculosis* GyrB inhibitors

5.1.2.1.1. Chemical synthesis and characterization

Confident by the promising result for asinex lead compound **D11**, we designed a library with the goal of obtaining a lead series with tractable SAR and potencies better than the identified virtual screening hit. A library of 28 molecules were designed and taken up for synthesis. It was decided to retain the left and linking core in the further structure- activity exploration and the structural diversity was brought in by modifying the right hand substituent's.

A library of twenty eight molecules consisting eight urea, eight thiourea and twelve amide derivatives at second position of 2-amino-5-phenylthiophene-3-carboxamide moiety was synthesised by following 3 step synthetic protocols as shown in **Figure 4.3** in material and method section**.** In the first step, phenylacetaldehyde on reaction with cyanoacetamide and sulphur powder in presence of morpholine produced compound **II**, which was an example of Gewald's reaction with an aldehyde. Reactions of compound **II** with substituted aryl/alkyl isocyanates/isothiocyanates under basic or thermal conditions produced no reaction. Then we

converted the free amine group of compound **II** to HCl salt by passing dry HCl gas into a solution in THF. In the last step of synthetic route, we reacted the compound **III** with various substituted aromatic & aliphatic isocyanates under microwave irradiation conditions to achieve compounds (**S1-8**), while various substituted aromatic & aliphatic isothiocyanates to yielded compounds (**S9-16**) and also with various carboxylicacidchlorides afforded compounds (**S17-28**) in good yields. The general procedure and spectral analysis of all the 28 compounds are represented in Annexure-I.

5.1.2.1.2. *In vitro* GyrB ATPase assay, DNA supercoiling assay, antimycobacterial potency and cytotoxicity studies of the synthesized molecules

5.1.2.1.2a. DNA GyrB enzyme inhibition and SAR

All the molecules inhibited GyrB ATPase activity, with IC_{50} values ranging between 0.8 ± 0.58 to 71.42 ± 1.72 μM. In the GyrB assay, out of the 28 compounds tested, 26 compounds displayed GyrB inhibitory IC_{50} <50 μM, out of which 16 compounds demonstrated IC_{50} < 15 μM, 5 compounds showed IC_{50} < 5 μM and 1 compound was found to inhibit GyrB activity even at sub micromolar concentration (IC_{50} 1 μM). Compound **S23** emerged as the most promising lead with and GyrB inhibitory IC_{50} of 0.8 ± 0.58 μM.

Dose-response curve was plotted for the most potent compound **S23** using GraphPad Prism software by taking log (inhibitor concentration) on the x-axis and response (% inhibition) on the y-axis as shown in **Figure 5.31** while the standard novobiocin showed an IC_{50} of 180 ± 3.9 nM.
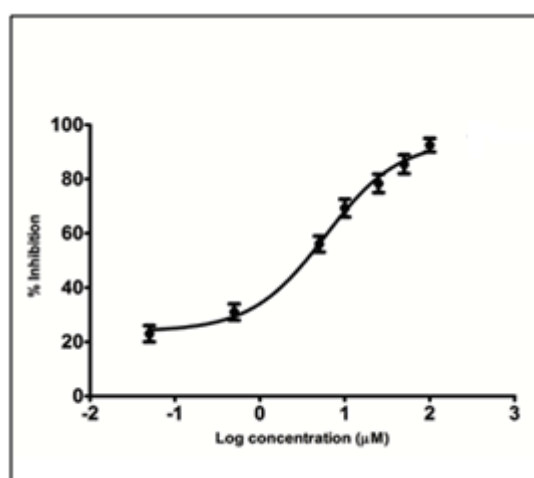
Figure 5.31: Dose-response curve of most active compound **S23**.

To study the SAR, we carried out docking studies of all the synthesized compounds together with lead compound **D11** using XP mode of Glide module. With respect to structure-activity relationship study we explored various substitutions at second position of 2-amino-5-phenylthiophene-3-carboxamide moiety. Out of the various substitutions attempted in synthesis, the urea and amide derivatives turned out to be the most promising leads as compared to thiourea derivatives.

The most promising lead compound **S23** also belonged to the amide group. Information on the common properties of the binding groups was essential for resolving the type of inhibitor binding to the target protein. In order to understand the interaction profile of the molecules reported from the assay, compounds were docked to the GyrB ATPase domain of *M. smegmatis* retrieved from PDB (PDB ID: 4B6C). An initial validation of the active site pocket was performed by re-docking the crystal ligand (6-(3,4-dimethylphenyl)-3-[[4-[3-(4-methylpiperazin-1-yl)propoxy]phenyl]amino]pyrazine-2-carboxamide), with the active site residues of the *M. smegmatis* GyrB protein. Re-docking results showed that the ligand exhibited similar interactions as that of the original crystal structure which was further confirmed with RMSD of 0.86Å. The docking studies gave us an insight into the differences in the binding pattern of the molecules used in the present study at the active site of the protein which probably explained the diverse activity profile displayed by these molecules. Our SAR study started with urea containing compounds (**S1-8**). The effect of various substituted phenyl/aliphatic substitution at the R position was explored. As shown in **Table 5.16**, the activity of most of the compounds was found in the in the range of 0.8±0.58 μM to 23.955±1.66 μM against GyrB. The docking results further validated the *in vitro* GyrB findings with urea derivatives (**S1-8**) revealing the good docking scores in the range of -8.39 to -9.36 kcal mol^{-1}. A closer look at the interaction profile of these molecules revealed that the carboxamide -NH_2 group was involved in an important hydrogen bonding interaction with Asp79 (**Figure 5.32**). This interaction was believed to be critical in improving the bioactivity. Phenyl substituted at R position (**compound S5**) turned out to be most active compound from this set (GyrB IC$_{50}$= 1.833±0.22 μM and *M. tuberculosis* supercoiling IC$_{50}$=1.32±0.39 μM). While compound with substituted 4-toluyl at R position (**compound S6**) led to decreased potency compared to other compounds from this subset (GyrB IC$_{50}$=23.955±1.66 μM and *M. tuberculosis* supercoiling IC$_{50}$=>25 μM). A closer analysis of both the compounds revealed that, due to more hydrophobic group at R position (Phenyl) the compound was involved in more hydrophobic interaction which was earlier demonstrated to be crucial for activity and

specificity (**Figure 5.32**). On the other side, closer analysis of 4-toluyl substituted group (**compound S6**) failed to retain the hydrophobic interaction as 4-toluyl group was placed outside the active site pocket (**Figure 5.33**).
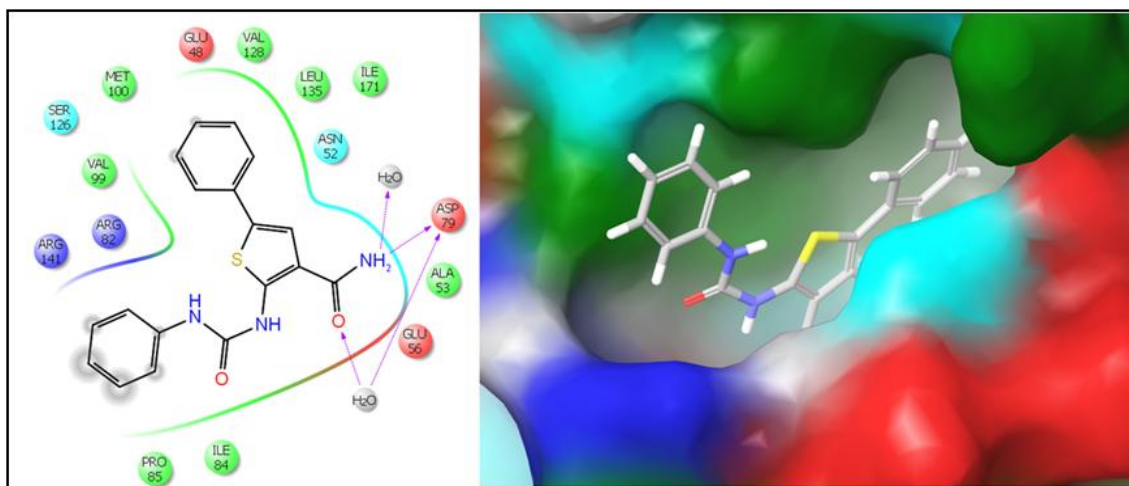
Figure 5.32: Binding pose and its interaction pattern of the compound **S5.**
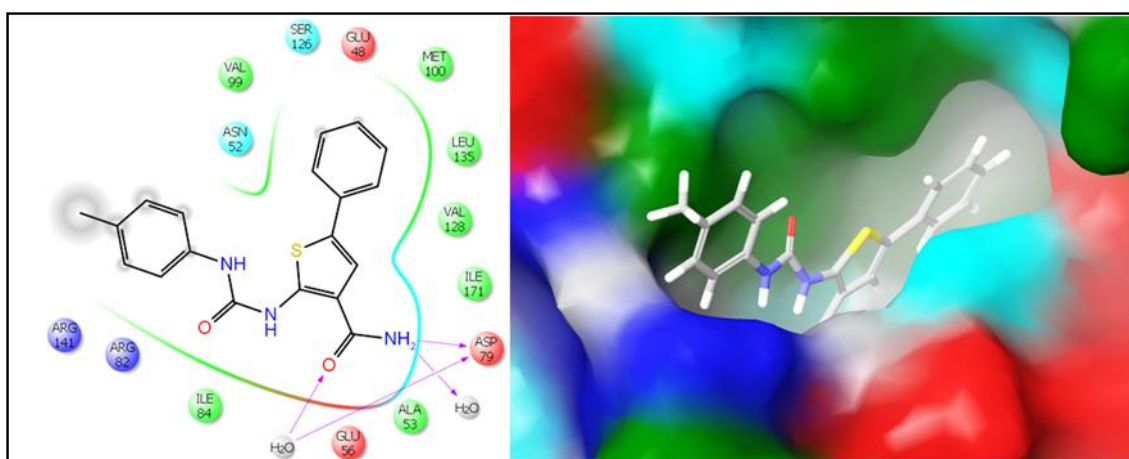
Figure 5.33: Binding pose and its interaction pattern of the compound **S6.**

In the second subset of compounds (**S9-16**), the effect of thiourea substitution was investigated to understand the effect of similar substituted phenyl/aliphatic substitution at R position as that of the previous set of compounds. Here, all the compounds showed satisfactory *in vitro* GyrB inhibitory activity in the range of 2.459±0.53 μM to 71.42±1.72 μM. The docking score of these set of compounds was found in the range of -9.38 to -10.38 kcal/mol. SAR study revealed that toluyl, benzyl and isopropyl group at R position (**compound S14-16**) is showed good inhibition against the GyrB protein whereas compound substituted with 4-chlorophenyl and phenyl at R position (**compound S10** and **S13**) led to

decreased activity. A closer study at the interaction pattern of the active leads showed that these molecules oriented deeply into the hydrophobic cavity wherein it was found to be stabilized by the hydrogen bonding interaction with Asp79 amino acid residue as well hydrophobic interactions; analogous to the one observed in the lead molecule **D11**.
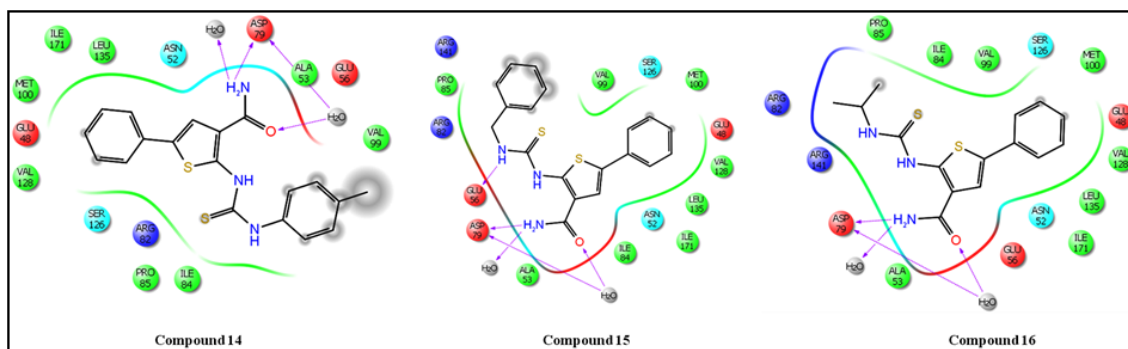
Figure 5.34: Binding pose and its interaction pattern of the compound **S14**, **S15** and **S16**.

The predicted binding pose of the less active compounds (**S10** and **S13**) suggested that these molecules were found to be in a slightly different orientation/pose compared to that of active compounds and also because of this orientation it pushed the chlorophenyl and phenyl group away from the cavity which made the compound less active (**Figure 5.35**). This was also supported by the low docking score of -6.12 and -.6.50 kcal/mol respectively.
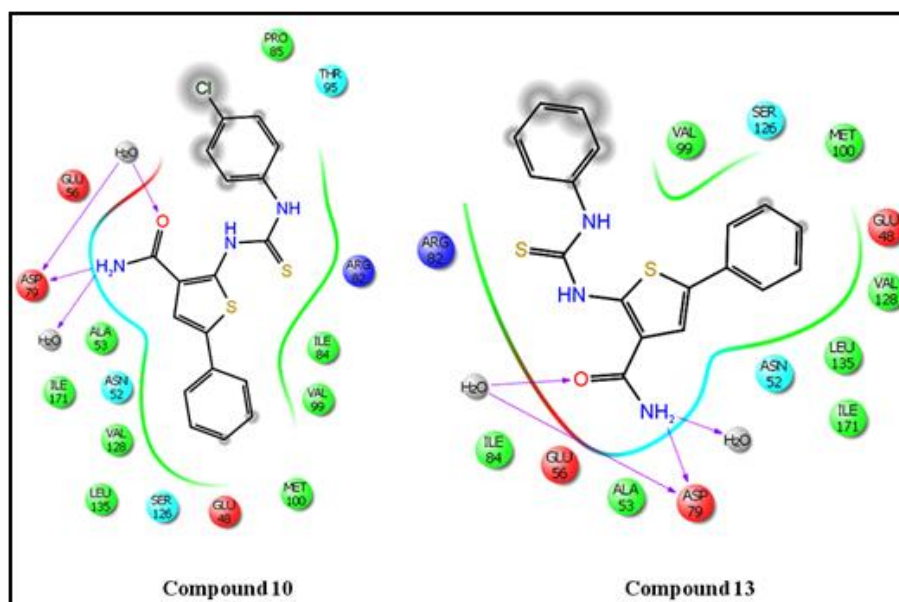
Figure 5.35: Binding pose and its interaction pattern of the compound **S10** and **S13**.

118

In the third subset of compounds, amide derivatives (**S17-28**) were synthesized by substituting various substituted phenyl/heteroaryl/aliphatic acyclic and cyclic substitution at R position as shown in **Table 5.16**. Here out of 12 compounds 4 compounds showed activity >10 μM, while 6 compounds showed activity >25 μM and other 2 compounds were not much active in GyrB inhibition assay. The phenyl substituted compound at R position (**S23**) turned out to be most promising compound among all the compounds having IC$_{50}$ of 0.8±0.58 μM in *M. smegmatis* GyrB assay and 0.76±0.25 μM in *M. tuberculosis* supercoiling assay.

The binding analysis of active compounds was further analyzed in more detail to understand its binding pattern. The binding analysis of most active compound in the active site of *M. smegmatis* GyrB protein revealed that the compound was stabilized by the hydrogen bonding interaction with Asp79 amino acid residue as well as water mediated hydrogen bond. Apart from hydrogen bonding interaction the phenyl ring of compound **S23** was involved in *cation-pi* interaction with Arg82 amino acid residue, this interaction was also observed in the reference crystal ligand. The compound was well inserted in to the active site pocket where phenyl core showed the hydrophobic interactions with Ala53, Ile171, Leu135, Val128, Met100, Val99 and Ile84 amino acid residues (**Figure 5.36**). The other compounds from this set were found to be active against *M. tuberculosis* GyrB. The binding analysis of all the compounds revealed that they were well docked in the active site cavity of the protein, where they were stabilized by important interaction with Asp79 as well as water mediated hydrogen bond. Amide substituted compounds turned out to be most active and a closer analysis of all these active compounds in the *M. smegmatis* GyrB protein revealed that all the compounds made favorable interactions with important amino acid residues such as with Asp79 as well as water mediated hydrogen bond with the good fitness having all the hydrogen bond distance less than 2.5Å which yielded stable protein-ligand complex. Here all the compounds except compound **S27** were involved in *cation-pi* interaction with Arg82 amino acid residue. Probably because of this loss of interaction compound **S27** exhibited moderately activity (**Figure 5.37**) and also the absence of *pi-electron* cloud in the pentyl moiety which was an important aspect in hydrophobic interactions made the compound **S27** less active as compared to compound **S23**.
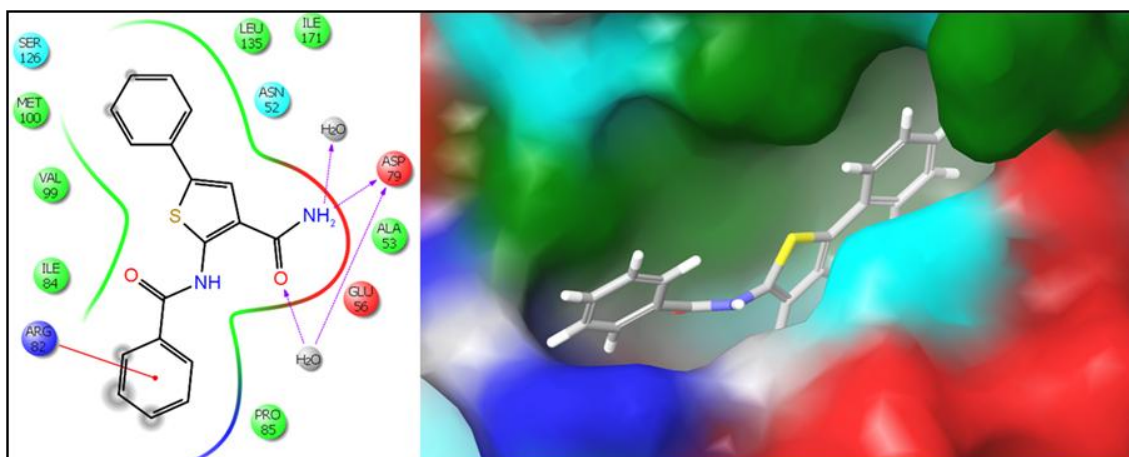
Figure 5.36: Binding pose and its interaction pattern of the compound **S23.**
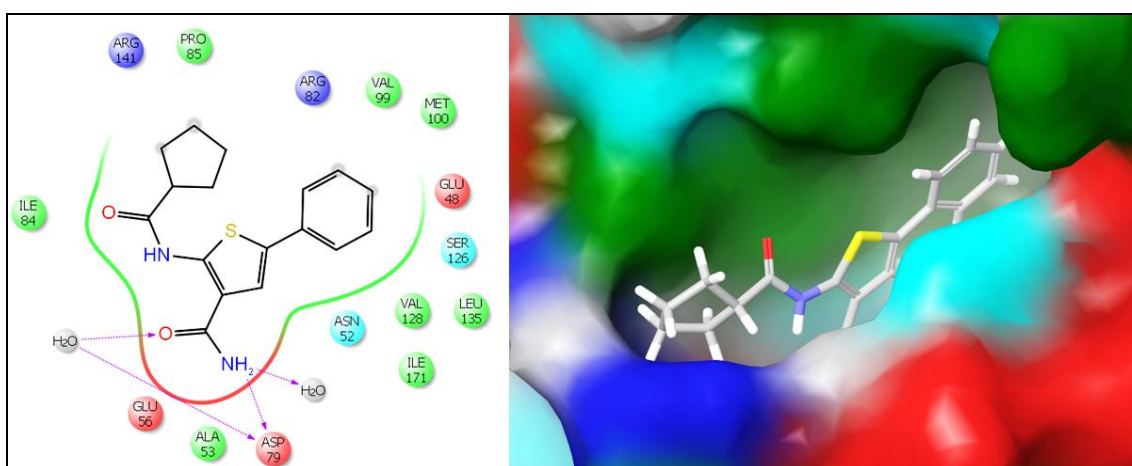
Figure 5.37: Binding pose and its interaction pattern of the compound **S27.**

5.1.2.1.2b. *M. tuberculosis* **supercoiling assay**

The assay was performed using the DNA supercoiling kit as per the protocol described in material and method section 4.1.1.3.4. The reactions were performed on *M. tuberculosis* DNA gyrase enzyme dose dependently with about 8 concentrations starting from 100, 50, 25, 12.5, 6.25, 3.125, 1.56 and 0.75 µM. The most active compound **S23** showed an IC_{50} of 0.76±0.25 µM as illustrated in **Figure 5.38**. Novobiocin was considered as a standard compound in this assay. IC_{50} was calculated based on relative quantification using Image lab software.
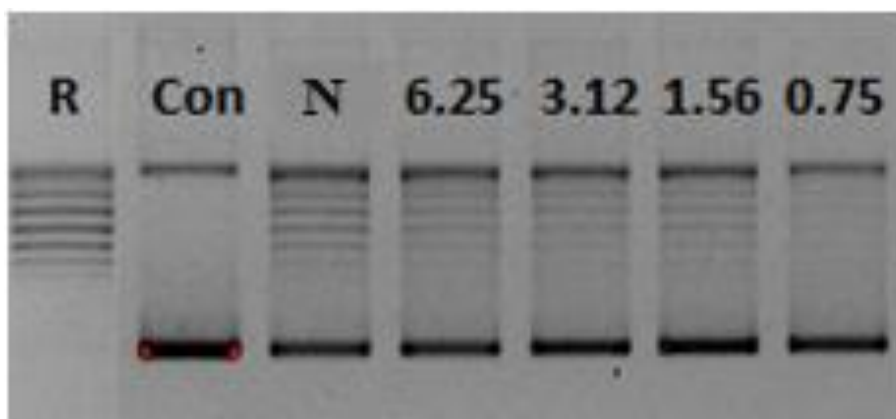
Figure 5.38: Inhibitory profile of *M. tuberculosis* DNA gyrase supercoiling activity by compound **S23**.

5.1.2.1.2c. *In vitro M. tuberculosis* screening

All the synthesized compounds were also screened for their *in vitro* anti-tubercular activity were further screened for their in vitro antimycobacterial activity against M. tuberculosis H37Rv by microplate Alamar blue assay method as described in material and method section 4.1.1.3.6. All the synthesized compounds showed activity against *M. tuberculosis* with MIC ranging from 4.84 to 80.70 µM. Out of the 28 molecules tested 12 molecules showed MIC less than 25 µM and 7 molecules exhibited MIC less than 10 µM, while the remaining 9 molecules did not show good activity. All the compounds were less potent than isoniazid, rifampicin and moxifloxacin. Most active compound **S23** (MIC of 4.84 µM) was found to be more potent than EMB (MIC of 7.64 µM).

5.1.2.1.2d. *In vitro* cytotoxic studies

The safety profile of all the synthesized compounds was assessed by testing their *in vitro* cytotoxicity in RAW 264.7 cells at 100 µM concentration using MTT assay described in material and method section 4.1.1.3.7. Almost all the tested compounds demonstrated a good safety profile with very low inhibitory potential. Compounds inhibited within a range of 32.06-40.34%. Furthermore, the most active compound **S23** exhibited 34.67% inhibition at 100 µM concentration of the drug, reflecting its safety profile in the eukaryotes. Cytotoxic results of all the compounds are illustrated in the **Table 5.16**.

5.1.2.1.2e. Biophysical characterization

Furthermore, the most potent analogue was evaluated for thermal stability of the protein-ligand complex using biophysical DSF experiment. Compound **S23** displayed a T_M shift of 2.5°C (T_M = 48.5°C) compared with the native protein (T_M = 46°C), a repercussion of strong binding of the ligand to the protein and highly correlated with its GyrB IC_{50} of 0.8±0.58µM. A higher or positive shift of melting temperature (T_M) of protein-ligand complex compared to the native protein T_M signified a better stabilization of the protein-ligand complex, which in turn would reflect on the inhibitor binding as depicted in the **Figure 5.39.**
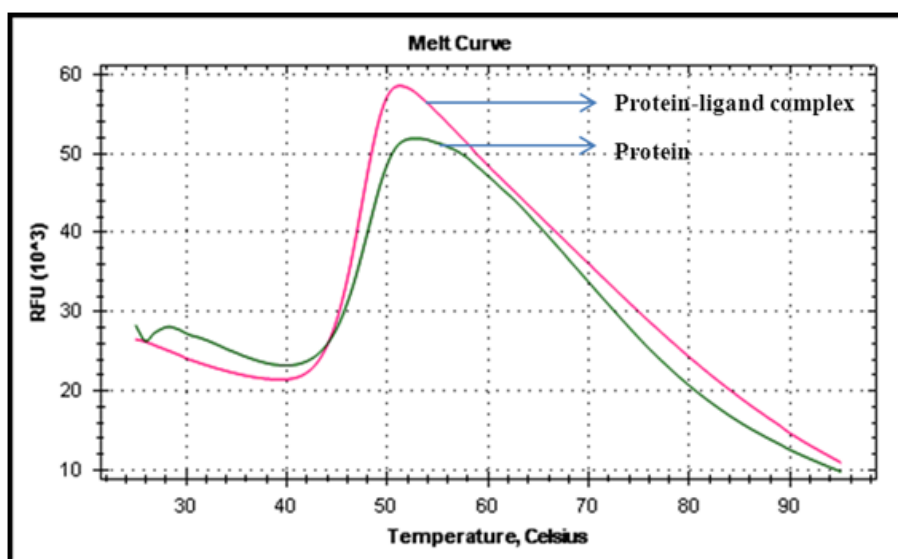
Figure 5.39: DSF experiment for compound **S23** showing an increase in thermal stability between the native *M. smegmatis* protein (green) and *M. smegmatis* protein-ligand complex.

Table 5.16: *In vitro* biological evaluation of the synthesized derivatives.
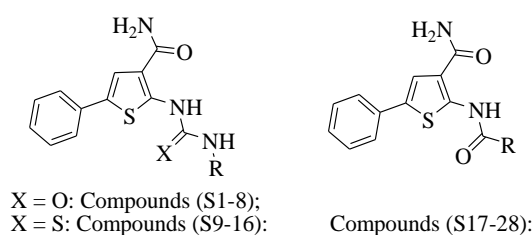
X = O: Compounds (S1-8);
X = S: Compounds (S9-16):   Compounds (S17-28):

Compound	R$_1$	*M. smegmatis* GyrB assay (IC$_{50}$)	*M. tuberculosis* Supercoiling assay (IC$_{50}$)	MIC (µM)	Cytotoxicity (% inhibition at 100µM)
S1	4-Bromophenyl	12.17±0.52	>25	15.02	37.58
S2	4-Chlorophenyl	3.142±0.69	2.97±0.44	8.42	38.20
S3	4-Fluorophenyl	11.45±1.22	9.88±0.37	17.60	33.69
S4	4-Nitrophenyl	12.83±0.97	10.92±0.45	16.3	37.32
S5	Phenyl	1.833±0.22	1.32±0.39	9.27	37.26
S6	4-Toluyl	23.955±1.66	>25	35.61	37.62
S7	Benzyl	10.7581±0.63	8.89±0.79	18.51	32.97
S8	Isopropyl	6.478±0.32	6.17±0.71	10.24	36.07
S9	4-Bromophenyl	10.87±0.57	9.63±0.65	18.0	35.57
S10	4-Chlorophenyl	71.42±1.72	>25	80.70	36.10
S11	4-Fluorophenyl	48.91±1.16	>25	67.38	32.06
S12	4-Nitrophenyl	32.48±0.63	>25	78.5	40.34
S13	Phenyl	70.33±1.82	>25	70.82	32.77
S14	4-Toluyl	2.459±0.53	2.97±0.46	8.50	34.83
S15	Benzyl	28.25±0.72	17.81±0.98	34.05	36.07
S16	Isopropyl	16.22±0.66	9.25±0.86	19.59	35.48
S17	4-Chlorophenyl	6.69±0.41	5.82±0.47	8.76	38.52
S18	4-Nitrophenyl	8.913±0.75	6.77±0.64	8.48	35.86
S19	Napthyl	28.558±1.72	>25	24.96	36.77
S20	Pyrazin-2-yl	18.36±1.31	>25	38.58	34.31

Contd.

Compound	R₁	*M. smegmatis* GyrB assay (IC$_{50}$)	*M. tuberculosis* Supercoiling assay (IC$_{50}$)	MIC (μM)	Cytotoxicity (% inhibition at 100μM)
S21	1H-Indole-2-yl	22.02±0.86	18.21±0.84	34.62	36.25
S22	4-penoxyphenyl	17.33±1.14	8.85±0.29	15.09	35.83
S23	Phenyl	0.8±0.58	0.76±0.25	4.84	37.64
S24	Acetyl	19.12±0.38	11.82±0.66	24.03	37.51
S25	Propionyl	11.75±0.81	5.62±0.62	22.81	39.41
S26	*n*-Butyryl	3.57±0.54	3.14±0.51	10.85	39.83
S27	Cyclopentyl	42.17±1.18	>25	39.72	39.71
S 8	Cyclohexyl	10.19±0.75	9.83±0.43	9.48	38.96
Novobiocin	-	180±3.9	0.046±0.45	nd	81.67
Isoniazid	-	nd	nd	0.66	nd
Rifampicin	-	nd	nd	0.23	nd
Ofloxacin	-	nd	nd	2.16	nd
Ethambutol	-	nd	nd	7.64	Nd

5.1.3. Highlights of the study

In the present study, 25 compounds were discovered using an e-pharmacophore modelling and subsequent *in vitro* screening that resulted in IC$_{50}$ of 1.5±0.12 μM which was subsequently optimized by a combination of modelling, and synthetic chemistry. Hit expansion of the lead by chemical synthesis led to improved inhibitor with an IC$_{50}$ of 0.8±0.58 μM along with *M. tuberculosis* MIC of 4.84 μM. Total 28 compounds were synthesized and evaluated biologically. Most of the synthesized compounds showed good GyrB inhibition and 2-benzamido-5-phenylthiophene-3-carboxamide (compound **S23**) was found to be the most active compound with IC$_{50}$ of 0.8±0.58 μM in *M. smegmatis* GyrB as well as *M. tuberculosis* supercoiling IC$_{50}$ of 0.76±0.25 μM (**Figure 5.40**).
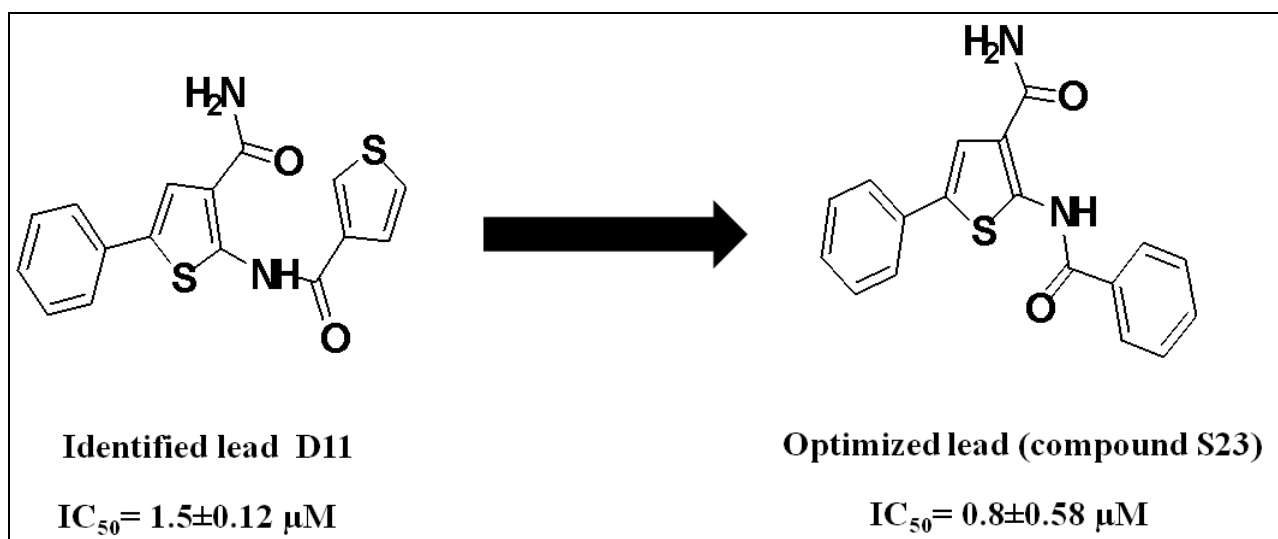
Figure 5.40: Optimized lead **S23** after synthesis.

Identified lead D11

IC_{50}= 1.5±0.12 µM

Optimized lead (compound S23)

IC_{50}= 0.8±0.58 µM

5.2. DEVELOPMENT OF *M. TUBERCULOSIS* L-ALADH INHIBITORS AS POTENTIAL ANTI-TUBERCULAR AGENTS

M. tuberculosis L-AlaDH catalyzes the oxidative deamination of L-alanine to pyruvate and ammonia (catabolic reaction) or, in the reverse direction, the reductive amination of pyruvate to L-alanine (biosynthetic reaction). A recent analysis involving microarray and other data had identified this enzyme to be among the top three drug targets, especially against persistence. Since no inhibitors were reported till date for *M. tuberculosis* L-AlaDH, in the present work we took an effort to design some novel inhibitors for *M. tuberculosis* L-AlaDH.

5.2.1. Design and development of *M. tuberculosis* L-AlaDH inhibitors

In the present study we utilized structure based virtual screening protocol described in the material and method section, to identify newer scaffolds as potential *M. tuberculosis* L-AlaDH leads.

5.2.1.1. Design and identification of *M. tuberculosis* L-AlaDH inhibitors based on NAD$^+$ binding site

In the present study, the crystal structure of the protein L-AlaDH from *M. tuberculosis* (PDB code: 2VHW) was retrieved from protein data bank (PDB) and was utilized for molecular modeling. First cofactor (NAD$^+$) bound to the protein was re-docked with the *M. tuberculosis* L-AlaDH and the output file was used to identify a pharmacophore hypothesis to be further utilized for screening database compounds of Asinex.

5.2.1.1a. e-Pharmacophore of NAD+

The crystal structure of the protein L-AlaDH from *M. tuberculosis* (PDB code: 2VHW) was used for structure-based pharmacophore modeling. Till date as no inhibitors were reported for L-AlaDH, in this study we attempted to utilize the co-factor NAD$^+$ bound with the protein along with pyruvate as substrate for the generation of an e-pharmacophore hypothesis. The asymmetric unit of AlaDH consisted of six chains and the subunit of L-AlaDH was built up of two distinct domains, the substrate-binding domain and the NAD-binding domain, connected by two α helices. The reference ligand NAD$^+$ was re-docked with the active site residues of the *M. tuberculosis* L-AlaDH protein to validate the active site cavity. The ligand exhibited a Glide score of -11.42 kcal mol^{-1} and was found in the vicinity of important amino

acids like Asp270, Val298, Thr178, Ser220, Lys203, Asp198, Met301, Ile267, Ser134, Leu240 and Ala179. Re-docking results (**Figure 5.41a**) showed that the compound exhibited similar interactions as that of the original crystal structure and showed a RMSD of 0.897 Å (**Figure 5.41b**). The result of this docking was used to ascertain the pharmacophoric features of *M. tuberculosis* L-AlaDH. The binding mode of the NAD^+ ligand to the *M. tuberculosis* L-AlaDH protein was defined by the interaction pattern of its pharmacophore.

a) Docking Interaction

b) Superimposition of docked pose of NAD+ to the original pose of NAD+
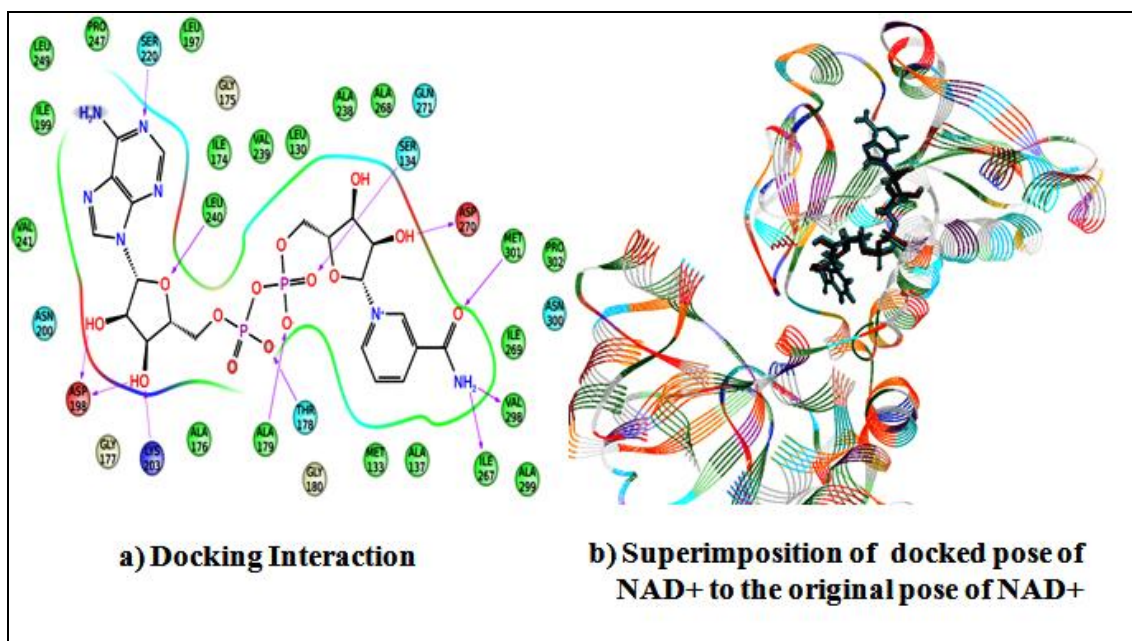
Figure 5.41: (a) XP docking showing interactions of NAD^+ with the active site residues of *M. tuberculosis* L-AlaDH protein. (b) Superimposition of docked pose of the NAD^+ to the original pose of the NAD^+.

Pharmacophore hypotheses were developed by mapping Glide XP energetic terms onto pharmacophore sites which was calculated based on the structural and energy information between the protein and the ligand using Phase module. The results of the e-pharmacophore rank of the best pharmacophoric features are given in **Table 5.17**. The e-pharmacophore features involved five donor molecules and two acceptor groups (**Table 5.17** and **Figure 5.42a**). The ranking was not taken as a sole foundation for the selection of the vital functional groups but also the Glide XP docking results were considered in support of the e-pharmacophore generated. The energy contribution between the ligand and every amino acid in the binding site were the key things in the ligand receptor complex. Among the seven pharmacophore sites *i.e.* four hydrogen bond donor (D16, D17, D19, D22, D23), and two hydrogen bond acceptor (A2 and A12) generated by t he structure based pharmacophore for

127

the *M. tuberculosis* L-AlaDH inhibition, significant five sites D17, D19, D22 A2 and A12 were selected by the e-pharmacophore method script on the basis of their energy scores and pharmacophoric features distance. The D16 and D17 having 2.39 Å distance and D22 and D23 having 1.75 Å distance, which was very close to each features and also they had same energy score, so in the final hypothesis D16 and D23 were deleted (**Figure 5.42b**).

Table 5.17: Scores of Hypothesis in e-pharmacophore.

Rank	Feature label	Score	Type
1	D16	-0.8	D[a]
2	D17	-0.8	D
3	D19	-0.75	D
4	A2	-0.7	A[b]
5	A12	-0.7	A
6	D22	-0.7	D
7	D23	-0.7	D

[a] Donor
[b] Acceptor

The important sites obtained in the e-pharmacophore such as D16, D17, D19, D22, D23 corresponded to the important amino acid residues such as Lys203, Asp198, Asp270, Ile267, Val298 and A2, A12 corresponded to Ser220 and Met301 residues. The five point e-pharmacophore was then utilized for the virtual screening of commercial database Asinex using a protocol as summarized in **Figure 5.43**. The option implying "find matches" to the hypothesis in Maestro was used. Thousand hits with pharmacophoric features similar to the known ligand were then obtained.
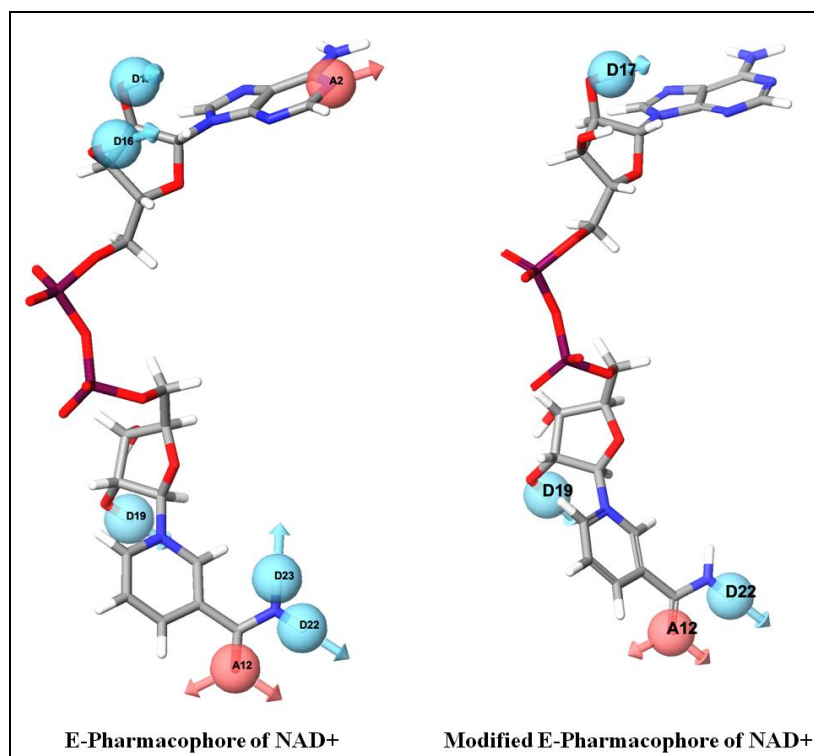
Figure 5.42: (a) The energy based pharmacophoric features of NAD$^+$. (b) Modified energy based pharmacophoric features of NAD$^+$.

5.2.1.1b. Virtual screening of pharmacophore screened database compounds

Virtual screening uses computer based methods to discover new ligand on the bases of biological structure. The basic goal of the virtual screening was the reduction of the enormous virtual chemical space of small organic molecules, to synthesize or screen against a specific target protein, to a manageable number of the compound that could inhibit with a highest chance to lead to a drug candidate. Also the virtual screening workflow option was performed to pre-filter ligands. The virtual screening options for HTVS, SP and Glide XP docking were all checked to be executed. A fit value was a measure of how well the ligand fitted to the pharmacophore. Therefore, the hits with a high fit value were probably very active. In this study, the hits retrieved by the e-pharmacophore model using Phase with a fit value above 1.0 were considered as potential hits and was carried forward for HTVS (**Figure 5.43**). Top compounds from HTVS resulting in a score of $\geq$ -6.0 kcalmol^{-1} were subjected to another round of docking by Glide SP. HTVS did primary screening and then secondary was the SP docking. The survivors of these preliminary screening would progress to Glide XP docking. The results of the above virtually screened ligands with the known ligand (NAD$^+$) were further given for Glide XP docking to find hydrogen-bond interactions, electrostatic

interaction, hydrophobic enclosure, and π-π stacking interactions and the results showed scores ranging from -7.47199 to -10.523 kcalmol^{-1}. Final short listing of possible lead compounds were based on visual inspection of the important amino acid residues involved in binding that included hydrogen bonding with Lys203, Asp198, Ser220, Ser134, Asp270, Leu240 and Ala238.

Figure 5.43: Virtual screening workflow for L-AlaDH.

5.2.1.1c. Molecular docking studies

In order to understand how these ligands bind to the enzyme, hits molecules were taken for docking studies by using Glide (version 5.7, Schrodinger, LLC, New York, NY, 2011) and GOLD 5.1.2 program. The total 100 compounds selected from the SP were further subjected to Glide XP docking. Here, we report five compounds from the Glide XP docking study with the best Glide scores (-7.47199 to -10.523) and Gold score (50.5-72.57), which suggest strong protein-ligand interactions. The chemical structures of these lead compounds are illustrated in **Figure 5.44** and **Figure 5.45** represented the binding modes of these five lead molecules and their interacting residues.
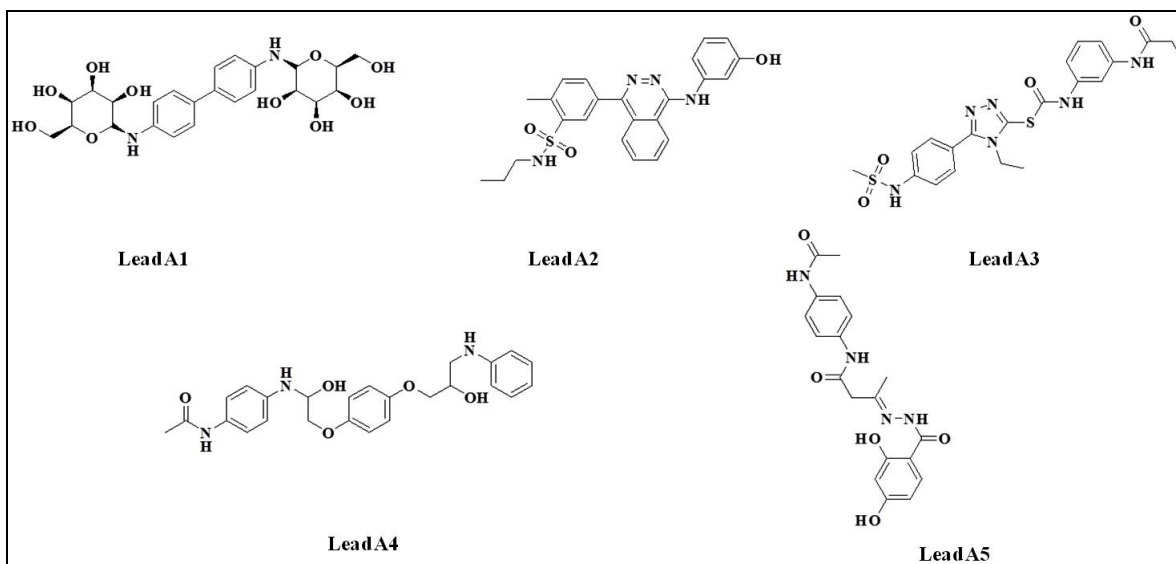
Figure 5.44: 2D structures of top five hits after virtual screening.

All the selected top five hits showed good docking score and interaction with important amino acids such as Lys203, Asp198, Ser220, Ser134, Asp270, Leu240 and Ala238. All the top hits were well fit in the active site cavity of the protein. The binding pattern of top five hits is represented in **Figure 5.46**. The top five hits with their docking score, H-Bond and important interactions are reported in **Table 5.18**. Further the final hits, which were procured from Asinex database, were screened initially at 100 μM concentration for enzyme inhibition and later at 50 μM and 25 μM against *M. tuberculosis* L-AlaDH using an assay based on the spectrophotometric determination of the reaction product pyruvate by 96-well plate format in Perkin Elmer Victor V3 Spectrophotometer.
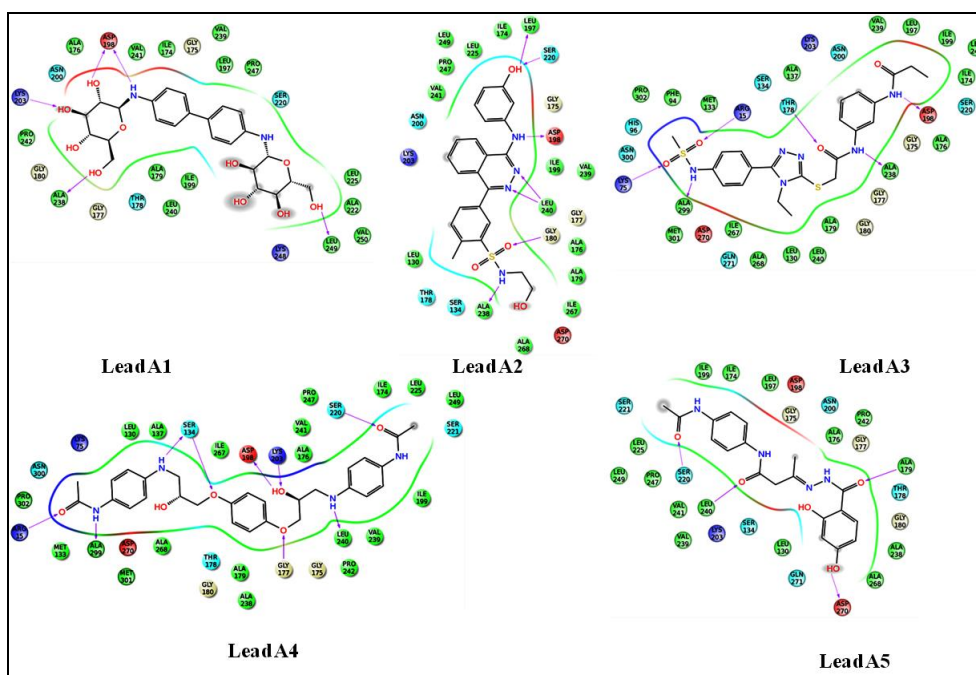
Figure 5.45: Protein-ligand contacts of *M. tuberculosis* L-AlaDH with the top five hit obtained using virtual screening.
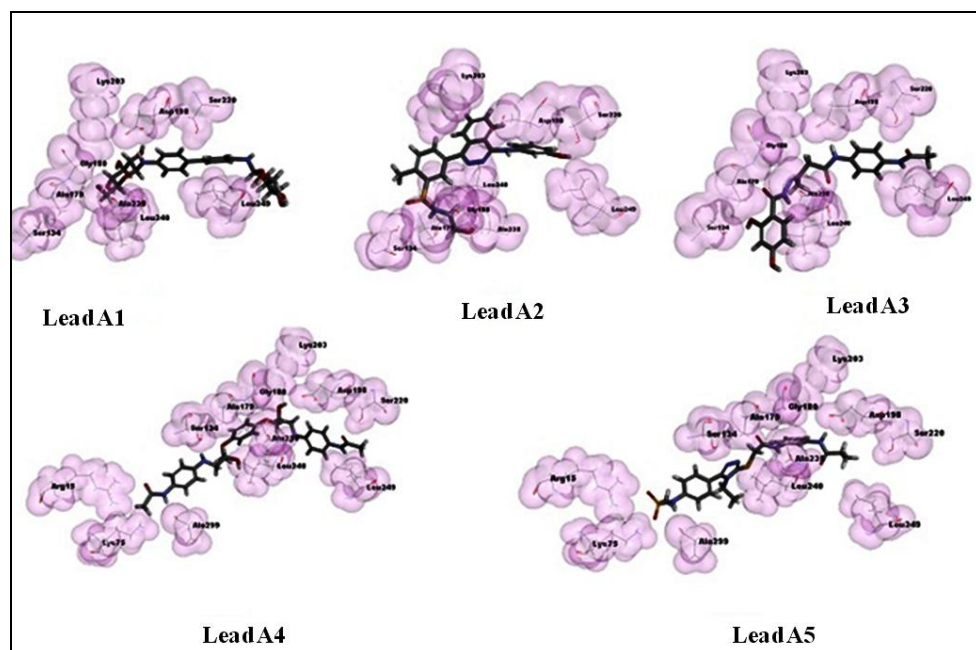
Figure 5.46: Binding pattern of top five hits in the *M. tuberculosis* L-AlaDH active site.

Table 5.18: Docking score, fitness, hydrogen bond interaction and GOLD score of best fit ligands.

Ligand	Fitness	Docking score	Glide score	H-Bond	GOLD Score	Interaction
Lead A1	1.34	-10.52	-10.523	9	58.9	Asp198,Ser220,Lys203,2Ser134, Arg15,Ala299,Gly177,Leu240
Lead A2	1.63	-9.88	-9.880	5	54.44	Asp198,Ser220,2Lys203,Asn200
Lead A3	1.17	-7.50	-7.509	5	58.43	Asp270,Ala178,Asp198,Leu240, Ser220
Lead A4	1.23	-7.47	-7.471	7	72.57	Asp198,Thr178,Ala238,Ala299, Lys75,Arg15
Lead A5	1.34	-7.01	-7.926	7	50.5	Leu137,Ser220,Asp198,Leu240, Gly180,Ala238

5.2.1.1d. Enzyme kinetics of *M. tuberculosis* L-AlaDH

Kinetic and mechanistic studies of L-AlaDH from several species showed that the enzyme followed a predominantly ordered mechanism, with NAD^+ and NADH binding occurring first in the oxidative deamination and reductive amination direction, respectively [Agren D. et al., 2008]. Initially we measured the concentration by range finding experiment at which the *M. tuberculosis* L-AlaDH enzyme worked, later substrate alanine and NAD^+ concentration were also measured. Then, we performed Michaelis–Menten kinetics to determine K_m and V_{max} for alanine and NAD^+. The K_m and V_{max} were found to be 0.049 mM and 1.071 absorbance units (AU) respectively. Similarly for NAD^+ the K_m and V_{max} were found to be 0.53 mM and 0.37 AU respectively (**Figure 5.47**).
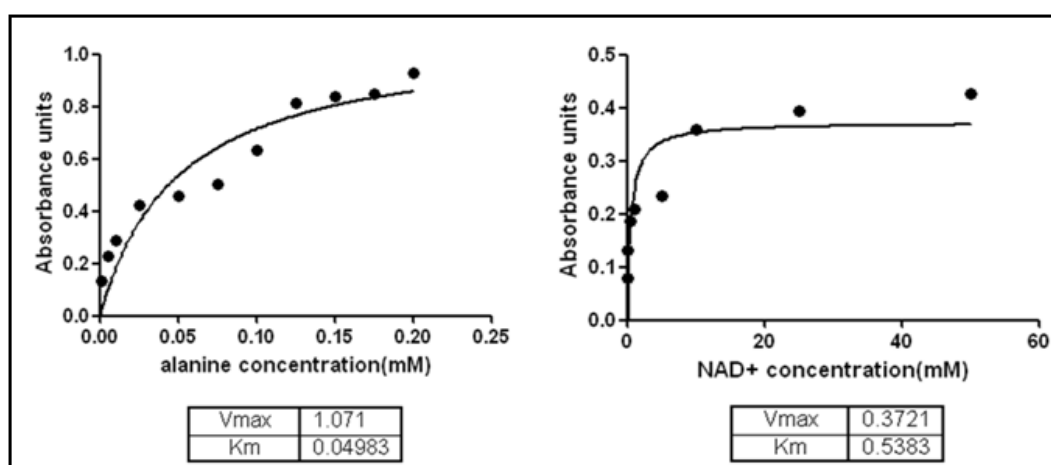
Figure 5.47: Enzyme kinetics of alanine and NAD^+.

5.2.1.1e. *In vitro* **enzyme inhibition of** *M. tuberculosis* **L-AlaDH**

Photometric determination of L-AlaDH activity was accomplished by measuring the rate of the production of NADH that accompanied the conversion of alanine into pyruvate in the oxidative deamination. The five most promising candidates exhibited IC_{50} values in the range of 35-80 μM, and the IC_{50} of two most active compounds **Lead A1** and **Lead A4** were found to be 35.54 and 36.84 μM respectively. These hits also showed high docking score and good no. of H-bond interaction which correlated with *in vitro* enzymatic inhibition studies. The IC_{50} values are represented in **Table 5.19**.

Table 5.19: Activity table showing the IC_{50} value of all the five top hits obtained through virtual screening.

Leads	IC_{50} μM
Lead A1	35.54±0.33μM
Lead A2	80.37±1.10 μM
Lead A3	51.529±1.25 μM
Lead A4	36.84±0.30 μM
Lead A5	73.84±2.23 μM

5.2.1.1f. Highlight of the study

The main objective of the present study was to identify the first set of inhibitors for *M. tuberculosis* L-AlaDH enzyme by using structure-based modeling. The availability of the crystal structure bound with co-factor of *M. tuberculosis* L-AlaDH was explored using pharmacophore model based on interaction energy and docking, to yield diverse leads. Structure based pharmacophore and virtual screening of Asinex database retrieved five top hit compounds with good docking score and interaction pattern. *In vitro* enzymatic inhibition studies of these five ligands yielded two compounds (**Lead A1** and **Lead A4**) with good IC_{50} of 35.54 and 36.84 μM, respectively (**Figure 5.48**).
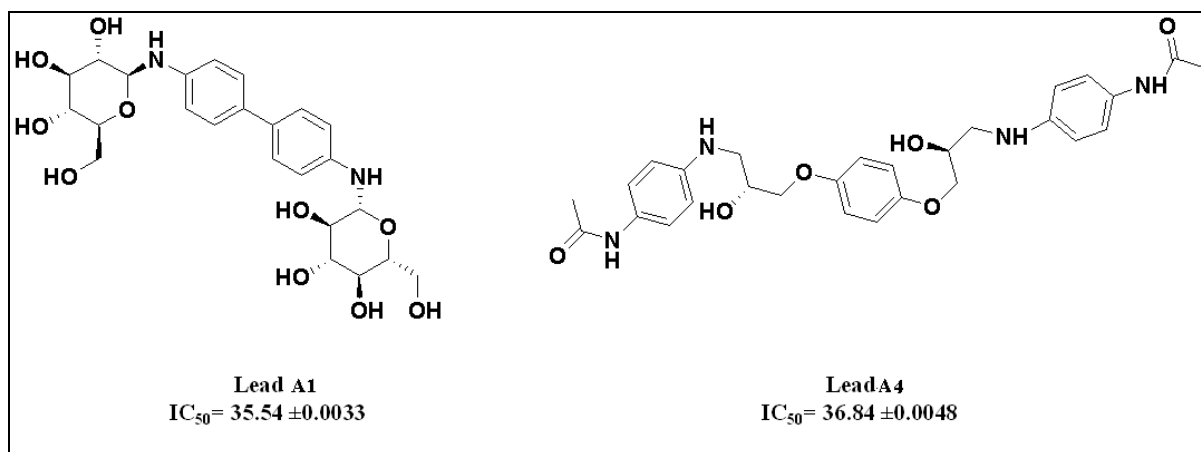
Figure 5.48: Identified lead compound through structure based virtual screening.

5.2.1.2. Design and identification of *M. tuberculosis* L-AlaDH inhibitors based on N_6-methyl adenosine bound protein

5.2.1.2a. Design of lead molecules

In the present study, crystal structure of the *M. tuberculosis* L-AlaDH in complex with N_6-methyl adenosine (PDB: 4LMP) having resolution of 1.95Å was used as a framework for structure based virtual screening of *in house* database consist is of 3000 diverse structured compounds to identify leads against this enzyme.

Analysis of the crystal structure of 4LMP revealed that the reference inhibitor in the AlaDH active site formed hydrogen-bonding network with Ser220, Asp198 and Leu240 active site residues. The reference ligand was re-docked with the active site residues of the *M. tuberculosis* AlaDH to validate the active site cavity. The ligand exhibited Glide score of -5.50 kcal/mol and was found in the vicinity of amino acids Ser220, Asp198 and Leu240, Ile174, Leu197, Asn200, Gly177, Ala176, Val241, Val239, Ile199 and Leu249. Re-docking results showed that the compound exhibited similar interactions as that of the original crystal structure with RMSD of 0.87Å suggesting reliability of the docking method. The superimposition of Glide docked conformation with co-crystal of 4LMP is shown in **Figure 5.49**.

Pharmacophore hypotheses were developed by mapping Glide XP energetic terms onto pharmacophore sites, and these energies were calculated based on the structural and energetic information between the protein and the ligand using Phase module having the default set of chemical features. The number of pharmacophore sites was set to ten and the total number of

pharmacophore sites derived was six with three donors (D), two ring aromatic (R) and one acceptor (A). The energy score of e-pharmacophore is represented in **Table 5.20**. Further based on energy score four features (D10, D11, A2 and R13) were selected and used for virtual screening. The six point and four point e-pharmacophores are shown in **Figure 5.50** which were then utilized for the virtual screening of *in house* database.
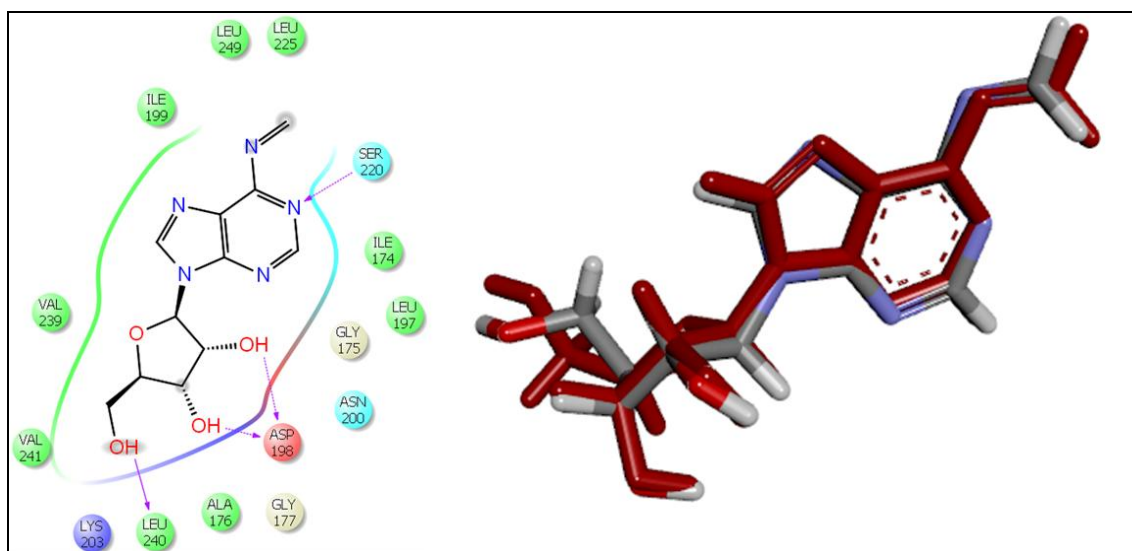
Figure 5.49: (a) Interactions of N_6-methyl adenosine with the active site residues of *M. tuberculosis* L-AlaDH protein. (b) Superimposition of docked pose (Red) of the N_6-methyl adenosine to the original pose of the N_6-methyl adenosine (Gray).

Table 5.20: Energy score of e-pharmacophore of N_6-methyl adenosine.

Rank	Feature label	Score	Type
1	D11[a]	-0.8	D
2	D10	-0.76	D
3	A2 [b]	-0.56	A
4	D9	-0.56	D
5	R13 [c]	-1.04	R
6	R12	-0.57	R

[a] Donor
[b] Acceptor
[c] Ring aromatics
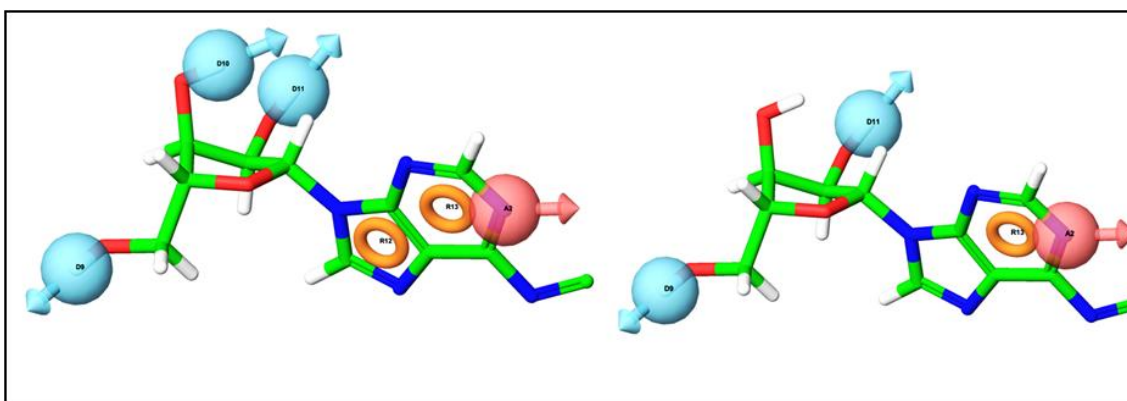
Figure 5.50: Energy based pharmacophoric features of N_6-methyl adenosine.

Compounds retrieved by e-pharmacophore filter using Phase with a fit value above 1.0 were considered as potential hits and were carried forward for high-throughput virtual screening. Compounds resulting with a score of $\leq$ -4.0 kcal mol^{-1} were subjected to another round of docking by Glide XP. Glide XP combined accurately, physics-based scoring terms and thorough sampling and resulted in compounds with docking scores between -6.649 to -5.45 kcal mol^{-1}. Final shortlisting of hit compounds was based on visual inspection of the important amino acid residues involved in binding that included hydrogen bonding with Ser220, Leu240, and Asp198.

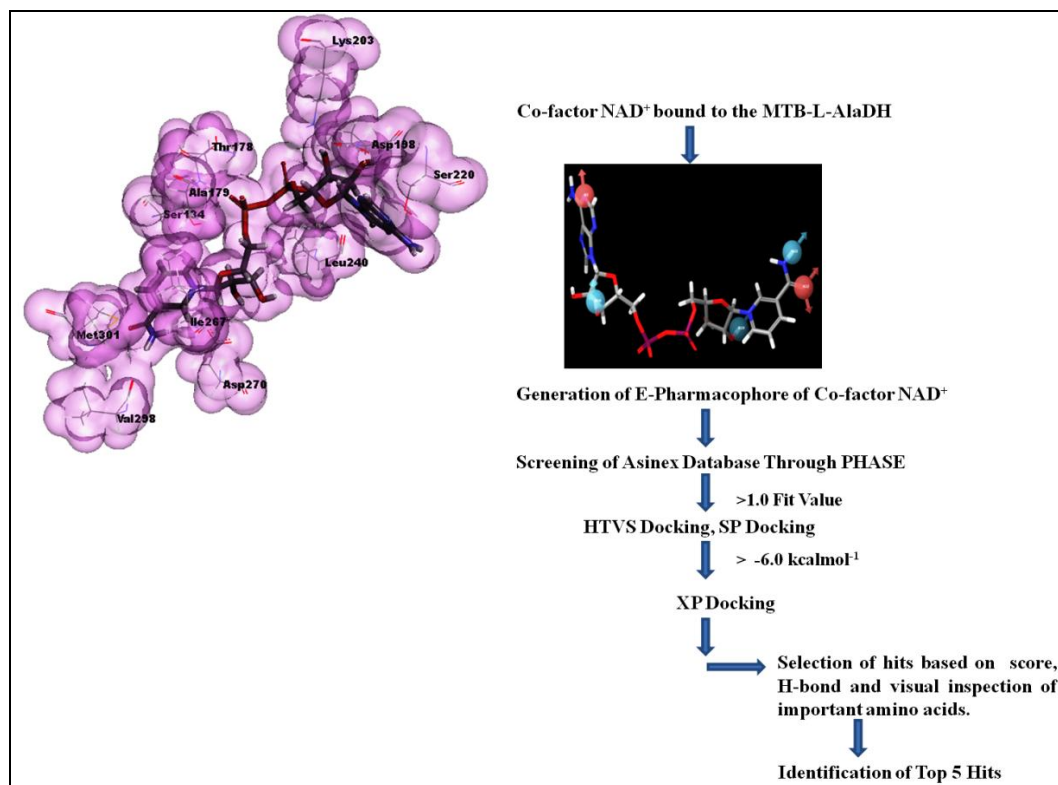In order to understand how these ligands bind to the enzyme, final hit molecules obtained from Glide XP were further evaluated with GOLD 5.1.2 program to confirm their potency. Thus we had selected top ten compounds from the Glide XP docking study with no violations of drug likeliness properties with the best Glide scores -6.649 to -5.45kcal mol^{-1} and GOLD scores (50.12-65.78), suggesting strong protein-ligand interactions. The chemical structures of these five compounds are illustrated in **Figure 5.51**. All these top hits showed good docking score and interaction with important amino acids residues and were well fit in the active site cavity of the protein. The docking score, fitness, H-bond and important interactions of these hits are represented in **Table 5.21**.
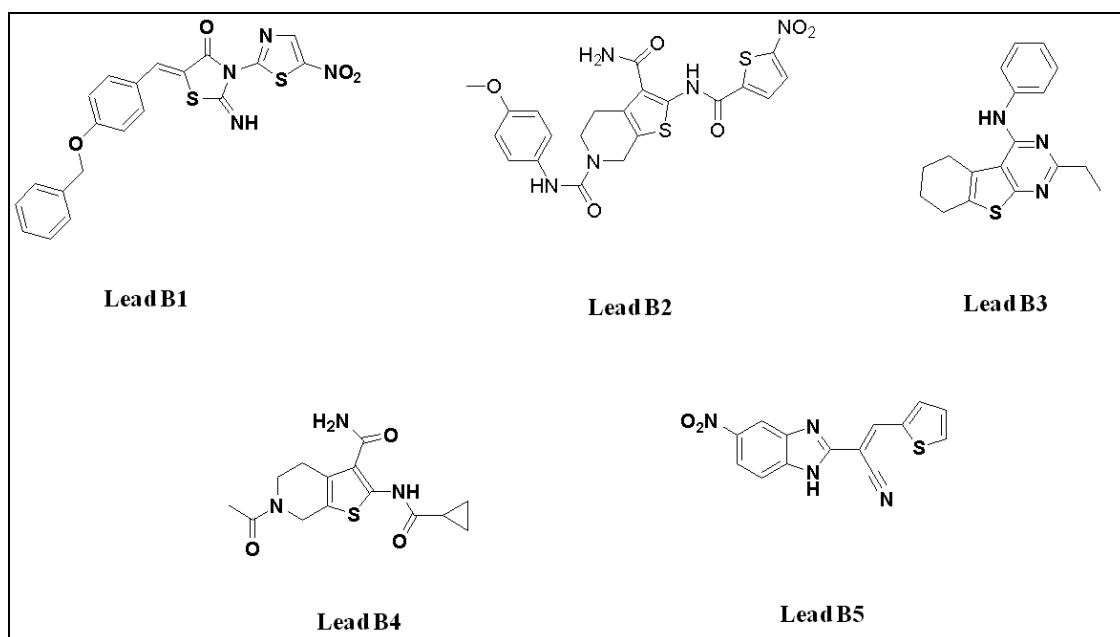
Figure 5.51: Chemical structures of top five compounds after virtual screening.

Table 5.21: The fitness, docking score, hydrogen bond interaction and GOLD score of top five ligands.

Ligand	Fitness	Docking Score	H-Bond	GOLD Score	Interaction
Lead B1	1.34	-6.92	3	62.17	Ser220, Lys203
Lead B2	1.56	-7.21	5	60.41	Ala238, Lys203, Ser220, Leu240,Thr178
Lead B3	1.67	-5.71	3	62.57	Ser220, Lys203, Ala238
Lead B4	1.23	-6.09	4	65.78	Ser220, Lys203,Thr178
Lead B5	1.43	-5.95	3	56.89	Ser220, Lys203, Leu240

5.2.1.2b. *M. tuberculosis* **L-AlaDH enzyme inhibition studies**

Further the final hits, from *in house* database, were screened initially at 50 μM concentration and later 25 μM and 10 μM respectively against *M. tuberculosis* L-AlaDH using an assay based on the spectrophotometric determination of the reaction product pyruvate by 96-well plate format in Perkin Elmer Victor V3 Spectrophotometer. In the initial screening all the compounds showed good percentage inhibition in the range of 40.0 to 56.6%. Thus IC_{50} values were calculated using non-linear regression analysis using GraphPad Prism software for all the compounds. All the compounds showed activity with IC_{50} ranging from 6.77±0.02

138

µM to 25.12±0.06 µM (**Table 5.22**). We identified (Z)-5-(4-benzyloxy)benzylidene-2-imino-3-(5-nitrothiazol-2-yl)thiazolidin-4-one **(Lead B1)** and 2-(5-nitrothiophene-2-carboxamido)-4,5-dihydro-N6-(4-methoxyphenyl)thieno[2,3-c]pyridine-3,6(7H) dicarboxamide **(Lead B2)** as potential inhibitors for *M. tuberculosis* L-AlaDH. Compounds showed a docking score of -6.92 and -7.21 kcal/mol respectively. Both the compounds are showed best activity among the ten compounds with the IC_{50} of 6.77 µM and 8.17 µM respectively.

Table 5.22: Activity table showing the IC_{50} value of all the ten hits obtained through virtual screening.

Leads	IC_{50} µM
Lead B1	6.77±1.12µM
Lead B2	8.17±1.25µM
Lead B3	15.10±1.75µM
Lead B4	20.12±1.00 µM
Lead B5	21.34±1.80 µM

Based on the two identified hit, we undertook synthesis of various analogues and evaluated for its biological activity against *M. tuberculosis* L-AlaDH for establishing SAR, to evaluate antimycobacterial activity in active and dormant *M. tuberculosis* and cytotoxicity. Docking of the **Lead B1** within the active site of the *M. tuberculosis* L-AlaDH protein is illustrated in **Figure 5.52**. Though the **Lead B1** showed one hydrogen bonding with Ser134 with a well fitted pose in the active site in the hydrophobic pocket within the vicinity of Ile199, Pro247, Leu255, Leu249, Leu197, Ile174, Ala126, Leu127, Ala179, Leu130, Ala176 and few polar amino acid residues Gln121, Asp198, Thr178, Ser220 respectively. The binding pattern within the active site pocket of the crystal ligand and reference ligand was quite similar and additionally the *cation-pi* between Lys203 and the ligand constituted for a stable binding profile of the molecule.
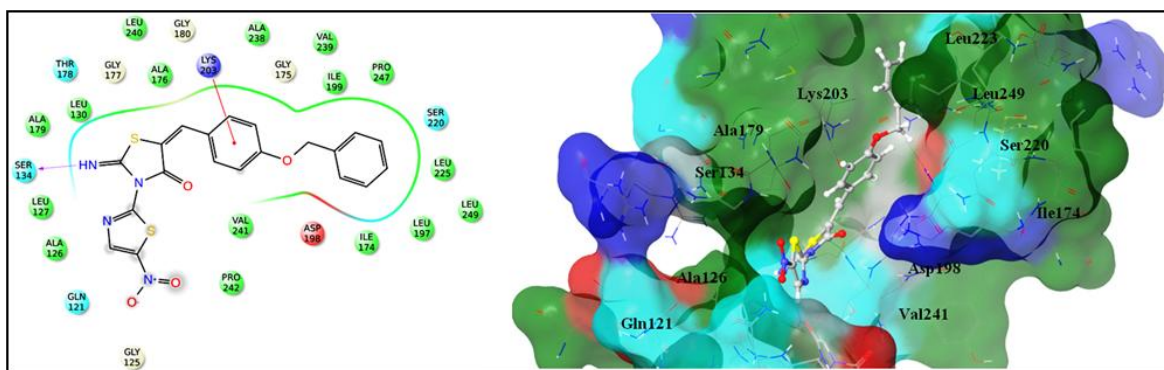
Figure 5.52: Binding pose and the interaction pattern of the **Lead 1**.

The docking orientation of **Lead B2** is representation in **Figure 5.53**, where the following interactions were observed at the binding site. The NO_2 group on thiophene ring was involved in hydrogen bonding interaction with Ser220, which was also observed in reference ligand. Further the amide NH_2 group on pyridine was stabilized by two hydrogen bonding interaction with Leu240 and Ala238 amino acid residues. The compound was found in the proximity of various hydrophobic amino acids such as Ile199, Pro247, Leu255, Leu249, Leu197, Ile174, Ala126, Leu127, Ala179, Leu130, and Ala176 where it showed hydrophobic interactions. Apart from these interactions the compound was further stabilized by *cation-pi* interaction with Lys203 amino acid residue.
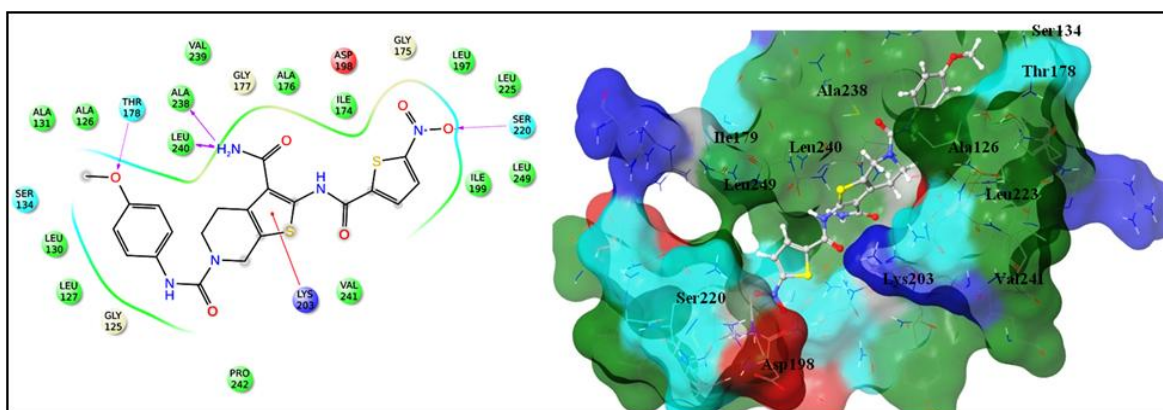
Figure 5.53: Binding pose and the interaction pattern of the **Lead B2**.

5.2.1.2c. Lead optimization

A library of 30 molecules, comprising of fifteen iminothiazolidine-4-one derivatives (compound **4a-o**) based on **Lead B1** and another fifteen 4,5,6,7-tetrahydrothieno[2,3-c]pyridine-3-carboxamide derivatives (compound **11-25**) based on **Lead B2** were synthesised

as shown in **Schemes 1** and **2** described in material and method section. Synthesis of chloroacetamides **2 a-o** was carried out by treating different substituted aromatic amines with chloroacetyl chloride under reflux conditions in benzene. In next step cyclisation of substituted chloroacetamide were accomplished by treating with KSCN in acetone under reflux conditions to yield iminothiazolidine-4-one (**3 a-o**). In final step, the target molecules **4** (**a-o**) were achieved by reaction of compounds **3 a-o** with 4-benzyloxybenzaldehyde using sodium acetate in acetic acid under thermal conditions.

For the second set of compounds, the conversion of N-Boc protected 4-piperdone (**5**) to *tert*-butyl 2-amino-3-carbamoyl-4,5-dihydrothieno[2,3-c]pyridine-6(7H)-carboxylate (**6**) was based on Gewald reaction, which was performed by treating compound **5** with cyanoacetamide, sulphur powder and morpholine using EtOH as solvent at room temperature. Compound **6** on direct reaction with substituted benzoyl chloride was not successful, so we used mixed anhydride instead of benzoyl chloride derivatives. The mixed anhydride (**8a-c**) was synthesised by treating compound corresponding benzoic acids (**7a-c**) with ethyl chloroformate and in the next step the synthesised mixed anhydrides were reacted with compound **6** under microwave reaction conditions using NaH as base and dry THF as solvent to yield corresponding 2-carboxamides (**9a-c**). Further deprotection of Boc was carried out by treating with TFA in dichloromethane at room temperature. In final step, the secondary free amine was treated with acetyl chloride/benzoyl chloride using Et$_3$N in dichloromethane and with CH$_3$I/PhCH$_2$Br using NaH as base under microwave irradiation to get compounds compounds (11-25). The general procedure and spectral analysisi of all the 30 compounds are represented in Annexure-II.

5.2.1.2d. *M. tuberculosis* L-AlaDH enzyme inhibition studies for synthesized compounds

The synthesized compounds were assayed for the inhibition of *M. tuberculosis* L-AlaDH at concentrations ranging from 25 μM to 0.5 μM. In the initial screening all the synthesized compounds showed good percentage inhibition in the range of 40.0 to 86.6%. Thus IC$_{50}$ values were calculated using non-linear regression analysis using GraphPad Prism software for all the compounds from both series. All the synthesized compounds showed activity with IC$_{50}$ ranging from 0.58±0.02 μM to 22.31±0.06 μM (**Table 5.23** and **5.24**). Twenty three compounds out of thirty synthesized compounds were found to be more potent than the initially identified **Lead B1** and **B2** (IC$_{50}$ of 6.77± 0.12 μM and 8.17± 0.18 μM). From the first series of iminothiazolidine-4-one derivatives, compounds **4n** and **4o** were found to be

most potent *M. tuberculosis* L-AlaDH inhibitor with IC_{50} 1.34±0.01 and 1.74±0.03 μM, while in the second series of 4,5,6,7-tetrahydrothieno[2,3-c]pyridine-3-carboxamide derivatives compound **12** and **14** were found to be most active compound with IC_{50} of 0.58±0.02 and 0.64±0.06 μM. Dose-response curves were plotted for the two most potent compounds (**4n** and **4o**) from series 1 and another two most active compound (**12** and **14**) from series 2 using GraphPad Prism software by taking log (inhibitor concentration) on the x-axis and response (% inhibition) on the y-axis as shown in **Figure 5.54A** and **5.54B.**
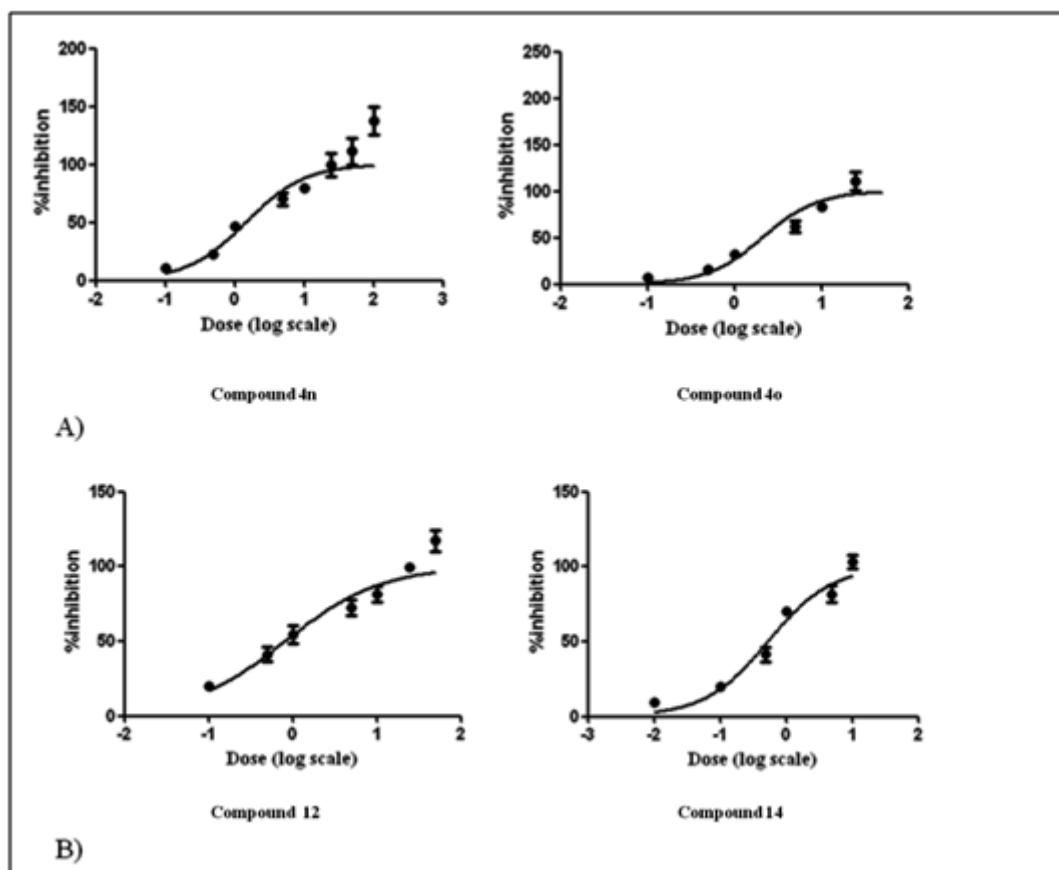
Figure 5.54: Dose-response curves for selected *M. tuberculosis* L-AlaDH inhibitors.

Further to support the activity we performed docking for these compounds. As shown in activity **Table 5.23**, most of the compounds exhibited good IC_{50} in the range of 1.34 to 22.31 μM against L-AlaDH with six compounds showed better activity than the lead compound **B1** (IC_{50}= 6.77 μM). Additionally, all of these inhibitors occupied a narrow potency range, indicating tolerability for a wide variety of substituent's on the R_1 position. The 4-chlorophenyl, 4-florophenyl group substituents (4b and 4c) at the R_1 position displayed good *M. tuberculosis* L-AlaDH inhibitory activity, while 4-bromophenyl substituted group (4a) showed moderately activity. Compounds containing the combination of the nitrophenyl group

at *meta* and *para* position at R_1 (4e and 4f) provided good *M. tuberculosis* L-AlaDH inhibitory activity, while introduction of 2-nitrophenyl group at R_1 position (4d) also provided moderately inhibitory activity. The compound substituted with 2,4-dichlorophenyl, 3-chloro-2-methylphenyl, pyrimidin-2-yl, pyridin-2-yl, 6-methylpyridin-2-yl and simple phenyl groups at R_1 (**4g-4l**) resulted in good *in vitro M. tuberculosis* L-AlaDH inhibitory activity in the range of 3.49±0.06 to 2.27±0.04 μM, while substitution with a 2,5-dimethylphenyl and 2,6-dimethylphenyl (**4n-4o**) led to emerged as a most potent compounds compared to other compounds from this series. This was well supported by the interaction profile of the molecules in the docking studies. Compound **4n** (Z)-5-(4-(benzyloxy)benzylidene)-2-imino-3-(2,5-dimethylphenyl)thiazolidin-4-one from the series 1 showed highest docking score of -7.50 kcal/mol which correlated well with its potency in the enzyme assay (IC_{50}=1.34±0.01 μM). Closer analysis of this compound in the protein active site revealed hydrogen bonding interactions with the Thr178. In addition to hydrogen bonding interactions, the compound was further stabilized by *cation-pi* stacking interaction with the phenyl ring of Lys203. The compound also showed hydrophobic interaction with Leu130, Ala131, Leu127, Pro128, Ala126, Pro242, Ala238, Val239, Leu197, Leu249, Ile174, Ile199, Leu225, Ala176 and Ala179 amino acid residues. Some polar contact was also observed between the compound and protein such as Asn200, Ser220, Ser134 and Gln271 (**Figure 5.55**). Further *in silico* investigation into binding profile of the molecules in the *M. tuberculosis* L-AlaDH domain revealed the importance of the hydrophobic interactions in increasing the specificity of the molecule towards the protein.
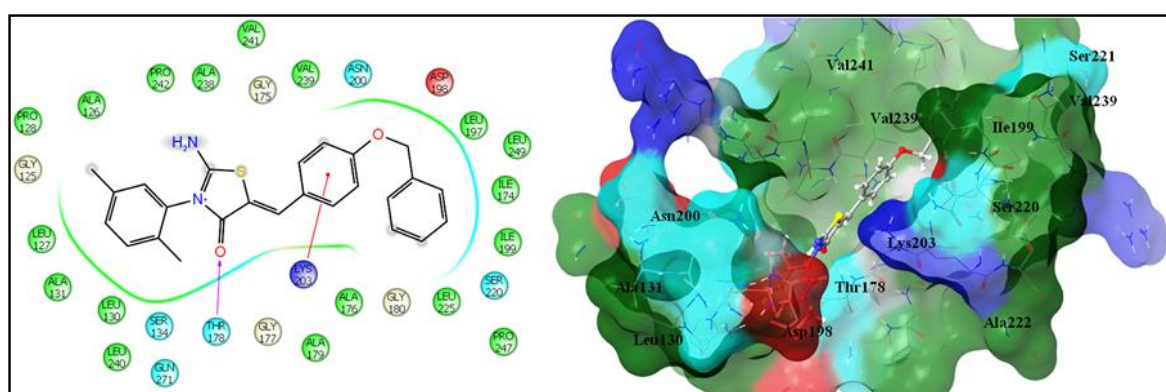
Figure 5.55: Binding pose and the interaction pattern of the compound **4n**.

The other active compound **4o** (Z)-5-(4-(benzyloxy)benzylidene)-2-imino-3-(2,6-dimethylphenyl)thiazolidin-4-one from this series also showed good binding energy of -6.90 kcal/mol which was further analyzed in more detail to understand its binding pattern. The

143

oxygen atom of benzyloxy group was fpound to interact with Ser220, analogous to the one observed in the reference crystal ligand. Apart from this, 2,6-dimethylphenyl ring interacted with Lys203 *via cation-pi* interaction. In the active site cavity the compound also made some polar contacts with Thr178, Asn200, Ser221 and Asp198 amino acid residues as well as hydrophobic interactions with Leu130, Ala131, Leu127, Pro128, Ala126, Pro242, Ala238, Val239, Leu197, Leu249, Ile174, Ile199, Leu225, Ala176 and Ala179 amino acid residues (**Figure 5.56**).
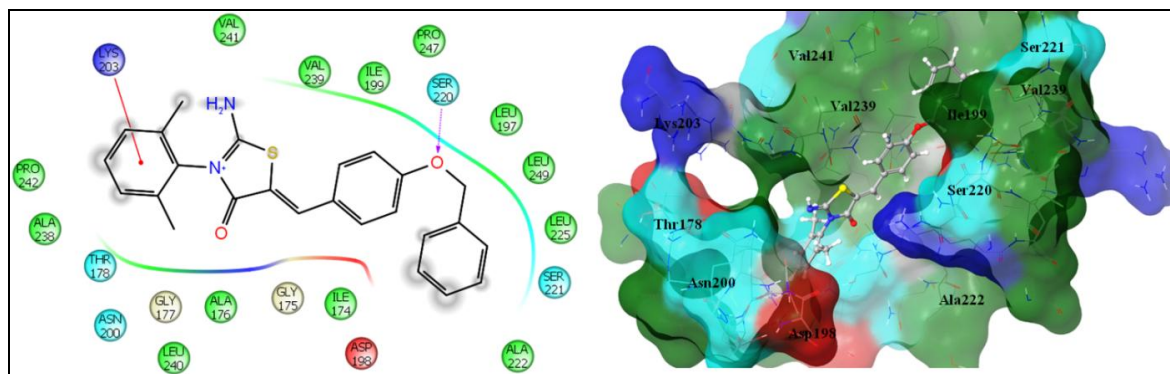
Figure 5.56: Binding pose and the interaction pattern of the compound **4o**.

The second **Lead B2** was also selected for further optimization, on which the structural modification was carried out in order to increase the binding ability. Thus, we have synthesized a series of 4,5,6,7-tetrahydrothieno[2,3-c]pyridine-3-carboxamide derivatives. Among the synthesised derivatives twelve compounds inhibited *M*. *tuberculosis* L-AlaDH with an IC_{50} of less than 1 μM (**Table 5.24**). Binding analysis of two most active compounds from this series (**12** and **14**) showed that both the compounds were well docked in the active site cavity of AlaDH protein with the docking score of -7.50 and -7.89 kcal/mol respectively. From the docking results, the formation of hydrogen bonds and hydrophobic interactions with the active site were predicted to be the most important factors affecting the inhibitory potency of these compounds. Compound **12** was involved in two hydrogen bonding interactions with Ser220, Leu197 amino acid residues. Apart from this, the compound was further stabilized by *cation-pi* interaction with Lys203 amino acid residue. The acetyl and 4-chloro group were found to make polar contacts with Ser221 and Thr178 amino acid residues. The compound was found to inserted in to the hydrophobic cavity where was stabilized by various hydrophobic amino acid such as Ile174, Ile199, Leu225, Leu249, Ala22, Pro247, Val239, Pro242, Val241, Leu241, Leu240 Ala179, Ala238 and Ala176 (**Figure 5.57**).
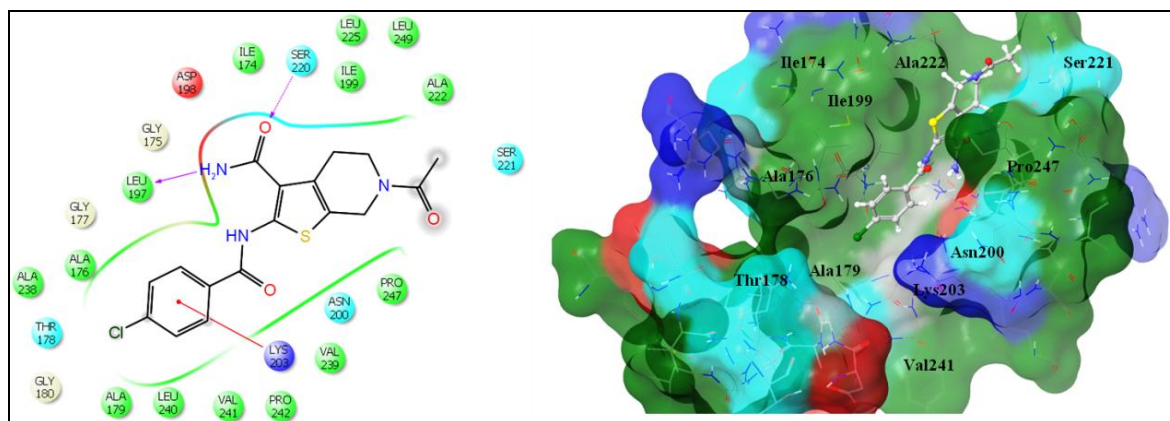
Figure 5.57: Binding pose and the interaction pattern of the compound **12**.

The predicted binding pose of the second most active compound (**14**) suggested that the observed improved potency arised due to the extensive hydrophobic interactions predicted to be formed with the side chains of Ile174, Ile199, Leu225, Leu249, Ala22, Pro247, Val239, Pro242, Val241, Leu241, Leu240 Ala179, Ala238 and Ala176 amino acid residues (**Figure 5.58**). The binding energy of the compound **14** was also found to be of -7.89 kcal/mol. The *cation-pi* interaction formed between the pyridine ring of compound **14** and Lys203 resulted in good activity, and additional hydrogen-bond interactions were observed with amino acid residues Leu240 and Lys203 which made the compound more fit in to the active site of protein.
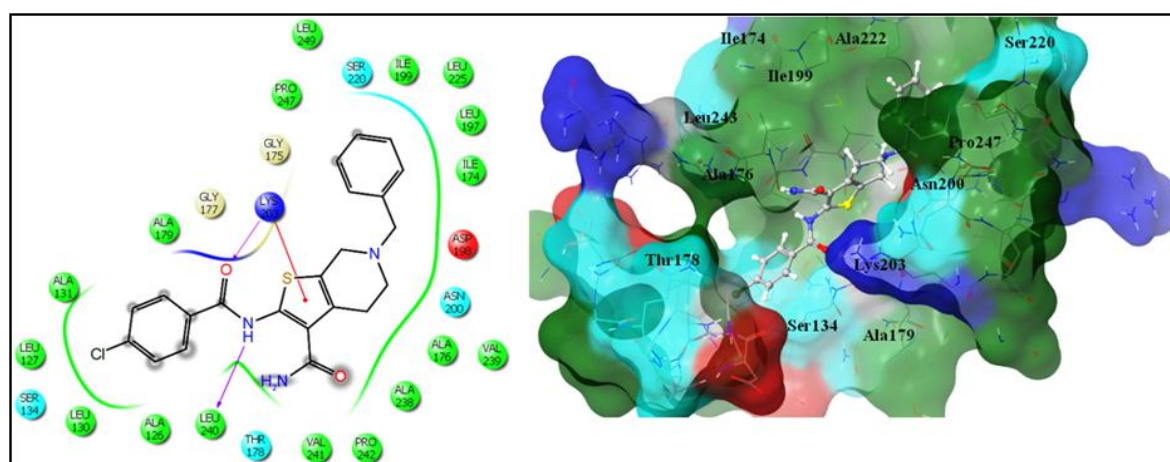
Figure 5.58: Binding pose and the interaction pattern of the compound **14**.

5.2.1.2e. *In vitro* dormant *M. tuberculosis* model

J.C. Betts et al. have established an *in vitro* model, in which nutrient starvation caused *M. tuberculosis* to arrest growth, minimized aerobic metabolism and became resistant to existing

145

antitubercular drugs while maintaining viability. Nutrient starvation may therefore mimic some of the features of *M. tuberculosis* during the persistent state. Moreover their protein expression profile of this model indicated that AlaDH was over expressed 6.04 times. Owing to its simplicity, reproducibility and ease of handling, we utilized this model for testing our novel potent AlaDH inhibitors aimed at persistent bacteria. In this model, cultures of *in vitro* grown *M. tuberculosis* bacteria were subjected to nutrient depletion by growing the culture in PBS (Phosphate buffer saline) for 6 weeks. Nutrient starvation using this method triggered a dormancy response in the bacilli that was termed non-replicating persistence (NRP), a physiological state thought to mimic the one exhibited by *M. tuberculosis* during various stages of persistent infection. After 6 weeks, the culture was treated with the synthesized and standard drugs (INH, RIF, Moxifloxacin) at a concentration of 10 µg/ml in a tube and incubated at 37°C for 7 days. The treated cell suspensions were diluted 10-fold up to 10^{-6} using Middlebrook 7H9 medium supplemented with OADC and were plated in 48 well plates in triplicates. The plates were incubated at 37°C for 4 weeks and the wells with visible bacterial growth were counted as positive and MPN values were calculated using standard statistical methods [Joanna C., *et al.*, 2002]. At 10 µg/ml concentration, standard first line anti-TB drugs INH and RIF reduced ~1.2 and 2.0 log bacterial reduction respectively whereas the DNA gyrase inhibitor moxifloxacin showed high activity with ~2.5 log bacterial reduction. When compared to INH all the eighteen screened compounds showed better activity with ~2.0 to 3.2 log bacterial reduction. Seventeen compounds were found to be more potent than RIF, and nine compounds (**4c, 4g, 4o, 11, 16, 19, 23-25**) were found to be more potent than moxifloxacin. Compound **24** (*tert*-butyl 2-(4-(benzyloxy)benzamido)-3-carbamoyl-4,5-dihydrothieno[2,3-c]pyridine-6(7H)-carboxylate) and **25** (6-benzyl-2-(4-(benzyloxy)benzamido)-4,5,6,7-tetrahydrothieno[2,3-c]pyridine-3-carboxamide) were found to be more promising with ~3.2 log bacterial reduction (**Figure 5.59** and **5.60**). These compounds also inhibited *M. tuberculosis* L-AlaDH with IC$_{50}$ of < 1 µM.
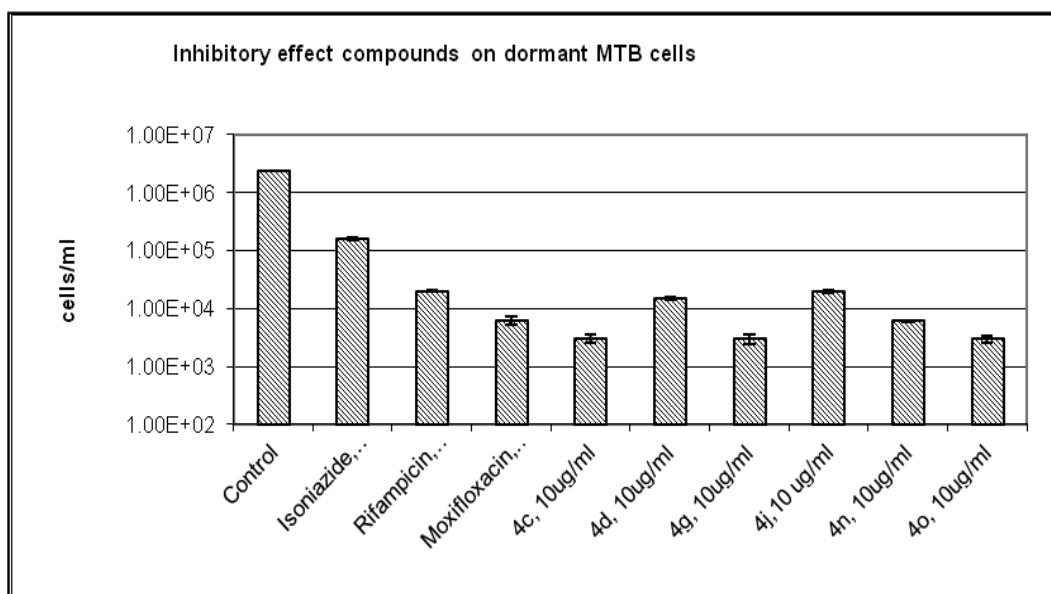
Figure 5.59: Bactericidal effect of **4c, 4d, 4g, 4j, 4n** and **4o** on dormant *M. tuberculosis* cells. Cells were treated with the compounds (10 µg/ml) for 7 days at 37°C. The viability of both treated and untreated cells was tested by MPN assay. The error bars represent standard deviation.
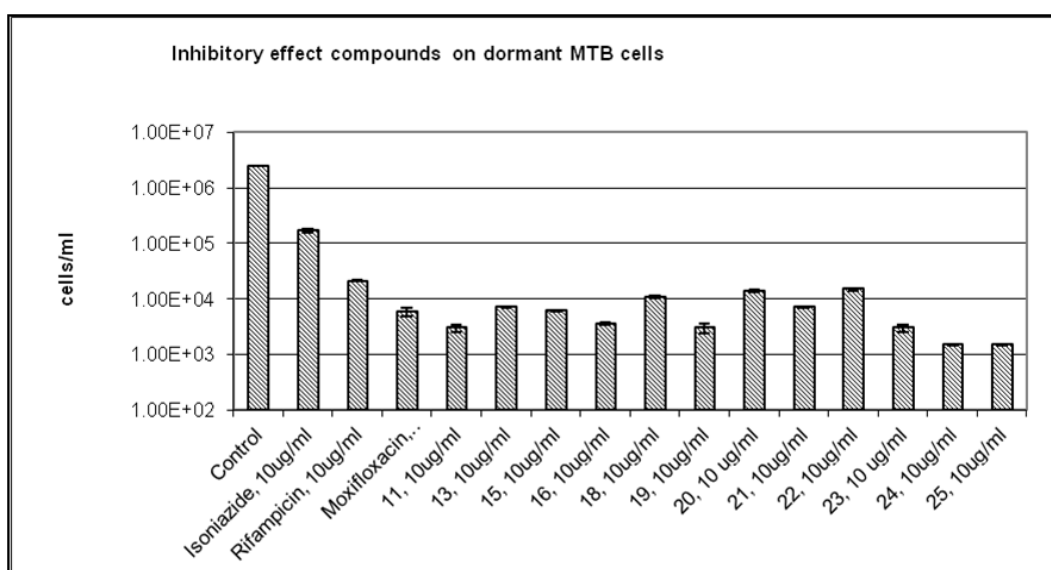
Figure 5.60: Bactericidal effect of **11, 13, 15-16, 18-25** on dormant *M. tuberculosis* cells.

5.2.1.2f. *In vitro* active *M. tuberculosis* model

All the synthesized compounds were also screened for their *in vitro* anti-tubercular activity were further screened for their *in vitro* antimycobacterial activity against *M. tuberculosis* H37Rv by microplate Alamar blue assay method. The MIC was determined for each

compound which was measured as the minimum concentration of compound required to completely inhibit the bacterial growth. INH, ETH, RIF and moxifloxacin were used as reference compounds for comparison. The MIC values of the synthesized compounds along with the standard drug for comparison are presented in **Table 5.23** and **5.24**. All the synthesized compounds showed activity against *M. tuberculosis* with MIC ranging from 1.53 to 60.38 μM. Six compounds (**4k, 4m, 14, 18, 22** and **24**) inhibited *M. tuberculosis* with MIC of < 2 μM. All the compounds were less potent than INH, RIF and moxifloxacin. Sixteen compounds were found to be more potent than ETH (MIC of 7.64 μM).

5.2.1.2g. *In vitro* cytotoxicity studies

The safety profile of all the synthesized compounds was evaluated by testing their *in vitro* cytotoxicity in mouse macrophage cell line (RAW 264.7) at 50 μM concentration using MTT assay [Scudiero D.A., *et al.*, 1988] Since *M. tuberculosis* resides inside the macrophage, the monocyte macrophage cell lines (RAW 264.7) were mostly used for tuberculosis research; in order to check whether the screened compounds were not toxic towards macrophages but toxic to the bacteria. Almost all the tested compounds demonstrated a good safety profile with very low inhibitory potential. Compounds inhibited within a range of 4.71-59.67%. Furthermore, the most active compound **4n** and **4o** from first series and compounds **12** and **14** from second series had 38.67 and 45.81 and 37.32 and 38.43% inhibition respectively at 50 μM concentration of the drug, reflecting its safety profile in the eukaryotes, cytotoxic results of all the compounds are illustrated in the **Tables 5.23** and **5.24.**

5.2.1.2h. Biophysical characterization

The stabilization of two active compounds from both the series were investigated using biophysical technique called DSF by measuring the fluorescence of the native protein and protein-ligand complexes in presence of a fluorescent dye whose fluorescence increasedd when exposed to non polar residues of the protein and reach the maximum when the protein denatured. A higher or positive shift of melting temperature (T_M) of protein-ligand complex compared to the native protein T_M signified a better stabilization of the protein-ligand complex, which in turn reflected on the inhibitor binding. The most potent compounds **4n** and **4o** from first series display good positive shifts towards the *M. tuberculosis* L-AlaDH protein (4.6°C and 1.4°C), whereas the second series compounds **12** and **14** shows 1.7°C and 1.8°C

positive shifts towards the *M. tuberculosis* L-AlaDH protein which further was re-ascertained for their stabilization towards the protein (**Figure 5.61**). The native protein melting temperature was 46.20°C; whereas the protein complexed with ligand showed melting temperature of 49.90°C to 51.80 °C proving the stabilization of the ligand towards the desired protein *M. tuberculosis* L-AlaDH.

Compound 4n
Protein, T_m = 47.20°C
Protein with ligand, T_m = 51.80°C

Compound 4o
Protein, T_m = 47.20°C
Protein with ligand, T_m =48.60°C

Where, ——— *represents Protein Melting curve*
——— *represents Protein complexes with ligand melting curve*

A)

Compound 12
Protein, T_m = 46.70°C
Protein with ligand, T_m = 48.40°C

Compound 14
Protein, T_m = 46.10°C
Protein with ligand, T_m =47.90°C

Where, ——— *represents Protein Melting curve*
——— *represents Protein complexes with ligand melting curve*

B)

Figure 5.61: DSF experiment for most active compounds from both series (**4n**, **4o**, **12** and **14**).

Table 5.23: Biological activities of synthesized compounds based on lead 2.
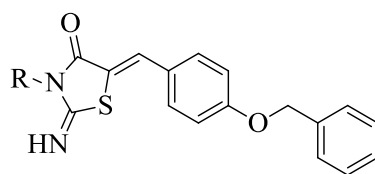
4a-o

Compound	R	AlaDH IC$_{50}$	*M. tuberculosis* MIC in μM	Cytotoxicity at 50 μM (RAW 264.7 cells) % inhibition
4a	4-Bromophenyl	22.31±0.06	3.35	7.825
4b	4-Chlorophenyl	7.01±0.05	7.42	16.370
4c	4-Fluorophenyl	8.55±0.02	7.72	10.516
4d	2-Nitrophenyl	15±0.03	58	24.375
4e	3-Nitrophenyl	5.56±0.01	14.50	52.878
4f	4-Nitrophenyl	6.16±0.05	7.23	17.269
4g	2,4-Dichlorophenyl	3.49±0.06	13.76	13.776
4h	3-Chloro-2-methylphenyl	12.96±0.04	14.40	59.672
4i	Pyrimidin-2-yl	7.52±0.03	4.02	26.627
4j	Pyridin-2-yl	2.12±0.01	8.06	37.232
4k	6-Methylpyridin-2-yl	9.44±0.08	1.94	25.078
4l	Phenyl	2.27±0.04	16.19	37.875
4m	2,4-Dimethylphenyl	6.08±0.001	1.88	36.839
4n	2,5-Dimethylphenyl	1.34±0.01	15.09	45.818
4o	2,6-Dimethylphenyl	1.74±0.03	60.38	38.676
Isoniazid		NA	0.72	ND
Rifampicin		NA	0.15	ND
Ethambutol		NA	7.64	ND
Moxifloxacin		NA	1.24	ND

NA indicates not active, ND indicates not determined.

Table 5.24: Biological activities of synthesized compounds based on lead 2.
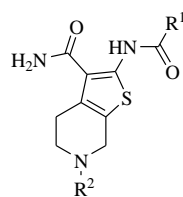
11-25

Compound	R_1	R_2	AlaDH IC_{50}	*M. tuberculosis* MIC in µM	Cytotoxicity at 50µM (RAW 264.7 cells) % inhibition
11	4-Chlorophenyl	Benzoyl	1.5±0.0233	28.47	42.50
12	4-Chlorophenyl	Acetyl	0.64±0.06	4.13	38.43
13	4-Chlorophenyl	Methyl	0.67±0.03	8.95	38.52
14	4-Chlorophenyl	t-Butyloxycarbonyl	0.58±0.03	1.79	37.32
15	4-Chlorophenyl	Benzyl	1.14±0.03	3.67	11.11
16	4-Phenoxyphenyl	Benzoyl	1.11±0.03	3.47	4.71
17	4-Phenoxyphenyl	Acetyl	0.66±0.01	6.11	32.91
18	4-Phenoxyphenyl	Methyl	0.73±0.03	1.85	58.87
19	4-Phenoxyphenyl	t-Butyloxycarbonyl	1.12±0.06	6.33	26.85
20	4-Phenoxyphenyl	Benzyl	0.78±0.04	3.58	23.60
21	4-Benzyloxyphenyl	Benzoyl	0.80±0.01	12.93	13.66
22	4-Benzyloxyphenyl	Acetyl	0.63±0.003	1.56	11.60
23	4-Benzyloxyphenyl	Methyl	1.22±0.01	15.35	37.59
24	4-Benzyloxyphenyl	t-Butyloxycarbonyl	0.64±0.02	1.53	52.10
25	4-Benzyloxyphenyl	Benzyl	0.81±0.08	12.57	23.99
Isoniazid	-	-	NA	0.72	ND
Rifampicin	-	-	NA	0.15	ND
Ethambutol	-	-	NA	7.64	ND
Moxifloxacin	-	-	NA	1.24	ND

NA indicates not active, ND indicates not determined.

5.2.1.2i. Highlights of the study

In summary, we identified and synthesized a novel thiazolidine and '2-aminothiophene' derivatives from a structure based virtual screening of *in house* database consisting of 2500 compounds. Most of the compounds showed potent *M. tuberculosis* L-AlaDH inhibition and *M. tuberculosis* MIC in active as well as dormant model. Compound **4n** and **4o** from first series and compound **12** and **14** from second series showed potency (**Figure 5.62),** selectivity, and no cytotoxicity up to 50 μM and emerged as valid leads for further development.
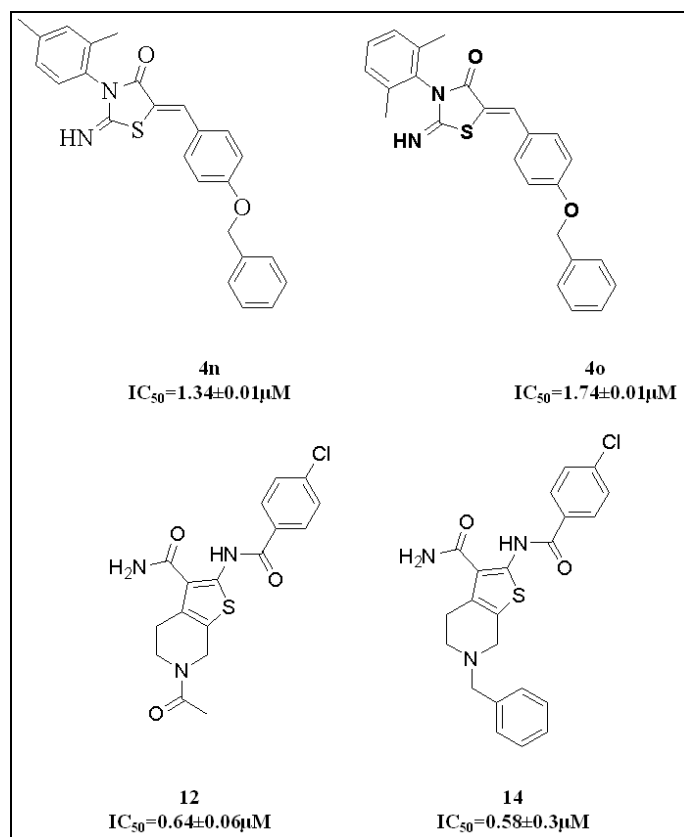
Figure 5.62: Optimized lead after virtual screening.

Chapter 6

SUMMARY AND CONCLUSION

Resistance, the man-made amplification of a natural phenomenon has allowed the resurgence of *M. tuberculosis* in its new virulent forms of MDR and XDR-TB; rendering the presently available anti-tubercular drug regime inadequate to address the many inherent and emerging challenges of treatment. **Mycobacterial DNA GyrB** and **L-AlaDH** are attractive but relatively less exploited targets for anti-tubercular drug discovery and hence holds immense potential for the development of novel agents that are not impacted by target mediated cross-resistance associated with previously reported drugs.

Utilizing the structure based and ligand based drug design methods, novel inhibitors were identified as potential DNA GyrB leads. Using structure based virtual screening total 25 compounds were identified, out of which, 10 molecules exhibited IC_{50} in the range of <10 μM in *M. smegmatis* GyrB assay whereas *M. tuberculosis* supercoiling activity 13 compounds were found in the range of <15 μM. The best compound was found to be lead **D11** having IC_{50} of 1.5± 0.12 μM in *M. smegmatis* GyrB and 1.16±0.25 μM in *M. tuberculosis* supercoiling assay. Further their tight binding with the protein was biophysically confirmed by DSF. This lead compound **D11** was further taken up for hit expansion by chemical synthesis, and about 28 molecules were synthesized and characterized in our laboratory. Using ligand based virtual screening, total 15 compounds were identified but all the compounds did not show much promising activity; thus they were not taken for further lead optimization.

The 28 analogues developed *via* chemical synthesis in the hit expansion step as potential GyrB inhibitors were further evaluated for their GyrB inhibitory potential by *in vitro M. smegmatis* GyrB assay and *M. tuberculosis* supercoiling assay. The binding affinity of the most potent ligand was further evaluated by DSF experiments. Further the active hits were subjected to a whole cell screening against *M. tuberculosis* $H_{37}Rv$ strain to understand their bactericidality and *in vitro* cytotoxicity against RAW 264.7 celline for understanding their safety profile. Most of the synthesized compounds showed good GyrB inhibition and 2-

benzamido-5-phenylthiophene-3-carboxamide (compound **S23**) was found to be the most active compound with IC_{50} of 0.8±0.58 μM in *M. smegmatics* GyrB as well as *M. tuberculosis* supercoiling IC_{50} of 0.76±0.25 μM and inhibited drug sensitive *M. tuberculosis* with MIC of 4.84 μM and was non-cytotoxic at 100 μM.

In case of ***M. tuberculosis* L-AlaDH** potential candidates were identified using an e-pharmcophore based high throughput virtual screening protocol. Total 10 compounds were identified through the two approaches and two lead compounds (**Lead B1** and **Lead B2**) were identified which showed an IC_{50} of 6.77 μM and 8.17 μM when tested for *M. tuberculosis* L-AlaDH activity. Based on the two identified hit, we undertook synthesis of various analogues and evaluated for its biological activity against *M. tuberculosis* L-AlaDH for establishing SAR, both in active and dormant *M. tuberculosis* and cytotoxicity. Total 30 analogues for ***M. tuberculosis* L-AlaDH** inhibitors were synthesized and characterized in our laboratory.

In a similar fashion, 30 analogues developed from series 2 as potential ***M. tuberculosis* L-AlaDH** inhibitors were also evaluated for their biological profile using an assay based on enzyme inhibition studies in microtitre plate containing desired substrate and enzyme concentrations. The spectrophotometric determination of the reaction product NADH that accompanied the conversion of L-alanine into pyruvate in the oxidative deamination was measured at 340nm in heat controlled microplate reader PerkinElmer Victor X3 instrument. Among the compounds four compounds (**4n, 4o, 12** and **14**) emerged as most potent inhibitors displaying inhibition of *M. tuberculosis* L-AlaDH with IC_{50} values ranging from 0.58±0.02 to 1.74±0.03 μM and were non-cytotoxic at 50 μM. Some of these synthesized compounds also showed good activity against nutrient starved dormant *M. tuberculosis* cells. The binding affinity of the most potent inhibitors was further confirmed biophysically DSF. In conclusion, the class of compounds described here of promising lead compounds for further optimization and development to yield best novel drugs aimed to combat ever present and ever-increasing bacterial infections. The study also provided the basis for further chemical optimization of these potent inhibitors as potential anti-tubercular agents.

FUTURE PERSPECTIVES

The type II topoisomerase, DNA gyrase and the L-AlaDH are absent in humans but essential in microbial pathogens, suggesting that it as potential targets for the development of novel antibacterial compounds. The present study focused on utilizing the pharmaceutical underexploited domains of DNA GyrB and L-AlaDH as potential anti-tubercular target thus offers an excellent opportunity to address the ever increasing problem of bacterial resistance and to develop an effective treatment for TB.

The study describes the development of one chemically diverse series of molecules as potential DNA gyrase inhibitors and two lead series as potential L-AlaDH inhibitors. The molecules reported here displayed considerable *in vitro* enzyme efficacy and bactericidality against *M. tuberculosis* $H_{37}Rv$ strain and some the molecules in L-AlaDH inhibitors showed good activity in dormant model of *M. tuberculosis*. Although these results are encouraging, lead optimization is needed to build in an efficient pharmacokinetic and a pharmacodynamic profile and to achieve an adequate safety profile to ensure that the dose to man would be in an acceptable range.

The advancement of any of the candidate compounds presented in this thesis along a drug development path would require a significant investment in medicinal chemistry, preclinical and clinical studies.

REFERENCES

Adachi T., Mizuuchi M., Robinson E.A., Appella E., Odea M.H., Gellert M., Mizuuchi K. DNA sequence of the *E. coli* gyrB gene: application of a new sequencing strategy. *Nucleic Acids Res.* **1987**, 15, 771-784.

Agren D., Stehr M., Berthold C.L., Kapoor S., Oehlmann W., Singh M., Schneider G. Three-dimensional structures of apo and *holo*-L-alanine dehydrogenase from *Mycobacterium tuberculosis* reveal conformational changes upon coenzyme binding. *J. Mol. Biol.* **2008**, 377, 1161-1173.

Ali J. A., Jackson A.P., Howells A.J., Maxwell A. The 43-kilodalton N-terminal fragment of the DNA gyrase B protein hydrolyzes ATP and binds coumarin drugs. *Biochem.* **1993**, 32, 2717-2724.

Ann M Ginsberg., Melvin Spigelman. Challenges in tuberculosis drug research and development. *Nat. Med.* **2007**, 13, 290-294.

Angehrn P., Goetschi E., Gmuender H. A new DNA gyrase inhibitor subclass of the cyclothialidine family based on a bicyclic dilactam-lactone scaffold synthesis and antibacterial properties. *J. Med. Chem.* **2011**, 54, 2207-2224.

Axten J.M., Brooks, G., Brown P., Davies, D., Gallagher T.F., Markwell, R.E., Miller W.H., Pearson N.D., Seefeld, M. WO004058144, 2004.

Andersen A.B., Andersen P., Ljungqvist L. Structure and function of a 40,000 molecular-weight protein antigen of *Mycobacterium tuberculosis*. *Infect Immun*. **1992**, 60, 2317-2323.

Barrera L. The basics of clinical bacteriology. In: Palomino J.C., Leao S.C. and Ritacco V., Eds., *Tuberculosis*: *From Basic Science to Patient Care*, Sao Paulo, **2007**, 93-112. www.TuberculosisTextbook.com.

Barros D. Recent advances in TB drug development-novel *Mycobacterium tuberculosis* DNA gyrase inhibitors. In: 40th Union World Conference on Lung Health; Cancun, Mexico. Paris, France: International Union against Tuberculosis and Lung Disease; 3–7 December **2009**.

Bax B.D., Chan P.F., Eggleston D.S., Fosberry A., Gentry D.R., Gorrec F., Giordano I., Hann M.M., Hennessy A., Hibbs M., Huang J., Jones J., Brown K.K., Lewis C.J., May E.W., Saunders M.R., Singh O., Spitzfaden C.E., Shen C., Shillings A., Theobald A.J., Wohlkonig N.D., Pearson N.D., Gwynn M.N. Type IIA topoisomerase inhibition by a new class of antibacterial agents. *Nature*. **2010**, 466, 935-940.

Bernstein J., Lott W.A., Steinberg B.A., Yale H.L. Chemotherapy of experimental tuberculosis. V. Isonicotinic acid hydrazide (nydrazid) and related compounds. *Am. Rev. Tuberc.* **1952**, 65, 357-364.

Betts J.C., Lukey P.T., Robb L.C., McAdam R.A., Duncan K. Evaluation of a nutrient starvation model of *Mycobacterium tuberculosis* persistence by gene and protein expression profiling. *Mol. Microbiol*. **2002**, 4, 717-731.

Binda G., Domenichini E., Gottardi A., Orlandi B., Ortelli E., Pacini B., Fowst G. Rifampicin, a general review. *Arzneimittelforschung*. **1971**, 12, 1907-1977.

Bayer R., Wilkinson D. Directly observed therapy for tuberculosis: history of an idea. *Lancet*. **1995**, 345, 1545-1548.

Bhowruth V., Dover L.G., Besra G.S. Tuberculosis chemotherapy: recent developments and future perspectives. *Prog. Med. Chem*. **2007**, 45, 169-203.

Balasubramanian V., Solapure S., Iyer H., Ghosh A., Sharma S., Kaur P., Sambandamurthy V. K. Bactericidal activity and mechanism of action of AZD5847, a novel oxazolidinone for treatment of tuberculosis. *Antimicrob Agents Chemother*. **2014**, 58, 495-502.

Black M.T., Stachyra T., Platel D., Girard A.M., Claudon M., Bruneau J.M., Miossec C. Mechanism of action of the antibiotic NXL101, a novel nonfluoroquinolone inhibitor of bacterial type II topoisomerases. *Antimicrob Agents Chemother*. **2008,** 52, 3339-3349.

Brino L., Urzhumtsev A., Mousli M., Bronner C., Mitschler A., Oudet P., Moras D. Dimerization of *E. coli* DNA-gyrase B provides a structural mechanism for activating the ATPase catalytic center. *J. Biol. Chem*. **2000**, 275, 9468-9475.

Brvar M., Perdih A., Renko M., Anderluh G., Turk D., Solmajer T. Structure-based discovery of substituted 4,5'-bithiazoles as novel DNA gyrase inhibitors. *J. Med. Chem.* **2012**, 55, 6413-6426.

Boehm H. J., Boehringer M., Bur D., Gmuender H., Huber W., Klaus W., Mueller F. Novel inhibitors of DNA gyrase: 3D structure based biased needle screening, hit validation by biophysical methods, and 3D guided optimization. A promising alternative to random screening. *J. Med. Chem.* **2000**, 43, 2664-2674.

Bobesh K.A., Renuka, J. Jeankumar V.U., Shruti S.K., Sridevi J.P., Yogeeswari P., Sriram D. Extending the N-linked aminopiperidine class to the mycobacterial gyrase domain: Pharmacophore mapping from known antibacterial leads. *Eur. J. Med. Chem.* **2014**, 85, 593-604.

Cole S.T., Brosch R., Parkhill J., Garnier T., Churcher C.; Harris D., Gordon S. V., Eiglmeier K., Gas S., Barry C.E. 3rd., Tekaia F., Badcock K., Basham D., Brown D., Chillingworth T., Connor R., Davies R., Devlin K., Feltwell T., Gentles S., Hamlin N., Holroyd S., Hornsby T., Jagels K., Krogh A., McLean J., Moule S., Murphy L., Oliver K., Osborne J., Quail M. A., Rajandream M.A., Rogers J., Rutter S., Seeger K., Skelton J., Squares R., Squares S., Sulston J. E., Taylor K., Whitehead S., Barrell B.G. Deciphering the biology of *Mycobacterium tuberculosis* from the complete genome sequence. *Nature.* **1998**, 393, 537-544.

Cohen J. Infectious disease. Approval of novel TB drug celebrated-with restraint. *Science.* **2013**, 339, 130.

Chopra S., Matsuyama K., Tran, T., Malerich J. P., Wan B., Franzblau S. G., Madrid P. B. Evaluation of gyrase B as a drug target in *Mycobacterium tuberculosis*. *J. Antimicrob. Chemother.* **2012**, 67, 415-421.

Champoux J.J. DNA topoisomerases: structure, function, and mechanism. *Annual review of biochem.* **2001**, 70, 369-413.

Costenaro L., Grossmann J.G., Ebel C., Maxwell A. Modular structure of the full-length DNA gyrase B subunit revealed by small-angle X-ray scattering. *Structure.* **2007**, 15, 329-339.

Critchlow S.E., Maxwell A. DNA cleavage is not required for the binding of quinolone drugs to the DNA gyrase-DNA complex. *Biochem.* **1996**, 35, 7387-7393.

Charifson P.S., Grillot A.L., Grossman T.H., Parsons J.D., Badia M., Bellon S., Deininger D.D., Drumm J.E., Gross C.H., LeTiran A., Liao Y., Mani N., Nicolau D.P., Perola E., Ronkin S., Shannon D., Swenson L.L., Tang Q., Tessier P.R, Tian S.K, Trudeau M., Wang T., Wei Y., Zhang H., Stamos D. Novel dual-targeting benzimidazole urea inhibitors of DNA gyrase and topoisomerase IV possessing potent antibacterial activity: intelligent design and evolution through the judicious use of structure-guided design and structure–activity relationships. *J. Med. Chem.* **2008**, 51, 5243-5263.

Chan K., Knaak, T., Satkamp L., Humbert O., Falkow S., Ramakrishnan L. Complex pattern of *Mycobacterium marinum* gene expression during long-term granulomatous infection. *Proc. Natl. Acad. Sci.* **2002**, 99, 3920-3925.

Chen J.M., Alexander D.C., Behr M.A., Liu J. *M. bovis* BCG vaccines exhibit defects in alanine and serine catabolism. *Infect. Immun.* **2003**, 71, 708-716.

Dalton T., Cegielski P., Akksilp S., Asencios L., Campos Caoili. J., Cho S.N., Erokhin V.V., Ershova J., Gler M.T., Kazennyy B.Y., Kim H.J., Kliiman K., Kurbatova E., Kvasnovsky C., Leimane V., van der Walt. M., Via L.E., Volchenkov G.V., Yagui M.A., Kang H., Global PETTS Investigators., Akksilp R., Sitti W., Wattanaamornkiet W., Andreevskaya S.N., Chernousova L.N., Demikhova O.V., Larionova E.E., Smirnova T.G., Vasilieva I.A., Vorobyeva A.V., Barry CE 3rd., Cai Y., Shamputa I.C., Bayona J., Contreras C., Bonilla C., Jave O., Brand J., Lancaster J., Odendaal R., Chen M.P., Diem L., Metchock B., Tan K., Taylor A., Wolfgang M., Cho E., Eum S.Y., Kwak H.K., Lee J., Lee J., Min S., Degtyareva I., Nemtsova E.S, Khorosheva T., Kyryanova E.V., Egos G., Perez M.T., Tupasi T., Hwang S.H., Kim C.K., Kim S.Y., Lee H.J., Kuksa L., Norvaisha I., Skenders G., Sture I., Kummik T., Kuznetsova T., Somova T., Levina K., Pariona G., Yale G., Suarez C., Valencia E., Viiklepp P. Prevalence of and risk factors for resistance to second-line drugs in people with multidrug-resistant tuberculosis in eight countries: a prospective cohort study. *Lancet.* **2012**, 380, 1406-1417.

Disratthakit A., Doi N. *In vitro* activities of DC-159a, a novel fluoroquinolone, against mycobacterium species. *Antimicrob. Agents Chemother.* **2010** 54, 2684-2686.

Drlica K., Hiasa H., Kerns R., Malik M., Mustaev A., Zhao X. Quinolones: action and resistance updated. *Curr. Top. Med .Chem.* **2009**, 9, 981-998.

Ferrero L., Cameron B., Manase B. Cloning and primary structure of *staphyylococcous aureus* DNA topoisomerase-IV: a primary target for fluoroquinolones. *Mol. Microbiol.* **1994**, 13, 641-653.

Franzblau S.G., Witzig R.S., McLaughlin J.C., Torres P., Madico G., Hernandez A., Degnan M.T., Cook M.B., Quenzer V.K., Ferguson R.M., Gilman R.H.J. Rapid, low-technology MIC determination with clinical *Mycobacterium tuberculosis* isolates by using the microplate Alamar Blue assay. *Clin. Microbiol.* **1998**, 36, 362-366.

Godreuil S., Tazi L., Bañuls A.L. Pulmonary tuberculosis and *Mycobacterium tuberculosis*: modern molecular epidemiology and perspectives. Encyclopedia of infectious diseases: modern methodologies. *Edited by M. Tibayrenc. John Wiley & Sons, Inc., Hoboken*, NJ. **2007,** 1-29.

Gellert M., O Dea M.H., Itoh T., Tomizawa J. Novobiocin and coumermycin inhibit DNA supercoiling catalyzed by DNA gyrase. *Proc. Natl. Acad. Sci.* **1976**, 73, 4474-4478.

Glaser B.T., Malerich J.P., Duellman S.J., Fong J., Hutson C., Fine R.M., Keblansky B., Tang M.J., Madrid P.B. A high-throughput fluorescence polarization assay for inhibitors of gyrase B. *J. Biomol. Screen.* **2011**, 16, 230-238.

Gilbert E.J., Maxwell A. The 24 kDa N-terminal sub-domain of the DNA gyrase B protein binds coumarin drugs. *Mol. Microbiol.* **1994**, 12, 365-373.

Giffin M.M., Modesti L., Raab R.W., Wayne L.G., Sohaskey C.D. ald of *Mycobacterium tuberculosis* encodes both the alanine dehydrogenase and the putative glycine dehydrogenase. *J. Bacteriol.* **2012**, 194, 1045-1054.

Gold, Version 5.1.2, Cambridge Crystallographic Data Centre, Cambridge, UK.

Hameed P.S., Raichurkar A., Madhavapeddi P., Menasinakai S., Sharma S., Kaur P., Sriram D. Benzimidazoles: Novel mycobacterial gyrase inhibitors from scaffold morphing. *ACS Med. Chem. Lett.* **2014**, 5, 820-825.

Hu T., Chang S., Hsieh T. Identifying Lys359 as a critical residue for the ATP-dependent reactions of Drosophila DNA topoisomerase II. *J. Biol. Chem*. **1998**, 273, 9586-9592.

Holdgate G.A., Tunnicliffe A., Ward W.H., Weston S.A., Rosenbrock G., Barth P.T., Timms D. The entropic penalty of ordered water accounts for weaker binding of the antibiotic novobiocin to a resistant mutant of DNA gyrase: a thermodynamic and crystallographic study. *Biochem.* **1997**, 36, 9663-9673.

Heide L. Genetic engineering of antibiotic biosynthesis for the generation of new aminocoumarins. *Biotechnol. Adv*. **2009**, 27, 1006-1014.

Hutter B., Dick T. Increased alanine dehydrogenase activity during dormancy in *Mycobacterium smegmatis*. *FEMS Microbiol Lett*. **1998,** 167, 7-11.

Ishizaki Y., Hayashi C., Inoue K., Igarashi M., Takahashi Y., Pujari V., Nomoto A. Inhibition of the First Step in Synthesis of the Mycobacterial Cell Wall Core, Catalyzed by the GlcNAc-1-phosphate Transferase WecA, by the Novel Caprazamycin Derivative CPZEN-45. *J. Biol. Chem*. **2013**, 288, 30309-30319.

Jain A., Mondal R. Extensively drug-resistant tuberculosis: current challenges and threats. *FEMS Immunol Med Microbiol*. **2008**, 53, 145-150.

Jackson A.P., Maxwell A. Identifying the catalytic residue of the ATPase reaction of DNA gyrase. *Proc. Natl. Acad. Sci. USA*. **1993**, 90, 11232-11236.

Jones D., H. J. Metzger A. Schatz, S.A.Waksman . Control of gram-negatives in experimental animals by streptomycin. *Science*. **1994**, 100, 103-105.

Renuka J., Reddy K.I., Srihari K., Jeankumar V.U., Shravan M., Sridevi J.P., Yogeeswari P., Babu K.S., Sriram D. Design, synthesis and biological evaluation of substituted benzofurans as DNA gyrase B inhibitors of *Mycobacterium tuberculosis*. *Bioorg. Med. Chem*. **2014**, 17, 4924-4934.

Jeong J.A., Baek E.Y., Kim S.W., Choi J.S., Oh J.I. Regulation of the ald Gene Encoding Alanine Dehydrogenase by AldR in *Mycobacterium smegmatis*. *J. Bacteriol*. **2013**, 195, 3610-3620.

Koch R. Die Aetiologie der Tuberkulose. A model for the mechanism of strand passage by DNA gyrase. *Berl. Klin. Wochenschr.* **1882**, 19, 221-230. [Reprint *Am. Rev. Tuberc.*, 1932, *25*, 285-323].

Kreuzer K.N., Cozzarelli N.R. Formation and resolution of DNA catenanes by DNA gyrase. *Cell.* **1980**, 20, 245–254.

Kampranis S.C., Bates A.D., Maxwell A. A model for the mechanism of strand passage by DNA gyrase. *Proc. Natl. Acad. Sci. USA.* **1999**, 96, 8414-8419.

Kale R.R., Kale M.G., Waterson D., Raichurkar A., Hameed S.P., Manjunatha M.R., Ghorpade S.R. Thiazolopyridone ureas as DNA gyrase B inhibitors: Optimization of antitubercular activity and efficacy. *Bioorg. Med. Chem. Lett.* **2014**, 24, 870-879.

Laurenzi M., Ginsberg A., Spigelman M. Challenges associated with current and future TB treatment. Infectious Disorders-Drug Targets (Formerly Current Drug Targets-Infectious Disorders), **2007**, 7, 105-119.

Lee M.P., Hsieh T.S. Linker insertion mutagenesis of Drosophila topoisomerase II. Probing the structure of eukaryotic topoisomerase II. *J. Mol. Biol.* **1994**, 235, 436-437.

Li W., Wang J.C. Footprinting of yeast DNA topoisomerase II lysyl side chains involved in substrate binding and interdomainal interactions. *J. Biol. Chem.* **1997**, 272, 31190-31195.

Lewis R.J., Singh O.M., Smith C.V., Skarzynski T., Maxwell A., Wonacott A.J., Wigley D.B. The nature of inhibition of DNA gyrase by the coumarins and the cyclothialidines revealed by X-ray crystallography. *EMBO J.* **1996**, 15, 1412-1420.

Lafitte D., Lamour V., Tsvetkov P. O., Makarov A. A., Klich M., Deprez P., Gilli R. DNA gyrase interaction with coumarin-based inhibitors: the role of the hydroxybenzoate isopentenyl moiety and the 5'-methyl group of the noviose. *Biochem.* **2002**, 41, 7217-7223.

Lubbers T., Angehrn P., Gmunder H., Herzig S., Kulhanek J. Design, synthesis, and structure–activity relationship studies of ATP analogues as DNA gyrase inhibitors. *Bioorg. Med. Chem. Lett.* **2000**, 10, 821-826.

Lewis R.J., Singh O.M., Smith C.V., Skarzynski T., Maxwell A., Wonacott A.J., Wigley D.B. The nature of inhibition of DNA gyrase by the coumarins and the cyclothialidines revealed by X-ray crystallography. *EMBO J.* **1996**, 15, 1412-1420.

Ling, B., Sun, M., Bi, S., Jing, Z., Liu, Y. Molecular dynamics simulations of the coenzyme induced conformational changes of *Mycobacterium tuberculosis* L-alanine dehydrogenase. *J. Mol. Graph. Model.* **2012**, 35, 1-10.

Ling, B., Bi, S., Sun, M., Jing, Z., Li, X., Zhang, R. Molecular dynamics simulations of mutated *Mycobacterium tuberculosis* L-alanine dehydrogenase to illuminate the role of key residues. *J. Mol. Graph. Model.* **2014**, 50, 61-70.

Malone L., Schurr A., Lindh H., Mckenzie D., Kiser J.S., Williams J.H. The effect of pyrazinamide (aldinamide) on experimental tuberculosis in mice. *Am. Rev. Tuberc.* **1952**, 65, 511-518.

Ma Z., Lienhardt C., McIlleron H., Nunn A., Wang X. Global tuberculosis drug development pipeline: the need and the reality. *Lancet.* **2010**, 375, 2100-2109.

Makarov V., Lechartier B., Zhang M., Neres J., van der Sar A. M., Raadsen S. A., Cole S. T. Towards a new combination therapy for tuberculosis with next generation benzothiazinones. *EMBO Mol. Med.* **2014,** 6, 372-383.

Migliori G.B., Sotgiu G., Gandhi N.R., Falzon D., DeRiemer K., Centis R., Park S.K. Drug resistance beyond extensively drug-resistant tuberculosis: individual patient data meta-analysis. *Eur Respir J.* **2013**, 42, 169-179.

Mdluli K., Ma Z. *Mycobacterium tuberculosis* DNA gyrase as a target for drug discovery. *Infect. Disord. Drug Targets.* **2007**, 7, 159-68.

Manchester, I.J., Dussault, D.D., Rose, A.J., Boriack-Sjodin, A., Uria-Nickelsen, M., Ioannidis, G., Bist, S., Fleming, P., Hull, G.K. Discovery of a novel azaindole class of antibacterial agents targeting the ATPase domains of DNA gyrase and Topoisomerase IV. *Bioorg. Med. Chem. Lett*., **2012**, 22, 5150-5156.

Mizuuchi K., O'Dea M.H., Gellert M. DNA gyrase: subunit structure and ATPase activity of the purified enzyme. *Proc. Natl. Acad. Sci. USA.* **1978**, 75, 5960-5963.

McCarthy J.D. Computational approaches to structure-based drug design. *Pharma. Thera.* **1999**, 84, 179-191.

Nikonenko B.V., Protopopova M., Samala R., Einck L., Nacy C.A. Drug therapy of experimental tuberculosis (TB): improved outcome by combining SQ109, a new diamine antibiotic, with existing TB drugs. *Antimicrob. Agents Chemother.* **2007**, 51, 1563-1565.

Neil Thomson. Mechanism of action of DNA gyrase.

Oblak M., Grdadolnik S.G., Kotnik M., Jerala R., Filipic M., Solmajer T. *In silico* fragment-based discovery of indolin-2-one analogues as potent DNA gyrase inhibitors. *Bioorg. Med. Chem. Lett.* **2005**, 15, 5207-5210.

Orphanides G., Maxwell A. Evidence for a conformational change in the DNA gyrase-DNA complex from hydroxyl radical footprinting. *Nucleic Acids Res.* **1994**, 22, 1567-1575.

Pantel A., Petrella S., Matrat S., Brossier F., Bastian S., Reitter D., Aubry A. DNA gyrase inhibition assays are necessary to demonstrate fluoroquinolone resistance secondary to gyrB mutations in *Mycobacterium tuberculosis. Antimicrob. Agents Chemother.* **2011,** 55, 4524-4529.

Parish T., Smith D.A., Roberts G., Betts J., Stoker N.G. The senX3–regX3 two-component regulatory system of *Mycobacterium tuberculosis* is required for virulence. *Microbiol.* **2003**, 149, 1423-1435.

Pethe K., Bifani P., Jang J., Kang S., Park S., Ahn S., No Z. Discovery of Q203, a potent clinical candidate for the treatment of tuberculosis. *Nat. Med.* **2013**, 19, 1157-1160.

Raviglione M.C. The new Stop TB Strategy and the Global Plan to Stop TB, 2006-2015. Bull World Health Organ. **2007**, 85, 327.

Rattan A. Mechanisms of resistance to fluoroquinolones. *Natl. Med. J. India.* **1999**, 12, 162-164.

Raynaud C., Etienne G., Peyron P., Lanéelle M. A. Daffé, M. Extracellular enzyme activities potentially involved in the pathogenicity of *Mycobacterium tuberculosis. Microbiol.* **1998**, 144, 577-587.

Rivers E.C., Mancera R.L. New anti-tuberculosis drugs in clinical trials with novel mechanisms of action. *Drug Dev.Today*. **2008**, 13, 1090-1098.

Russell D.G. Who puts the tubercle in tuberculosis? *Nature Rev. Microbiol.* **2007,** 5, 39-47.

Rai S.P., Panda B.N. Outcome in Multidrug Resistant Tuberculosis patients with ambulatory treatment; *Indian J. Tuberc*. **2004**, 51, 33-36

Redgrave L.S., Sutton S.B., Webber M.A., Piddock L.J. Fluoroquinolone resistance: mechanisms, impact on bacteria, and role in evolutionary success. *Trend microbiol*. **2014**, 8, 438-445.

Roca J., Wang J.C. The capture of a DNA double helix by an ATP-dependent protein clamp: a key step in DNA transport by type II DNA topoisomerases. *Cell*. **1992**, 71, 833-840.

Roca J., Wang J.C. DNA transport by a type II DNA topoisomerase: evidence in favor of a two-gate mechanism. *Cell.* **1994**, 77, 609-616.

Ronkin S.M., Badia M., Bellon S., Grillot A.L., Gross C.H, Grossman T.H,, Mani N., Parsons J.D., Stamos D., Trudeau M., Wei Y., Charifson P.S. Discovery of pyrazolthiazoles as novel and potent inhibitors of bacterial gyrase, *Bioorg. Med. Chem. Lett*. **2010**, 20, 2828-2831.

Reck F., Alm R., Brassil P., Newman J., Dejonge B., Eyermann C.J., Breault G., Breen J., Comita-Prevoir J., Cronin M., Davis H., Ehmann D., Galullo V., Geng B., Grebe T., Morningstar M., Walker P., Hayter B., Fisher S. Novel N-Linked Aminopiperidine Inhibitors of Bacterial Topoisomerase Type II: Broad-Spectrum Antibacterial Agents with Reduced hERG Activity. *J. Med. Chem*. **2011**, 54, 7834-7847.

Smith I. "*Mycobacterium tuberculosis* pathogenesis and molecular determinants of virulence." *Clin Microbiol Rev*. **2003**, 16, 463-496.

Singh, G., Singh, G., Jadeja, D., & Kaur, J. Lipid hydrolyzing enzymes in virulence: *Mycobacterium tuberculosis* as a model system. *Crit. Rev. Biochem. Mol.* **2010**, 36, 259-269.

Kaufmann S.H. How can immunology contribute to the control of tuberculosis? *Nat. Rev. Immunol*. **2001**, 1, 20-30.

Schatz, A., Waksman S.A. Effect of streptomycin upon *Mycobacterium tuberculosis* and related organisms. *Proc. Soc. Exptl. Biol. & Med*. **1944**, 57, 244-248.

Solanki R.N. Drug-Resistant Tuberculosis: New Challenges. *Indian J Chest Dis Allied Sci.* **2012**, 54, 159-160.

Sharma S.K., Mohan A. Multidrug-resistant tuberculosis. *Indian J Med Res.* **2004**, 120, 354-376

Shah N.S., Wright A., Bai G.H., Barrera L., Boulahbal F., Martín-Casabona N., Drobniewski F., Gilpin C., Havelková M., Lepe R., Lumb R., Metchock B., Portaels F., Rodrigues M.F., Rüsch-Gerdes S., Van Deun A., Vincent V., Laserson K., Wells C., Cegielski J.P.Worldwide emergence of extensively drug-resistant tuberculosis. *Emerg. Infect. Dis.* **2007**, 13, 380-87.

Stanley S.A., Grant S.S., Kawate T., Iwase N., Shimizu M., Wivagg C., Hung D.T. Identification of novel inhibitors of *Mycobacterium tuberculosis* growth using whole cell based high-throughput screening. *ACS Chem. Biol.* **2012**, 7, 1377-1384.

Sacksteder K.A., Protopopova M., Barry C.E., Andries K., Nacy C.A. Discovery and development of SQ109: a new antitubercular drug with a novel mechanism of action. *Future Microbiol.* **2012**, 7, 823-837.

Shen L.L., Kohlbrenner W. E., Weigl D., Baranowski J. Mechanism of quinolone inhibition of DNA gyrase. Appearance of unique norfloxacin binding sites in enzyme-DNA complexes. *J. Biol. Chem.* **1989**, 264, 2973-2978.

Shen, L.L. Quinolone interactions with DNA and DNA Gyrase. *Methods Mol. Biol*. **2001**, 95, 171-184.

Smith C.V., Maxwell A. Identification of a residue involved in transition-state stabilization in the ATPase reaction of DNA gyrase. *Biochem.* **1998**, 37, 9658-9667.

Sherer B.A., Hull K., Green O., Basarab G., Hauck S., Hill P., Loch J.T 3rd., Mullen G., Bist S., Bryant J., Boriack-Sjodin A., Read J., DeGrace N., Uria-Nickelsen M., Illingworth R.N., Eakin A.E. Pyrrolamide DNA gyrase inhibitors: optimization of antibacterial activity and efficacy. *Bioorg. Med. Chem. Lett.* **2011**, 21, 7416-7420.

Shirude P.S., Madhavapeddi P., Tucker J. A., Murugan K., Patil V., Basavarajappa H., Raichurkar A.V., Humnabadkar V., Hussein S., Sharma S., Ramya V.K., Narayan, C.B., Balganesh T.S., Sambandamurthy V.K. Aminopyrazinamides: novel and specific GyrB inhibitors that kill replicating and nonreplicating *Mycobacterium tuberculosis*. *ACS. Chem. Biol*. **2013**, 8, 519-523.

Shahul H.P., Solapure S., Mukherjee K., Nandi V., Waterson D., Shandil R., Balganesh M., Sambandamurthy V.K., Raichurkar A.K., Deshpande A., Ghosh A., Awasthy D., Shanbhag G., Sheikh G., McMiken H., Puttur J., Reddy J., Werngren J., Read J., Kumar M., R, M., Chinnapattu M., Madhavapeddi P., Manjrekar P., Basu R., Gaonka, S.,Sharma S., Hoffner S., Humnabadkar V., Subbulakshmi V., Panduga V. Optimization of pyrrolamides as mycobacterial GyrB ATPase inhibitors: structure activity relationship and in vivo efficacy in the mouse model of tuberculosis. *Antimicrob. Agents Chemother*. **2014**, 58, 61-70.

Sherer B.A., Hull K., Green O., Basarab G., Hauck S., Hill P., Loch J.T 3rd., Mullen G., Bist S., Bryant J., Boriack-Sjodin A., Read J., DeGrace N., Uria-Nickelsen M., Illingworth R.N., Eakin A.E. Pyrrolamide DNA gyrase inhibitors: optimization of antibacterial activity and efficacy. *Bioorg. Med. Chem. Lett.* **2011**, 21, 7416-7420.

Sugino A., Higgins N.P., Brown P.O., Peebles C.L., Cozzarelli N.R., Energy coupling in DNA gyrase and the mechanism of action of novobiocin. *Proc. Natl. Acad. Sci*. **1978**, 75, 4838-4842.

Sugino A., Cozzarelli N.R. The intrinsic ATPase of DNA gyrase. *J Biol. Chem*. **1980**, 255, 6299-6306.

Shahul, H.P., Waterson, D. 2-(Piperidin-1-yl)-4-azolyl-thiazole-5-carboxylic acid derivatives against bacterial infections. US Patent,2012,0022107Al.

Siranosian K.J., Ireton K., Grossman, A.D. Alanine dehydrogenase (ald) is required for normal sporulation in Bacillus subtilis. *J. Bacteriol.* **1993**, 175, 6789-6796.

Salam N.K., Nuti R., Sherman W. Novel method for generating structure-based pharmacophores using energetic analysis. *J. Chem. Inf. Model.* **2009**, 49, 2356-2368.

Singh K.D., Kirubakaran P., Nagarajan S., Sakkiah S., Muthusamy K., Velmurgan D., Jeyakanthan, J. Homology modeling, molecular dynamics, e-pharmacophore mapping and docking study of Chikungunya virus nsP2 protease. *J. Mol. Modeling*. **2012**, 18, 39-51.

Sandeep R.G., Manoj G.K., Charles D.M., Shahul H.P., Anand Kumar V.R. Thiazolo [5, 4-B] pyridine and oxazolo [5, 4- B]pyridine derivatives as antibacterial agents. WIPO Patent. 2009, 147431A1.

Sriram D., Yogeeswari P., Basha J.S., Radha D.R, Nagaraja V. Synthesis and antimycobacterial evaluation of various 7-substituted ciprofloxacin derivatives. *Bioorg. Med. Chem*. **2005**, 13, 5774-5778.

Salina E., Ryabova O., Kaprelyants A., Makarov V. New 2-Thiopyridines as Potential Candidates for Killing both Actively Growing and Dormant *Mycobacterium tuberculosis* Cells. *Antimicrob. Agents Chemother*. **2014**, 58, 55-60.

Scudiero D.A., Shoemaker R.H., Paull K.D., Monks A., Tierney S., Nofziger T.H., Boyd M. R. Evaluation of a soluble tetrazolium/formazan assay for cell growth and drug sensitivity in culture using human and other tumor cell lines. *Cancer Res*. **1988**, 48, 4827-4833.

Thomas J.P., Baughn, C.O., Wilkinson R.G, Shepherd R.G. A new synthetic compound with antituberculous activity in mice: ethambutol (dextro-2,2'-(ethylenediimino)-di-l-butanol). *Am. Rev. Respir. Dis*. **1961**, 83, 891-893.

Tingey A.P., Maxwell A. Probing the role of the ATPoperated clamp in the strand-passage reaction of DNA gyrase. *Nucleic Acids Res.* **1996**, 24, 4868-4873.

Tamura J.K., Gellert M. Characterization of the ATP binding site on Escherichia coli DNA gyrase. Affinity labeling of Lys-103 and Lys-110 of the B subunit by pyridoxal 5'-diphospho-5'-adenosine. *J. Biol. Chem*. **1990**, 265, 21342-21349.

Tsai F.T., Singh O.M., Skarzynski T., Wonacott A.J., Weston S., Tucker A., Pauptit R.A., Breeze A.L., Poyser J.P., O'Brien R., Ladbury J.E., Wigley D.B. *Proteins.* **1997**, 28, 41-52.

Tripathi S.M., Ramachandran R. Overexpression, purification, crystallization and preliminary X-ray analysis of Rv2780 from *Mycobacterium tuberculosis* H37Rv. *Acta Crystallographica Section F: Structural Biology and Crystallization Communications*. **2008**, 64, 367-370.

Taylor R.D., Jewsbury P.J., Essex J.W. A review of protein-small molecule docking methods. *J. Comput. Aided Mol. Des.* **2002**, 16, 151-166.

Villemagne B., Crauste C., Flipo M., Baulard A.R., Déprez B., Willand, N. Tuberculosis: the drug development pipeline at a glance. *Eur. J. Med. Chem.* **2012**, 51, 1-16.

Jeankumar V.U., Renuka J., Santosh P., Soni V., Sridevi J. P., Suryadevra P., Yogeeswari P., Sriram D. Thiazole–aminopiperidine hybrid analogues: Design and synthesis of novel *Mycobacterium tuberculosis* GyrB inhibitors. *Eur. J. Med. Chem*. **2013**, 70, 140-153.

Jeankumar V.U., Renuka J., Pulla V.K., Soni V., Sridevi J.P., Suryadevara P., Shravan M., Medishetti R., Kulkarni P., Yogeeswari P., Sriram D. Development of novel N-linked aminopiperidine-based mycobacterial DNA gyrase B inhibitors: Scaffold hopping from known antibacterial leads. *Int. J. Antimicrob. Agents*. **2013**, 43, 269-278.

Jeankumar V.U., Renuka J., Kotagiri S., Saxena S., Kakan S.S., Sridevi J.P., Yellanki S., Kulkarni P., Yogeeswari P., Sriram D. Gyrase ATPase domain as an antitubercular drug discovery platform: Structure-based design and lead optimization of nitothiazolyl carboxamide analogues. *ChemMedChem*. **2014**, 9, 1850-1859.

Venkatraman V., Pérez-Nueno V.I., Mavridis L., Ritchie D.W. Comprehensive comparison of ligand-based virtual screening tools against the DUD data set reveals limitations of current 3D methods. *J. Chem. Inf. Model.* **2010**, 50, 2079-2093.

Wayne L.G., Hayes L.G. An *in vitro* model for sequential study of shiftdown of *Mycobacterium tuberculosis* through two stages of nonreplicating persistence. *Infect. Immun.* **1996**, 64, 2062-2069.

Williams N.L., Maxwell A. Probing the two-gate mechanism of DNA gyrase using cysteine cross-linking. *Biochem*. **1999**, 38, 13502-13511.

Williams N.L., Howells A., Maxwell A. Locking the ATP-operated clamp of DNA gyrase: probing the mechanism of strand passage. *J. Mol. Biol*. **2001**, 306, 969-984.

Wigley D.B., Davies G.J., Dodson E.J., Maxwell A., Dodson G. Crystal structure of an N-terminal fragment of the DNA gyrase B protein. *Nature*. **1991**, 351, 624-629.

Zumla A., Nahid P., Cole S. T. Advances in the development of new tuberculosis drugs and treatment regimens. *Nat Rev Drug Discov.* **2013**, 12, 388-404.

ANNEXURE-I

Synthetic procedure and characterization of 2-amino-5-phenylthiophene-3-carboxamide derivatives.

1. *Preparation of compound II*

To the stirred solution of phenylacetaldehyde (4.00 g, 33.3 mmoles), cyanoacetamide (2.94 g, 35.0 mmoles) in ethanol was added morpholine (4.30 mL, 49.9 mmoles) and stirred for few minutes then sulphur powder (1.06 g, 33.3 mmoles) was added and allowed to stir for 7 h. The reaction mixture was concentrated and the obtained solids were washed with H2O ($3 \times$ 60 mL), cold ethanol (2×10 mL), dried in vacuum oven to get compound **II** (6.10 g, 84%) as a yellow solid. ESI(MS) showed desired mass and carried to next step.

2. *Preparation of compound III*

Compound **II** (6.10 g) in THF was taken in 250 mL 3 neck RB flash equipped with N_2-balloon outlet. Dry HCl gas generated from conc.HCl/conc.H_2SO_4 reaction setup was purged through the solution till the saturation point. The obtained solids were filtered directly and washed with THF (2×40 mL), dried in oven to get compound 3 (4.50 g) as an off-white solid.

3. *Preparation of compounds S1-8*

3.1. *2-(3-(4-Bromophenyl)ureido)-5-phenylthiophene-3-carboxamide (S1)*

Compound **3** (0.3 g, 1.18 mmoles) and 4-bromophenylisocyanate (0.26 g, 1.29 mmoles) were taken in ethanol (2 mL) and subjected to microwave irradiation at 130 °C for 20 min. the reaction mixture was diluted with EtOAc and washed with H_2O (3×20 mL), the separated organic layer was dried over anhy Na_2SO_4 and evaporated to get crude compound. Then purified by trituration with CH_2Cl_2/hexanes to get title compound (0.42 g, 84%) as an Off-

white solid. MS(ESI) 417 [M+H]$^+$. ^{1}H NMR (300 MHz, CDCl$_3$): δ 9.45 (s, 2H), 7.81 (d, J = 7.5 Hz, 2H), 7.69–7.45 (m, 7H), 7.36–7.26 (m, 3H); ^{13}C NMR (75 MHz, CDCl$_3$) δ 172.6, 166.9, 156.2, 138.4, 133.9, 132.8(2C), 130.2(2C), 128.3, 127.2(2C), 126.7, 125.1(2C), 125.0, 119.7, 116.1. Anal calcd for C$_{18}$H$_{14}$BrN$_3$O$_2$S: C, 51.93; H, 3.39; N, 10.09 % Found C, 51.99; H, 3.47; N, 10.12 %.

3.2. 2-(3-(4-Chlorophenyl)ureido)-5-phenylthiophene-3-carboxamide (S2)

MS(ESI) 372 [M+H]$^+$. Yield 79%; ^{1}H NMR (300 MHz, CDCl$_3$): δ 9.48 (s, 2H), 7.72–7.54 (m, 4H), 7.51 (s, 1H), 7.48–7.29 (m, 7H); ^{13}C NMR (75 MHz, CDCl$_3$) δ 173.4, 167.2, 158.8, 138.7, 134.1, 133.0(2C), 131.4(2C), 129.6, 128.0(2C), 127.4, 124.9(2C), 123.7, 118.9, 117.3. Anal calcd for C$_{18}$H$_{14}$ClN$_3$O$_2$S: C, 58.14; H, 3.79; N, 11.30 % Found C, 58.19; H, 3.77; N, 11.42 %.

3.3. 2-(3-(4-Fluorophenyl)ureido)-5-phenylthiophene-3-carboxamide (S3)

MS(ESI) 356 [M+H]$^+$. Yield 74%; ^{1}H NMR (300 MHz, CDCl$_3$): δ 9.52 (s, 2H), 7.78 (s, 2H), 7.74–7.63 (m, 4H), 7.58–7.36 (m, 5H), 7.27 (s, 1H); ^{13}C NMR (75 MHz, CDCl$_3$) δ 172.9, 168.4, 159.4, 139.3, 135.3, 133.9(2C), 132.6(2C), 130.7, 129.2(2C), 128.5(2C), 125.4, 122.6, 119.4, 116.9. Anal calcd for C$_{18}$H$_{14}$FN$_3$O$_2$S: C, 60.83; H, 3.97; N, 11.82 % Found C, 60.89; H, 4.02; N, 11.92 %.

3.4. 2-(3-(4-Nitrophenyl)ureido)-5-phenylthiophene-3-carboxamide (S4)

MS(ESI) 383 [M+H]$^+$. Yield 81%; ^{1}H NMR (300 MHz, DMSO-d_6): δ 10.24 (s, 2H), 8.19 (d, J = 7.8 Hz, 2H), 7.81–7.73 (m, 4H), 7.67–7.42 (m, 6H); ^{13}C NMR (75 MHz, DMSO-d_6) δ 179.1, 169.0, 160.2, 138.9, 136.6, 134.5(2C), 133.9(2C), 131.5, 128.0(2C), 127.3(2C), 126.2, 124.3, 120.6, 117.0. Anal calcd for C$_{18}$H$_{14}$N$_4$O$_4$S: C, 56.54; H, 3.69; N, 14.65 % Found C, 56.58; H, 3.72; N, 14.82 %.

3.5. 5-Phenyl-2-(3-phenylureido)thiophene-3-carboxamide (S5)

MS(ESI) 338 [M+H]$^+$. Yield 83%; ^{1}H NMR (300 MHz, CDCl$_3$): δ 9.98 (s, 2H), 7.76–7.68 (m, 3H), 7.63–7.47 (m, 4H), 7.39–7.18 (m, 6H); ^{13}C NMR (75 MHz, CDCl$_3$) δ 179.6, 168.4, 160.2, 137.3, 133.9, 133.0(2C), 132.2(2C), 130.2, 127.8(2C), 127.2, 124.3(2C), 121.3, 117.7, 116.9. Anal calcd for C$_{18}$H$_{15}$N$_3$O$_2$S: C, 64.08; H, 4.48; N, 12.45 % Found C, 64.19; H, 4.52; N, 12.51 %.

3.6. 5-Phenyl-2-(3-(p-tolyl)ureido)thiophene-3-carboxamide (S6)

MS(ESI) 352 [M+H]$^+$. Yield 74%; ^{1}H NMR (300 MHz, CDCl$_3$): δ 10.17 (s, 2H), 7.90 (s, 1H), 7.67–7.54 (m, 4H), 7.48–7.36 (m, 3H), 7.31–7.18 (m, 4H), 2.43 (s, 3H); ^{13}C NMR (75 MHz, CDCl$_3$) δ 176.2, 169.2, 160.6, 136.2, 133.6, 133.0, 131.4(2C), 129.4(2C), 126.4(2C), 125.2, 124.6(2C), 121.6, 118.6, 117.0, 22.5. Anal calcd for C$_{19}$H$_{17}$N$_3$O$_2$S: C, 64.94; H, 4.88; N, 11.96 % Found C, 65.04; H, 4.92; N, 12.01 %.

3.7. 2-(3-Benzylureido)-5-phenylthiophene-3-carboxamide (S7)

MS(ESI) 352 [M+H]$^+$. Yield 79%; ^{1}H NMR (300 MHz, CDCl$_3$): δ 10.11 (s, 2H), 7.74 (d, J = 8.1 Hz, 2H), 7.69–7.53 (m, 6H), 7.49–7.33 (m, 4H), 4.50 (s, 3H); ^{13}C NMR (75 MHz, CDCl$_3$) δ 174.6, 168.4, 161.1, 137.4, 134.2, 133.2, 130.5(2C), 129.4(2C), 127.3(2C), 124.6, 124.0(2C), 123.3, 117.7, 116.1, 42.5. Anal calcd for C$_{19}$H$_{17}$N$_3$O$_2$S: C, 64.94; H, 4.88; N, 11.96 % Found C, 65.07; H, 4.96; N, 12.13 %.

3.8. 2-(3-Isopropylureido)-5-phenylthiophene-3-carboxamide (S8)

MS(ESI) 304 [M+H]$^+$. Yield 87%; ^{1}H NMR (300 MHz, CDCl$_3$): δ 9.63 (s, 2H), 7.72–7.54 (m, 4H), 7.42 (s, 1H), 7.36–7.27 (m, 3H), 4.09–4.05 (m, 1H), 1.21 (d, J = 12.0 Hz, 6H); ^{13}C NMR (75 MHz, CDCl$_3$) δ 178.6, 166.3, 160.2, 136.2, 135.9, 131.5(2C), 128.4, 126.2(2C),

119.7, 117.3, 42.6, 24.1(2C). Anal calcd for $C_{15}H_{17}N_3O_2S$: C, 59.38; H, 5.65; N, 13.85 % Found C, 59.47; H, 5.69; N, 13.93 %.

4. *Preparation of compounds S9-16*

4.1. *2-(3-(4-Bromophenyl)thioureido)-5-phenylthiophene-3-carboxamide (S9)*

Compound **3** (0.3 g, 1.18 mmoles) and 4-bromophenylisothiocyanate (0.28 g, 1.29 mmoles) were taken in ethanol (2 mL) and subjected to microwave irradiation at 130 °C for 20 min. the reaction mixture was diluted with EtOAc and washed with H_2O (3× 20 mL), the separated organic layer was dried over anhy Na_2SO_4 and evaporated to get crude compound. Then purified by washing with cold ethanol, hexanes to get title compound (0.45 g, 88%) as an Off-white solid. MS(ESI) 433 [M+H]$^+$. ^{1}H NMR (300 MHz, CDCl$_3$): δ 10.33 (s, 2H), 7.78 (d, *J* = 7.8 Hz, 2H), 7.71–7.60 (m, 3H), 7.48–7.33 (m, 5H), 7.29 (d, *J* = 7.8 Hz, 2H); ^{13}C NMR (75 MHz, CDCl$_3$) δ 177.6, 167.4, 159.4, 137.3, 136.4, 134.4(2C), 133.4(2C), 129.2, 126.1(2C), 125.3, 125.0(2C), 124.6, 119.9, 117.2. Anal calcd for $C_{18}H_{14}BrN_3OS_2$: C, 50.00; H, 3.26; N, 9.72 % Found C, 50.08; H, 3.37; N, 9.82 %.

4.2. *2-(3-(4-Chlorophenyl)thioureido)-5-phenylthiophene-3-carboxamide (S10)*

MS(ESI) 388 [M+H]$^+$. Yield 80%; ^{1}H NMR (300 MHz, CDCl$_3$): δ 9.62 (s, 2H), 7.74–7.58 (m, 3H), 7.55–7.49 (m, 3H), 7.4–7.26 (m, 6H); ^{13}C NMR (75 MHz, CDCl$_3$) δ 176.3, 166.4, 159.4, 139.2, 135.3, 133.6(2C), 132.6(2C), 128.4, 128.2(2C), 126.8, 125.1(2C), 122.6, 119.4, 118.0. Anal calcd for $C_{18}H_{14}ClN_3OS_2$: C, 55.73; H, 3.64; N, 10.83 % Found C, 55.81; H, 3.72; N, 11.02 %.

4.3. *2-(3-(4-Fluorophenyl)thioureido)-5-phenylthiophene-3-carboxamide (S11)*

MS(ESI) 372 [M+H]$^+$. Yield 72%; ^{1}H NMR (300 MHz, CDCl$_3$): δ 9.78 (s, 2H), 7.99 (s, 1H), 7.81–7.66 (m, 6H), 7.58–7.39 (m, 5H); ^{13}C NMR (75 MHz, CDCl$_3$) δ 171.7, 167.6, 160.2, 138.4, 136.8, 134.1(2C), 133.0(2C), 131.4, 128.6(2C), 126.9(2C), 124.3, 121.4, 120.0, 117.6. Anal calcd for C$_{18}$H$_{14}$FN$_3$OS$_2$: C, 58.20; H, 3.80; N, 11.31 % Found C, 58.29; H, 3.88; N, 11.42 %.

4.4. *2-(3-(4-Nitrophenyl)thioureido)-5-phenylthiophene-3-carboxamide (S12)*

MS(ESI) 399 [M+H]$^+$. Yield 71%; ^{1}H NMR (300 MHz, DMSO-d_6): δ 9.94 (s, 2H), 8.12 (d, *J* = 7.8 Hz, 2H), 7.78–7.69 (m, 3H), 7.66–7.44 (m, 7H); ^{13}C NMR (75 MHz, DMSO-d_6) δ 178.3, 168.2, 161.1, 137.6, 137.2, 133.0(2C), 132.2(2C), 130.5, 127.2(2C), 126.0(2C), 124.5, 123.8, 119.4, 116.9. Anal calcd for C$_{18}$H$_{14}$N$_4$O$_3$S$_2$: C, 54.26; H, 3.54; N, 14.06 % Found C, 54.28; H, 3.62; N, 14.12 %.

4.5. *5-Phenyl-2-(3-phenylthioureido)thiophene-3-carboxamide (S13)*

MS(ESI) 354 [M+H]$^+$. Yield 78%; ^{1}H NMR (300 MHz, CDCl$_3$): δ 10.28 (s, 2H), 7.73–7.65 (m, 4H), 7.60–7.42 (m, 5H), 7.38–7.19 (m, 4H); ^{13}C NMR (75 MHz, CDCl$_3$) δ 178.3, 166.9, 161.1, 136.9, 134.4, 133.3(2C), 131.5(2C), 128.5, 126.9(2C), 125.3, 123.4(2C), 122.2, 119.3, 116.4. Anal calcd for C$_{18}$H$_{15}$N$_3$OS$_2$: C, 61.16; H, 4.28; N, 11.89 % Found C, 61.19; H, 4.42; N, 12.01 %.

4.6. *5-Phenyl-2-(3-(p-tolyl)thioureido)thiophene-3-carboxamide (S14)*

MS(ESI) 368 [M+H]$^+$. Yield 69%; ^{1}H NMR (300 MHz, CDCl$_3$): δ 10.21 (s, 2H), 7.92 (s, 1H), 7.64–7.55 (m, 4H), 7.49–7.38 (m, 3H), 7.33–7.21 (m, 4H), 2.41 (s, 3H); ^{13}C NMR (75 MHz, CDCl$_3$) δ 175.3, 168.5, 161.0, 137.5, 134.3, 133.3, 132.1(2C), 130.6(2C), 127.4(2C), 126.8, 125.1(2C), 123.4, 119.6, 117.7, 21.7. Anal calcd for C$_{19}$H$_{17}$N$_3$OS$_2$: C, 62.10; H, 4.66; N, 11.43 % Found C, 62.14; H, 4.62; N, 11.52 %.

4.7. 2-(3-Benzylthioureido)-5-phenylthiophene-3-carboxamide (S15)

MS(ESI) 368 [M+H]$^+$. Yield 73%; ^{1}H NMR (300 MHz, CDCl$_3$): δ 10.18 (s, 2H), 7.77 (d, J = 7.8 Hz, 2H), 7.69–7.60 (m, 4H), 7.49–7.32 (m, 6H), 4.48 (s, 3H); ^{13}C NMR (75 MHz, CDCl$_3$) δ 171.9, 167.3, 162.3, 136.9, 135.1, 134.5, 131.4(2C), 128.2(2C), 126.9(2C), 125.3, 124.2(2C), 122.5, 119.4, 117.3, 43.2. Anal calcd for C$_{19}$H$_{17}$N$_3$OS$_2$: C, 62.10; H, 4.66; N, 11.43 % Found C, 62.19; H, 4.74; N, 11.58 %.

4.8. 2-(3-Isopropylthioureido)-5-phenylthiophene-3-carboxamide (S16)

MS(ESI) 320 [M+H]$^+$. Yield 64%; ^{1}H NMR (300 MHz, CDCl$_3$): δ 9.76 (s, 2H), 7.69–7.58 (m, 3H), 7.41–7.29 (m, 5H), 4.11–4.07 (m, 1H), 1.23 (d, J = 11.4 Hz, 6H); ^{13}C NMR (75 MHz, CDCl$_3$) δ 177.3, 167.4, 160.6, 137.4, 136.3, 132.6(2C), 129.0, 127.4(2C), 120.6, 116.8, 41.8, 24.3(2C). Anal calcd for C$_{15}$H$_{17}$N$_3$OS$_2$: C, 56.40; H, 5.36; N, 13.15 % Found C, 56.47; H, 5.39; N, 13.23 %.

5. Preparation of compounds S17-28

5.1. 2-(4-Chlorobenzamido)-5-phenylthiophene-3-carboxamide (S17)

To the stirred solution of compound **2** (0.3 g, 1.37 mmoles) in CH$_2$Cl$_2$ (12 mL) at 0 °C was added Et$_3$N (0.39 mL, 2.75 mmoles) followed by 4-chlorobenzoylchloride (0.21 mL, 1.64 mmoles) and stirred the reaction at room temperature for 4 h. the reaction mixture was diluted with CH$_2$Cl$_2$ and washed with H$_2$O (3 × 15 mL). The separated organic layer was dried over anhy.Na$_2$SO$_4$ and evaporated to get crude compound, purified by triturating with CH$_2$Cl$_2$/hexanes to get compound **17** (0.36 g, 73 %) as pale yellow solid.

MS(ESI) 357 [M+H]$^+$. ^{1}H NMR (300 MHz, DMSO-d_6): δ 10.12 (s, 2H), 7.81 (d, J = 7.8 Hz, 2H), 7.73-7.62 (m, 4H), 7.59-7.43 (m, 5H); ^{13}C NMR (75 MHz, CDCl$_3$) δ 178.4, 166.5,

158.3, 136.4, 134.6, 132.9(2C), 132.2(2C), 128.9, 128.4, 129.8, 127.3(2C), 126.8, 124.6(2C), 120.6. Anal calcd for $C_{18}H_{13}ClN_2O_2S$: C, 60.59; H, 3.67; N, 7.85 % Found C, 60.61; H, 3.72; N, 7.92 %.

5.2. 2-(4-Nitrobenzamido)-5-phenylthiophene-3-carboxamide (S18)

MS(ESI) 368 [M+H]$^+$. Yield 88%; ^{1}H NMR (300 MHz, DMSO-d_6): δ 9.86 (s, 2H), 8.08 (d, J = 8.4 Hz, 2H), 7.72 (d, J = 8.1 Hz, 2H), 7.56–7.38 (m, 7H); ^{13}C NMR (75 MHz, DMSO-d_6) δ 176.4, 169.3, 164.7, 154.5, 136.8, 135.4, 133.4(2C), 132.6(2C), 130.2, 127.4, 126.8(2C), 125.2(2C), 123.5, 119.7. Anal calcd for $C_{18}H_{13}N_3O_4S$: C, 58.85; H, 3.57; N, 11.44 % Found C, 58.94; H, 3.62; N, 11.52 %.

5.3. 2-(1-Naphthamido)-5-phenylthiophene-3-carboxamide (S19)

MS(ESI) 373 [M+H]$^+$. Yield 90%; ^{1}H NMR (300 MHz, CDCl$_3$): δ 10.48 (s, 1H), 9.92 (s, 1H), 8.01–7.85 (m, 3H), 7.78–7.64 (m, 6H), 7.54 (s, 1H), 7.49–7.33 (m, 4H); ^{13}C NMR (75 MHz, CDCl$_3$) δ 175.4, 167.4, 160.6, 153.1, 139.6, 137.2, 134.5, 133.0, 132.5, 131.4, 130.3(2C), 129.4, 127.8(2C), 127.1, 126.0 125.6, 125.1, 124.8, 122.6, 120.3. Anal calcd for $C_{21}H_{16}N_2OS$: C, 73.23; H, 4.68; N, 8.13 % Found C, 73.34; H, 472; N, 8.22 %.

5.4. N-(3-Carbamoyl-5-phenylthiophen-2-yl)pyrazine-2-carboxamide (S20)

MS(ESI) 325 [M+H]$^+$. Yield 76%; ^{1}H NMR (300 MHz, DMSO-d_6): δ 8.28–8.12 (m, 4H), 7.73 (d, J = 7.8 Hz, 2H), 7.49 (s, 2H), 7.47–7.33 (m, 4H); ^{13}C NMR (75 MHz, DMSO-d_6) δ 180.2, 169.0, 162.3, 156.4, 144.9, 139.2, 136.2, 133.2(2C), 133.0, 130.8(2C), 126.6, 124.5, 120.6. Anal calcd for $C_{15}H_{12}N_4OS$: C, 60.79; H, 4.08; N, 18.91 % Found C, 60.81; H, 4.12; N, 18.99 %.

5.5. N-(3-Carbamoyl-5-phenylthiophen-2-yl)-1H-indole-2-carboxamide (S21)

MS(ESI) 362 $[M+H]^+$. Yield 82%; ^{1}H NMR (300 MHz, DMSO-d_6): δ 10.92 (s, 1H), 9.34 (s, 2H), 7.88–7.62 (m, 4H), 7.56–7.42 (m, 5H), 7.40–7.31 (m, 3H); ^{13}C NMR (75 MHz, DMSO-d_6) δ 178.3, 169.2, 161.4, 146.3, 139.6, 137.3, 133.3, 132.1(2C), 131.3, 130.4(2C), 129.6, 128.4, 127.6, 127.0, 126.8, 125.3, 124.3, 121.5. Anal calcd for $C_{20}H_{15}N_3O_2S$: C, 66.46; H, 4.18; N, 11.63 % Found C, 66.51; H, 4.22; N, 11.79 %.

5.6. 2-(4-Phenoxybenzamido)-5-phenylthiophene-3-carboxamide (S22)

MS(ESI) 415 $[M+H]^+$. Yield 91%; ^{1}H NMR (300 MHz, DMSO-d_6): δ 10.24 (s, 1H), 8.08 (d, $J = 8.1$ Hz, 2H), 7.90 (d, $J = 8.1$ Hz, 2H), 7.84–7.74 (m, 3H), 7.69–7.44 (m, 6H), 7.42–7.33 (m, 4H); ^{13}C NMR (75 MHz, DMSO-d_6) δ 176.4, 167.2, 163.5, 162.6, 161.4, 142.3, 138.2, 136.1, 133.2(2C), 132.1, 130.5(2C), 128.7(2C), 127.3(2C), 126.8, 125.1(2C), 124.2, 122.4(2C), 119.4. Anal calcd for $C_{24}H_{18}N_2O_3S$: C, 69.55; H, 4.38; N, 6.76 % Found C, 69.58; H, 4.52; N, 6.89 %.

5.7. 2-Benzamido-5-phenylthiophene-3-carboxamide (S23)

MS(ESI) 323 $[M+H]^+$. Yield 72%; ^{1}H NMR (300 MHz, DMSO-d_6): δ 9.85 (s, 1H), 7.92–7.81 (m, 5H), 7.78–7.56 (m, 5H), 7.48–7.37 (m, 3H); ^{13}C NMR (75 MHz, DMSO-d_6) δ 179.1, 166.5, 160.2, 137.4, 135.2, 132.8(2C), 132.1, 130.3(2C), 127.4, 126.1(2C), 125.0(2C), 124.8, 122.4, 120.6. Anal calcd for $C_{18}H_{14}N_2O_2S$: C, 67.06; H, 4.38; N, 8.69 % Found C, 67.08; H, 4.42; N, 8.79 %.

5.8. 2-Acetamido-5-phenylthiophene-3-carboxamide (S24)

MS(ESI) 261 $[M+H]^+$. Yield 76%; ^{1}H NMR (300 MHz, DMSO-d_6): δ 9.45 (s, 1H), 7.81 (d, $J = 7.2$ Hz, 2H), 7.74 (bs, 2H), 7.63–7.54 (m, 3H), 7.31 (s, 1H), 2.07 (s, 3H); ^{13}C NMR (75

MHz, DMSO-d_6) δ 181.2, 167.4, 163.4, 138.3, 136.1, 133.6(2C), 131.4, 129.7(2C), 124.9, 121.5, 26.9. Anal calcd for $C_{13}H_{12}N_2O_2S$: C, 59.98; H, 4.65; N, 10.76 % Found C, 60.03; H, 4.72; N, 10.79 %.

5.9. 5-Phenyl-2-propionamidothiophene-3-carboxamide (S25)

MS(ESI) 275 [M+H]$^+$. Yield 84%; ^{1}H NMR (300 MHz, DMSO-d_6): δ 9.36 (s, 1H), 7.84 (d, J = 7.2 Hz, 2H), 7.66–7.54 (m, 3H), 7.33 (s, 1H), 7.29 (s, 2H), 2.27 (q, J = 7.2 Hz, 2H), 1.11 (t, J = 7.2 Hz, 3H); ^{13}C NMR (75 MHz, DMSO-d_6) δ 180.4, 166.6, 164.2, 139.4, 133.2(2C), 130.6, 128.4(2C), 126.4, 123.8, 121.5, 31.4, 12.1. Anal calcd for $C_{14}H_{14}N_2O_2S$: C, 61.29; H, 5.14; N, 10.21 % Found C, 61.38; H, 5.22; N, 10.29 %.

5.10. 2-Butyramido-5-phenylthiophene-3-carboxamide (S26)

MS(ESI) 289 [M+H]$^+$. Yield 82%; ^{1}H NMR (300 MHz, DMSO-d_6): δ 9.61 (s, 1H), 7.87 (d, J = 7.2 Hz, 2H), 7.63–7.33 (m, 6H), 2.32 (t, J = 7.2 Hz, 2H), 1.48–1.44 (m, 2H), 1.01 (t, J = 7.5 Hz, 3H); ^{13}C NMR (75 MHz, DMSO-d_6) δ 182.6, 168.4, 167.3, 137.6, 134.1(2C), 132.1, 129.7(2C), 124.8, 123.2, 122.4, 38.4, 21.1, 10.7. Anal calcd for $C_{15}H_{16}N_2O_2S$: C, 62.48; H, 5.59; N, 9.71 % Found C, 62.58; H, 5.69; N, 9.99 %.

5.11. 2-(Cyclopentanecarboxamido)-5-phenylthiophene-3-carboxamide (S27)

MS(ESI) 315 [M+H]$^+$. Yield 70%; ^{1}H NMR (300 MHz, DMSO-d_6): δ 10.62 (s, 1H), 7.83 (d, J = 7.8 Hz, 2H), 7.60–7.39 (m, 6H); ^{13}C NMR (75 MHz, DMSO-d_6) δ 177.6, 166.5, 163.2, 139.6, 133.2(2C), 132.1, 128.4(2C), 127.3, 125.4, 120.4, 48.4, 29.8(2C), 24.1(2C). Anal calcd for $C_{17}H_{18}N_2O_2S$: C, 64.94; H, 5.77; N, 8.91 % Found C, 64.98; H, 5.82; N, 9.02 %.

5.12. 2-(Cyclohexanecarboxamido)-5-phenylthiophene-3-carboxamide (S28)

MS (ESI) 329 [M+H]$^+$. Yield 74%; ^{1}H NMR (300 MHz, DMSO-d_6): δ 9.72 (s, 1H), 7.81 (d, J = 7.8 Hz, 2H), 7.58–7.42 (m, 5H), 7.31 (s, 1H), 2.29–2.26 (m, 1H), 1.78–1.48 (m, 10H); ^{13}C NMR (75 MHz, DMSO-d_6) δ 178.4, 165.9, 164.3, 138.5, 134.0(2C), 133.2, 127.2(2C), 125.2, 123.2, 120.6, 46.2, 27.9(2C), 24.3(2C), 24.0. Anal calcd for $C_{18}H_{20}N_2O_2S$: C, 65.83; H, 6.14; N, 8.53 % Found C, 65.94; H, 6.22; N, 8.62 %.

ANNEXURE-II

1. Synthetic procedure and characterization data of iminothiazolidine-4-one derivatives.

1.1. *General procedure for synthesis of N-substituted chloroacetamides (2a-o)*

Compound **1** (1.0 equiv.) and chloroacetyl chloride (1.0 equiv.) were taken in benzene and the reaction mixture was refluxed for 6 h. after completion of the reaction monitored by TLC, the reaction mixture was diluted with EtOAc and washed with sat NaHCO$_3$, H$_2$O and brine. The combined organic layer was dried over anhyd. Na$_2$SO$_4$, evaporated to get compound corresponding **2a-o**.

1.2. *General procedure for synthesis of 3-substituted-2-iminothiazolidine-4-one (3a-o)*

Compound **2a-o** (1.0 equiv) and KSCN (1.6 equiv) were taken in dry acetone and refluxed for 2 h. The reaction mixture was concentrated and obtained solid was washed with H$_2$O and dried in vacuum oven to get corresponding 3-substituted-2-iminothiazolidine-4-one **3a-o**.

1.3. *General procedure for synthesis of compounds 4a-o)*

Compound **3a-o** (1.0 equiv), NaOAc (2.0 equiv) and 4-benzyloxybenzaldehyde (1.1 equiv) were taken in acetic acid and heated at 100 °C for 3 hours, the solids formed in the reaction mixture were filtered and washed with water, little amount of ethanol and hexanes to afford title compounds **4 (a-o)** as an off-white solid.

1.3.1. *5-(4-(Benzyloxy)benzylidene)-3-(4-bromophenyl)-2-iminothiazolidin-4-one (4a)*

ESI-MS 465 [M+H]$^+$. ^{1}H NMR (300 MHz, CDCl$_3$): δ 10.44 (s, 1H), 8.35 (d, J = 7.5 Hz, 2H), 7.72–7.29 (m, 5H), 7.11–6.88 (m, 7H), 5.20 (s, 2H); ^{13}C NMR (75 MHz, CDCl$_3$) δ 176.2, 163.9, 156.2, 144.3, 137.6, 136.6, 133.9(2C), 131.4, 130.5(2C), 128.4(2C), 126.4(2C), 126.0, 125.8(2C), 123.3(2C), 121.4, 117.7, 72.9. Anal calcd for C$_{23}$H$_{17}$BrN$_2$O$_2$S: C, 59.36; H, 3.68; N, 6.02 % Found C, 59.42; H, 3.77; N, 6.12 %.

1.3.2. 5-(4-(Benzyloxy)benzylidene)-3-(4-chlorophenyl)-2-iminothiazolidin-4-one (4b)

ESI-MS 421 [M+H]$^+$. ^{1}H NMR (300 MHz, CDCl$_3$): δ 10.71 (s, 1H), 8.12 (d, J = 7.8 Hz, 2H), 7.90 (s, 1H), 7.63–7.45 (m, 9H), 7.27 (d, J = 7.8 Hz, 2H), 5.22 (s, 2H); ^{13}C NMR (75 MHz, CDCl$_3$) δ 177.3, 164.5, 156.6, 145.4, 138.4, 135.9, 134.0(2C), 132.2(2C), 130.8(2C), 129.6(2C), 128.9(2C), 127.2, 126.7(2C), 124.8, 122.4, 118.6, 73.2. Anal calcd for C$_{23}$H$_{17}$ClN$_2$O$_2$S: C, 65.63; H, 4.07; N, 6.66 % Found C, 65.72; H, 3.97; N, 6.79 %.

1.3.3. 5-(4-(Benzyloxy)benzylidene)-3-(4-fluorophenyl)-2-iminothiazolidin-4-one (4c)

ESI-MS 405 [M+H]$^+$. ^{1}H NMR (300 MHz, DMSO-d_6): δ 8.44 (d, J = 8.1 Hz, 2H), 7.82 (s, 1H), 7.72 (s, 1H), 7.68–7.49 (m, 4H), 7.38–7.21 (m, 5H), 7.09 (d, J = 7.8 Hz, 2H), 5.24 (s, 2H); ^{13}C NMR (75 MHz, DMSO-d_6) δ 179.1, 165.4, 158.3, 146.3, 139.4, 136.8, 135.2(2C), 133.2(2C), 130.3(2C), 130.3(2C), 129.0(2C), 128.2, 127.8(2C), 125.3, 123.6, 119.7, 74.2. Anal calcd for C$_{23}$H$_{17}$FN$_2$O$_2$S: C, 68.30; H, 4.24; N, 6.93% Found C, 68.42; H, 4.37; N, 7.09 %.

1.3.4. 5-(4-(Benzyloxy)benzylidene)-2-imino-3-(2-nitrophenyl)thiazolidin-4-one (4d)

ESI-MS 432 [M+H]$^+$. ^{1}H NMR (300 MHz, DMSO-d_6): δ 8.31 (d, J = 8.4 Hz, 1H), 7.99 (d, J = 8.1 Hz, 1H), 7.84–7.69 (m, 4H), 7.63–7.38 (m, 7H), 7.09–6.99 (d, J = 7.8 Hz, 2H), 5.19 (s, 2H); ^{13}C NMR (75 MHz, DMSO-d_6) δ 177.1, 162.9, 153.3, 148.3, 144.4, 141.4, 137.8, 136.3(2C), 134.7(2C), 133.0(2C), 132.1, 130.5, 129.0, 128.8, 126.4, 125.8, 124.2(2C), 119.1, 72.0. Anal calcd for C$_{23}$H$_{17}$N$_3$O$_4$S: C, 64.03; H, 3.97; N, 9.74 % Found C, 64.12; H, 3.99; N, 9.89 %.

1.3.5. 5-(4-(Benzyloxy)benzylidene)-2-imino-3-(3-nitrophenyl)thiazolidin-4-one (4e)

ESI-MS 432 [M+H]$^+$. ^{1}H NMR (300 MHz, DMSO-d_6): δ 9.99 (s, 1H), 8.91 (s, 1H), 8.29 (d, J = 7.2 Hz, 1H), 8.01–7.89 (m, 3H), 7.81–7.64 (m, 4H), 7.60–7.24 (m, 3H), 7.11 (d, J = 7.8 Hz, 2H), 5.24 (s, 2H); ^{13}C NMR (75 MHz, DMSO-d_6) δ 176.3, 164.8, 154.6, 147.3, 145.2, 142.8, 138.2, 137.1(2C), 135.6(2C), 133.3(2C), 133.0, 132.1, 129.6, 129.2, 127.2, 125.4, 125.0(2C), 118.8, 73.1. Anal calcd for C$_{23}$H$_{17}$N$_3$O$_4$S: C, 64.03; H, 3.97; N, 9.74 % Found C, 64.16; H, 4.05; N, 9.85 %.

1.3.6. 5-(4-(Benzyloxy)benzylidene)-2-imino-3-(4-nitrophenyl)thiazolidin-4-one (4f)

ESI-MS 432 [M+H]$^+$. ^{1}H NMR (300 MHz, DMSO-d_6): δ 10.20 (s, 1H), 8.43 (d, J = 7.5 Hz, 2H), 7.88 (d, J = 7.2 Hz, 2H), 7.74–7.54 (m, 6H), 7.51–7.39 (m, 4H), 5.21 (s, 2H); ^{13}C NMR (75 MHz, DMSO-d_6) δ 177.4, 162.9, 156.6, 148.4, 146.2, 141.5, 139.0, 138.2(2C), 134.6(2C), 133.9(2C), 133.3, 132.1(2C), 130.5, 129.7(2C), 127.4, 125.4(2C), 119.1, 73.1. Anal calcd for $C_{23}H_{17}N_3O_4S$: C, 64.03; H, 3.97; N, 9.74 % Found C, 64.16; H, 4.05; N, 9.85 %.

1.3.7. 5-(4-(Benzyloxy)benzylidene)-3-(2,4-dichlorophenyl)-2-iminothiazolidin-4-one (4g)

ESI-MS 455 [M+H]$^+$. ^{1}H NMR (300 MHz, CDCl$_3$): δ 9.49 (s, 1H), 8.13 (s, 1H), 7.92 (d, J = 7.2 Hz, 1H), 7.76 (s, 1H), 7.67–7.56 (m, 4H), 7.49–7.37 (m, 6H), 5.29 (s, 2H); ^{13}C NMR (75 MHz, CDCl$_3$) δ 172.3, 162.3, 155.6, 142.4, 138.4, 137.2, 136.4, 135.2(2C), 133.9(2C), 132.6, 133.3, 132.4(2C), 130.9, 128.4(2C), 126.6, 125.2, 123.4, 118.2, 74.9. Anal calcd for $C_{23}H_{16}Cl_2N_2O_2S$: C, 60.67; H, 3.54; N, 6.15 % Found C, 60.76; H, 3.65; N, 6.25 %.

1.3.8. 5-(4-(Benzyloxy)benzylidene)-3-(3-chloro-2-methylphenyl)-2-iminothiazolidin-4-one (4h)

ESI-MS 435 [M+H]$^+$. ^{1}H NMR (300 MHz, CDCl$_3$): δ 10.45 (s, 1H), 7.92 (s, 1H), 7.80–7.56 (m, 6H), 7.47–7.11 (m, 6H), 5.23 (s, 2H), 2.25 (s, 3H); ^{13}C NMR (75 MHz, CDCl$_3$) δ 173.4, 163.5, 154.7, 141.3, 139.2, 138.1, 137.2, 136.0(2C), 134.2(2C), 133.5, 134.2, 130.2(2C), 129.4, 127.2(2C), 125.3, 124.6, 121.5, 117.9, 74.3, 16.2. Anal calcd for $C_{24}H_{19}ClN_2O_2S$: C, 66.28; H, 4.40; N, 6.44 % Found C, 66.36; H, 4.45; N, 6.54 %.

1.3.9. 5-(4-(Benzyloxy)benzylidene)-2-imino-3-(pyrimidin-2-yl)thiazolidin-4-one (4i)

ESI-MS 389 [M+H]$^+$. ^{1}H NMR (300 MHz, DMSO-d_6): δ 9.45 (s, 1H), 8.41 (d, J = 8.4 Hz, 2H), 7.88 (s, 1H), 7.78–7.54 (m, 4H), 7.39 (d, J = 8.1 Hz, 2H), 7.30–7.09 (m, 4H), 5.19 (s, 2H); ^{13}C NMR (75 MHz, CDCl$_3$) δ 174.6, 166.5, 158.2, 142.2(2C), 136.3, 133.0, 129.9(2C), 128.2(2C), 127.5, 126.2, 124.8(2C), 123.6, 123.0(2C), 121.6, 118.4, 73.6. Anal calcd for $C_{21}H_{16}N_4O_2S$: C, 64.93; H, 4.15; N, 14.42 % Found C, 64.96; H, 4.25; N, 14.51 %.

1.3.10. 5-(4-(Benzyloxy)benzylidene)-2-imino-3-(pyridin-2-yl)thiazolidin-4-one (4j)

ESI-MS 388 [M+H]$^+$. ^{1}H NMR (300 MHz, DMSO-d_6): δ 9.22 (s, 1H), 8.02 (d, J = 8.1 Hz, 1H), 7.84 (s, 1H), 7.72–7.63 (m, 4H), 7.54 (d, J = 8.1 Hz, 2H), 7.44–7.34 (m, 3H), 7.18–6.88 (m, 3H), 5.18 (s, 2H); ^{13}C NMR (75 MHz, DMSO-d_6) δ 171.6, 164.6, 160.2, 144.9, 137.4, 134.6, 133.9(2C), 133.0, 129.0(2C), 128.3, 127.4, 126.6, 125.4(2C), 124.3, 123.4, 121.0(2C), 117.7, 74.2. Anal calcd for $C_{22}H_{17}N_3O_2S$: C, 68.20; H, 4.42; N, 10.85 % Found C, 68.26; H, 4.54; N, 10.91 %.

1.3.11. 5-(4-(Benzyloxy)benzylidene)-2-imino-3-(6-methylpyridin-2-yl)thiazolidin-4-one (4k)

ESI-MS 402 [M+H]$^+$. ^{1}H NMR (300 MHz, DMSO-d_6): δ 8.94 (s, 1H), 7.81 (s, 1H), 7.72 (d, J = 8.1 Hz, 2H), 7.53–7.39 (m, 6H), 7.24–7.02 (m, 4H), 5.21 (s, 2H), 2.48 (s, 3H); ^{13}C NMR (75 MHz, DMSO-d_6) δ 166.4, 163.6, 157.2, 153.5, 146.4, 139.5, 137.4, 134.4(2C), 133.2, 129.4(2C), 127.4, 126.0, 124.2(2C), 123.2, 121.4, 120.6(2C), 118.8, 73.6, 22.5. Anal calcd for $C_{23}H_{19}N_3O_2S$: C, 68.81; H, 4.77; N, 10.47 % Found C, 68.96; H, 4.94; N, 10.51 %.

1.3.12. 5-(4-(Benzyloxy)benzylidene)-2-imino-3-phenylthiazolidin-4-one (4l)

ESI-MS 387 [M+H]$^+$. ^{1}H NMR (300 MHz, CDCl$_3$): δ 8.88 (s, 1H), 7.78 (s, 1H), 7.63–7.51 (m, 4H), 7.36–7.20 (m, 5H), 7.11–6.93 (s, 5H), 5.18 (s, 2H); ^{13}C NMR (75 MHz, CDCl$_3$) δ 171.3, 162.9, 154.2, 143.3, 136.6, 134.3(2C), 133.6(2C), 132.4, 130.4(2C), 129.1(2C), 127.6(2C), 126.1, 125.3(2C), 124.1, 123.4, 117.9, 71.8. Anal calcd for $C_{23}H_{18}N_2O_2S$: C, 71.48; H, 4.69; N, 7.25 % Found C, 71.56; H, 4.74; N, 7.31 %.

1.3.13. 5-(4-(Benzyloxy)benzylidene)-3-(2,4-dimethylphenyl)-2-iminothiazolidin-4-one (4m)

ESI-MS 415 [M+H]$^+$. ^{1}H NMR (300 MHz, CDCl$_3$): δ 7.81 (s, 1H), 7.72–7.62 (m, 4H), 7.58 (s, 1H), 7.42–7.18 (m, 5H), 7.02–6.90 (m, 3H), 5.24 (s, 2H), 2.42 (s, 3H), 2.33 (s, 3H); ^{13}C NMR (75 MHz, CDCl$_3$) δ 169.9, 161.6, 153.6, 144.7, 137.5, 135.1(2C), 134.2(2C), 133.2, 130.9(2C), 129.3, 128.4, 126.4(2C), 126.1, 125.4, 124.7, 124.1, 123.6, 119.7, 73.3, 25.1, 23.4. Anal calcd for $C_{25}H_{22}N_2O_2S$: C, 72.44; H, 5.35; N, 6.76 % Found C, 72.56; H, 5.44; N, 6.81 %.

1.3.14. 5-(4-(Benzyloxy)benzylidene)-3-(2,5-dimethylphenyl)-2-iminothiazolidin-4-one (4n)

ESI-MS 415 $[M+H]^+$. ^{1}H NMR (300 MHz, CDCl$_3$): δ 9.45 (s, 1H), 7.78 (s, 1H), 7.73–7.65 (m, 4H), 7.46–7.21 (m, 4H), 7.06–6.93 (m, 4H), 5.22 (s, 2H), 2.40 (s, 3H), 2.29 (s, 3H); ^{13}C NMR (75 MHz, CDCl$_3$) δ 172.9, 162.5, 154.6, 146.3, 138.6, 136.3(2C), 135.6(2C), 134.4, 132.3(2C), 130.6, 129.6, 127.6(2C), 125.6, 124.6, 124.0, 123.5, 121.4, 120.1, 74.2, 23.2, 18.9. Anal calcd for C$_{25}$H$_{22}$N$_2$O$_2$S: C, 72.44; H, 5.35; N, 6.76 % Found C, 72.49; H, 5.40; N, 6.88 %.

1.3.15. 5-(4-(Benzyloxy)benzylidene)-3-(2,6-dimethylphenyl)-2-iminothiazolidin-4-one (4o)

ESI-MS 415 $[M+H]^+$. ^{1}H NMR (300 MHz, CDCl$_3$): δ 8.91 (s, 1H), 7.81 (s, 1H), 7.69–7.54 (m, 5H), 7.38–7.20 (m, 4H), 7.09–6.91 (m, 3H), 5.17 (s, 2H), 2.46 (s, 3H), 2.38 (s, 3H); ^{13}C NMR (75 MHz, CDCl$_3$) δ 171.7, 163.7, 156.4, 147.6, 139.4, 137.4(2C), 136.3(2C), 134.4(2C), 133.3(2C), 132.4, 130.5(2C), 127.4(2C), 126.3, 125.2, 124.4, 123.4, 118.1, 73.6, 19.8. Anal calcd for C$_{25}$H$_{22}$N$_2$O$_2$S: C, 72.44; H, 5.35; N, 6.76 % Found C, 72.60; H, 5.46; N, 6.84 %.

2. Synthetic procedure and characterization data of 4,5,6,7-tetrahydrothieno[2,3-c]pyridine-3-carboxamide derivatives

2.1. *Preparation of tert-butyl 2-amino-3-carbamoyl-4,5-dihydrothieno[2,3-c]pyridine-6(7H)-carboxylate (6)*

To the stirred solution of Compound **5** (3.0 g, 15.07 mmol), 2-cyanoacetamide (1.51 g, 18.09 mmol), sulphur powder (1.06 g, 15.07 mmol) in Ethanol (40 mL) was added morpholine (3.21 mL, 33.15 mmol) and stirred the reaction mixture at room temperature for 9 h. the reaction mixture was concentrated, diluted with EtOAc and washed the organic layer with H$_2$O (3 × 40 mL). The separated organic layer was dried over anhydrous Na$_2$SO$_4$, evaporated and purified by column chromatography to get Compound **6** (3.67 g, 82%) as a light yellow solid. ESI-MS found 298 $[M+H]^+$. ^{1}H NMR (400 MHz, DMSO-d_6): δ 11.25 (s, 2H), 7.90 (s, 2H), 4.32 (s, 2H), 3.51 (t, J = 6.8 Hz, 2H), 3.04 (t, J = 6.8 Hz, 2H).

2.2. *General procedure for the preparation of compounds 8a-c*

4-Phenoxybenzoic acid (2.0 g, 9.34 mmol) was taken in a 100 mL single neck RB flask equipped with N$_2$-inlet, to this was added THF (30 mL), Et3N (2.69 mL, 18.68 mmol) and

Ethylchloroformate (0.93 mL, 9.80 mmol) at 0 °C and reaction mixture was allowed to stir at room temperature for 4 h. The reaction mixture was concentrated, diluted with ethyl acetate and washed the organic phase with H_2O (3 × 40 mL). The separated organic layer was dried over anhydrous Na_2SO_4, evaporated to get solid compound. The solids were washed with hexanes to get compound **8b** (2.60 g, 97%) as an Off-white solid. Similar procedure was followed for the synthesis of **8a** and **8c** starting with 4-chloro benzoic acid and 4-benzyloxy benzoic acid respectively. ESI-MS showed desired mass and carried to next step.

2.3. *Synthesis of compound 9a*

To the stirred solution of compound **6** (3.0 g, 10.10 mmol) in CH_2Cl_2 at 0 °C under N_2 atm, was added 4-chlorobenzoylchloride (1.42 mL, 11.11 mmol) followed Et_3N (2.91 mL, 20.20 mmol) and allowed to stir at room temperature for 7 h. The reaction mixture was concentrated and dissolved in EtOAc, washed with sat. $NaHCO_3$ (2×40 mL) and H_2O (2×60 mL). The separated organic layer was concentrated under vaccum and purified by flash chromatography to get compound **9a** (3.6 g, 82%) as light yellow solid.

2.4. *General procedure for the preparation of compounds 9a-c*

Compound **6** (1.00 equiv) in THF was taken in a microwave vial and added NaH (1.20 equiv), respective mixed anhydride (**8 a-c**) and subjected to microwave irradiation [Biotage initiator, temperature: 120 °C] for 20 min. The reaction mixture was quenched with sat. NH_4Cl and extracted into EtOAc. The organic layer was evaporated and the obtained solid product was triturated with CH_2Cl_2/Hexanes to get pure product.

2.5. *Synthesis of compounds 10 (a-c)*

To the stirred solution of compound **9 (a-c)** in CH_2Cl_2 at 0 °C under N_2 atm, was added TFA (2 volumes) and allowed to stir at room temperature for 2 h. The reaction mixture was concentrated to dryness and the obtained solids were washed with hexanes to afford compounds **10 (a-c)** respectively.

2.6. *General procedure for the synthesis of compounds 11-15, 16-20 and 20-25*

To the stirred solution of 2-(4-chlorobenzamido)-4,5,6,7-tetrahydrothieno[2,3-c]pyridine-3-carboxamide (**10a**) in DMF at 0 °C under N_2 atm was added Et_3N (1.5 equiv) followed by benzoyl chloride/acetyl chloride (1.2 equiv) and stirred the reaction mixture at room

temperature for 3 h. The reaction mixture was added ice and obtained solids were filtered and washed with H_2O, dried and purified by column chromatography using EtOAc/Hexanes as eluent to get compounds 11/12 respectively.

To the stirred solution of 2-(4-chlorobenzamido)-4,5,6,7-tetrahydrothieno[2,3-c]pyridine-3-carboxamide (**10a**) in MeOH at 0 °C under N_2 atm was added formaldehyde (for compound 13)/Benzaldehyde (for compound 15) (2.0 equiv) followed by $NaCNBH_3$ (1.2 equiv) and stirred the reaction mixture at room temperature for 3 h. The reaction mixture was quenched with ice, extracted with EtOAc. The organic layer was dried over anhy Na_2SO_4 and evaporated to get crude compound and purified by column chromatography using EtOAc/Hexanes as eluent. Similar procedure was followed with **10b** and **10c** to get final molecules.

2.6.1.   *6-Benzoyl-2-(4-chlorobenzamido)-4,5,6,7-tetrahydrothieno[2,3-c]pyridine-3-carboxamide (11)*

Yield: 78%; MS(ESI) *m/z* 440 [M+H]$^+$. ^{1}H NMR (300 MHz, DMSO-d_6): δ 10.42 (s, 1H), 9.63 (s, 2H), 8.01 (d, *J* = 7.2 Hz, 2H), 7.81 (d, *J* = 7.5 Hz, 2H), 7.72–7.63 (m, 5H), 4.72 (s, 2H), 3.93 (t, *J* = 7.8 Hz, 2H), 3.01 (t, *J* = 7.8 Hz, 2H); ^{13}C NMR (75 MHz, DMSO-d_6) δ 178.6, 169.8, 166.2, 161.9, 144.3, 140.5, 138.2, 137.6(2C), 136.9(2C), 135.5(2C), 133.4, 132.8(2C), 126.4, 125.9, 117.7, 47.9, 43.8, 19.6. Anal calcd for: $C_{22}H_{18}ClN_3O_3S$: C, 60.07; H, 4.12; N, 9.55 % Found C, 60.10; H, 4.27; N, 9.64%.

2.6.2.   *6-Acetyl-2-(4-chlorobenzamido)-4,5,6,7-tetrahydrothieno[2,3-c]pyridine-3-carboxamide (12)*

Yield: 79%; MS(ESI) *m/z* 378 [M+H]$^+$. ^{1}H NMR (300 MHz, DMSO-d_6): δ 9.42 (s, 1H), 8.64 (s, 2H), 7.92 (d, *J* = 8.1 Hz, 2H), 7.74 (d, *J* = 7.8 Hz, 2H), 4.84 (s, 2H), 3.90 (t, *J* = 7.8 Hz, 2H), 3.09 (t, *J* = 7.8 Hz, 2H), 2.25 (s, 3H); ^{13}C NMR (75 MHz, DMSO-d_6) δ 179.3, 170.1, 166.9, 162.6, 141.3, 137.5, 133.6(2C), 131.4(2C), 130.4, 126.0, 118.1, 46.4, 42.7, 22.5, 20.1. Anal calcd for: $C_{17}H_{16}ClN_3O_3S$: C, 54.04; H, 4.27; N, 11.12 % Found C, 54.10; H, 4.34; N, 11.24%.

2.6.3. 2-(4-Chlorobenzamido)-6-methyl-4,5,6,7-tetrahydrothieno[2,3-c]pyridine-3-carboxamide (13)

Yield: 81%; MS(ESI) m/z 350 [M+H]$^+$. ^{1}H NMR (300 MHz, DMSO-d_6): δ 10.12 (s, 1H), 7.89 (d, J = 8.1 Hz, 2H), 7.76 (d, J = 7.8 Hz, 2H), 7.47 (s, 2H), 4.60 (s, 2H), 3.78 (t, J = 7.8 Hz, 2H), 2.97 (t, J = 7.8 Hz, 2H), 2.61 (s, 3H); ^{13}C NMR (75 MHz, DMSO-d_6) δ 176.3, 165.4, 163.7, 140.3, 133.2, 131.9(2C), 129.6(2C), 124.5, 121.5, 117.9, 49.4, 44.8, 42.3, 18.0. Anal calcd for: $C_{16}H_{16}ClN_3O_2S$: C, 54.93; H, 4.61; N, 12.01 % Found C, 55.01; H, 4.74; N, 12.16%.

2.6.4. tert-butyl 3-carbamoyl-2-(4-chlorobenzamido)-4,5-dihydrothieno[2,3-c]pyridine-6(7H)-carboxylate (14)

Yield: 84%; MS(ESI) m/z 436 [M+H]$^+$. ^{1}H NMR (300 MHz, DMSO-d_6): δ 9.20 (s, 1H), 8.88 (s, 2H), 7.84 (d, J = 8.4 Hz, 2H), 7.69 (d, J = 8.1 Hz, 2H), 4.46 (s, 2H), 3.72 (t, J = 7.8 Hz, 2H), 3.15 (t, J = 7.8 Hz, 2H), 1.39 (s, 9H); ^{13}C NMR (75 MHz, DMSO-d_6) δ 180.3, 168.1, 162.9, 160.2, 139.9, 136.8, 132.9(2C), 130.3(2C), 128.4, 125.1, 116.1, 79.0, 47.4, 43.9, 26.1(3C), 19.2. Anal calcd for: $C_{20}H_{22}ClN_3O_4S$: C, 55.10; H, 5.09; N, 9.64 % Found C, 55.16; H, 5.13; N, 9.74%.

2.6.5. 6-Benzyl-2-(4-chlorobenzamido)-4,5,6,7-tetrahydrothieno[2,3-c]pyridine-3-carboxamide (15)

Yield: 72%; MS(ESI) m/z 426 [M+H]$^+$. ^{1}H NMR (300 MHz, DMSO-d_6): δ 10.64 (s, 1H), 9.27 (s, 2H), 7.94 (d, J = 8.1 Hz, 2H), 7.72 (d, J = 7.8 Hz, 2H), 7.54–7.46 (m, 5H), 3.72 (s, 2H), 3. 69 (s, 2H), 3.33 (t, J = 7.8 Hz, 2H), 2.91 (t, J = 7.8 Hz, 2H); ^{13}C NMR (75 MHz, DMSO-d_6) δ 180.6, 166.8, 162.2, 142.3, 141.5, 136.4, 133.2(2C), 132.9(2C), 130.5(2C), 130.0, 128.4, 127.8(2C), 125.4, 117.7, 63.9, 49.9, 46.4, 20.7. Anal calcd for: $C_{22}H_{20}ClN_3O_2S$: C, 62.04; H, 4.73; N, 9.87 % Found C, 62.10; H, 4.87; N, 9.94%.

2.6.6. 6-Benzoyl-2-(4-phenoxybenzamido)-4,5,6,7-tetrahydrothieno[2,3-c]pyridine-3-carboxamide (16)

Yield: 76%; MS(ESI) m/z 498 [M+H]$^+$. ^{1}H NMR (300 MHz, DMSO-d_6): δ 10.33 (s, 2H), 8.12–7.88 (m, 4H), 7.72–7.36 (m, 6H), 7.31–7.11 (m, 5H), 4.63 (s, 2H), 3.96 (t, J = 7.8 Hz, 2H), 3.12 (t, J = 7.8 Hz, 2H); ^{13}C NMR (75 MHz, DMSO-d_6) δ 181.6, 172.8, 169.2, 166.4,

162.5, 153.3, 137.5, 136.2, 135.3(2C), 133.9(2C), 132.4, 132.0, 130.5(2C), 128.6, 127.2(2C), 126.0(2C), 124.2(2C), 121.5, 118.2, 46.9, 43.4, 20.7. Anal calcd for: $C_{28}H_{23}N_3O_4S$: C, 67.59; H, 4.66; N, 8.45 % Found C, 67.70; H, 4.72; N, 8.53%.

2.6.7.   *6-Acetyl-2-(4-phenoxybenzamido)-4,5,6,7-tetrahydrothieno[2,3-c]pyridine-3-carboxamide (17)*

Yield: 81%; MS(ESI) m/z 436 [M+H]$^+$. ^{1}H NMR (300 MHz, DMSO-d_6): δ 9.66 (s, 1H), 8.08 (d, J = 8.1 Hz, 2H), 7.92–7.45 (m, 6H), 7.39–7.26 (m, 3H), 4.60 (s, 2H), 3.90 (t, J = 7.8 Hz, 2H), 3.15 (t, J = 7.8 Hz, 2H), 2.27 (s, 3H); ^{13}C NMR (75 MHz, DMSO-d_6) δ 180.7, 172.6, 168.3, 166.4, 160.5, 158.4, 136.8(2C), 135.2(2C), 134.8, 130.0(2C), 129.0, 126.9, 124.4(2C), 121.5, 117.0, 47.9, 44.4, 22.5, 20.0. Anal calcd for: $C_{23}H_{21}N_3O_4S$: C, 63.43; H, 4.86; N, 9.65 % Found C, 63.49; H, 4.92; N, 9.73%.

2.6.8.   *6-Methyl-2-(4-phenoxybenzamido)-4,5,6,7-tetrahydrothieno[2,3-c]pyridine-3-carboxamide (18)*

Yield: 84 %; MS(ESI) m/z 408 [M+H]$^+$. ^{1}H NMR (300 MHz, CDCl$_3$): δ 9.43 (s, 1H), 8.12 (d, J = 8.1 Hz, 2H), 7.72–7.63 (m, 3H), 7.44–7.26 (m, 6H), 4.12 (s, 2H), 3.60 (t, J = 7.8 Hz, 2H), 3.04 (t, J = 7.8 Hz, 2H), 2.32 (s, 3H); ^{13}C NMR (75 MHz, CDCl$_3$) δ 180.9, 174.3, 166.3, 161.4, 159.3, 137.6(2C), 136.4, 135.8(2C), 132.0(2C), 128.6, 127.6, 126.0, 123.3(2C), 116.1, 52.9, 48.4, 42.3, 19.2. Anal calcd for: $C_{22}H_{21}N_3O_3S$: C, 64.85; H, 5.19; N, 10.31 % Found C, 64.89; H, 5.22; N, 10.43%.

2.6.9.   *tert-butyl   3-carbamoyl-2-(4-phenoxybenzamido)-4,5-dihydrothieno[2,3-c]pyridine-6(7H)-carboxylate (19)*

Yield: 79 %; MS (ESI) m/z 494 [M+H]$^+$. ^{1}H NMR (300 MHz, DMSO-d_6): δ 8.01 (d, J = 8.4 Hz, 2H), 7.84 (s, 1H), 7.63–7.44 (m, 6H), 7.39–7.27 (m, 3H), 4.47 (s, 2H), 3.81 (t, J = 8.1 Hz, 2H), 3.21 (t, J = 8.1 Hz, 2H), 1.42 (s, 9H); ^{13}C NMR (75 MHz, DMSO-d_6) δ 180.7, 167.4, 164.4, 162.6, 158.7, 156.3, 134.6(2C), 133.3(2C), 130.4, 129.4, 127.2(2C), 126.0, 124.2(2C), 123.4, 117.9, 79.9, 49.3, 46.6, 27.9(3C), 18.7. Anal calcd for: $C_{26}H_{27}N_3O_5S$: C, 63.27; H, 5.51; N, 8.51 % Found C, 63.36; H, 5.63; N, 8.74%.

2.6.10.   *6-Benzyl-2-(4-phenoxybenzamido)-4,5,6,7-tetrahydrothieno[2,3-c]pyridine-3-carboxamide (20)*

Yield: 79 %; MS(ESI) *m/z* 484 [M+H]$^{+}$. ^{1}H NMR (300 MHz, DMSO-d_6): δ 9.97 (s, 1H), 8.08 (d, *J* = 7.8 Hz, 2H), 7.78–7.63 (m, 6H), 7.54–7.39 (m, 4H), 7.33–7.24 (m, 4H), 3.79 (s, 2H), 3.66 (s, 2H), 3.19 (t, *J* = 7.8 Hz, 2H), 3.01 (t, *J* = 7.8 Hz, 2H); ^{13}C NMR (75 MHz, DMSO-d_6) δ 179.4, 169.8, 164.6, 162.4, 160.2, 139.3, 138.4(2C), 136.4, 134.4(2C), 133.0, 132.7(2C), 130.3(2C), 129.0(2C), 127.6, 126.4(2C), 123.3, 125.4, 116.9, 64.8, 48.6, 46.6, 18.7. Anal calcd for: $C_{28}H_{25}N_3O_3S$: C, 69.54; H, 5.21; N, 8.69 % Found C, 69.60; H, 5.27; N, 8.84%.

2.6.11.   *6-Benzoyl-2-(4-(benzyloxy)benzamido)-4,5,6,7-tetrahydrothieno[2,3-c]pyridine-3-carboxamide (21)*

Yield: 79%; MS(ESI) *m/z* 512 [M+H]$^{+}$. ^{1}H NMR (300 MHz, DMSO-d_6): δ 9.34 (s, 1H), 8.01 (d, *J* = 7.8 Hz, 2H), 7.92–7.84 (m, 6H), 7.77–7.44 (m, 4H), 7.33–7.06 (m, 4H), 5.22 (s, 2H), 4.68 (s, 2H), 3.96 (t, *J* = 8.1 Hz, 2H), 3.13 (t, *J* = 7.8 Hz, 2H); ^{13}C NMR (75 MHz, DMSO-d_6) δ 180.7, 171.9, 168.4, 164.7, 160.9, 141.3, 139.6, 137.5(2C), 135.4, 134.5, 133.9(2C), 131.3(2C), 129.9, 128.2, 127.6(2C), 126.0, 125.1(2C), 124.5, 124.0, 117.3, 72.9, 48.4, 44.8, 19.6. Anal calcd for: $C_{29}H_{25}N_3O_4S$: C, 68.08; H, 4.93; N, 8.21 % Found C, 68.20; H, 4.98; N, 8.33%.

2.6.12.   *6-Acetyl-2-(4-(benzyloxy)benzamido)-4,5,6,7-tetrahydrothieno[2,3-c]pyridine-3-carboxamide (22)*

Yield: 81%; MS(ESI) *m/z* 450 [M+H]$^{+}$. ^{1}H NMR (300 MHz, DMSO-d_6): δ 10.06 (s, 1H), 7.98 (d, *J* = 8.1 Hz, 2H), 7.81–7.64 (m, 7H), 7.29 (d, *J* = 8.1 Hz, 2H), 5.24 (s, 2H), 4.63 (s, 2H), 3.91 (t, *J* = 7.8 Hz, 2H), 3.18 (t, *J* = 8.1 Hz, 2H), 2.34 (s, 3H); ^{13}C NMR (75 MHz, DMSO-d_6) δ 181.8, 171.6, 169.2, 165.3, 160.3, 138.4, 134.6(2C), 133.6(2C), 132.6, 130.5(2C), 128.6, 126.7, 123.4(2C), 123.0, 116.9, 71.8, 48.4, 46.6, 21.6, 19.8. Anal calcd for: $C_{24}H_{23}N_3O_4S$: C, 64.13; H, 5.16; N, 9.35 % Found C, 64.22; H, 5.22; N, 9.43%.

2.6.13. 2-(4-(Benzyloxy)benzamido)-6-methyl-4,5,6,7-tetrahydrothieno[2,3-c]pyridine-3-carboxamide (23)

Yield: 84 %; MS(ESI) m/z 422 [M+H]$^+$. ^{1}H NMR (300 MHz, CDCl$_3$): δ 10.42 (s, 1H), 7.99 (d, J = 8.1 Hz, 2H), 7.92 (s, 2H), 7.60–7.42 (m, 5H), 7.27 (d, J = 8.1 Hz, 2H), 5.23 (s, 2H), 4.09 (s, 2H), 3.43 (t, J = 8.1 Hz, 2H), 3.03 (t, J = 8.4 Hz, 2H), 2.36 (s, 3H); ^{13}C NMR (75 MHz, CDCl$_3$) δ 181.4, 172.3, 169.3, 160.4, 142.5, 139.3, 137.6(2C), 136.2(2C), 135.4(2C), 134.0, 130.5(2C), 128.1, 127.3, 118.2, 74.0, 54.9, 49.5, 43.3, 18.0. Anal calcd for: C$_{23}$H$_{23}$N$_3$O$_3$S: C, 65.54; H, 5.50; N, 9.97 % Found C, 65.69; H, 5.62; N, 10.03%.

2.6.14. tert-Butyl 2-(4-(benzyloxy)benzamido)-3-carbamoyl-4,5-dihydrothieno[2,3-c]pyridine-6(7H)-carboxylate (24)

Yield: 84 %; MS (ESI) m/z 508 [M+H]$^+$. ^{1}H NMR (300 MHz, DMSO-d_6): δ 9.45 (s, 2H), 9.22 (s, 1H), 7.92 (d, J = 8.4 Hz, 2H), 7.63 (d, J = 8.1 Hz, 2H), 7.58–7.49 (m, 3H), 7.33 (d, J = 8.7 Hz, 2H), 5.26 (s, 2H), 4.46 (s, 2H), 3.91 (t, J = 8.4 Hz, 2H), 3.18 (t, J = 8.1 Hz, 2H), 1.44 (s, 9H); ^{13}C NMR (75 MHz, DMSO-d_6) δ 182.7, 170.1, 166.6, 164.3, 156.6, 141.3, 136.2(2C), 135.6(2C), 133.9, 129.5(2C), 127.0, 126.4, 124.4(2C), 123.4, 118.8, 83.6, 74.0, 48.3, 45.4, 29.1(3C), 19.2. Anal calcd for: C$_{27}$H$_{29}$N$_3$O$_5$S: C, 63.89; H, 5.76; N, 8.28 % Found C, 63.96; H, 5.93; N, 8.44%.

2.6.15. 6-Benzyl-2-(4-(benzyloxy)benzamido)-4,5,6,7-tetrahydrothieno[2,3-c]pyridine-3-carboxamide (25)

Yield: 74 %; MS(ESI) m/z 498 [M+H]$^+$. ^{1}H NMR (300 MHz, DMSO-d_6): δ 9.54 (s, 1H), 7.94 (d, J = 7.8 Hz, 2H), 7.81–7.74 (m, 4H), 7.63–7.42 (m, 6H), 7.36–7.22 (m, 4H), 5.21 (s, 2H), 3.76 (s, 2H), 3.42 (s, 2H), 3.06 (t, J = 8.1 Hz, 2H), 2.99 (t, J = 8.1 Hz, 2H); ^{13}C NMR (75 MHz, DMSO-d_6) δ 180.6, 168.3, 162.6, 161.1, 138.6, 136.2, 134.7(2C), 132.4(2C), 133.2, 130.7(2C), 129.2, 128.2, 127.6(2C), 127.0(2C), 126.4(2C), 124.3, 123.4, 117.4, 72.9, 63.9, 51.6, 48.3, 19.2. Anal calcd for: C$_{29}$H$_{27}$N$_3$O$_3$S: C, 70.00; H, 5.47; N, 8.44 % Found C, 70.11; H, 5.52; N, 8.55%.

APPENDIX

LIST OF PUBLICATIONS

FROM THESIS WORK

1. Identification of Novel Inhibitors against *Mycobacterium tuberculosis* L-Alanine Dehydrogenase (MTB-L-AlaDH) through Structure-based Virtual Screening. **Shalini Saxena**, Parthiban Brindha Devi, Vijay Soni, Perumal Yogeeswari, Dharmarajan Sriram. *J. Mol. Graphics Modell*. **2014**, 47, 37–43.

2. Mycobacterial DNA gyrase B inhibitors: Ligand-based pharmacophore modeling and enzyme inhibition studies. **Shalini. Saxena,** Janupally Renuka, Variam Ullas Jeankumar, Perumal Yogeeswari, Dharmarajan Sriram. *Curr. Topics Med. Chem.* **2014,** 14, 1990-2005.

3. Discovery of novel mycobacterial DNA gyrase B inhibitors: In silico and in vitro biological evaluation. **Shalini Saxena**, Janupally Renuka, Perumal Yogeeswari, Dharmarajan Sriram. *Mol. imform*. **2014,** 33, 597-609.

4. Design and development of novel *Mycobacterium tuberculosis* L-alanine dehydrogenase inhibitors. **Shalini Saxena**, Ganesh Samala, Jonnalagadda Padma Sridevi, Parthiban Brindha Devi, Perumal Yogeeswari, Dharmarajan Sriram. *Eur. J. Med. Chem.* **2014, Accepted.**

5. Structure guided discovery of novel anti-tubercular agents targeting the gyrase ATPase domain. Variam Ullas Jeankumar#, **Shalini Saxena**#, Rahul Vats, Srilakshmi Rudra Reshma, Renuka Janupally, Jonnalagadda Padma Sridevi, Pushkar Kulkarni, Perumal Yogeeswari, Dharmarajan Sriram. *ACS Med Chem Letter*. **2014, Revised version communicated.**

6. Development of 2-amino-5-phenylthiophene-3-carboxamide derivatives as novel and potent inhibitors of Mycobacterium tuberculosis DNA GyrB domain. **Shalini Saxena**, Ganesh Samala, Janupally Renuka, Jonnalagadda Padma Sridevi, Perumal Yogeeswari, Dharmarajan Sriram. *Bioorg. Med. Chem.* **2014, Revised version communicated.**

OTHER PUBLICATIONS

1. Discovery of novel inhibitors targeting the *Mycobacterium tuberculosis* O-acetylserine sulfhydrylase (CysK1) using virtual high-throughput screening. Variam Ullas Jean kumar, Omer Poyraz, **Shalini Saxena**, Robert Schnell, Perumal Yogeeswari, Gunter Schneider, Dharmarajan Sriram. *Bioorg. Med. Chem. Lett.* **2013**, 23, 1182-1186.

2. Structure-Guided Design of Novel Thiazolidine Inhibitors of O-Acetyl Serine Sulfhydrylase from *Mycobacterium tuberculosis*. Omer Poyraz, Variam Ullas Jeankumar, **Shalini Saxena**, Robert Schnell, Martin Haraldsson, Perumal Yogeeswari, Dharmarajan Sriram, Gunter Schneider. *J. Med. Chem.* **2013,** 56, 6457-6466.

3. Gyrase ATPase Domain as an Antitubercular Drug Discovery Platform: Structure-Based Design and Lead Optimization of Nitrothiazolyl Carboxamide Analogues. Variam Ullas Jeankumar, Janupally Renuka, Sonali Kotagiri, **Shalini Saxena**, Shruti Singh Kakan, Jonnalagadda Padma Sridevi, Swapna Yellanki, Pushkar Kulkarni, Perumal Yogeeswari, Dharmarajan Sriram. ChemMedChem. **2014,** 9, 1850-1859.

4. Development of novel tetrahydrothieno[2,3-c]pyridine-3-carboxamide based *Mycobacterium tuberculosis* pantothenate synthetase inhibitors: Molecular hybridization from known antimycobacterial leads. Ganesh Samala, Parthiban Brindha Devi, Radhika Nallangi, Jonnalagadda Padma Sridevi, **Shalini Saxena**, Perumal Yogeeswari, Dharmarajan Sriram *Bioorg. Med. Chem.* **2014,** 22, 1938–1947.

5. Identification and development of 2-methylimidazo[1,2-a]pyridine-3-carboxamides as *Mycobacterium tuberculosis* pantothenate synthetase inhibitors. Ganesh Samala, Radhika Nallangi, Parthiban Brindha Devi, **Shalini Saxena**, Renu Yadav, Jonnalagadda Padma Sridevi, Perumal Yogeeswari, Dharmarajan Sriram. *Bioorg. Med. Chem*. **2014,** 22, 4223-4232.

6. Investigating structure–activity relationship and mechanism of action of antitubercular 1-(4-chlorophenyl)-4-(4-hydroxy-3-methoxy-5-nitrobenzylidene)pyrazolidine-3,5-dione [CD59]. Ganesh Samala, Shruti Singh Kakan, Radhika Nallangi, Parthiban Brindha Devi, Jonnalagadda Padma Sridevi, **Shalini Saxena**, Perumal Yogeeswari, Dharmarajan Sriram. *Int J Mycobacteriol.* **2014,** 3, 117-126.

7. Structure-guided design of novel thiazolidines as inhibitor of pantothenate synthetase from *Mycobacterium tuberculosis*. Parthiban Brindha Devi, Ganesh Samala, Jonnalagadda Padma Sridevi, **Shalini Saxena,** Mallika Alvala, Perumal Yogeeswari, Elena G Salina, Dharmarajan Sriram. *ChemMedChem.* **2014**, 9, 2538-2547.

8. Development of 2-(4-oxoquinazolin-3(4H)-yl) acetamide derivatives as novel enoyl-acyl carrier protein reductase (InhA) inhibitors for the treatment of tuberculosis. Ganesh S Pedgaonkar, Jonnalagadda Padma Sridevi, Variam Ullas Jean Kumar, **Shalini Saxena**, Parthiban Brindha Devi, Janupally Renuka, Perumal Yogeeswari, Dharmarajan Sriram. *Eur. J. Med. Chem.* **2014**, 86, 613-627.

9. Development of benzo[d]oxazol-2(3H)-ones derivatives as novel inhibitors of *Mycobacterium tuberculosis* InhA. Ganesh S Pedgaonkar, Jonnalagadda Padma Sridevi, Variam Ullas Jean Kumar, **Shalini Saxena**, Parthiban Brindha Devi, Janupally Renuka, Perumal Yogeeswari, Dharmarajan Sriram. *Bioorg. Med. Chem.* **2014**, 22, 6134-6145

10**.** Salicylanilide Diethyl Phosphates as Potential Inhibitors of Some Mycobacterial Enzymes. Martin Kratky, Eva Novotna, **Shalini Saxena,** Perumal Yogeeswari, Dharmarajan Sriram, Marketa Svarcová, and Jarmila Vinsova. *The Scientific World Journal*. **2014,** Volume 2014 (2014), Article ID 703053, 6 pages.

11. Enabling the (3+2) cycloaddition reaction to engineer a newer anti-tubercular lead acting through the inhibition of Gyrase ATPase domain: Lead optimization and structure activity profiling. Variam Ullas Jean Kumar, Janupally Renuka, Brahmam Medapi, **Shalini saxena**, Jonnalagadda Padma Sridevi Pushkar Kulkarni Perumal Yogeeswari, Dharmarajan Sriram. *Organic & Biomolecular Chemistry.* **2014**, **Accepted.**

12. Design of novel *Mycobacterium tuberculosis* pantothenate synthetase inhibitors: Virtual screening, synthesis and *in vitro* biological activities. Parthiban Brindha Devi, **Shalini Saxena,** Sridhar Jogula, Asireddy Parameshwar reddy, Jonnalagadda Padma Sridevi, Dharmarajan Sriram, Perumal Yogeeswari. *Molecular Informatics*. **2014, Accepted.**

PAPERS PRESENTED AT NATIONAL/INTERNATIONAL CONFERENCES

1. Devi, P.B., **Saxena, S**., Sriram, D., Yogeeswari, P., Screening and Identification of Potent Inhibitors against pantothenate synthetase- An important target *Mycobacterium tuberculosis* infection. 3rd ScienceOne Conference on Drug Discovery and Development (SCDDD), 21-23 January **2014**, Dubai.

2. Kakan, S.K., JeanKumar, V.U., Devi, P.B., **Shalini, S**., Sriram, D., Yogeeswari, P., Targeting *Mycobacterium tuberculosis* Lysine aminotransferase: Design, synthesis and in vitro evaluation of small molecule compounds. International Conference on "Drugs for the Future: Infectious Diseases", Antimicrobial Drug Discovery: Challenges and Perspectives, 27-28 March **2014**, NIPER, Hyderabad, India.

3. P. Santosh, V.U. Jean Kumar, **S. Saxena**, P. Yogeeswari, D. Sriram, In-Silico Design and Synthesis of Novel Nitrothiazole derivatives as potential inhibitors of MTB CysK1, 5th International Symposium of Drug development for Orphan/Neglected Diseases, 26-28 February **2013**, Lucknow.

BIOGRAPHY OF SHALINI SAXENA

Miss Shalini Saxena completed his Bachelor of Science and Master of Science in Biotechnology from Dr. Hari Singh Gour University Sagar, (M.P.). She has about 2.5 years of experience in Molecular Modelling and Drug Design at Central Drug Research Institute, Lucknow, from 2008-20010. She has been appointed as a Junior Research Fellow at Birla Institute of Technology and Science, Pilani, Hyderabad campus from 2011-2014 under the supervision of D. Sriram. She has published nineteen scientific publications in well-renowned international journals and presented papers at various national and international conferences.

BIOGRAPHY OF PROFESSOR. D. SRIRAM

D. Sriram is presently working in the capacity of Professor at Department of Pharmacy, Birla Institute of Technology and Science, Pilani, Hyderabad campus. He received his Ph.D. in 2000 from Banaras Hindu University, Varanasi. He has been involved in teaching and research for last 14 years. He has 250 peer-reviewed research publications to his credit. He has collaborations with various national and international organizations such as Karolinska institute, Sweden; the Indian Institute of Science, Bangalore and National Institute of Immunology, New Delhi. He was awarded the Young Pharmacy Teacher of the year award of 2006 by the Association of Pharmacy Teachers of India. He received ICMR Centenary year award in 2011. He has guided 8 Ph.D. students and 13 students are pursuing Ph.D currently. His research is funded by agencies like the UGC, CSIR, ICMR, DBT and DST.